NUMERICAL AND EXPERIMENTAL ANALYSIS OF SINGLE PILE FOUNDATION BEHAVIOR IN EXPANSIVE ANKARA CLAY

A THESIS SUBMITTED TO
THE GRADUATE SCHOOL OF NATURAL AND APPLIED SCIENCES
OF
MIDDLE EAST TECHNICAL UNIVERSITY

BY

SEFA YILDIRIM

IN PARTIAL FULFILLMENT OF THE REQUIREMENTS
FOR
THE DEGREE OF DOCTOR OF PHILOSOPHY
IN
CIVIL ENGINEERING

JULY 2025

Approval of the thesis:

NUMERICAL AND EXPERIMENTAL ANALYSIS OF SINGLE PILE FOUNDATION BEHAVIOR IN EXPANSIVE ANKARA CLAY

submitted by **SEFA YILDIRIM** in partial fulfillment of the requirements for the degree of **Doctor of Philosophy** i**n Civil Engineering, Middle East Technical University** by,

Prof. Dr. Naci Emre ALTUN
Dean, **Graduate School of Natural and Applied Sciences** _____

Prof. Dr. Erdem Canbay
Head of the Department, **Civil Engineering** _____

Prof. Dr. Erdal Çokça
Supervisor, **Civil Engineering, METU**

Examining Committee Members:

Prof. Dr. Seyhan Fırat
Civil Engineering, Gazi Uni. _____

Prof. Dr. Erdal Çokça
Civil Engineering, METU _____

Prof. Dr. Nihat Sinan Işık
Civil Engineering, Gazi Uni. _____

Assoc. Prof. Dr. Nabi Kartal Toker
Civil Engineering, METU _____

Assoc. Prof. Dr. Onur Pekcan
Civil Engineering, METU _____

Date: 02.07.2025

I hereby declare that all information in this document has been obtained and presented in accordance with academic rules and ethical conduct. I also declare that, as required by these rules and conduct, I have fully cited and referenced all material and results that are not original to this work.

Name Last name : Sefa Yıldırım

Signature :

ABSTRACT

NUMERICAL AND EXPERIMENTAL ANALYSIS OF SINGLE PILE FOUNDATION BEHAVIOR IN EXPANSIVE ANKARA CLAY

Yıldırım, Sefa
Doctor of Philosophy, Civil Engineering
Supervisor : Prof. Dr. Erdal Çokça

July 2025, 206 pages

Ankara, Türkiye, has a semi-arid climate, where moisture content variations in expansive soils cause swelling movements, potentially damaging lightweight structures. Pile foundations are commonly used in expansive soils when superstructure loads need to be transferred to depths where moisture change is ignorable. To design safe pile foundations in such conditions, it is crucial to determine the necessary anchorage depth to counteract uplift forces. The soil surrounding the pile in expansive clays is typically unsaturated, and matric suction significantly influences the mechanical behavior of the pile.

To achieve the objectives of this study, the Thornthwaite Moisture Index (TMI) was determined to classify the regional climate zone. Scanning Electron Microscope (SEM) images and X-ray Diffraction (XRD) results were analyzed to identify the soil mineralogy. The index properties of the soil were characterized through sieve and hydrometer analyses, specific gravity tests, Atterberg limits, compaction tests, free swell tests, and methylene blue tests. The mechanical behavior of the soil was investigated using direct shear, unconfined compression, triaxial, and one-dimensional consolidation tests. Additionally, the soil water retention curve (SWRC) was obtained using the axis translation, filter paper, and

salt solution methods. The findings were then combined to derive the parameters of the Barcelona Basic Model (BBM) for numerical modeling.

Furthermore, small-scale laboratory experiments were conducted to simulate the behavior of a single pile foundation in expansive clay. The displacement of the pile at varying anchorage depths was measured to determine the minimum required anchorage depth for a safe and stable design.

According to the results of the experiments carried out in the laboratory, it was observed that if 3/5 of the total length of the single piles is placed in the anchor zone in the Ankara clay, there will be no movement of the pile. This study shows that Ankara-Cubuk clay, which is very difficult to predict the behavior and model because of the change in material properties depending on the water content, can be modeled using the BBM method.

Keywords: Clay, Expansive Soil, Pile Foundation, SWRC, BBM, FEM

ÖZ

ŞİŞEN ANKARA KİLİNDE TEKİL KAZIK TEMEL DAVRANIŞININ SAYISAL VE DENEYSEL ANALİZİ

Yıldırım, Sefa
Doktora, İnşaat Mühendisliği
Tez Yöneticisi: Prof. Dr. Erdal Çokça

Temmuz 2025, 206 sayfa

Ankara, Türkiye, zemindeki su içeriği değişimlerinin şişme hareketlerine neden olduğu ve potansiyel olarak hafif yapılara zarar veren yarı kurak bir iklime sahiptir. Kazıklı temeller, üstyapı yüklerinin su içeriği değişiminin önemsiz olduğu derinliklere aktarılması gereken şişen zeminlerde yaygın olarak kullanılmaktadır. Bu tür koşullarda güvenli kazık temel tasarımı için, kaldırma kuvvetlerine karşı koymak üzere gerekli ankraj derinliğini belirlemek çok önemlidir. Şişen killerde kazığı çevreleyen zemin tipik olarak doymamış durumdadır ve matrik emme kazığın mekanik davranışını önemli ölçüde etkiler.

Bu çalışmanın amaçlarına ulaşmak için, Thornthwaite Nem İndisi (TMI) bölgesel iklim zonunu sınıflandırmak için tespit edilmiştir. Zemin mineralojisini tanımlamak için Scanning Electron Microscope (SEM) görüntüleri ve X-ray Diffraction (XRD) sonuçları analiz edilmiştir. Zeminin indeks özellikleri elek ve hidrometre analizleri, özgül ağırlık testleri, Atterberg limitleri, kompaksiyon testleri, serbest şişme testleri ve metilen mavisi testleri ile tanımlanmıştır. Zeminin mekanik davranışı direkt kesme, serbest basınç, üç eksenli ve tek boyutlu konsolidasyon deneyleri kullanılarak incelenmiştir. Ayrıca, zemin su tutma eğrisi (SWRC) eksen öteleme, filtre kağıdı ve tuz çözeltisi yöntemleri kullanılarak elde edilmiştir. Bulgular daha

sonra sayısal modelleme için Barselona Basic Modeli'nin (BBM) parametrelerini belirlemek üzere birleştirilmiştir.

Ayrıca, şişen kilde tekil kazıklı temelin davranışını simüle etmek için küçük ölçekli laboratuvar deneyleri yapılmıştır. Kazığın farklı ankraj derinliklerindeki yer değiştirmesi ölçülerek güvenli ve stabil bir tasarım için gerekli minimum ankraj derinliği belirlenmiştir. Laboratuvarda yapılan deneylerin sonuçlarına göre, tek kazıkların toplam uzunluğunun 3/5'i Ankara kilinde ankraj bölgesine yerleştirilirse kazığın hareket etmeyeceği gözlemlenmiştir. Bu çalışma, su içeriğine bağlı olarak malzeme özelliklerindeki değişim nedeniyle davranışını tahmin etmenin ve modellemenin çok zor olduğu Ankara-Çubuk kilinin BBM yöntemi kullanılarak modellenebileceğini göstermektedir.

Anahtar Kelimeler: Şişen Zemin, Kazık Temel, SWRC, BBM, FEM

Dedicated to My Family

ACKNOWLEDGMENTS

First and foremost, I would like to express my deepest gratitude to my advisor, Prof. Dr. Erdal Çokça, for believing in me and supporting me through every challenge I encountered in this long and demanding marathon. Balancing a full-time job with PhD studies was never easy, especially during the COVID-19 pandemic when I had to freeze my studies for an entire year. There were times when continuing seemed almost impossible, but Prof. Çokça was always there with his encouraging words, steady support, and unwavering belief in me. His ability to motivate, guide, and lift me up through the most difficult moments is something I will never forget. I have learned so much from him — not only about geotechnical engineering but also about academic integrity, perseverance, and mentorship. One of my greatest goals is to become a professor like him one day: supportive, inspiring, and truly devoted to his students' success.

I am profoundly thankful to Assoc. Prof. Dr. Nabi Kartal Toker, whose endless support in the laboratory made this research possible. I must have asked him millions of questions, and yet he always responded with care and generosity. He not only taught me every detail of the experimental procedures but also guided everyone in the lab with kindness and wisdom. In my case, he treated me like one of his own students, and this thesis simply could not have been completed without his unwavering help.

My sincere thanks go to Prof. Dr. Nihat Sinan Işık, whose insightful comments during my thesis committee meetings greatly enriched the quality of this study. I truly appreciate the effort he made by traveling to METU multiple times, always contributing valuable perspectives.

I would also like to thank Prof. Dr. Seyhan Fırat for kindly accepting to be part of my thesis committee despite his extremely busy schedule, and for taking on the role of committee chair. His presence and support are deeply appreciated.

A special thanks to Assoc. Prof. Dr. Onur Pekcan, who was not only a member of my committee but also a psychological support throughout this journey. His thoughtful conversations, motivation, and encouraging words came at just the right times and helped me keep going.

I am also deeply grateful to Dr. Melih Kenanoğlu, one of the most important contributors to this study. He not only taught me how to conduct all the unsaturated soil tests but also spent countless hours helping me interpret the results and guiding me with his brilliant mind and generous heart. His support is unforgettable, and I feel truly lucky to have him as a close friend.

I am thankful to everyone in the Soil Mechanics Laboratory for their support. In particular, Kamber Abi, a legend among everyone who has ever worked in the lab, is always the go-to person for any kind of help. Thanks to Ulaş Abi for our thoughtful discussions and his practical suggestions on test procedures.

I would also like to thank my lab mates, who over time became like family to me. Listed here in alphabetical order — Dr. Berkan Söylemez, Elife Çakır, Emre Duman, Hayri Güzel (I will never forget the night he stayed with me in the lab and helped while I was exhausted and overwhelmed), Moutasem Zarzour, Tuğçe Aktaş, and Dr. Yılmaz Emre Sarıçiçek — and many other friends whose names may not be mentioned but whose presence I truly value. Working alongside such dedicated, kind, and supportive people made this long journey not only manageable but also filled with friendship and unforgettable memories. I'm genuinely grateful to have shared this path with each of them.

My heartfelt thanks go to my closest friends, Dr. Sarper Demirdöğen, Emre Odabaşı, and Moutasem Zarzour, who shared not only the challenges of academic life but also stood by me during one of the most physically demanding parts of this research — collecting and transporting tons of clay samples from various locations in Ankara. Their help during this exhausting process meant a great deal to me, and I truly appreciate their generosity, strength, and unwavering friendship.

Many thanks to Yasemin Er and Alaa Elsaid for their invaluable companionship throughout the entire PhD journey. Their excellent presentation skills were a great source of help, especially when I needed support preparing for seminars, committee meetings, and my thesis defense. I am also grateful for their keen eye and technical help in fixing formatting issues and improving the overall appearance of the thesis. Their friendship and assistance have been truly appreciated every step of the way.

Finally, I owe the deepest gratitude to my beloved family, whose unwavering support has been the foundation of this journey. I thank my mother, Şeriman Yıldırım, for her endless prayers and wishes, always believing in the best for me. To my father, Mehmet Yıldırım, whose wisdom, advice, and steadfast presence have guided me throughout every stage of my life — thank you for being my greatest supporter.

I am also deeply grateful to my precious sisters, Dr. Merve Yıldırım and Dr. Şafak Yıldırım, the most valuable people in my life. Their constant encouragement, unconditional love, and belief in me have been a source of strength throughout this journey. No matter how difficult things became, they always knew how to lift my spirits and remind me of my worth. I feel truly lucky and proud to have them by my side, not only as sisters but as lifelong companions.

At the beginning of this long PhD journey, I was fortunate to have the prayers and emotional support of my late grandmother and aunt — Emine Yıldırım and Hatice Yıldırım — whom I sadly lost during the COVID-19 pandemic. Their love and presence remain in my heart, and I dedicate this achievement to their memory.

TABLE OF CONTENTS

ABSTRACT v

ÖZ vii

ACKNOWLEDGMENTS x

TABLE OF CONTENTS xiii

LIST OF TABLES xx

LIST OF FIGURES xxii

LIST OF ABBREVIATIONS xxix

LIST OF SYMBOLS xxxi

CHAPTERS

1. INTRODUCTION 1

1.1. Research Objectives 2

1.2. Expansive Soil 3

1.3. Active Zone Depth 3

1.4. Development of the Design Parameters 6

2. LITERATURE REVIEW 7

2.1. Clay Mineralogy 7

2.1.1. Kaolinite 9

2.1.2. Illite 9

2.1.3. Montmorillonite 10

2.2. Expansive Soil 10

2.2.1. Global Distribution of the Expansive Soil 10

2.2.2. Expansive Soils in Türkiye 13

2.3. Identification and Classification of Expansive Clays....16
2.3.1. Signs for the Existence of Expansive Soil on the Field....16
2.3.2. Climate....17
2.3.3. Active Zone Depth....18
2.3.4. Direct Tests for Determination of Swelling Parameters....20
2.3.4.1. Swell Potential....21
2.3.4.2. Swell Pressure....22
2.3.4.3. Modified Free Swell Test....23
2.3.4.4. Lateral Swell Test....24
2.3.5. Laboratory Tests to Identify and Classify Expansive Soils and Determine Swell Parameters....25
2.3.5.1. Sieve and Hydrometer Tests....25
2.3.5.2. Specific Gravity Test....26
2.3.5.3. Atterberg Limits Test....26
2.3.5.4. Compaction Test....32
2.3.6. Laboratory Tests for Mineralogical Identification of Expansive Soil....34
2.3.6.1. Methylene Blue Test....34
2.3.6.2. X-Ray Diffraction Analysis....37
2.3.6.3. Scanning Electron Microscope (SEM)....40
2.4. Soil Water Retention Curve (SWRC) Measurements....40
2.4.1. Suction Measurement Techniques for SWRC....44
2.4.1.1. Axis Translation Method....45
2.4.1.2. Filter Paper Method....46
2.4.1.3. Salt Solution Method....48
2.5. Barcelona Basic Model (BBM)....49

2.5.1. Determining Barcelona Basic Model Parameters 54
2.6. Pile Foundation in Expansive Soil 56
2.6.1. Adhesion Factor 56
2.6.2. Uplift Factor 58
3. FIELD AND LABORATORY STUDIES 61
3.1. Site selection 62
3.2. Determination of Thornthwaite Moisture Index (TMI) 65
3.3. Soil Collection and Preparation Process 66
3.3.1. Soil Collection Process 66
3.3.2. Preparation of Soil Samples for the Laboratory Tests 68
3.4. Laboratory Tests 69
3.4.1. Atterberg Limit Tests 69
3.4.1.1. Shrinkage Limit Tests 69
3.4.2. Specific Gravity Test 72
3.4.3. Sieve and Hydrometer Tests 72
3.4.4. Compaction Test 73
3.4.5. Modified Free Swell Test 74
3.4.6. Swelling Potential and Swelling Pressure Tests 74
3.4.7. One-Dimensional Consolidation Test Using Incremental Loading 76
3.4.8. Direct Shear Tests 76
3.4.9. Unconfined Compression Tests 79
3.4.10. X-Ray Diffraction (XRD) Test 81
3.4.11. Scanning Electron Microscope (SEM) 82
3.4.12. Methylene Blue Test 83
3.4.13. Shrinkage Curve 83

3.5. Soil Water Retention Curve (SWRC) Development Tests 85
3.5.1. Vapor Equilibrium Method 85
3.5.2. Filter Paper Method 87
3.5.3. Axis Translation Method 89
3.6. Determination of Barcelona Basic Model Parameters 90
3.6.1. Additional Laboratory Tests to Determine Barcelona Basic Model Parameters 91
3.6.1.1. Evaporation Test to Determine Critical Water Content 92
3.6.1.2. Unsaturated 1-D Consolidation Test 92
3.6.1.3. Simplified Unsaturated Triaxial Tests 93
3.6.1.4. Saturated Triaxial CD Tests 94
3.6.2. Calibration of Barcelona Basic Model Parameters 94
3.6.2.1. The slope of elastic compression line (κ) 94
3.6.2.2. The slope of the critical state line (M) 95
3.6.2.3. The Slope of the Saturated Virgin Compression Line (λ(0)) 95
3.6.2.4. Slope of Apparent Tensile Strength vs. Suction (k) 95
3.6.2.5. Loading-Collapse (LC) Parameters (r, β) 95
3.6.2.6. The preconsolidation pressure (p_0*) 96
3.6.2.7. General optimization process for BBM parameters 96
4. TEST RESULTS AND DISCUSSION 97
4.1. Soil Collection 97
4.2. Thornthwaite Moisture Index (TMI) Determination for Cubuk-Ankara 99
4.3. Soil Index and Classification Tests 102
4.3.1. Atterberg Limit Tests 102
4.3.2. Shrinkage Limit Tests 102

4.3.3. Specific Gravity 103
4.3.4. Grain Size Distribution 103
4.3.5. Activity of the soil 103
4.3.6. Compaction Test 104
4.4. Swell Potential-Pressure 104
4.5. Hydraulic Tests 105
4.5.1. Shrinkage Curve 105
4.4.2. Evaporation Test 106
4.4.3. Soil Water Retention Curve 107
4.4.3.1. Axis Translation Method 107
4.4.3.2. Filter Paper Method 108
4.4.3.3. Salt Solution Method 110
4.4.3.4. SWRC Determination 111
4.5. Mechanical Tests 115
4.5.1. Unconfined Compression Test 115
4.5.2. Direct Shear Test 118
4.6. Investigation of the Mineralogy of Ankara Expansive Clay 119
4.6.1. Methylene Blue Test Results 119
4.6.2. Scanning Electron Microscope (SEM) 121
4.6.3. Energy-Dispersive X-ray Spectroscopy (EDX) Analysis of Cubuk-Ankara Clay 123
4.6.4. X-Ray Diffraction (XRD) Result 123
4.7. Determination of Barcelona Basic Model Parameters 125
4.7.1 The slope of the elastic compression line (κ) 125
4.7.2. The slope of the critical state line (M) 127

4.7.3. The slope of the saturated virgin line (λ(0)) 128
4.7.4. Suction Contribution to Apparent Cohesion (k) 128
4.7.5. Loading-Collapse (LC) Parameters (r, β) 130
4.7.6. The preconsolidation pressure (p_0*) 130
4.7.7. General optimization process for BBM parameters 131
5. LABORATORY MODEL TESTS 141
5.1. Model Tests in PVC Meter Test Set-up 141
5.2. Laboratory Size Model Tests in the 15.2 cm diameter, 5 cm height mold for Pile Foundation in Expansive Clay 141
5.2.1. Preparation of pile and drainage pipes 141
5.2.2. Preparation of the soil for the test 142
5.2.3. Preparation of the soil for the test with anchorage zones 144
5.2.4. Saturating the test setup and measuring pile movement 145
5.2.5. Laboratory Test Results 146
5.3. Determination of Adhesion Factors 149
5.4. Determination of Adhesion Factors 150
6. NUMERICAL ANALYSIS RESULTS OF THE LABORATORY MODEL TEST 153
6.1. RS-2 Numerical Model 153
6.2. Boundary Conditions 154
6.3 Analysis Results 155
6.4. Sensitivity Analysis for λ(0), κ, r, β, p_c, k and M parameters 156
7. CONCLUSIONS AND RECOMMENDATIONS FOR FUTURE RESEARCH 161
7.1. Conclusion 161

7.2. Recommendations For Future Research 163
REFERENCES 165
APPENDICES
A. FIGURES TO EXPLAIN THE PARAMETERS OF BBM FROM INTERNET 179
B. TMI AND CLAY MINERALOGY IDENTIFICATION 186
C. XRD 188
D. SEM PHOTOS 190
E. EDX GRAPHS 194
F. GRAPHICAL ABSTRACT OF THE RESEARCH 200
G. CURRICULUM VITAE 205

LIST OF TABLES

TABLES

Table 2.1. Thorntwaite Moisture Index for the Different Climate Types (Thornthwaite, 1948; Ikizler, 2018) 17
Table 2.2. Depth of Design Suction Change for Cities in Australia (Adopted from AS2870, 2011) 19
Table 2.3. Relationship between TMI and depth of soil suction (Adopted from AS2870, 2011) 19
Table 2.4. USBR Classification for expansive soils 21
Table 2.5. Expansive soil classification (Adopted Sridharan and Prakash, 2000) 21
Table 2.6. Classification of the soil based on the expansion index (Nelson, 2015) 22
Table 2.7. Swelling pressure effect on asphalt and concrete surface (Pruška and Šedivý, 2017) 23
Table 2.8. Classification of Expansive Soil using FSI (Bureau of Indian Standards 1987) 24
Table 2.9. Skempton, 1953 Classification of Clay based on activity 27
Table 2.10. Skempton, 1953 Activity values for typical clay minerals (Nelson, 2015) 27
Table 2.11. Previous studies to classify expansive soils using Atterberg limits and clay content 28
Table 2.12. Empirical Predictions for Expansive Soils (Hergul, 2012) 31
Table 2.13. Typical values of maximum dry densities and corresponding optimum water contents (Germaine and Germaine, 2009) 34
Table 2.14. Typical values of CEC and SSA for different clay minerals (Mitchell and Soga,2005, modified from Nelson, 2015) 36
Table 2.15. Interatomic spaces for common minerals in soil (Mitchell, 2005) 39

Table 2.16. Advantages and disadvantages of different designations on SWRC (Fredlund, 2012) 41
Table 2.17. SWRC empirical equations (Leong and Wijaya, 2023)..... 42
Table 2.18. Common techniques for soil suction measurements (Modified after Lu and Likos, 2004) 44
Table 2.19. Relative humidity of common types of salts and corresponding total suctions (Kenanoğlu, 2023) 49
Table 2.20. The required parameters for the BBM (Adopted from Kenanoğlu, 2023) 55
Table 3.1.Measurement Conditions for the XRD Test 82
Table 3.2. Kenanoglu and Toker (2024) proposal for determining BBM parameters and tests done in this study..... 91
Table 4.1. Results of some rapid tests on the collected soils..... 97
Table 4.2. TMI calculation spreadsheet for the Cubuk region 101
Table 4.3. Relative humidity of salts and corresponding total suctions (ASTM E104.02, Kenanoğlu, 2023)..... 110
Table 4.4. Determination of p_s 129
Table 4.5. C_c and $\lambda(s)$ values..... 130
Table 4.6. Final BBM parameters after the optimization process 132
Table 5.1. Determination of adhesion factor (α) from the undrained shear strength (c_u) (Coduto, 1994; modified from Cherubini and Vessia, 2008)..... 150
Table 5.2. Adhesion factor determination..... 150
Table 6.1. BBM parameters used in the RS-2 software..... 155
Table B.1. Latitude degree and monthly correction coefficient values 186
Table B.2. Adjustment coefficient calculation equations 187
Table C.1. XRD peak list for Cubuk clay..... 189

LIST OF FIGURES

FIGURES

Figure 1.1. Forces acting on the pile in expansive soil (Modified from Chen, 1975) 4
Figure 1.2. A typical pile foundation design under lightweight structures (Nelson and Miller, 1997; Alnmr et al., 2023) 5
Figure 2.1. Components of a variety of clay minerals (Mitchell and Soga, 2005) ... 8
Figure 2.2. Distribution of Expansive Soils in the USA (Nelson et al, 2015) 11
Figure 2.3. Distribution of Expansive Soils in China (Shi et al., 2002) 12
Figure 2.4. Distribution of Expansive Soils in Australia (Richards et al., 1983) 13
Figure 2.5. The general distribution of TMI in Turkiye (Ikizler, 2018) 18
Figure 2.6. Water content variations in a variety of locations in Tanzania (Lucian, 2011) 20
Figure 2.7. The relationship between swell ratio, initial water content, and dry density (Sapaz, 2004) 25
Figure 2.8. Location of Kaolinites Illites and Montmorillonites on the Plasticity Chart (Holtz, Kovacs, and Sheahan 2011, Nelson 2015) 29
Figure 2.9. Classification of Expansive soils based on clay contents and activities (Seed, Woodward and Lundgren, 1962; Chen, 1975) 30
Figure 2.10. Relationship between plasticity index and swelling potential (Chen, 1975) 30
Figure 2.11. Compaction Curve (Germaine and Germaine, 2009) 33
Figure 2.12. Compaction Curves for different soil textures (Gérmaine and Gérmaine, 2009) 33
Figure 2.13. The schematic graph to perform methylene blue test (Cokca, 2002) . 35
Figure 2.14. Potential expansion of the clay according to CEC and activity (Nelson and Miller, 1992; Nelson, 2015). 37
Figure 2.15. X-ray diffraction according to Bragg's law (Mitchell, 2005) 38

Figure 2.16.SEM images of kaolinite, illite and montmorillonite (Murray, 2007, Adopted from Özkan, 2021) 40
Figure 2.17. Properties of Soil Water Retention Curve (SWRC) (Soltani et al., 2019) 43
Figure 2.18. Effect of stress history and method on SWRC (Fredlund, 2012)..... 43
Figure 2.19. Sketch of the oedometer cell for axis translation method (Kenanoğlu, 2023) 45
Figure 2.20. Sketch of filter paper (Shen et al., 2013)..... 47
Figure 2.21. Salt solution desiccator (Fredlund, 2012)..... 49
Figure 2.22. Barcelona Basic Model yield surfaces in p-q-s plane (Alonso et al., 1999) 50
Figure 2.23. Effect of different loading paths on LC curve (Alonso, Gens, and Josa, 1990) 54
Figure 2.24. Forces acting on a pile in expansive soils (Nelson, 2015)..... 59
Figure 3.1. Golbasi Clay Sample-1 63
Figure 3.2. Golbasi Clay Sample-2 and MFSI Test..... 63
Figure 3.3. Cubuk Clay Sample-1 and Free Swell Test..... 64
Figure 3.4. Cubuk Clay Sample-2 and Modified Free Swell Tests 64
Figure 3.5. Batikent and Yuvakoy soil samples and Modified Free Swell Tests ... 65
Figure 3.6. Location of the Soil Sample 66
Figure 3.7. Soil Collection Process..... 67
Figure 3.8. Disturbed Soil samples taken from different depths and water content measurements..... 68
Figure 3.9. Soil Preparation stages before the laboratory tests..... 69
Figure 3.10. Atterberg Limits LL and PL Tests..... 69
Figure 3.11. Linear shrinkage limit test..... 70
Figure 3.12. Shrinkage limit determination by using mercury 71
Figure 3.13. Specific gravity (G_S) photos..... 72
Figure 3.14. Compaction test photos 73
Figure 3.15. Tempering of the clay samples for compaction test..... 74

Figure 3.16. Apparatus to measure swelling potential and swelling pressure 75
Figure 3.17. Direct Shear Test Apparatus 77
Figure 3.18. Direct Shear Testing Procedures 78
Figure 3.19. Interface Direct Shear Test Apparatus 79
Figure 3.20. Unconfined Compression Specimen Preparation 80
Figure 3.21. Tempering Unconfined Compression Test Specimens 81
Figure 3.22. QUANTA 400F Field Emission SEM 82
Figure 3.23. Methylene blue test apparatuses 83
Figure 3.24. Shrinkage curve test process 85
Figure 3.25. Salt solution test preparations 86
Figure 3.26. Salt solution specimens for water content and volume measurements 86
Figure 3.27. Filter paper test preparations 88
Figure 3.28. Filter paper method volume measurements at the end of the test 89
Figure 3.29. Axis translation method, test preparation 90
Figure 3.30. Evaporation test measurements 92
Figure 3.31. Specimen preparation for unsaturated triaxial tests 93
Figure 3.32. Unsaturated triaxial testing process 93
Figure 3.33. Triaxial CD test setup 94
Figure 4.1. Water content change with depths in Cubuk, Ankara 98
Figure 4.2. USBR plasticity chart 102
Figure 4.3. Grain size distribution 103
Figure 4.4. Compaction curve 104
Figure 4.5. Swelling Potential vs Pressure 105
Figure 4.6. Shrinkage curve 106
Figure 4.7. Evaporation test 106
Figure 4.8. SWRC data points gained from the axis translation method 108
Figure 4.9. SWRC data points gained from the filter paper method 109
Figure 4.10.SWRC data points gained from the salt solution 111
Figure 4.11. SWRC all data points 112

Figure 4.12. Ankara-Cubuk clay SWRC all data points 112
Figure 4.13. Ankara-Cubuk clay SWRC all data points with volumetric water content 113
Figure 4.14. Ankara-Cubuk clay SWRC all data points with the degree of saturation 113
Figure 4.15. Ankara-Cubuk clay SWRC with Van Genuchten fitting 114
Figure 4.16. Ankara-Cubuk clay SWRC with volumetric water content (Van Genuchten fitting) 114
Figure 4.17. Ankara-Cubuk clay SWRC with degree of saturation (Van Genuchten fitting) 115
Figure 4.18. Undrained Shear Strength (cu) values for different compaction curve points 116
Figure 4.19. Undrained Shear Strength (c_u) values for different shrinkage curve points 117
Figure 4.20. Direct shear test results of (a) clay, (b) concrete-clay interface 118
Figure 4.21. Methylene blue test result 119
Figure 4.22. SEM image with 1000x magnification 121
Figure 4.23. SEM image with 25000x magnification 122
Figure 4.24. X-Ray Diffraction (XRD) Result for the Cubuk-Ankara clay 124
Figure 4.25. Unsaturated 1-D compression test result for specimen with the water content of 19 percent 126
Figure 4.26. Unsaturated 1-D compression test result for specimen with the water content of 21 percent 126
Figure 4.27. Unsaturated 1-D compression test result for specimen with the water content of 23 percent 127
Figure 4.28. The slope of the critical state line (M) 127
Figure 4.29. BBM prediction of triaxial CD tests with the minimum deviation .. 128
Figure 4.30. Determination of suction contribution to apparent cohesion (k) 129
Figure 4.31. Model prediction curves for normalized deviatoric stress under 100 kPa confining pressure 132

Figure 4.32. Model prediction curves for normalized deviatoric stress under 400 kPa confining pressure 133
Figure 4.33. Experimental result vs BBM prediction for initial water content of 19% 133
Figure 4.34. Experimental result vs BBM prediction for initial water content of 21% 134
Figure 4.35. Experimental data vs BBM prediction for initial water content of 23% 134
Figure 4.36. Experimental results vs BBM prediction for saturated condition 135
Figure 4.37. LC curves and k line for the clay with 19, 21, 23 % of water contents under 100 kPa confining pressure 135
Figure 4.38. LC curves and k line for the clay with 19, 21, 23 % of water contents under 400 kPa confining pressure 136
Figure 4.39. Stress paths, critical state lines, and yield surfaces in the p-q plane under 100 kPa confining pressure 136
Figure 4.40. Stress paths, critical state lines, and yield surfaces in the p-q plane under 400 kPa confining pressure 137
Figure 4.41. Critical state lines, and yield surfaces under 100 kPa confining pressure 137
Figure 4.42. Critical state lines, and yield surfaces under 400 kPa confining pressure 138
Figure 4.43. Yield surfaces, k line and LC curves under 100 kPa confining pressure 138
Figure 4.44. Yield surfaces, k line and LC curves under 400 kPa confining pressure 139
Figure 5.1. PVC meter size laboratory test setup 141
Figure 5.2. Preparation of piles 142
Figure 5.3. Preparation of clay for the lab size test setup 143
Figure 5.4. Installation of piles and drains in the test setup 143
Figure 5.5. Preparation of test setup with anchorage zones 144

Figure 5.6. Test setup photos during and after the experiment 146
Figure 5.7. (a) Fully saturated set-up sketch, (b) Pile movement over time 147
Figure 5.8. (a) 2.5 cm in active, 2.5 cm in anchor zone set-up, (b) Pile movement over time 148
Figure 5.9. (a) 2 cm in active, 3 cm in anchor zone set-up, (b) Pile movement over time 149
Figure 6.1. Axisymmetric RS-2 model 154
Figure 6.2. RS2 Analysis Results 155
Figure 6.3. Sensitivity Analysis for $\lambda(0)$ 156
Figure 6.4. Sensitivity Analysis for κ 156
Figure 6.5. Sensitivity Analysis for r 157
Figure 6.6. Sensitivity Analysis for β 157
Figure 6.7. Sensitivity Analysis for p_c 158
Figure 6.8. Sensitivity Analysis for k 158
Figure 6.9. Sensitivity Analysis for M 159
Figure A.1. *Comparison of p-q-Sr diagram and p-q-s diagram.* 179
Figure A.2. BBM model demonstration 179
Figure A.3. Figure to explain the parameters of BBM yield surface 180
Figure A.4. Figure for BBM (yield surface) 180
Figure A.5. Figure to explain the parameters of BBM 181
Figure A.6. *Figure to explain the parameters of BBM yield surface* 181
Figure A.7. *Figure to explain the parameters of BBM (Alonso et al., 1990)* 182
Figure A.8. *Figure to explain the parameters of BBM yield surface* 182
Figure A.9. *Yield surface in the p´-q plane* 183
Figure A.10. Normal consolidation line and unloading-reloading (swelling) lines for an isotropic compression test 183
Figure A.11. An incremental consolidation pressure change due to movement of point from A´ to A´´ 184
Figure A.12. Relationship between preconsolidation stresses p_0 and p_0* (Alonso et al., 1990) 184

Figure A.13. The yield surface in Barcelona Basic Model (modified after Gens, 1995)..... 185
Figure C.1. XRD results from evaluatıon of Cubuk clay. 188
Figure C.2. XRD results from evaluatıon of Cubuk clay 188
Figure C.3. Minerals determined in Cubuk clay from XRD test..... 189
Figure D.1. SEM photos 190
Figure D.2. SEM photos 191
Figure D.3. SEM photos 192
Figure D.4. SEM photos 193
Figure E.1. EDX Graphs 194
Figure E.2. EDX Graphs 195
Figure E.3. EDX Graphs 196
Figure E.4. EDX Graphs 197
Figure E.5. EDX Graphs 198
Figure E.6. EDX Graphs 199
Figure F.1. Site Selection 200
Figure F.2. Laboratory Tests 201
Figure F.3. SWRC 201
Figure F.4. Minerological Analyses 202
Figure F.5. Interface Direct Shear Test between concrete and clay 202
Figure F.6. Laboratory model setup 202
Figure F.7. BBM Model 203
Figure F.8. Computer, Axisymmetric RS-2 model 204
Figure F.9. Recommendation for pile design in Cubuk-Ankara clay..... 204

LIST OF ABBREVIATIONS

AEV	Air Entry Value
AFNOR	Association Française de Normalisation
AMB	The area covered by one methylene blue molecule (130×10^{-20} m^2 according to Hang and Brindley, 1970)
AN	Avogadro's Number (6.02×10^{23}/mol)
AS	Australian Standard
ASTM	American Society for Testing and Materials
BBM	Barcelona Basic Model
CEC	Cation Exchange Capacity
DSI	The State Hydraulic Works
EDX	Energy Dispersive X-ray Spectroscopy
EI	Expansion Index
FEM	Finite Element Model
FSI	Free Swell Index
HAE	High Air Entry
I	Heat Index
IS	Indian Standards
LC	Surfaces of Loading-Collapse
LL	Liquid Limit
MFI	Modified Free Swell Index

NMB	Normality of Methylene Blue
PE	Potential Evapotranspiration
PI	Plasticity Index
PL	Plastic Limit
RH	Relative Humidity
SEM	Scanning Electron Microscope
SI	Strength Increment
SSA	Specific Surface Area
SWRC	Soil Water Retention Curve
TMI	Thornthwaite Moisture Index
USBR	United States Bureau of Reclamation
USCS	Unified Soil Classification System
WMB	Weight of Dry Methylene Blue Used for Methylene Blue Solution
XRD	X-ray Diffraction

LIST OF SYMBOLS

F_u	Uplift force
Z_a	Active zone depth
β_u	Uplift factor
P_s	Swelling pressure
W	The withholding force
Q_d	Load acting on pile
L	Length of the pile
α	Adhesion factor
N_c	Bearing capacity factor
β	Uplift factor
Z_a	Active zone depth
Hs	Depth of soil suction change
θ	Angle of Diffraction
λ	Wavelength of the X-rays
d	Interatomic Spacing
M_f	Mass of Dry Filter Paper
M_2	Total Dry Mass
T_h	Hot Container’s Mass
M_w	Mass of Water in the Filter Paper
T_c	Cold Container's Mass
w_f	Water Content of the Filter Paper
Ψ	Suction
Υ_w	Density of the water
(MW)w	Molar weight of water
R	Ideal gas constant
T	Temperature
p	Net Stress

S	Suction
p_0	Pre-consolidation Pressure
p	Mean Net Stress
σ_1	Major Principal Stress
σ_3	Minor Principal Stress
u_a	Pore air pressure
u_w	Pore water pressure
v	Specific volume
$\lambda(s)$	Slope of the virgin line (constant suction)
p_c	Reference stress
N(s)	Specific volume corresponds to $\lambda(s)$
κ	Slope of the elastic compression line due to the suction change
p_{atm}	Atmospheric pressure
N (0)	Specific volume at the reference stress
$\lambda(0)$	Slope of the saturated virgin line
β	Hardening effect with suction
r	Ratio compression index at the high suctions and slope of the saturated virgin line
q	Deviatoric stress
p	Mean net stress
p_c	Preconsolidation pressure with suction
M	Critical state parameter
q	Deviatoric stress
f	Skin friction
c_u	Undrained shear strength of the soil
a	Adjustment Factor
c_v	Coefficient of consolidation
c_c	Compression index
c_r	Recompression index
q_u	Unconfined compression strength

$p`$	Mean effective stress
k	Suction Contribution to Apparent Cohesion
w	Gravimetric water content
w_{crt}	Critical water content
R	Ideal gas constant (8.31432 Joules/mole·K)
T	Absolute temperature
v	Volume of 1000 moles of liquid water (0.018 m^3)
c_r	The slope of the recompression line in the vertical stress (σ_v) vs. void ratio (e) space;
K_0	The lateral earth pressure coefficient
Φ'	Internal friction angle
M	Slope of the critical state line
c''	Apparent cohesion
p_s	Cohesion increment due to suction

CHAPTER 1

INTRODUCTION

This study holds significant implications for the field of geotechnical engineering and construction in regions with expansive clay soils, particularly in semiarid climates like Ankara, Türkiye.

The shrinkage and swelling behavior of expansive soils have been a recurring challenge for lightweight construction projects. Despite extensive investigations under various conditions, the behavior of expansive soils remains an active research topic. The findings of this study will provide clear insights into how the swelling phenomena of soil affect the performance of pile foundations in expansive clay soils. Such information will be invaluable for geotechnical engineers and construction professionals, enabling the design of more reliable and safe foundation systems by taking into account the mechanics and behavior of soils under changing conditions.

Expansive clays are frequently seen across the world in semi-arid or arid climate type and the behavior of these clays is generally an important concern for geotechnical engineers (Dafalla et al., 2012). Ankara, Turkiye is in a semi-arid climate type and expansive clays are distributed all over the city. The behavior of Ankara expansive clays may vary from region to region, and it can be affected by many factors such as confining pressure, over-consolidation ratio, and their mineralogy as all the other expansive clays. The active zone where the significant water content change occurs is directly related to the volumetric change in expansive soils. The soils are generally unsaturated in this zone, so defining unsaturated soil behavior is one of the key and challenging parts of working in expansive soils.

Geotechnical engineers use pile foundations so that swelling forces coming from the active zone can be carried out by the anchorage zone. A safe and detailed pile foundation design requires determining many parameters such as clay mineralogy, active zone depth, swelling potential and pressure of the soil, soil water retention curve, and engineering parameters of the clay to predict the behavior of the soil and its interactions with the pile.

The outcome of research carried out in the expansive soil of Ankara to develop guidelines and design parameters for the single concrete piles in expansive Ankara clay is presented in this thesis study.

1.1. Research Objectives

The main objective of this study is to establish design guidelines for piles constructed in expansive Ankara clay. To achieve this, comprehensive laboratory experiments are conducted to characterize the geotechnical properties of the clay in detail, thereby contributing to the understanding and prediction of similar soil behavior. Another key objective is to investigate the performance of piles embedded in expansive clay through both experimental studies and numerical analyses. Based on the predicted pile movements, the study ultimately aims to determine the minimum required anchorage depth to ensure safe and effective design.

The following steps are defined separately and gathered together to achieve the main objective.

Gathering soil samples all around Ankara to perform quick laboratory testing to determine their swelling pressures and decide which soil to select for further advanced testing to be used in this study.

Determining the Thornthwaite Moisture Index (TMI) specifically for the location of the selected clay samples.

Determining the index parameters for the soil by performing laboratory tests such as grain size distribution by performing sieve and hydrometer tests, free swell tests, and Atterberg limit tests.

Performing a compaction test to determine the optimum water content and maximum dry density of the soil.

Performing a consolidation test to determine the consolidation curve of the soil.

Determining the shear strength parameters of the soil and soil-pile interface by conducting direct shear tests.

Determining the behavior of a single pile in the Ankara expansive clay by conducting small-scale laboratory experiments.

Determining soil parameters required for the Barcelona Basic Model (BBM) numerical modeling.

The findings of this study will provide clear insights into how the swelling phenomena of soil affect the performance of pile foundations in expansive clay soils.

The graphical abstract of the research is presented in Appendix F.

1.2. Expansive Soil

Expansive soils have significant volume changes depending on their moisture content and are mostly found in arid and semi-arid regions. Increasing the moisture content causes a volumetric increase, which is known as swelling, and decreasing the moisture content causes a volumetric decrease, which is known as shrinkage. This volumetric change can cause serious damage to overlaying structures.

1.3. Active Zone Depth

The zone of the soil where moisture content variation can occur due to climatic changes contributes to the swelling-shrinking action. This zone is called the active zone.

TMI was found as -22.4 and the site is considered a semiarid climatic type according to Table 2.1. Depth of soil suction change was found to be less than 3m according to Table 2.3. Ergular and Ulusay (2001) performed a comprehensive study on Ankara expansive clay to determine the swelling parameters of 20 soil samples collected from different locations. The authors determined the active zone depth based on water content variations and suggest that it can be taken as 2 meters in Ankara.

Figure 1.1 shows a pile foundation in the expansive clay and the forces acting on it. Chen (1975) recommended the use of Equations 1.1 and 1.2 for the safe design of piles in expansive soil.

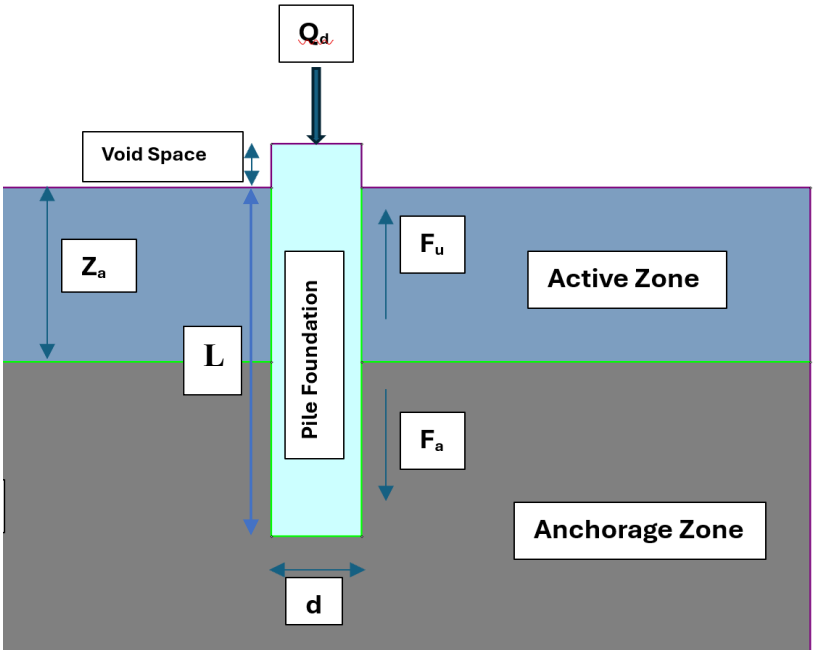

Figure 1.1. Forces acting on the pile in expansive soil (Modified from Chen, 1975)

$$F_u = \Pi \; d \; Z_a \; \beta \; P_s \qquad \textit{(Eq. 1.1)}$$

Where;

F_u : Uplift force

Z_a : Active zone depth

β : Uplift factor

P_s : Swelling pressure

$$W = \Pi\ d\ \alpha\ c_u(L - Z_a) + Q_d \qquad \textit{(Eq. 1.2)}$$

Where;

W : The withholding force

Q_d :Load acting on pile

L : The length of the pile

Solar panels, electricity poles and some structures are significantly affected by the volume change of expansive soils due to their lightweight. The use of pile foundations is a very common method for such structures. Figure 1.2 shows a typical pile foundation design under lightweight structures. The air space or sand gravel fills are used to prevent the volumetric increase in the active zone from affecting the structure, while the extended pile length is used to carry the structure by the stable ground in the anchorage zone and to balance the uplift forces acting on the pile from the active zone.

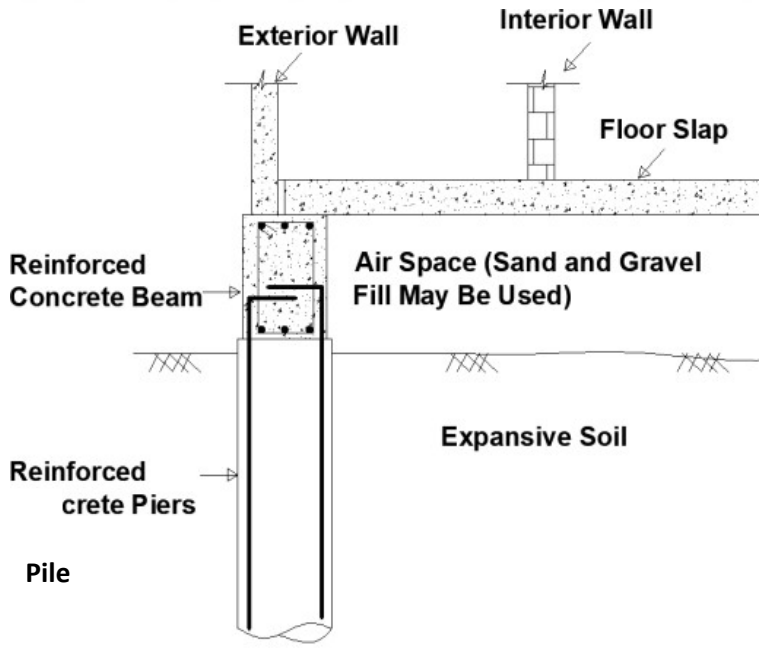

Figure 1.2. A typical pile foundation design under lightweight structures (Nelson and Miller, 1997; Alnmr et al., 2023)

The main purpose of the pile foundations analysis and design is to determine the safe diameter and length (US Army, 1998). Considering the equations above, it is necessary for the safe pile design to determine the adhesion factor α, bearing capacity factor N_c, uplift factor β_u, and active zone depth Z_a parameters to find the uplift and withholding forces acting on the pile (Chen, 1975).

1.4. Development of the Design Parameters

The design parameters developed in this study were based on laboratory and field tests carried out on expansive clays from Ankara, Türkiye. The volume change characteristics and shear strength of partially saturated expansive soils are known to be very sensitive to changes in moisture content and matric suction; therefore, for safe design, the effects of wetting of the tested soils on these parameters were considered.

The tests performed for the development of the design parameters under consideration were grouped into shear and interface shear strength tests, model tests, and numerical analysis. The shear tests included direct shear in the shear box apparatus and triaxial compression tests. Interface shear strength tests were performed in the shear box apparatus and were intended to determine the adhesion between soil and concrete and the effects of wetting on adhesion. The model tests were intended to determine the uplift factor and study the effects of wetting on the skin frictional resistance of small model piles. The Barcelona Basic Model is used for numerical analysis.

CHAPTER 2

LITERATURE REVIEW

2.1. Clay Mineralogy

The term “clay” can be used to refer to soil size and the type of mineral. The clay size generally refers to all particles in soil that are smaller than 0.002 mm. The term “clay mineralogy” refers to a special type of soil mineral that varies from other types of soil. The main characteristics that distinguish clay minerals from other soil types, rather than the particle size, are a negative electrical surcharge, plasticity, high resistance to weathering, and particle shapes. Although clay size refers to a particle that is finer than 0.002 mm, not all clay minerals are finer, and not all nonclay materials are coarser than 0.002 mm. Therefore, using two different terms, clay size and clay mineralogy, to describe the clay might be quite beneficial to avoid confusion (Mitchell and Soga, 2005).

Clays and clay mineralogy have been studied over the centuries due to their abundance on the earth and widespread usage in both geotechnical and agricultural industries. Behaviors and the properties of the clays are highly variable. Even in the same area and climate zone, clays might behave differently (Grim, R. E.,1962). Therefore, studying the natural soil and predicting its behavior might be quite challenging. The amount of clay in the soil has a great influence on soil behavior, as well as the mineralogical structure of the clay. A natural soil deposit can contain many different types of elements, but the most abundant ones are oxygen, silicon, hydrogen, and aluminum. In addition to these elements, calcium, sodium, potassium, magnesium, and carbon make up 99 percent of the Earth's crust. Different organizations of atoms in these most abundant elements can create the minerals in the soil. Although the amount of nonclay materials on the earth is

higher than the clay, the most influential materials that affect the behavior of the soils are clays and organic materials (Mitchell and Soga, 2005).

Clay mineral structure consists of a silica sheet, an octahedral sheet, water molecules, and ions. The variety of combinations of each component forms a different type of clay mineral. The different orientations of these components and the resulting some of the well-known clay minerals are sketched by (Mitchell and Soga, 2005) as shown in Figure 2.1. Silicon tetrahedron consists of 1 silica and 4 oxygens. Silica tetrahedra combine by sharing 3 of their oxygens with another silica tetrahedra and form silicate sheets. Similarly, a combination of aluminum or magnesium octahedral forms an octahedral sheet. The octahedral sheet is called Gibbsite (G) if the cations are mainly aluminum, and the octahedral sheet is called Brucite (B) if the cations are mainly magnesium. The terms 1:1 and 2:1 semibasic units refer to the combination of one silicate sheet to one octahedral sheet and two silicate sheets to one octahedral sheet, respectively. Kaolinite, smectite (montmorillonite), and illite are the most well-known main clay minerals (Verruijt, 2001).

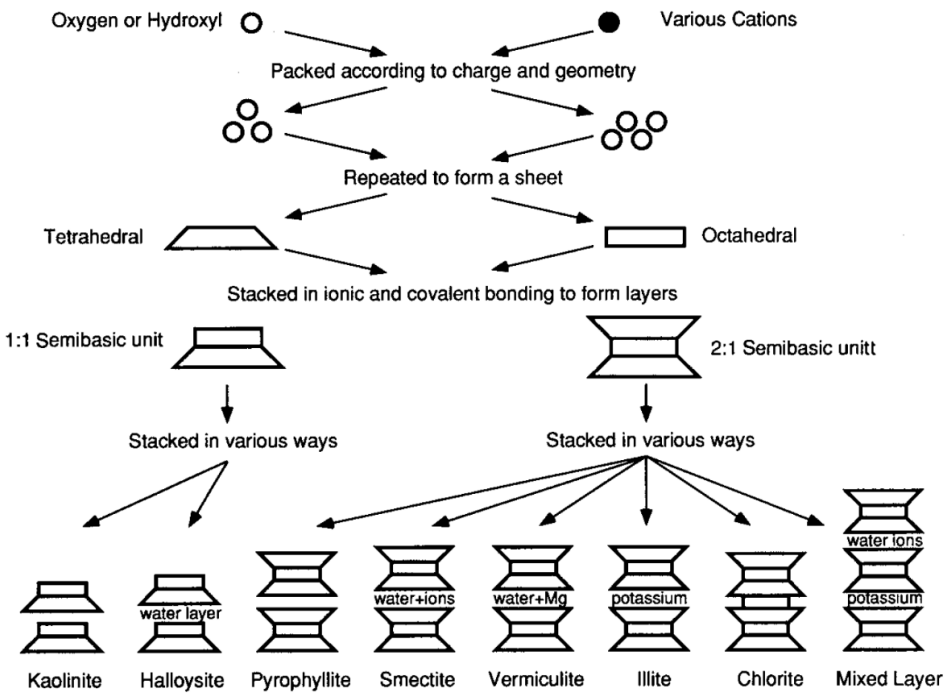

Figure 2.1. Components of a variety of clay minerals (Mitchell and Soga, 2005)

2.1.1. Kaolinite

Kaolinite consists of a 1:1 semistructural unit as shown in schematic diagrams in Figure 2.1. It has a very strong interlayer bonding between the silica and the octahedral sheet (Grim 1959). On the other hand, the bonds between the two semi-units are generally weak hydrogen bonds. Those weak hydrogen bonds are still capable of keeping several semi-units together (Nelson et al., 2015).

The thickness of nonhydrated kaolinite is about 7.2 angstroms. When it gets hydrated, the thickness might increase to 10.1 angstroms, and the difference of 2.9 angstroms shows the thickness of the water layer between the semiunits. The activity of kaolinite might differ between 0.33 and 0.46 (Skempton, 1953). The Cation exchange capacity (CEC) of kaolinite is generally between 1 to 6 meq/100 g. The Specific surface area is between 5 to 55 m^2/g according to (Mitchell and Soga, 2005), and 10 to 15 m^2/kg according to (Baker et al, 2017).

2.1.2. Illite

Illite is a mica-like clay mineral, and it is the most common type of clay mineral encountered in geotechnical engineering (Mitchell and Soga, 2005). The structure of illite consists of a 2:1 semistructural unit with two silica and one octahedral sheet, as shown in Figure 2.1. There are mostly potassium (K) cations between the adjacent units. The potassium cations form a strong bond to connect sheets. Illite is the only clay minerals that have potassium in its structure (Nelson et al., 2015). Therefore, determining potassium in clay is a very simple and quick identification of illite existence (Chittoori and Puppala 2011).

The thickness of illite structural units is around 10 Ångström. The activity of illite is typically 0.9 (Skempton, 1953). The Cation exchange capacity of illite is generally between 15 to 50 meq/100 g. The Specific surface area is between 80 to 120 m2/g according to (Mitchell and Soga, 2005).

2.1.3. Montmorillonite

Montmorillonite consists of a 2:1 semistructural unit as shown in schematic diagrams in Figure 2.1. The connections of the two adjacent units are provided with very weak van der Waals bonds. Therefore, these very weak bonds are easily breakable and only capable of connecting one or two units (Nelson et al., 2015).

The thickness of montmorillonite structural units is 9.6 angstrom or higher, depending on the type of cations it contains. The typical activity of montmorillonite is typically 1.5 and 7.2 for calcium and sodium montmorillonite (Skempton, 1953). The Cation exchange capacity of montmorillonites is generally between 80 to 150 meq/100 g. The Specific surface area is between 600 to 800 m^2/g according to (Mitchell and Soga, 2005).

2.2. Expansive Soil

Expansive soils have significant volume changes depending on their moisture content and are mostly found in arid and semi-arid regions. Increasing the moisture content causes a volumetric increase, which is known as swelling, and decreasing the moisture content causes a volumetric decrease, which is known as a shrinkage phenomenon. This volumetric change behavior can cause serious damage to overlaying structures (Al-Mukhtar, Lasledj, & Alcover, 2010; Al-Rawas, Hago, & Al-Sarmi, 2005; Basma & Tuncer, 1991; Cokca, 2001; Rao, Rahardjo, & Fredlund, 1988; Rosenbalm & Zapata, 2017).

2.2.1. Global Distribution of the Expansive Soil

Nelson et al. (2015) stated that the swelling shrinkage behavior of the soils has been reported in 6 continents and 40 countries worldwide and shared the general expansive soil distribution in the United States as shown in Figure 2.2. The study states that expansive soils are not only limited to as shown in Figure 2.2, but there are also considerable amounts of expansive soils, which are quite severe, in other parts of North America.

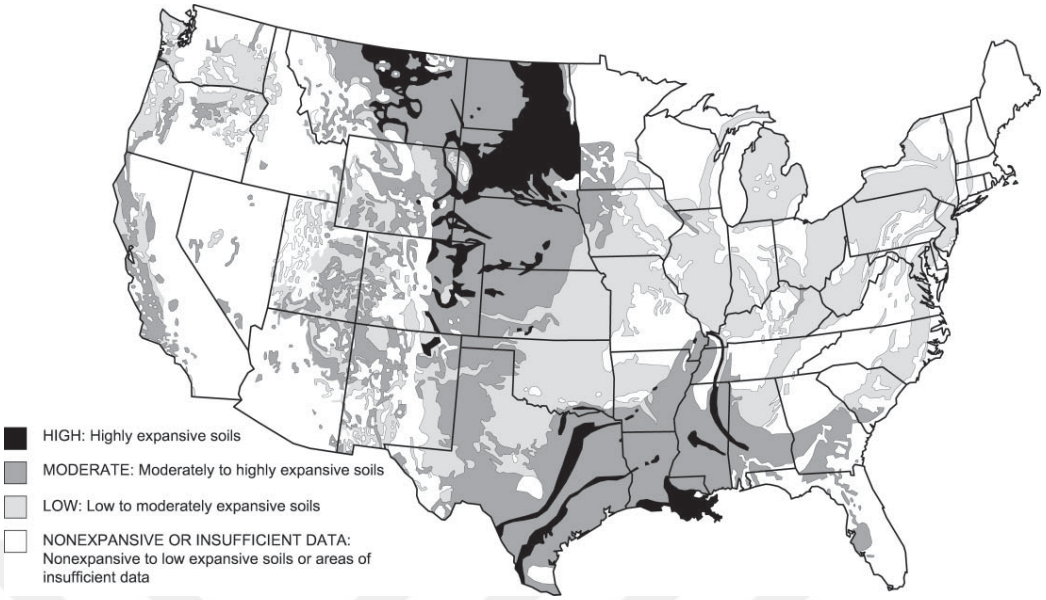

Figure 2.2. Distribution of Expansive Soils in the USA (Nelson et al, 2015)

Expansive behavior causes cracks in foundations, and damage on lightweight structures such as floors and basement walls. The annual average cost spent on expansive soil-related infrastructure damages is 9 billion dollars in the United States of America (Lyons & Ross, 2015).

Shi et al. (2002) state that expansive soil is a common problematic soil that is distributed all around the world. China is one of the countries that contains a high amount of expansive soil. 20 provinces and regions roughly about 600,000 km^2 areas are covered by expansive soils in China. The annual structural damage cost due to the swelling-shrinkage behavior of the expansive soil is more than 1 billion US dollars in China. Figure 2.3 shows the general expansive soil distribution in China taken from (Shi et al., 2002).

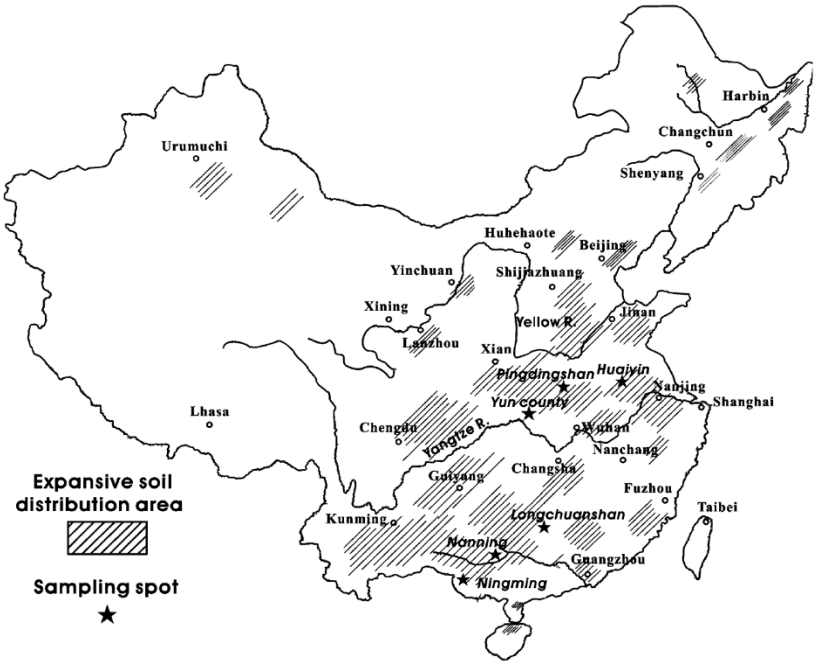

Figure 2.3. Distribution of Expansive Soils in China (Shi et al., 2002)

Verma and Maru state that 20 percent of India is covered by expansive soil. The most common regions that contain a high amount of expansive clays are the Deccan Plateau, Andhra Pradesh, Uttar Pradesh, Karnataka, Maharastra, and some parts of Gujarat. Black Cotton type of expansive soil is the most dominant soil in the Malwa region in India (Verma and Maru, 2013).

Australia is another country that faces many challenges due to the presence of expansive soils. Six of the eight capital cities in Australia are covered by expansive soils (Ahmed, Evans, & Imteaz, 2016). According to (Richards et al., 1983), 20 percent of Australia is covered by expansive soil as shown in Figure 2.4 and most of them are in the semi-arid climate zone. In the semi-arid zones, reddish brown clay with some amount of bentonite results in swelling shrinkage behavior and creates Australian gilgais, which is an Australian word that means small waterholes (Wagner, 2002).

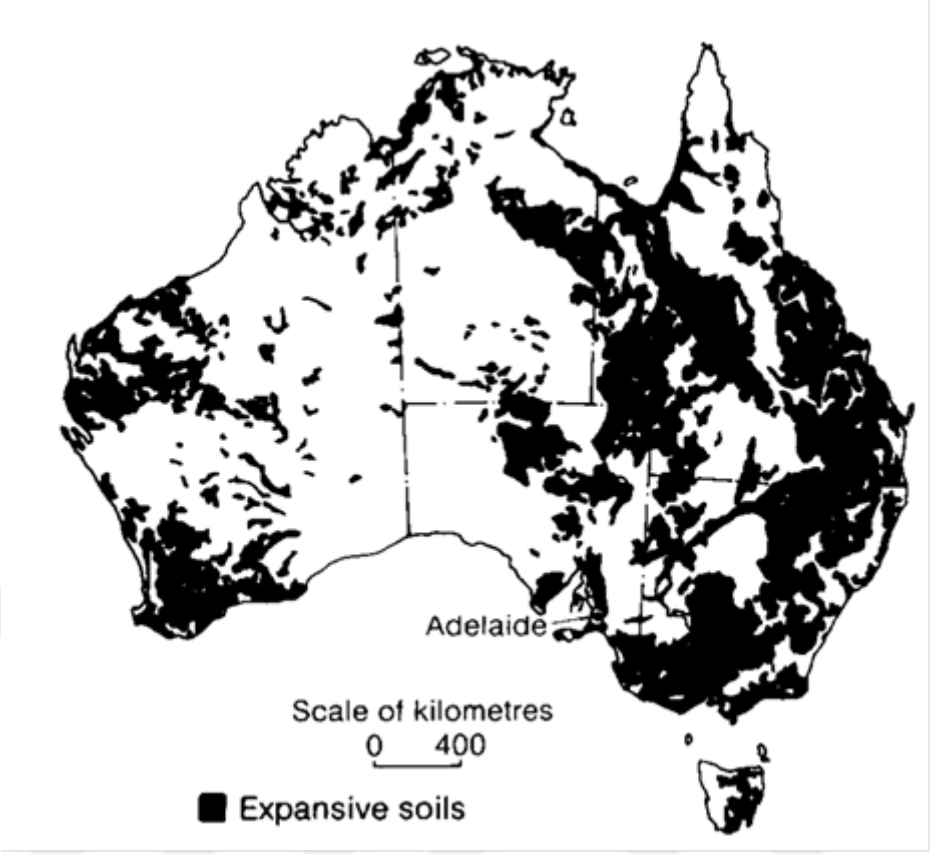

Figure 2.4. Distribution of Expansive Soils in Australia (Richards et al., 1983)

2.2.2. Expansive Soils in Türkiye

Çokça (1991) worked on determining the swelling characteristics of Ankara clay. He worked on a variety of clays in the Ankara region and developed a new classification method using the methylene blue test and clay content to predict swelling potential.

Çokça (2001) studied the stabilization of expansive soil with a variety of fly ashes from Soma and Tuncbilek thermal power plants in Türkiye with a variety of curing times. He found that adding fly ashes reduced the swelling potential up to 68 percent when Tuncbilek Fly ash was used. (Ünver, Lav, & Çokça, 2021) studied Ankara expansive clay from the Akyurt-Ankara. They aimed to reduce the swelling potential of high plastic Ankara expansive clay and increase the strength of the soil. They reported that adding lime for the stabilization of expansive clay is a more effective approach than adding fly ash for stabilization.

Nalbantoglu and Gucbilmez (2001) worked on expansive clay in Cyprus and stated that adding 15 percent Soma fly ash and 3 percent lime reduced the swelling potential of Cyprus expansive clay to almost zero. They indicate that after adding fly ash and lime, the structure of the expansive clay becomes silt-sand-like structures. Nalbantoglu and Tawfiq (2006) studied the stabilization of Northern Cyprus expansive clay by adding olive cake residue. 3 percent of olive cake residue was found to be efficient in decreasing swelling pressure and increasing the strength of the soil significantly. Therefore, they highlighted that olive cake residue can be used as a good environmentally friendly alternative to be used for the stabilization of expansive soils.

Yilmaz and Karacan (2002) determine both the geotechnical parameters and the mineralogy of expansive clays in the Erbaa Basin by performing both field and laboratory tests. Comparing the swelling potential of expansive soils, they indicate that overconsolidated soils with higher strength contain less potential to cause damage, regardless of their high swelling potential.

Ergüler and Ulusay (2003) studied expansive clay taken from 20 different locations in Ankara and identified the factors that affect swelling behavior. When water contents increased to 30 percent or higher, they observed a significant decrease in swelling potential. They reported that active zone depth is between 1 to 2 meters in Ankara. They also showed that anisotropy is one of the critical factors that has a significant impact on swelling behavior. Comparing the vertical and horizontal swelling, they found that horizontal swelling is much higher than vertical swelling. This is especially very critical for retaining walls and lateral swelling might cause significant damage to drainage systems (Ozer, Ulusay, & Isik, 2011).

Mollamahmutoğlu, Yılmaz, and Güngör (2005) worked on the stabilization of expansive clay with fly ash in Bursa, Türkiye. They stated that adding 35 percent of fly ash can stabilize the Bursa expansive clay (a liquid limit of around 80 percent) and reduce the swelling pressure to a tolerable level to use in highway construction.

Kalkan and Bayraktutan (2007) show the existence of expansive clay in Oltu-Narman in Erzurum. According to their study, swelling potential and pressure of the clay in that region vary between 3.1 - 6.0 percent and 181 - 267 kPa, respectively. The plasticity index of the clay was reported as between 22 and 42 percent.

Oncu and Bilsel (2018) investigated the stabilization of expansive clay in Cyprus, adding waste marble powder and marble dust. Based on the laboratory tests, the researchers showed that the addition of 10 percent marble powder or 5 percent marble dust results significant reduction in swelling potential and a significant increase in compressive strength. Using waste material as a stabilization agent is both an environmentally friendly solution and a good alternative to other stabilization agents.

Deliktaş and Çokça (2020) worked on several Ankara expansive clays from Bilkent University Campus, Middle East Technical University Campus, and Ege Plaza in Ankara and investigated the relationship between the swelling capacity of the Ankara expansive clay and its undrained strength. The study showed that the shear strength of the Ankara Clay was reduced by 70 percent when the clay had 10 percent of swelling and reduced by 90 percent when 100 percent of swelling occurred.

Özdemir, Kalkan and Turhan (2024) determine the properties of Ankara clay in Ayas region. They stated that the swelling potential of the clay varies with depth. In Ayas-clay, swelling potential varies between 3.9 percent to 6.9 percent, and the max swelling pressure they determined was 37.5 kPa.

Türkiye is one of the countries that has expansive clays in a variety of regions. This has been demonstrated above by numerous studies carried out in different regions in Türkiye. Ankara is located in a semi-arid climate zone where expansive soil behavior is an important concern. As can be seen from the above studies, the identification, behavioral determination, and stabilization of the Ankara expansive clay is an important research topic and continues to be important at present.

2.3. Identification and Classification of Expansive Clays

The behavior of the expansive clay depends on many factors. Mitchell and Soga (2005) group these factors into two groups: environmental and compositional factors. Compositional factors are the type of minerals, adsorbed cations, and the amount in the soil, pore water distribution in the soil, grain size distribution, and the shapes of the particles. Environmental factors are confining pressure, temperature, soil fabric, water content, density, and the availability of water.

Both compositional and environmental factors can have a significant impact on the behavior of the soil. Therefore, both site investigations and laboratory tests can be essential to define the soil and determine its engineering properties.

2.3.1. Signs for the Existence of Expansive Soil on the Field

Chen (2012) suggests that geotechnical engineers gather as much information as possible for the site before starting work on a soil investigation. Topography, surficial geology, existing structures, drilling and sampling, and performing in-situ tests such as standard penetration tests can help geotechnical engineers to have a comprehensive idea about the soil. Therefore, it would be unwise for engineers to skip site investigation to avoid some extra cost for a project.

One of the main signs of the existence of expansive soil is crack patterns in the soil and cracks in the structures. These damages highly increase the amount of project costs. Even minor cracks in the properties might be an early sign of bigger damage (Radevsky, 2001).

Lightweight structures are much more likely to be affected by expansive behavior because they cannot apply enough pressure to prevent upward movement. Therefore, observation of differential movements between the houses and the sidewalks would be a sign of the presence of expansive soil.

Expansive soil shows a volumetric increase when there is available water to absorb. Therefore, a local volumetric increase adjacent to local water sources is a sign of expansive soil presence (Wise and Hudson, 1971).

2.3.2. Climate

The swelling and shrinkage action in the soil is related to the amount of water in the soil. The moisture content increments or decreases cause the behavioral change in the soil. The availability of water and the potential change in the moisture content are directly related to climate. Therefore, the climate has a significant influence on the behavior of the expansive clays (Karunarathne, 2016).

Thornthwaite (1948) used climate factors of temperature and rainfall to determine average potential evapotranspiration (PE). When the average PE is more than the monthly rainfall, the condition is defined as a water deficit. In contrast, if monthly rainfall is higher than the average potential evapotranspiration (PE), the excess water is stored up to the maximum capacity of 100 mm in the soil. When the amount of excess water exceeds the maximum capacity of storage, the condition is defined as a water surplus. Thornthwaite suggested calculating the Thornthwaite Moisture Index (TMI) parameter using monthly water surplus-deficit and potential evapotranspiration data that may occur in the region to identify different climate types.

Table 2.1. Thorntwaite Moisture Index for the Different Climate Types (Thornthwaite, 1948; Ikizler, 2018)

Climate Type	Thornthwaite Moisture Index (TMI)
(A) Perhumid	>100
(B_4) Humid	80 to 100
(B_3) Humid	60 to 80
(B_2) Humid	40 to 60
(B_1) Humid	20 to 40
(C_2) Moist Subhumid	0 to 20
(C_1) Dry Subhumid	-20 to 0
(D) Semiarid	-40 to -20
(E) Arid	-60 to -40

In Türkiye, there may be significant variations in the amount of precipitation and temperature averages from region to region. Therefore, the TMI value should be calculated separately for each region. Figure 2.5 shows the general distribution of TMI in Turkiye.

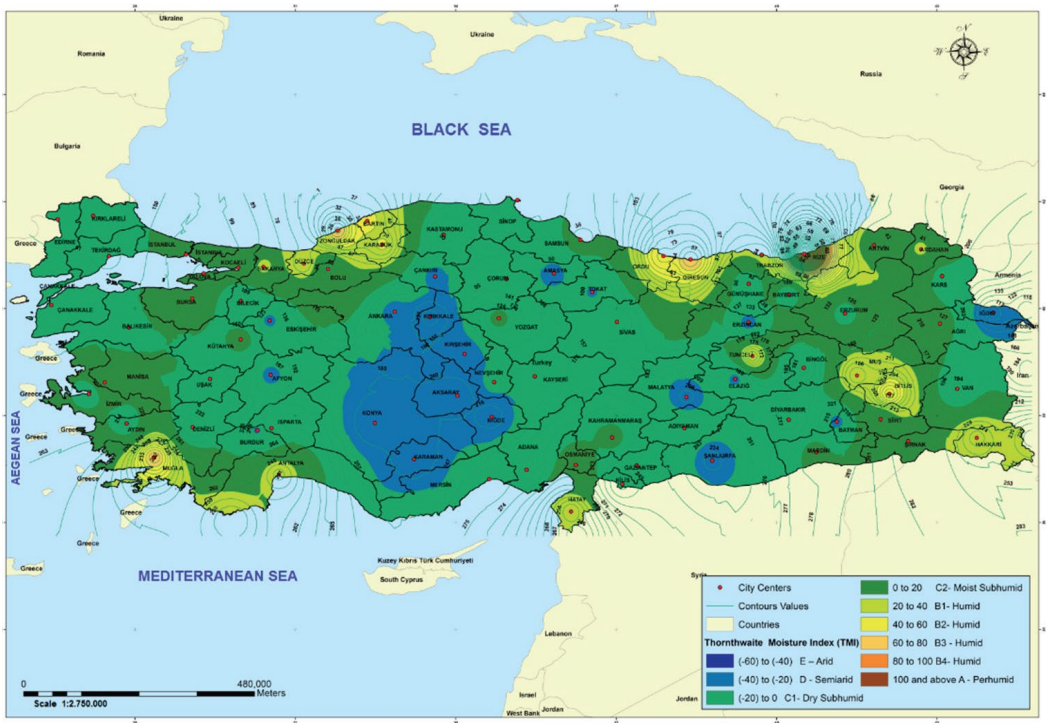

Figure 2.5. The general distribution of TMI in Türkiye (Ikizler, 2018)

2.3.3. Active Zone Depth

The zone of the soil where moisture content variation can occur due to climatic changes contributes to the swelling-shrinking action. This zone is called the active zone. The existing drainage or irrigation water can change the depth of the active zone (Nelson, 2015).

The active zone depth can vary from location to location in a site, and it can be determined by plotting the liquidity index and soil depth profile over different seasons. In the western part of the United States, the active zone depth can reach up to 15 meters. On the other hand, active zone depth varies between 1.5 to 3 meters in Houston, 2.1 to 4.6 meters in Dallas, 3 to 9 meters in San Antonio, and 3 meters in Denver (Das, 2011).

An Australian standard of AS2870 (2011) defines the Hs for the cities shown in Table 2.2. It is also indicated that TMI values can be used to determine the Hs using Table 2.3. It is noted that if the water table elevation is lower than the depth of the design soil suction change, Hs should be taken equal to the depth of the water table.

Table 2.2. Depth of Design Suction Change for Cities in Australia (Adopted from AS2870, 2011)

Cities in Australia	Depth of soil suction change (H_s) m
Adelaide	4.0
Albury/Wodonga	3.0
Brisbane/Ipswich	1.5 – 2.3
Gosford	1.5 – 1.8
Hobart	2.3 – 3.0
Hunter Valley	1.8 – 3.0
Launceston	2.3 – 3.0
Melbourne	1.8 – 2.3
Newcastle	1.5 – 1.8
Perth	1.8
Sydney	1.5 – 1.8
Toowoomba	1.8 – 2.3

Table 2.3. Relationship between TMI and depth of soil suction (Adopted from AS2870, 2011)

TMI	Depth of soil suction change (H_s) m
>10	1.5
≥-5 to 10	1.8
≥-15 to ≤-5	2.3
≥-25 to ≤-15	3.0
≥-40 to ≤-25	4.0
≤-40	>4.0

Lucian, 2011 stated that volumetric increase due to water content change over seasons occurs only in the active zone. The author measured the water content over depth in a variety of locations in September and April which are the driest and wettest months in Tanzania to determine active zone depth as shown in Figure 2.6. He found that active zone depth in Tanzania is between 1.5 meters and 2 meters.

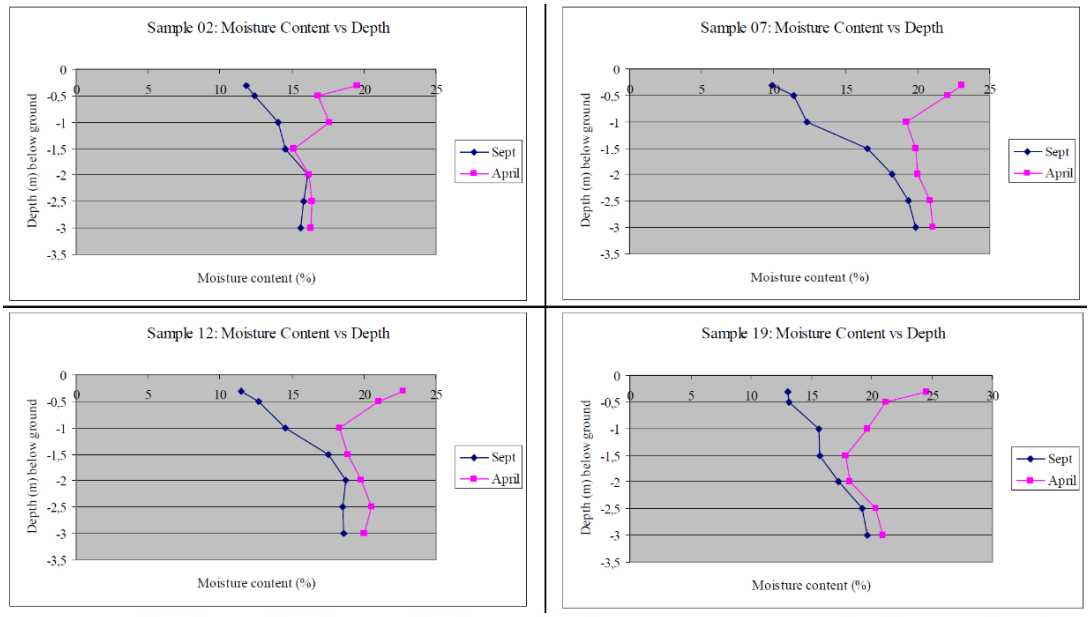

Figure 2.6. Water content variations in a variety of locations in Tanzania (Lucian, 2011)

Ergular and Ulusay, 2001 performed a comprehensive study on Ankara expansive clay to determine the swelling parameters of 20 soil samples collected from different locations. The authors determined the active zone depth based on water content variations and suggested that it can be taken 2 meters in Ankara.

2.3.4. Direct Tests for Determination of Swelling Parameters

Swelling parameters are swelling potential and swelling pressure. These parameters can either be directly measured with some specific tests in the soil laboratory tests or can be obtained using some empirical formulas or charts by the index parameters of the soil (Sapaz, 2004).

2.3.4.1. Swell Potential

Swelling potential defines an expansive soil's ability to increase volume when water is added (Holtz, Kovacs, & Sheahan, 1981). ASTM D5890-11 describes the free swell percentage as the ratio of volume change over the initial volume, as shown in Equations 2.1 and 2.2. ASTM D4546-14 suggests using an oedometer ring to prevent lateral movements, so volumetric increments can be defined as increments in height. Therefore, swelling potential can be simply determined as the height increment of the specimen over the initial height of the specimen.

$$\text{Free Swell Percentage} = \frac{\text{Vf} - \text{Vi}}{\text{Vi}} \times 100 \qquad (Eq.\ 2.1)$$

$$\text{Free Swell Percentage} = \frac{\text{Hf} - \text{Hi}}{\text{Vi}} \times 100 \qquad (Eq.\ 2.2)$$

Table 2.4. USBR Classification for expansive soils

Swelling Potential	Degree of Expansion
>25	Very high
5 - 25	High
1.5 - 5	Medium
0 – 1.5	Low

Table 2.5. Expansive soil classification (Adopted Sridharan and Prakash, 2000)

Swelling Potential from oedometer (%)	Clay Type	Degree of Expansion
<1	Non-swelling	Negligible
1 - 5	A mixture of swelling and non-swelling	Low
5 - 15	Swelling	Moderate
15 - 25	Swelling	High
>25	Swelling	Very high

The ASTM D-4829 suggests applying 7 kPa normal pressure to the specimen and soaking it in water. The ratio of the height increments to the initial height is described as the expansion index (EI). The soil can be classified by its expansion index according to Table 2.6 (Nelson, 2015).

$$EI = \frac{Final\ thickness - Initial\ thickness}{Initial\ thichness} \times 1{,}000 \qquad (Eq.\ 2.3)$$

Table 2.6. Classification of the soil based on the expansion index (Nelson, 2015)

Expansion Index (EI)	Expansion Potential
0 - 20	Very low
21 - 50	Low
51 - 90	Medium
91 - 130	High
>130	Very High

2.3.4.2. Swell Pressure

When expansive soils absorb water, they attempt to swell. If volume is prevented from expanding, the soil develops pressure, which is called swelling pressure. ASTM D4546-14 suggests three different methods to determine this stress. According to the first method, the soil can be allowed to swell freely and then apply stress to force it to return to its initial volume. The applied pressure can be defined as swelling pressure. The second method prevents soil from having volume increase by applying additional stress to the soil when it attempts to swell. This method is also known as the constant volume method. When there is no further volume increment attempt in the soil, the final applied pressure is defined as swell pressure. The last method is applying alternative loads to the specimen and measuring the swelling pressure for different swell pressures.

The amount of deformation caused by the swelling pressure depends on the type of structure to be overlaid. If the stress, caused by the overlying structure, is lower than the swell pressure, some level of damage to the upper structure may be observed. Pruška and Šedivý (2017) studied a different type of cracks that can occur on asphalt and concrete surfaces when different ranges of swelling pressure are applied as shown in Table 2.7.

Table 2.7. Swelling pressure effect on asphalt and concrete surface (Pruška and Šedivý, 2017)

Swelling Pressure (kPa)	Evaluation	Asphalt Surface	Concrete Surface
<30	Negligible	No deformation	Virtually impossible
30 - 60	Increased	Little noticeable deformation	First signs of cracks
60 - 100	High	Slight undulations	Clear visible cracks
>100	Very high	Significant undulations	Significant cracks

2.3.4.3. Modified Free Swell Test

The modified free swell test is the easiest and quickest test to determine the swelling potential of the soil. 10 grams of soil passes No: 40 sieve is required to perform the test. Then the soil samples should be divided into two portions and each portion should be placed in 100 ml cylinders. One of the cylinders should be filled with distilled water and the other with kerosene. After 24 hours of waiting the ratio of the difference in volume of soil in the distilled water and kerosene over the volume of the soil in the kerosene defines the free swell index (FSI). The test can be performed in both according to the standards ASTM D5890 for geosynthetic liners and IS 2720 for natural soils. FSI can be used for the classification of the soil.

$$FSI = \frac{Volume\ of\ soil\ in\ water - Volume\ of\ soil\ in\ kerosene}{Volume\ of\ soil\ in\ kerosene} \times 100 \qquad (Eq.\ 2.4)$$

Table 2.8. Classification of Expansive Soil using FSI (Bureau of Indian Standards 1987)

Degree of Expansion	Free Swell Index (FSI)
Low	< 50
Medium	50 - 100
High	100 - 200
Very High	>200

2.3.4.4. Lateral Swell Test

Water adsorption in an expansive clay causes a volumetric expansion. This expansion is not limited to vertical but also lateral movements. Although the vertical pressure is generally higher than the lateral pressure in the soil, depending on the geology and the stress history, vertical pressures might be balanced by the pressure that comes from the overlying soils. Therefore, the impact of the lateral swell pressure on the geotechnical structures might be critical to be considered (Ito and Azam, 2013).

Sapaz (2004) conducted a series of laboratory tests in the Middle East Technical University's soil laboratory using a thin wall oedometer technique to determine lateral swell pressure and a constant volume swell test for the vertical pressure. The study showed that the initial moisture content and the dry strength of the clay are important influencing factors in lateral and vertical swell pressure. The author reported that increments in the initial water content cause a decrease in both vertical and lateral swell pressure. A constant increment in the initial dry density causes an increment in both vertical and lateral swell pressure. The ratio of lateral to vertical swelling pressure was identified as the swelling pressure ratio, and the study found that it is between 0.59 and 0.86 according to a variety of tests

performed under different conditions, as shown in Figure 2.7. On the other hand, Ertekin (1991) indicates that in some cases swelling ratio can be higher than 1.0.

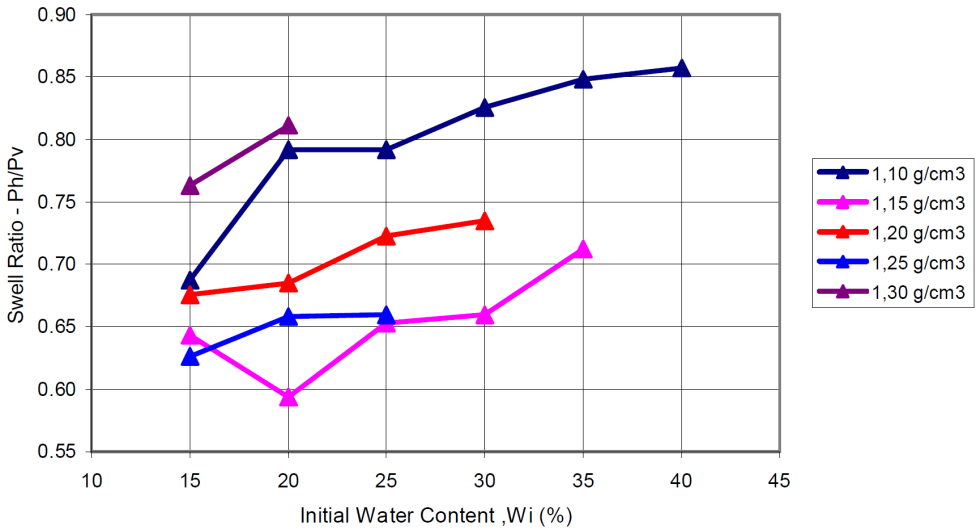

Figure 2.7. The relationship between swell ratio, initial water content, and dry density (Sapaz, 2004)

2.3.5. Laboratory Tests to Identify and Classify Expansive Soils and Determine Swell Parameters

2.3.5.1. Sieve and Hydrometer Tests

The soil consists of coarse materials such as sand and gravel and fine materials such as clay and silt. The sieve and hydrometer tests can be conducted to determine the grain size distribution for coarse and fine materials. The combination of them can provide geotechnical engineers amount of each material in the soil from clay to boulders. The procedures to perform these tests are explained in the ASTM standards of D6913 – 04, 2009, for the sieve test and D7928 – 17, 2017 for the hydrometer test (Germaine and Germaine, 2009).

One of the most critical influential factors of the expansive behavior of the soil is the clay content and it can be easily determined from the grain size distribution (Basma, Al-Homoud, & Husein, 1995). Also, the percentage of clay content can be used to calculate the activity of the clay, which is a useful parameter for the classification of the soil.

2.3.5.2. Specific Gravity Test

The specific gravity is the ratio of the mass of the soil to the mass of the water at 4 °C in the same volume. Determining the specific gravity is very important for geotechnical engineering because it is required to be known for almost all geotechnical tests. The procedure to perform the test is explained in the ASTM D854-06e1, 2006 (Germaine and Germaine, 2009).

Expansive soil data collected from 119 international case studies show that the specific gravity (Gs) of most expansive clays ranges between 2.5 and 2.9 (Jalal et al., 2021). Ergular and Ulusay (2001) state that the GS of Ankara soil can be changed between 2.52 and 2.66 based on 20 tested soil samples taken from different locations in Ankara.

2.3.5.3. Atterberg Limits Test

Atterberg limits tests are performed to determine the liquid limit (LL), plastic limit (PL), and Shrinkage limit (SL) for the soil. The liquid limit is the water content where the consistency of the soil changes from fluid-like behavior to a plastic behavior. The plastic limit is a water content where the consistency of the soil changes from plastic behavior to semi-solid behavior. Similarly, shrinkage limits are the boundary between semi-solid behavior to solid behavior. Most of the natural soils are determined between the boundaries of plastic limits and liquid limits. These limits were first developed by A. Atterberg (1911) for the classification of agricultural soils and then standardized by Casagrande, in 1932. Liquid and plastic limits are also used to determine the plasticity index (PI) as it is the difference between these two parameters as shown in Equation 2.5. High PI values indicate that the soil shows plastic behavior in a high range of water contents. Using the parameters PI and clay percentage in the clay, Skempton (1953) determined a term activity as shown in Equation 2.6 (Germaine and Germaine, 2009). Table 2.9 classifies the clay into three groups based on their activity and Table 2.10 shows the typical activity values for some clay minerals.

The detailed description of conducting Atterberg limits tests is explained in the ASTM standards of D4318, 2017, and D4943, 2018.

Atterberg limits, plasticity index, and the activity of the soil are related to clay mineralogy and the clay fraction in the soil, similar to the swelling characteristics of the soil. Therefore, many researchers used these parameters to predict the degree of expansions. Table 2.11 summarizes the previous studies that correlate liquid limit, plasticity index, and the clay content of the soil to the degree of expansion. Figure 2.8 shows the location of montmorrilite, illite and kaolinite on the plasticity chart. The figure indicates that clay minerals with higher plasticity index tend to have higher expansion.

$$PI = LL - PL \qquad (Eq.\ 2.5)$$

$$Activity = \frac{PI}{Clay\ Content\ (\%)} \qquad (Eq.\ 2.6)$$

Table 2.9. Skempton, 1953 Classification of Clay based on activity

Activity	Soil Classification
<0.75	Inactive
0.75-1.25	Normal
>1.25	Active

Table 2.10. Skempton, 1953 Activity values for typical clay minerals (Nelson, 2015)

Activity	Mineral
0.33-0.46	Kaolinite
0.9	Illite
1.5	Ca Montmorillonite
7.2	Na Montmorillonite

Table 2.11. Previous studies to classify expansive soils using Atterberg limits and clay content

Resources	SL	LL	PI	Clay content (%)	Swelling Potential (%)	Degre of Expansion
Altmeyer,1955	<12					Noncritical
	10-12					Marginal
	>10					Critical
Holtz and Gibb, 1956	>15		<18	<15	<10	Low
	10-16		15-28	13-23	10-30	Medium
	7-12		25-41	13-20	20-30	High
	<11		>35	>28	>30	Very High
Terzaghi and Peck,			<15			Low
1967			10-35			Medium
			20-55			High
			>55			Very High
Raman, 1967	<15		<12			Low
	15-30		12-23			Medium
	30-40		23-32			High
	>40		>32			Very High
Sowers and Sowers,	>12		<15			Low
1970	10-12		15-30			Moderate
	<10		>30			High
Peck et al., 1974			<15			Low
			10-35			Medium
			20-35			High
			>35			Very High
Snethen et al., 1977		>60	>35		>1.5	High
		50-60	25-35		0.5-1.5	Moderate
		<50	<25		<0.5	Low
USAEWES		<50			<0.5	Low
Classification (O'Neil		50-60			0.5-1.5	Marginal
and Poorymoayed,		>60			>1.5	High
1980)						
Pitts, 1984; Kalantari,		<50	<25			Low
1991		50-60	25-35			Marginal
		>60	>35			High

Table 2.11. (continued)

Chen, 1988	>60		>95	>10	Very High
	40-60		60-95	3-10	High
	30-40		30-60	1-5	Medium
	<30		<30	<1	Low
Bowels,1988		<15			Low
		10-35			Medium
		20-55			High
		>35			Very High
Kay, 1990	<20				Low
	20-40				Moderate
	40-70				High
	>70				Very High

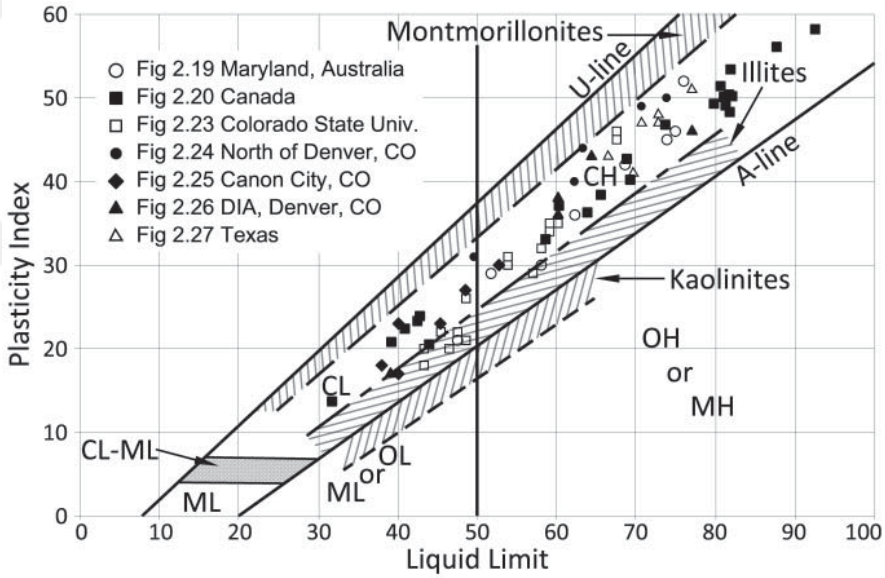

Figure 2.8. Location of Kaolinites Illites and Montmorillonites on the Plasticity Chart (Holtz, Kovacs, and Sheahan 2011, Nelson 2015)

Seed, H. B., Woodward, R. J., and Lundgren, R. (1962) showed that the degree of expansiveness is related to the clay content and activity, and it can be classified into 4 groups: low, medium, high, and very high as shown in Figure 2.9. On the other hand, Figure 2.10 shows that different researchers found different relationships between plasticity index and swelling potential. Therefore, although it is obvious that the plasticity of the soil is related to swelling potential, swelling

potential calculated by this graph can show different amounts of swell. Conducting relevant laboratory tests to determine each parameter of the plasticity index and swelling pressure might be necessary if exact values are needed.

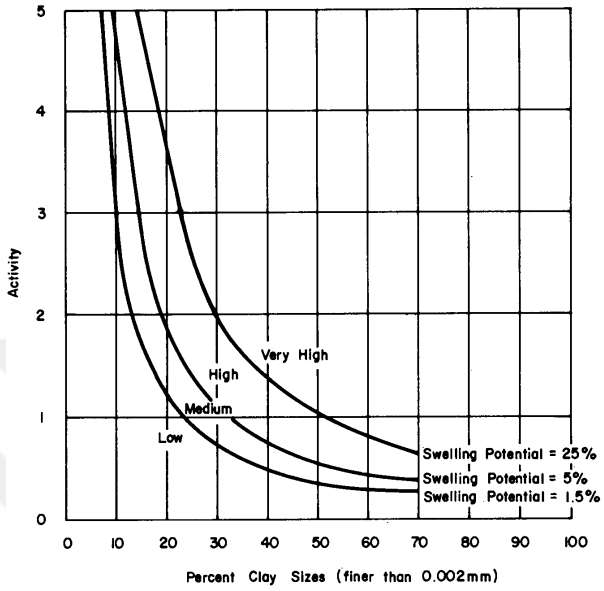

Figure 2.9. Classification of Expansive soils based on clay contents and activities (Seed, Woodward and Lundgren, 1962; Chen, 1975)

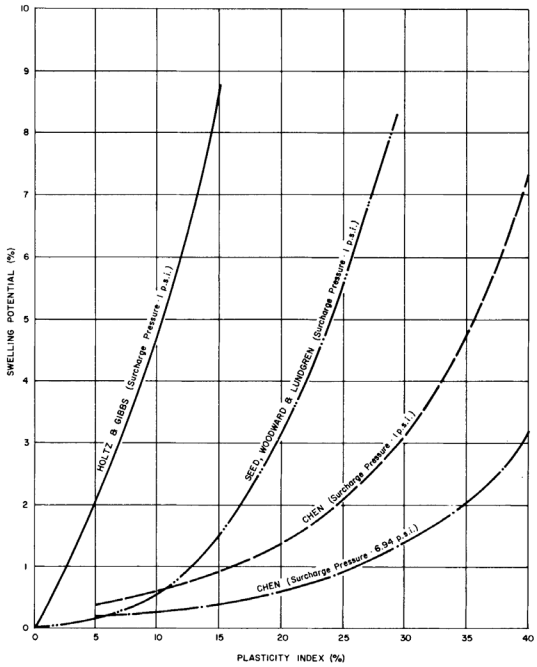

Figure 2.10. Relationship between plasticity index and swelling potential (Chen, 1975)

In addition to previous charts and tables to classify expansive soils, many resources found an empirical relationship between swelling pressure and index parameters. Hergul (2012) collected past empirical predictions of swelling pressure as shown in Table 2.12.

Table 2.12. Empirical Predictions for Expansive Soils (Hergul, 2012)

Researchers	Relationships Based on	Proposed Empirical Equation
Seed et al., 1962(b)	Activity (A) and Clay Content (C)	$S_p = 3.6x10^{-5}(A^{2.44})(C^{3.44})$
	Plasticity Index (PI)	$S_p = 3.6x10^{-5}(M)(PI^{2.44})$ where M=60 for natural and M=100 for artificial soils
Van der Merve, 1964	Correction Factor (F), Thickness of Non-Expansive Layer (D), Thickness of Expansive Layer (H)	$\Delta H = F \times e^{-0.377D} \times (e^{-0.377H} - 1)$
Komornik and David, 1969	Liquid Limit (LL), Initial Water Content (wo) and Dry Unit Weight (gd) (gd in kg/m3)	$\text{Log } P_s = -2.132 + 0.0208LL + 0.000665\gamma_d - 0.0269\, w_0$
Nayak and Christensen, 1971	Plasticity Index (PI), Initial Water Content (w_o) and Clay Content (C)	$S_p = (0.00229PI)(1.45C)/w_0 + 6.38$
		$P_s = (3.58x10^{-2})\, PI^{1.12}\, C^2/w_0^2 + 3.79$ (P_s in psi)
Vijayvergia anf Ghazzaly, 1973	Liquid Limit (LL), Initial Water Content (w_o) and Dry Unit Weight (γ_d) (γ_d in lb/ft^3)	$\text{Log } S_p = (0.44LL - w_o + 5.5) / 12$
		$\text{Log } S_p = 0.0526\, \gamma_d + 0.033LL - 6.8$
Schnider et al., 1974	Plasticity Index (PI) and Initial Water Content (w_o)	$\text{Log } S_p = 0.9(PI/w_0) - 1.19$
Johnson and Snethen, 1978	Thickness of Expansive Layer (H), Plasticity Index (PI), Initial Water Content (w_o)	$S_p = 23.82 + 0.7346PI - 0.1458H - 1.7w_0 + 0.00225PIw_0 - 0.0088PI\,H$
		$S_p = -9.18 + 1.5546PI + 0.08424H + 0.1w_0 - 0.0432\, PI\, w_0 - 0.0215\, PIH$
Weston, 1980	Weighted Liquid Limit (LL_w), Surcharge Load (σ_v), Initial Water Content (w_0)	$S_p = 0.00411(LL_w)^{4.17}\, \sigma_v^{-3.86}\, w_0^{-2.33}$
Chen, 1988	Plasticity Index (PI)	$S_p = 0.2558e^{0.383(PI)}$
TxDOT, 1999	Plasticity Index (PI)	Sp = 0.217(PI)-2.9 (For Optimum Conditions) S_p = 0.294(PI)-2.9 (For Average Conditions with PI<60))
Thomas et al., 2000	Clay Content (C), Cation Exchange Capacity (CEC), Liquid Limit (LL), Swell Index (C_s)	Unified Expansive Soil Index (ESI) Estimation
Ergüler and Ulusay, 2003	Liquid Limit (LL), Methylene Blue Value (MBV), Clay Content (C), Plastic Limit (PL), Plasticity Index (PI), Water Content at 24 h (w_{max24}), Water Content at 72 h ($wmax_{72}$), Percent of Smectite (S_m)	S_p and P_s Values Estimated from Various Equations
Kariuki and van der Meer, 2004	Activity (A), Cation Exchange Activity (CEA), Saturated Standard Mositure (SSP), Linear Extensibility Percentage (LEP)	Unified Expansive Soil Index (ESI) Estimation
Avşar, Ulusay and Ergüler, 2005	Liquid Limit (LL), Methylene Blue Value (MBV), Clay Content (C), Plasticity Index (PI)	S_p and P_s Values Estimated from Various Equations
Yılmaz, 2009	Liquidity Index (LI)	$S_p = 2.0981e^{(-1.7196LI)}$
Yılmaz and Kaynar, 2011	Liquid Limit, Cation Exchange Capacity (CEC), Activity (A)	$S_p = 9.223x10^{-2}LL + 2.041x10^{-2}A + 5.535x10^{-2}CEC - 0.153$

2.3.5.4. Compaction Test

The main purpose of the compaction test is to determine the compaction characteristics of the maximum dry density and the optimum water content of the soil. The test aims to provide a curve that demonstrates the dry densities for different water content values when standard energy is implemented a soil for compaction. The ASTM D698 standard named standard effort test, specifies that energy is 600 kN-m/m3. Other methods can be used to perform compaction tests as modified effort (2700 kN-m/m^3) or the Harvard compaction tests. The procedures of modified effort compaction tests are explained in detail in ASTM D1557. This method uses larger types of equipment that enable geotechnical engineers to use larger soil particles and better simulate the field condition (Germaine and Germaine, 2009). Similarly, the Harvard compaction test uses smaller apparatuses and is used for fine soils (Wilson, 1970).

Figure 2.11 demonstrates an example compaction curve. The black square points represent the dry density for each corresponding water content. The best-fit line that connects all data points is named the compaction curve. The peak point on the compaction curve corresponds to the optimum water content on the x-axis and the maximum dry density on the y-axis. The part of the curve with higher water content than the optimum water content is defined as wet of optimum and reversely the part of the curve with less water content than the optimum water content is defined as dry of optimum. A sequence of degree of saturation (S) curves can be drawn on the graph to determine the corresponding degree of saturation for each data point (Germaine and Germaine, 2009).

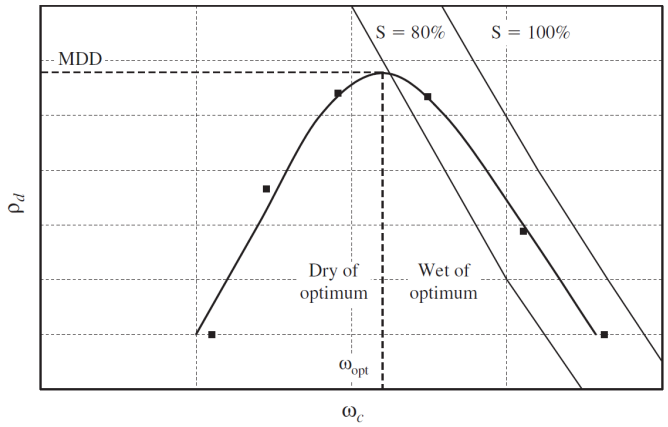

Figure 2.11. Compaction Curve (Germaine and Germaine, 2009)

The type of soil has a great influence on the compaction curve as shown in Figure 2.12. Soil with a high amount of coarse material generally tends to have high dry density and low optimum water content. Oppositely, soil with high amounts of fine material like silts and clay tends to have low dry density and high water content. Typical values for maximum dry densities and corresponding optimum water contents are shown in Table 2.13.

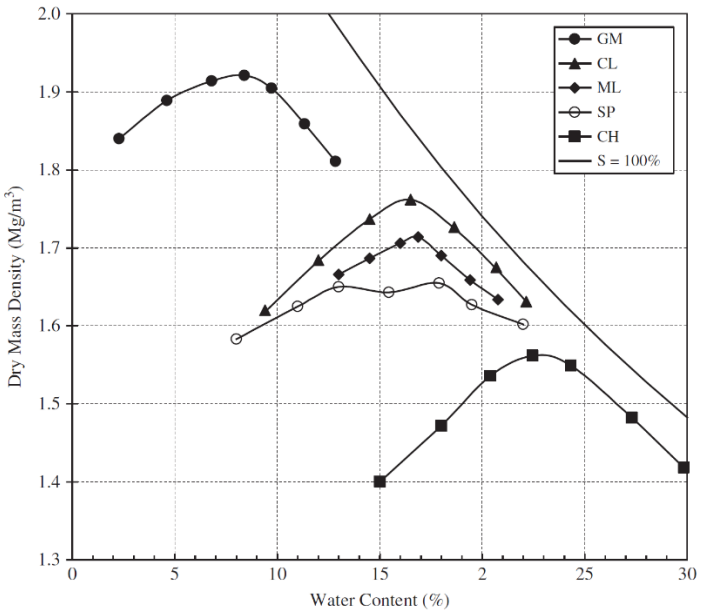

Figure 2.12. Compaction Curves for different soil textures (Germaine and Germaine, 2009)

Table 2.13. Typical values of maximum dry densities and corresponding optimum water contents (Germaine and Germaine, 2009)

Soil	ρ_{max} (Mg/m^3)	ω_{opt} (%)	Method
Maine Clay*	1.80	17.7	Harvard Miniature
Vicksburg Buckshot Clay**	1.56	22.8	D698
Annapolis Clay**	1.75	16.6	D698
Vicksburg Silt**	1.70	17.1	D698
Well-graded clean gravels, gravel-sand mixtures***	2.0 to 2.2	8 to 11	D698
Poorly graded clean gravels, gravel-sand mix***	1.8 to 2.0	11 to 14	D698
Silty gravels, poorly graded gravel-sand-silt***	1.9 to 2.2	8 to 12	D698
Clayey gravels, poorly graded gravel-sand-clay***	1.8 to 2.1	9 to 14	D698
Well-graded clean sands, gravelly sands***	1.8 to 2.1	9 to 16	D698
Poorly graded clean sands, sand-gravel mix***	1.6 to 1.9	12 to 21	D698
Silty sands, poorly graded sand-silt mix***	1.8 to 2.0	11 to 16	D698

Akgün et al. (2017) studied the hydraulic conductivity of the Ankara clay to determine if it can be used as a clay liner. According to the data set they provided, high plasticity Ankara clays have an optimum water content between 22 and 28 percent, and maximum dry density between 13.9 and 14.4 kN/m^3.

2.3.6. Laboratory Tests for Mineralogical Identification of Expansive Soil

Clay fraction and the mineralogical composition of the clays play an important role in dominating the swelling behavior of the soil. Although it is quite beneficial to identify the mineralogical components of the soil, it might require some costly sophisticated equipment (Cokca, 2002).

2.3.6.1. Methylene Blue Test

The methylene blue test was first developed in France to determine the amount of clays in aggregates (Taylor, 1985; Cokca, 1991). The test is economical and

practical to determine the surface area of a clay particle and cation exchange capacity, and it can be correlated with index soil laboratory tests to evaluate swelling potential (Türköz and Tosun, 2011). The surface area of a clay particle is a useful parameter to identify the type of mineral and it can provide how much water the clay particle can absorb (Cokca, 2002). Therefore, it is considered a direct reflection of clay mineralogy and an indirect indicator for the expansion of soil (Fityus and Smith, 2000; Cokca, 2002).

The test procedure according to a France standard ANFOR (1993) was schematized by (Cokca, 2002) can be seen in Figure 2.13.

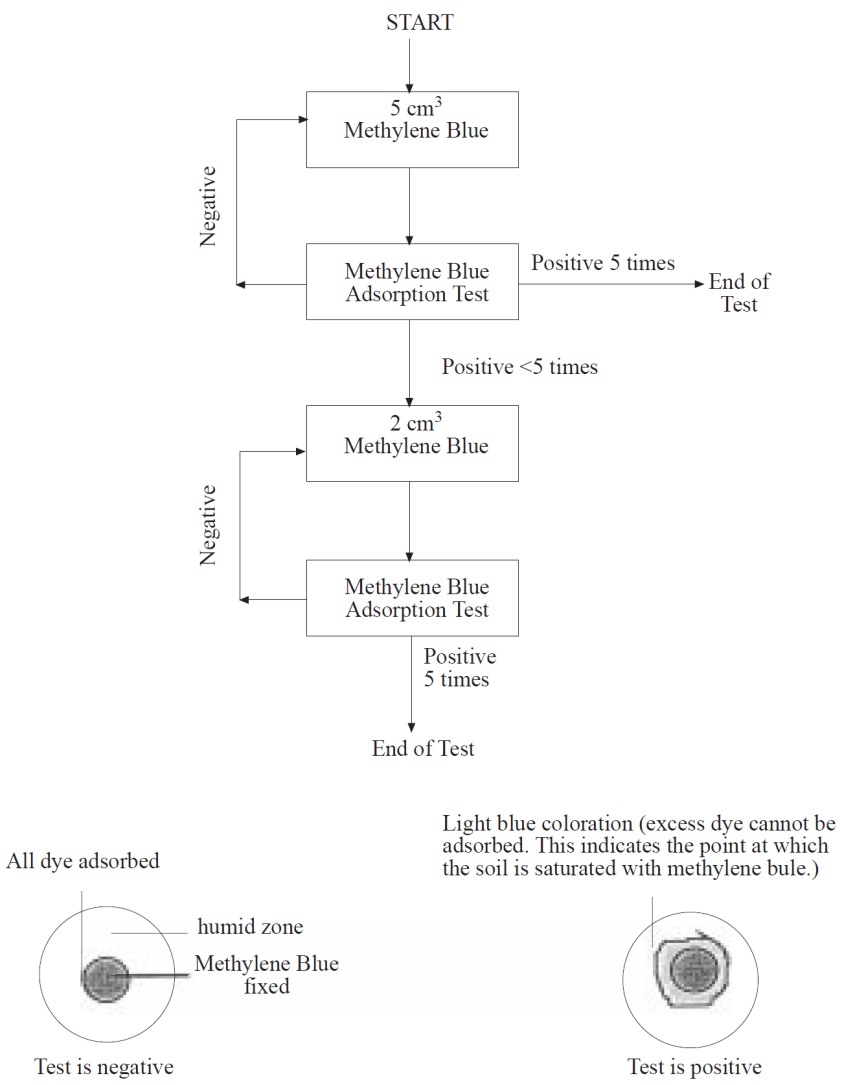

Figure 2.13. The schematic graph to perform methylene blue test (Cokca, 2002)

The specific surface area (SSA) and cation exchange capacity (CEC) are the most common parameters that are being used for the identification of clay particles. The clay particles have negative surcharged surfaces. The total amount of cations to neutralize the negative surface of the clay particles is defined as cation exchange capacity (CEC). Active clays that have a higher potential to swell have higher CEC. The SSA is the total surface area of clay particles in a unit weight of soil. SSA increases when the particle size of clay decreases. The clay with higher SSA might have a higher potential to adsorb water and expand. However, if there is a considerable amount of organic material in the clay, the swelling capacity may be low even though the SSA is high. Therefore, SSA might not directly reflect the expansion of soil (Jury, Gardner, and Gardner, 1991; Nelson, 2015). Table 2.14 shows the typical values of CEC and SSA for different clay minerals. Figure 2.14 shows the potential expansion according to CEC and activity.

Table 2.14. Typical values of CEC and SSA for different clay minerals (Mitchell and Soga,2005, modified from Nelson, 2015)

Clay Mineral	Cation Exchange Capacity (CEC) (meq/100g)	Specific Surface Area (m^2/g)
Kaolinite	1-6	5-55
Illite	15-50	80-120
Montmorillonite	80-150	600-800

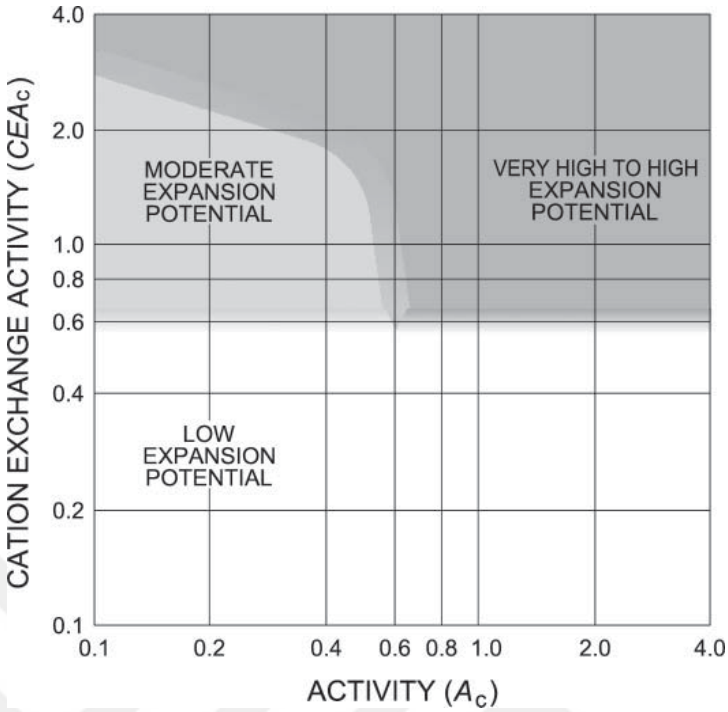

Figure 2.14. Potential expansion of the clay according to CEC and activity (Nelson and Miller, 1992; Nelson, 2015).

2.3.6.2. X-Ray Diffraction Analysis

X-ray diffraction analysis is one of the most common types of methods to determine soil composition and specifically to identify fine-grain minerals. Different X-ray diffraction peaks represent different minerals. A combination of this knowledge with simple grain size distribution can help to define soil and help to predict its behavior (Mitchell, 2005).

X-rays consist of wavelengths between 0.01 and 100 Å (Angstrom). Mitchell (2005) states that when a high-speed X-ray electron is sent to the soil, it either displaces one of the electrons from the target material's inner shell and lowers the vacancy of the material or it might not strike an electron and replace any electrons. X-rays with different wavelengths can be filtered before sending them to the target soil sample. Therefore, it is possible to send an X-ray with a single wavelength. Copper radiation with a wavelength of 1.54 Å (Angstrom) is most used to identify the soils (Mitchell, 2005). Figure 2.15 shows the diffraction of X-rays from target

material according to Bragg's law as defined in Equation 2.7. The angle of diffraction (θ) is dependent on the interatomic spacing (d), which is identical for each mineral. In Equation 2.7, (n) is the order of diffraction that can be any whole number and (λ) is the wavelength of the X-rays.

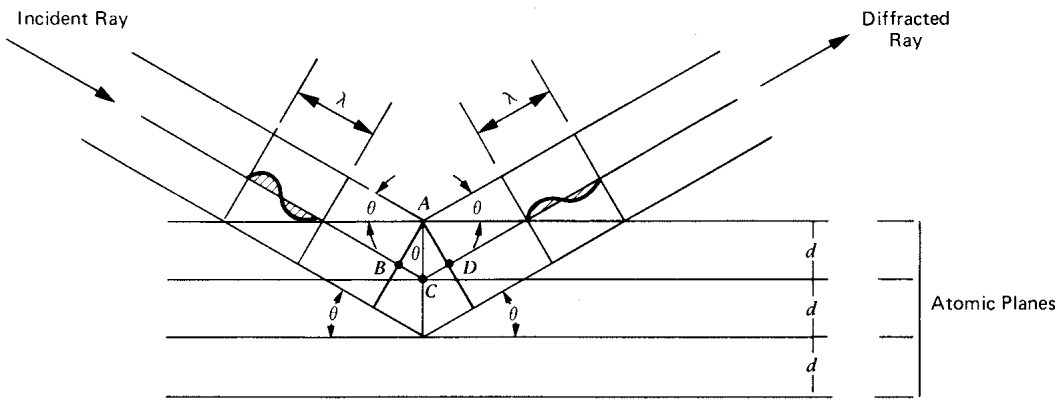

Figure 2.15. X-ray diffraction according to Bragg's law (Mitchell, 2005)

$$n\lambda=2d\sin\theta \qquad \textit{(Eq. 2.7)}$$

The reflected X-rays from different angles and intensities are collected by a detector. Each peak intensity corresponding to different diffraction angles represents a different mineral in the soil. Table 2.15 shows the interatomic space (d) for different common types of minerals in soil.

Table 2.15. Interatomic spaces for common minerals in soil (Mitchell, 2005)

d (Å)	Mineral[a]	*d* (Å)	Mineral[a]
14	*Mont. (VS) Chl. Verm. (VS)*[b]	2.93–3.00	Felds.
12	*Sepiolite,* heated corrensite	2.89–2.90	Carb.
10	*Illite, Mica (S), Halloysite*	2.86	Felds.
9.23	Heated Verm.	2.84	Carb. *Chl.*
7	*Kaol. (S). Chl.*	2.84–2.87	*Chl.*
6.90	*Chl.*	2.73	Carb.
6.44	Attapulgite	2.61	Attapulgite
6.39	*Felds.*	2.60	Verm., Sepiol.
4.90–5.00	Illite, Mica, Halloysite	2.56	Illite (VS), Kaol.
4.70–4.79	*Chlor. (S)*	2.53–2.56	Chlor., Felds., Mont.
4.60	Verm. (S)	2.49	Kaol. (VS)
4.45–4.50	Illite (VS), Sepiolite	2.46	Quartz, heated Verm.
4.46	Kaol.	2.43–2.46	Chlorite
4.36	Kaol.	2.39	*Verm.,* Illite
4.26	Quartz (S)	2.38	*Kaol.*
4.18	Kaol.	2.34	Kaol. (VS)
4.02–4.04	Felds. (S)	2.29	Kaol. (VS)
3.85–3.90	Felds.	2.28	Quartz, Sepiol.
3.82	Sepiol.	2.23	Illite, Chl.
3.78	Felds.	2.13	Quartz, Mica
3.67	Felds.	2.05–2.06	Kaol. (WK)
3.58	Carbonate, Chl.	1.99–2.00	*Mica, Illite (S),* Kaol. Chl.
3.57	*Kaol. (VS), Chl.*	1.90	Kaol.
3.54–3.56	Verm.	1.83	Carb.
3.50	Felds., Chlor.	1.82	Quartz
3.40	Carb.	1.79	Kaol.
3.34	Quartz (VS)	1.68	Quartz
3.32–3.35	*Illite (VS)*	1.66	Kaolin
3.30	Carb.	1.62	Kaolin
3.23	Attapulgite	1.54B	Verm. (S), Quartz
3.21	Felds.	1.55	Quartz
3.20	Mica	1.58	Chl.
3.19	*Felds. (VS)*	1.53	Verm., Illite
3.05	Mont.	1.50	Ill. (S), Kaol.
3.04	Carb. (VS)	1.48–1.50	Kaol. (VS), Mont.
3.02	Felds.	1.45B	Kaol.
3.00	Heated Verm.	1.38	Quartz, Chl.
2.98	Mica (S)	1.31, 1.34, 1.36	Kaol. (B)

[a](B) = broad; (S) = strong; (VS) = very strong; (WK) = weak; Mont. = montmorillonite; Ch1. = chlorite; Verm. = vermiculite; Kaol. = kaolinite; Carb. = carbonate; Felds. = feldspar; Sepiol. = sepiolite.
[b]*Italics indicates (001) spacing.*

Sharma et al. (2012) stated that crystal structures can be used to identify the material and refer to the X-ray pattern as a fingerprint of the crystal structure. X-ray diffraction analysis can be used in a wide variety of fields. Bunaciu et al. (2015) emphasize the importance of the test in the pharmaceutical industry, forensic science, microelectronics industry, and glass industry, in addition to geological applications.

2.3.6.3. Scanning Electron Microscope (SEM)

The scanning electron microscope (SEM) is a common method for the compositional analysis of fine soils. It has a magnification range of x20 to x150000 and makes it possible to reveal and identify clay particles. The limit of SEM is 100 angstrom but generally using lesser magnifications is sufficient to resolve clay particles in soil compositions. The typical SEM images for kaolinite, illite and montmorillonite are shown in Figure 2.16.

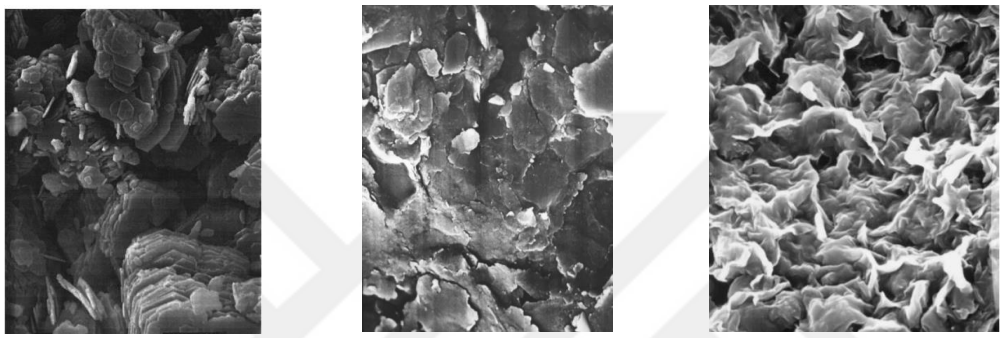

Kaolinite Illite Montmorillonite

Figure 2.16.SEM images of kaolinite, illite and montmorillonite (Murray, 2007, Adopted from Özkan, 2021)

2.4. Soil Water Retention Curve (SWRC) Measurements

Soil mechanics emerged around the 1930s as a discipline that considers only the saturated conditions of the soil. The concept of the suction effect on the soil was not known in those years. After that, the effect of negative pore pressure in the soil was recognized but ignored because it would reveal more conservative safety designs. In humid climate zones, water level elevations are quite high, so generally positive pore pressures occur in the soils. However, in arid and semi-arid regions where expansive soils exist, assuming the soil is fully saturated or ignoring the suction would not be tolerable. Later on, independent stress state parameters (Fredlund et al., 1978), volume change behavior (Fredlund and Morgenstern,1976), shear strength (Fredlund et al., 1978), and seepage analysis for the unsaturated soils were studied. Nevertheless, there was a lack of knowledge between theories and

practical geotechnical problems. This inadequacy has been mitigated by SWRC (Fredlund, 2012).

SWRC consists of a series of data points showing the correlation between water content (gravimetric or volumetric) or degree of saturation and suction (matric or total). It is generally drawn as matric suction on the logarithmic x-axis and volumetric water content on the y-axis (Rajesh et al., 2017; Soltani et al., 2019). Fredlund (2012) explained some advantages and disadvantages of defining SWRC with gravimetric water content, volumetric water content, or degree of saturation, as shown in Table 2.16.

Table 2.16. Advantages and disadvantages of different designations on SWRC (Fredlund, 2012)

Designation	Advantages	Disadvantages
Gravimetric water content, w	• Consistent with usage in classic soil mechanics • Most common means of measurement • Does not require a volume measurement • Reference value is a "mass of soil" which remains constant	• Does not allow differentiation between change in volume and change in degree of saturation • Does not yield the correct air-entry value when the soil changes volume upon drying
Volumetric water content, θ	• Is the basic form that emerges in the derivation of transient seepage and fluid storage in unsaturated soils • Commonly used in databases of results obtained in soil science and agronomy	• Requires a volume measurement • Rigorous definition requires a volume measurement at each soil suction • Is the designation least familiar and least used historically in geotechnical engineering
Degree of saturation, S	• Most clearly defines the air-entry value • Appears to be the variable most closely controlling unsaturated soil property functions	• Requires a volume measurement • Although volume measurements are required, the degree of saturation variable does not quantify overall volume change

Brooks and Corey (1964), van Genuchten (1980), and Fredlund and Xing (1994) models are the most common mathematical approaches to fit data points to create the SWRC (Lu and Likos, 2004). Different fitting models for SWRC are shown in Table 2.17.

Table 2.17. SWRC empirical equations (Leong and Wijaya, 2023)

Reference	*Equation*	*Input parameter*
van Genuchten (1980)	$w(s)=\frac{(w_s-w_r)}{\left[1+(a_v s)^{n_v}\right]^{m_v}}+w_r$	General notation: w_s = saturated water content w_r = residual water content s = soil suction a_v, n_v, m_v = van Genuchten (1980) empirical parameters s_2 = suction at the intersection between initial drying line and virgin drying line a_b = Brooks and Corey (1964) empirical parameter a_f, n_f, m_f, ψ_r= Fredlund and Xing (1994) empirical parameters b_d, c, d_d = Feng and Fredlund (1999) empirical parameters
Brooks and Corey (1964)	For $s < s_2$: $w(s)=w_s$ For $s \geq s_2$ $w(s)=\left(\frac{S_2}{S}\right)^{a_b}$	
Fredlund and Xing (1994)	$w(s)=\frac{w_s C(s)}{\left\{\ln\left[\exp(1)+\left(\frac{s}{a_f}\right)^{n_f}\right]\right\}^{m_f}}$ $C(s)=1\frac{\ln\left(1+\frac{s}{\psi_r}\right)}{\ln\left(1+\frac{10^6}{\psi_r}\right)}$	
Feng and Fredlund (1999)	$w(s)=\frac{w_s b_d+c\cdot s^{d_d}}{b_d+s^{d_d}}$	

The SWRC consists of three main zones: saturated (boundary effect zone as named in Figure 2.17), transition, and residual, and two important boundaries that separate those zones as air entry value (AEV) and residual suction value, as illustrated in Figure 2.17. Air entry value (AEV) is the boundary between the saturated zone and the transition zone. Under lower suction than AEV, the soil has the highest water content and becomes fully or nearly saturated. The zone describes the lower suction and the highest water content is described as a saturated zone. When a higher suction than AEV is applied to the soil, air entry to the soil begins and removes water. The main characteristic of the transition zone is the rapid decrease in water content when suction increases. Further increase in suction removes water in the soil until it reaches the residual suction value. At this boundary condition water that remains in the soil is tightly attached to the soil particles. Soil goes to the residual zone after a further increase in suction. In this zone, hydraulic flows become negligible, so the mobility of the water in the soil significantly decreases to vapor

equilibrium in pore air. The specimen prepared with different methods or stress histories can have different SWRC. Figure 2.18 shows SWRC determined from compacted, undisturbed, initially slurried, and slurried and then preconsolidated specimens.

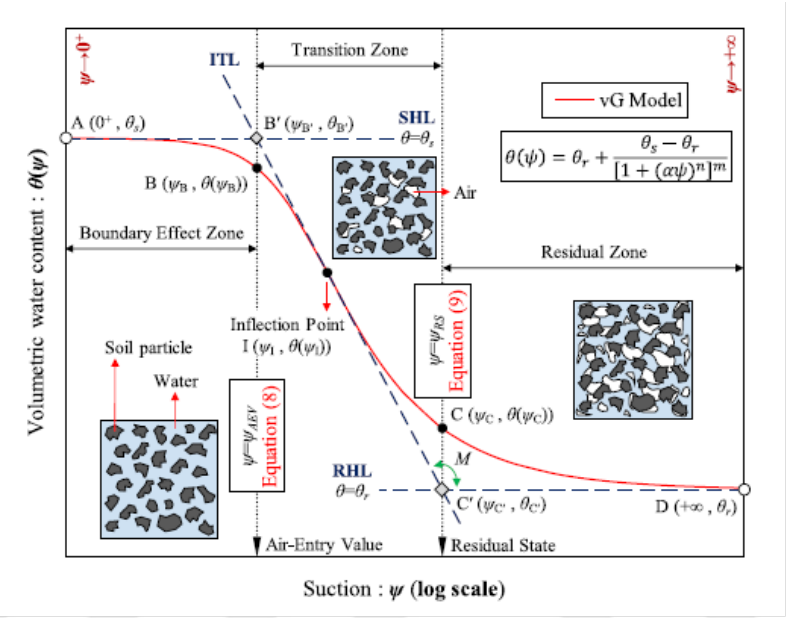

Figure 2.17. Properties of Soil Water Retention Curve (SWRC) (Soltani et al., 2019)

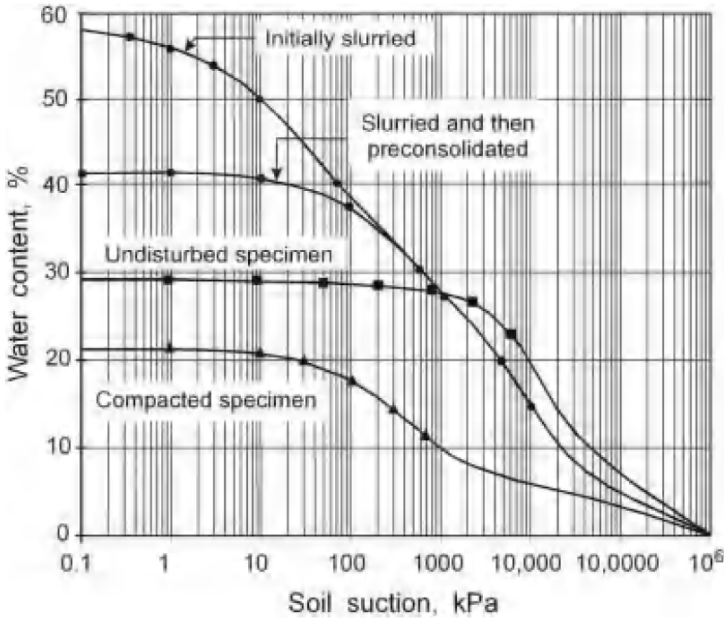

Figure 2.18. Effect of stress history and method on SWRC (Fredlund, 2012)

2.4.1. Suction Measurement Techniques for SWRC

Many different suction measurement techniques with different measurement ranges, complexities, and costs can be used to create SWRC. Some of these techniques with their recommended suction ranges and related references are given in Table 2.18 provided by Lu and Likos (2004).

Frelund (2012) stated that early laboratory equipment to measure SWRC consisted of large pressure chambers. Several soils could be tested at the same time, but it took a long time to test soils for different suction values. However, recent types of equipment are much smaller, allowing engineers to test different soils individually. The laboratory methods to create SWRC are generally categorized into two groups. First, the types of equipment that apply matric suction to the soil, and second, the types of equipment that apply controlled total suction. The methods used in this study (Axis translation, filter paper, and salt solution) are explained in the following sections.

Table 2.18. Common techniques for soil suction measurements (Modified after Lu and Likos, 2004)

Type of Suction	Technique	Suction Range (kPa)
Matric Suction	Tensiometers	0-100
	Axis translation	0-1500
	Contact filter paper	Entire range
Total Suction	Thermocouple psychrometers	100–8000
	Chilled-mirror hygrometers	1000–450000
	Resistance/capacitance sensors	Entire range
	Isopiestic humidity control	4000–400000
	Two-pressure humidity control	10000–600000
	Noncontact filter paper	1000–500000

2.4.1.1. Axis Translation Method

The axis translation technique is the first and most common suction-controlled method developed to measure SWRC (Hilf, 1956; Delage et al., 2008; Kenanoğlu, 2023). Negative pore water pressure may cause cavitation of water in conventional pressure measurement devices. That would make the measurements of matric suction impossible or unrealistic. Axis translation technique overcomes this problem by elevating pore air pressure while keeping the pore water pressure over a pressure that can cause cavitation. Therefore, the matric suction (u_a - u_w), the difference between pore air pressure and pore water pressure, can be kept under control. High air entry (HAE) discs or ceramics (maximum suction capacity of 1500 kPa) are required to be used in this method to prevent the entry of high-pressurized air into low-pressurized water systems (Lu and Likos 2004; Fredlund, 2012). Air entry through the ceramic might create air bubbles in the lower pressurized water compartment and cause errors in suction measurements. Preventing occurrence of the air bubbles can be achieved by regularly flushing the air bubbles (Fredlund, 1975; Kenanoğlu, 2023). A detailed sketch of the axis translation technique provided by Kenanoğlu (2023) can be seen in Figure 2.19.

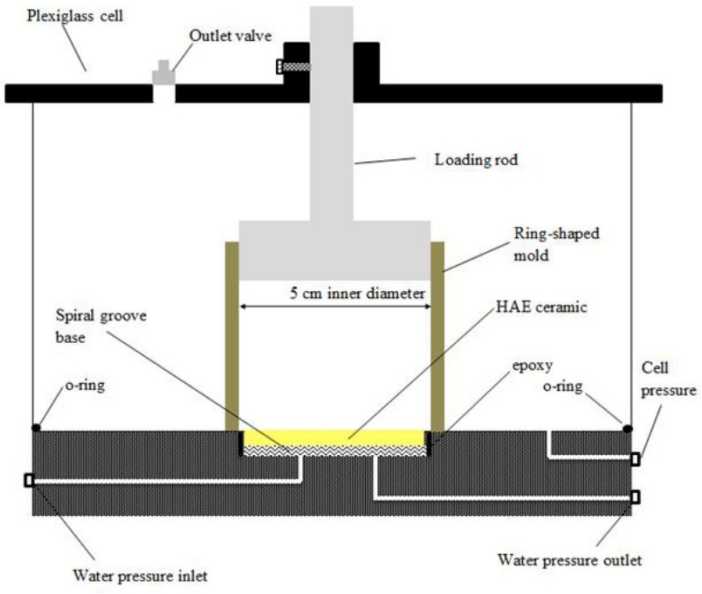

Figure 2.19. Sketch of the oedometer cell for axis translation method (Kenanoğlu, 2023)

2.4.1.2. Filter Paper Method

This method was first introduced by agronomists and soil scientists (Gardner, 1937; Shen et al., 2013). The filter paper method has become a frequently preferred suction measurement method by geotechnical engineers because it is the only method that can measure both total and matric suction in the same experiment, it is cost-effective because it requires minimum equipment, it can be used for all types of soil and it can be used in all suction ranges (Hamblin, 1981; Likos and Lu, 2002; Ridley et al., 2003; Mabirizi & Bulut, 2009; Shen et al., 2013). Figure 2.20 illustrates the general schematic sketch for the filter paper method. The filter paper in the middle of the two specimens has direct contact with the soil and it is used to measure the matric suction. The filter paper at the top without direct contact with the soil specimen is used to measure the total suction.

The test procedure is outlined in the ASTM D5298-03 standard. The standard suggests using Whatman No. 42 type of filter paper. For the matric suction measurements, three filter papers should be used. Top and bottom filter papers can protect the middle filter paper from getting any soil particles attached to it. The water directly transfers from the soil to the filter paper. For the total suction measurements, no contact with the soil specimen can be achieved using some wire netting as in Figure 2.20, or simply a small O ring can be located between the soil specimen and the filter paper. The water transfer from the soil to the filter paper occurs through the air (vapor equilibrium).

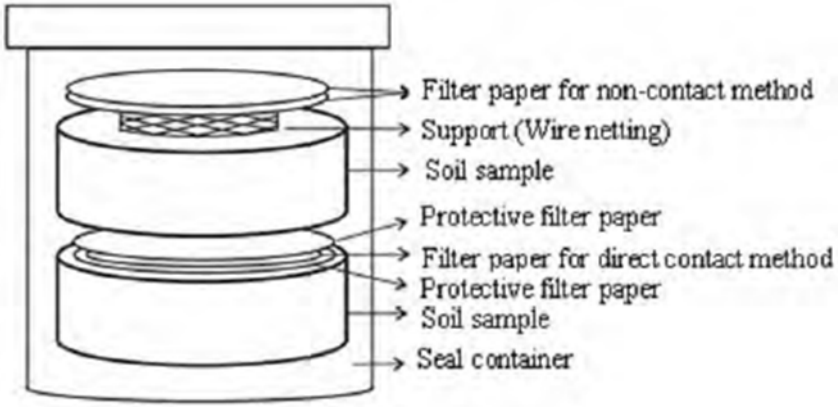

Figure 2.20. Sketch of filter paper (Shen et al., 2013)

The water content of the filter papers can be calculated using Equations from 2. 8 to 2.10.

$M_f = M_2 - T_h$ *(Eq. 2.8)*

$M_w = M_1 - M_2 + T_h - T_c$ *(Eq. 2.9)*

$$w_f = \frac{Mw}{Mf} \times 100 \quad \textit{(Eq. 2.10)}$$

Where;

M_f : Mass of dry filter paper (g)

M_2 : Total dry mass (g)

T_h : Hot container's mass (g)

M_w : Mass of water in the filter paper (g)

T_c : Cold container's mass (g)

w_f : Water content of the filter paper (g)

The total suction corresponding to the calculated water content of the filter paper (w_f) can be determined using Equations 2.11 and 2.12 (Wang et al.,2003; Shen et al., 2013) and the matric suction can be determined using Equations 2.13 and 2.14 (Bai et al., 2011; Shen et al., 2013).

$$\log \Psi_t = -0{,}070 w_f + 5.257 \text{ if } w \leq 41\% \quad \textit{(Eq. 2.11)}$$

$$\log \Psi_t = -1.194 w_f + 51.321 \text{ if } w > 41\% \quad \textit{(Eq. 2.12)}$$

$$\log \Psi_m = -0{,}0767 w_f + 5.493 \text{ if } w \leq 47\% \quad \textit{(Eq. 2.13)}$$

$$\log \Psi_m = -0{,}0120 w_f + 2.470 \text{ if } w > 47\% \quad \textit{(Eq. 2.14)}$$

2.4.1.3. Salt Solution Method

The salt solution method is a humidity-controlled technique to indirectly measure total suction from relative humidity. The temperature affects the relative humidity and therefore the total suction. The total suction can be calculated by Kelvin's equation (Equation 2.18). This method can provide a high suction application as can be seen in Table 2.20. A variety of salt solutions can be used to create different relative humidity and total suction to determine several data points for SWRC. Figure 2. 21 shows a general scheme of a desiccator where salt solutions are located at the bottom and specimens are elevated from the solution to prevent direct contact. ASTM E104.02 provides some relative humidity values for different types of salts. The corresponding total suctions can be calculated by using Equation 2.15. Table 2.19 shows five different types of salt, their relative humidity at 25 °C, and calculated total suction ranging approximately from 3.7 MPa to 74.5 MPa.

$$\Psi = \frac{-\Upsilon w R T}{(MW)_w} \ln(RH) \quad \textit{(Eq. 2.15)}$$

Where;

Ψ : Suction (kPa)

Υ_w : Density of the water

$(MW)_w$: Molar weight of water (18.016 g/mol)

R : Ideal gas constant (8.314 J/mol)

T : Temperature (Kelvin)

RH : Relative humidity

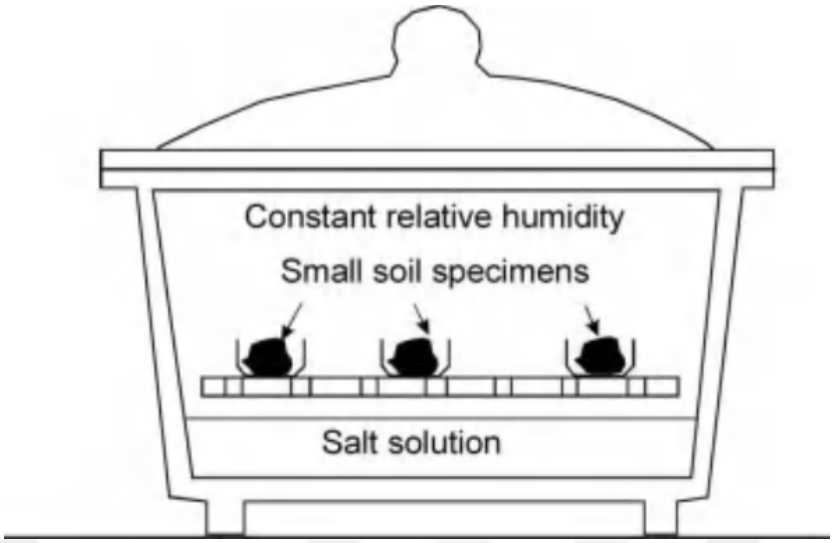

Figure 2.21. Salt solution desiccator (Fredlund, 2012)

Table 2.19. Relative humidity of common types of salts and corresponding total suctions (Kenanoğlu, 2023)

Chemical salts	Relative Humidity	Generated total suction (kPa)
K_2SO_4	97.3	3697
KNO_3	93.6	8932
KCl	84.2	23226
NaCl	75.3	38313
NaBr	57.6	74502

2.5. Barcelona Basic Model (BBM)

Barcelona Basic Model (BBM) is the most widely used constitutive model to define the behavior of the unsaturated soil (Wheeler et al, 2002). BBM simulates the swelling behavior of expansive soils better than its contemporaries. The model, developed by Alonso et al. (1990), extends the modified clay model considering net mean stress (p) and suction (s) as state variables. The net stress is defined as the difference between total mean stress and pore air pressure. The increment in suction decreases the swelling and increases the strength and the preconsolidation mean stress (p_0) in the soil. The BBM consists of two yield surfaces named suction

increase yield surface (SI) and loading-collapse yield surface as shown in Figure 2. 22 (Alonso et al., 1999).

$$p = \frac{\sigma_1 + 2\sigma_3}{3} - u_a \qquad \textit{(Eq. 2.16)}$$

$$q = \sigma_1 - \sigma_3 \qquad \textit{(Eq. 2.17)}$$

$$s = u_a - u_w \qquad \textit{(Eq. 2.18)}$$

Where;

p : Mean net stress

σ_1 : Major principal stress

σ_3 : Minor principal stress

s : Suction

u_a : Pore air pressure

u_w : Pore water pressure

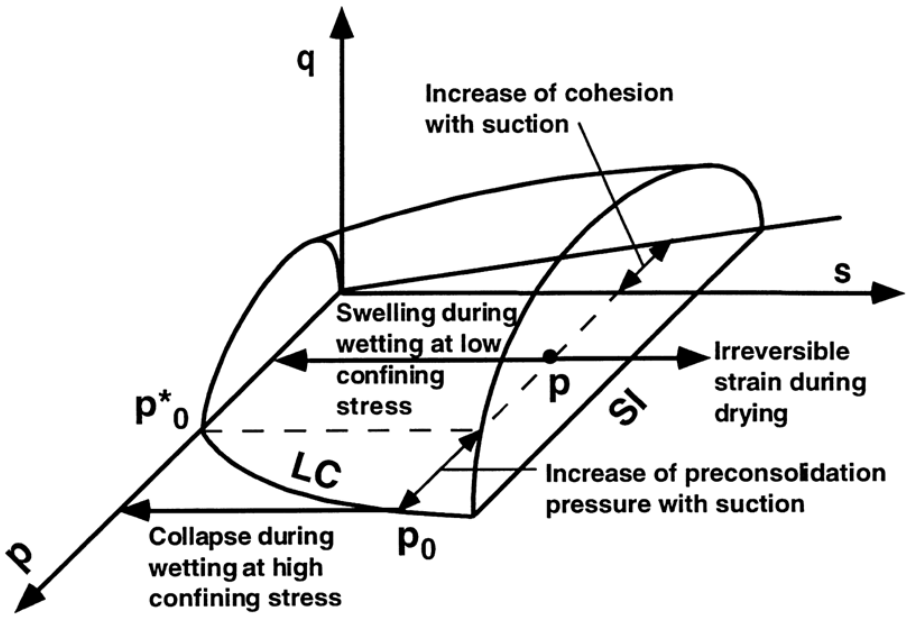

Figure 2.22. Barcelona Basic Model yield surfaces in p-q-s plane (Alonso et al., 1999)

The volume change can be defined using equations from Equation 2.19 to 2.24 under isotropic stress conditions. Additional figures for graphical explanation of BBM parameters are given in Appendix A.

$$v = N(s) - \lambda_s \times \ln(p/p_c) \quad \textit{(Eq. 2.19)}$$

$$d_v = -\kappa d_p/p \quad \textit{(Eq. 2.20)}$$

$$d_v = -\kappa_s \times d_s/(s + p_{atm}) \quad \textit{(Eq. 2.21)}$$

$$N(s) = N(0) - \kappa_s \times \ln(\frac{s + p_{atm}}{p_{atm}}) \quad \textit{(Eq. 2.22)}$$

$$p_0 = p_c \times (p_0^*/p_c)\text{^}(\frac{\lambda(s) - \kappa}{\lambda(0) - \kappa}) \quad \textit{(Eq. 2.23)}$$

$$\lambda(s) = \lambda(0) \times ((1 - r) \times e^{(-\beta \times s)} + r) \quad \textit{(Eq. 2.24)}$$

Where;

v : Specific volume

λ(s) : Slope of the virgin compression line (constant suction)

p_c : Reference stress

N(s) : Specific volume corresponds to λ(s)

κ : Slope of the elastic compression line due to the suction change

p_{atm} : Atmospheric pressure

N (0) : Specific volume at the reference stress

p_0* : Preconsolidation pressure in mean stress terms

λ(0) : Slope of the saturated virgin line

β : Hardening effect with suction

r : Ratio compression index at the high suctions and slope of the saturated virgin line (λ(0))

The yield surfaces of loading-collapse (LC) and suction increase (SI) in p-s space, as shown in Figure 2. 22, are defined in Equations 2.25 and 2.26 for volumetric plastic strain increments.

For LC Curve;

$$d\varepsilon_v^p = \frac{\lambda(0) - \kappa}{v}\frac{dp_0}{p_0^*} \qquad \textit{(Eq. 2.25)}$$

For SI Curve;

$$d\varepsilon_v^p = \frac{\lambda(s) - \kappa_s}{v}\frac{ds_0}{s_0 + p_{atm}} \qquad \textit{(Eq. 2.26)}$$

Modified Cam Clay (MCC) theory defines the elliptical yield surface in the p-q space as written in Equation 2.27.

$$F = q^2 + M^2(p + p_0)(p - p_c) = 0 \qquad \textit{(Eq. 2.27)}$$

The BBM model similarly defines the elliptical yield surface like modified cam clay model but extends it by considering the suction effect and using it as a state parameter as shown in Equation 2.28.

$$F = q^2 + M^2(p + p_0(p,s))(p - p_c(p,s)) = 0 \qquad \textit{(Eq. 2.28)}$$

Where;

q : Deviatoric stress

p : Mean net stress

p_c : Preconsolidation pressure with suction

M : Critical state parameter

The ratio of plastic shear strain to plastic volumetric strain is;

$$\frac{d\varepsilon_s^p}{d\varepsilon_v^p} = \frac{2q\alpha}{M^2\left(2p + ks - p_0\right)} \qquad \textit{(Eq. 2.29)}$$

Where;

α : Parameter to define flow rule

The parameter α is defined by Alonso et al. (1990) as

$$\alpha = \frac{M(M-9)(M-3)}{9(6-M)} \frac{1}{1-(\kappa/\lambda(0))} \qquad \textit{(Eq. 2.30)}$$

In Figure 2. 24, Alonso et al show the different loading-collapse (LC) that occurs in the soil as stress and suction change. The reduction in suction causes the LC curves to shift to the left side, causing wetting of the soil and therefore weakening. At a constant suction value, the SI line shows the suction increase value and the soil yields if the suction exceeds this value. A, B, C, D, E, F represent stress-suction paths and they stated that different suction and loading conditions acting on the soil will create different LC curves. In the experiments on 3 soil samples, they noted that different loading paths of the soil from point A to point F resulted in different LC curves. In the A-B-F path, the first sample is loaded from point A to point B in the saturated condition where suction is zero. In this case the soil showed plastic deformation causing the LC curve to shift to the right. Then the suction was increased by drying and moved to point F, but this path did not cause any plastic deformation because it remained within the LC curve. In the A-E-F path, the soil was first dried by applying internal suction and then loaded. The suction applied before loading made the soil stiffer and resulted in the LC curve being on the left compared to the first case. In the A-B-F path soil shows the highest volume change while in the A-E-F path soil shows the lowest volume change.

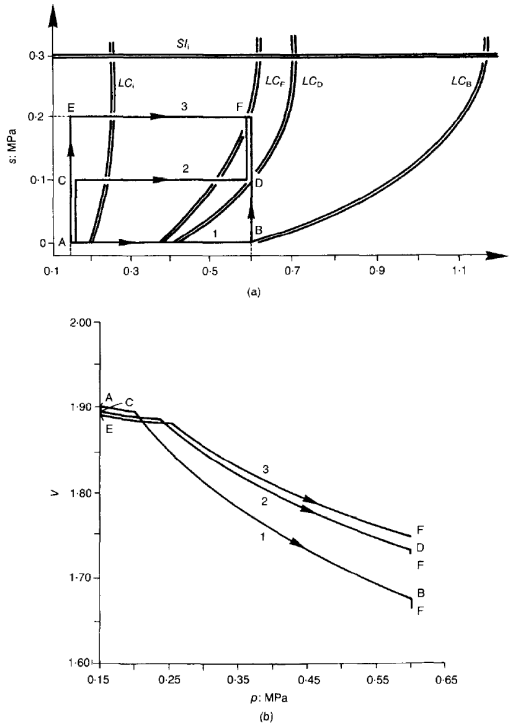

Figure 2.23. Effect of different loading paths on LC curve (Alonso, Gens, and Josa, 1990)

2.5.1. Determining Barcelona Basic Model Parameters

Gallipoli et al. (2010) proposed calibration methods to determine each BBM parameter. Researchers suggest suction-controlled isotropic compression tests to determine $\lambda(s)$, β, $N(0)$, and $p_c(s)$ parameters, saturated isotropic compression tests to determine $\lambda(0)$, suction-controlled unloading-reloading tests to determine elastic parameters of κ and κ_s and suction-controlled triaxial tests to determine the slope of the critical state line (M).

Zhang and Xiao (2013) conducted suction-controlled isotropic compression tests under the constant suction of 0, 100, 200,300 kPa and elastic unloading-reloading tests and used a modified state surface approach and Newton optimization technique to calibrate BBM parameters.

Zhang et al. (2016) proposed an alternative methodology to determine BBM parameters using suction-controlled oedometer tests instead of triaxial tests. They performed the tests under multiple constant suctions of 0, 100, 200, 300 and 400

kPa. The authors emphasize that it requires less time and lower cost compared to the suction-controlled triaxial tests.

Kenanoğlu (2023) classified the BBM parameters into three groups: the parameters to define the initial conditions, the loading-collapse (LC) curve, and the strength as shown in Table 2.20.

Kenanoglu and Toker (2024) state that soil laboratory testing for unsaturated soils requires costly equipment and a long testing time. Therefore, they proposed a practical framework to determine BBM parameters using a straightforward and rapid process rather than suction-controlled tests which are complex and require long testing time. Their proposed approach for determining BBM parameters comprises: 1 standard oedometer test, 2 triaxial CD tests, evaporation tests, 3 unsaturated K_0 tests, 4 unsaturated undrained tests, and a soil water retention curve. They provide step-by-step procedures that demonstrate calibration for each parameter.

Table 2.20. The required parameters for the BBM (Adopted from Kenanoğlu,2023)

Initial Conditions	**Loading-collapse (LC)**	**Strength**
The initial specific volume (v_0)	Reference stress (p_c)	Shear modulus of elastic state (G)
The initial suction (s_0)	The slope of the saturated virgin line ($\lambda(0)$)	The slope of the critical state line (M)
Saturated preconsolidation stress (p_0^*)	The slope of the elastic compression line (κ)	The contribution of suction to cohesion (k)
	Hardening effect with suction (β)	
	The slope of the compression line at the high suction values (r)	

2.6. Pile Foundation in Expansive Soil

The swelling or shrinkage behavior that may occur due to the change in water content in the expansive soils may cause serious damage to the structures located on them. The use of pile foundations is one of the common methods used to prevent damage to structures due to the behavior of the expansive soils. (Poulos, 1993; Xiao et al., 2011; Wu and Vanapalli, 2022).

Mittal, Samanta and Maurya (2025) stated that the use of pile foundations increases the strength of soils, increases the natural frequency of the soil-structure system and improves the seismic performance of the buildings built on it. Increasing the pile length reduces the amplification of seismic waves and thus makes the structures more stable in earthquakes.

Zhang and Acosta Martinez (2023) stated that pile foundations are often used in large solar farms with expansive soil, thus avoiding the damage to the structure caused by swelling pressures and the impact of strong winds acting on the lightweight structures above them.

In the design of pile foundations in expansive soils, the uplift forces acting on the pile due to the water content change in the active zone should be lower than the withholding forces acting on the pile in the anchoring zone. If this cannot be ensured, the uplift forces acting on the pile will cause the pile to move upward with the ground. In order to prevent this condition from occurring, the pile length should be increased and the pile should be inserted more into the anchorage zone and the forces acting on the pile should be equal to or higher than the uplift forces (Chen, 1975).

2.6.1. Adhesion Factor

The adhesion factor describes the strength reduction between the pile foundation and the soil and can be calculated from Equation 2.31 (Chen, 1975; Prakash and Sharma, 1991; Elsharief, Ahmed and Mohamedzein, 2016, Mulrosha and Arifin, 2021).

$f = \alpha \cdot c_u$ *(Eq. 2.31)*

Where;

f : skin friction

α : adhesion factor

c_u : undrained shear strength of the soil

According to Prakash and Sharma (1991), it is very difficult to determine the adhesion factor between soil and pile. The adhesion factor varies according to the type of pile as well as the consistency of the soil, water content, and the method of installation of the pile. If the concrete is wet, the strength of the clay in contact with the pile will decrease since there will be water transfer from the concrete to the soil.

Skempton (1959) stated that in London clay, the adhesion factor can vary between 0.3 and 0.6 for the bored piles. According to Mohan and Chandra (1961), it can be taken as 0.5 for the medium to hard clays.

According to Tjandra and Soemitro (2013), seasonal changes affect the adhesion factor significantly. A decrease in water content increases the undrained strength of the clay and the adhesion factor, while an increase in water content decreases the undrained strength of the clay and therefore the adhesion factor. Also, they stated that the adhesion factor may decrease over time in clays with shear strength less than 30kPa.

Elsharief, Ahmed, and Mohamedzein (2016) emphasize that the adhesion factor is a very important parameter for safe pile design in expansive clays. They found the interface shear strength value from the shear test between clay and concrete in direct shear apparatus in high plasticity clays and found the adhesion factor from the ratio of this value to the undrained shear strength of the clay. According to the authors' findings, the adhesion factor varies with the water content. At water contents lower than the plastic limit the adhesion factor remains constant at 0.45 for the high plastic clay they used in their study, while at water contents higher than the plastic limit the adhesion factor increases linearly.

2.6.2. Uplift Factor

The uplift factor (β_u) is the ratio of the uplift pressure to the swelling pressure of the soil as shown in Equation 2.32. Chen 1975 conducted experiments on 2-inch diameter and 6- and 9-inch-long pile foundations placed in expansive clay. The uplift pressure was found by calculating the stress that should be applied to prevent the movement of the pile due to the swelling of the soil. From the ratio of the uplift pressure to the swelling pressure of the soil, the uplift factor was found to be 0.15. This indicates that 15 percent of the swelling pressure causes the uplift pressure at the concrete pile foundation.

$$\beta_u = \frac{Uplift\ Pressure}{Swelling\ Pressure} \qquad \textit{(Eq. 2.32)}$$

Nelson (2015) stated that uplift skin friction will take place in the active zone while negative skin friction will occur in the anchorage zone, as shown in Figure 2.25. Nelson also recommended the use of Equation 2.31 used by Chen 1975 for pile foundations completely located in expansive clay but stated that different values have been used for the uplift factor according to different studies over time. Chen (1988) reported a range of 0.09 to 0.18 for the uplift factor, and Nelson and Miller (1991) reported a range of 0.1 to 0.25. According to the results of the experiment conducted at Colorado State University (CSU), which was performed on full-size (36 cm in diameter and 760 cm in length) drilled concrete piers and measured for 10 years, the uplift factor between concrete and expansive soil can vary between 0.4 and 0.6 (Benvenga, 2005; Nelson, 2015). Nelson 2015 evaluated all these different studies and results and concluded that it would be more accurate to use the results of the experiment conducted at CSU for the uplift factor because it uses full-scaled testing and long-term measurements.

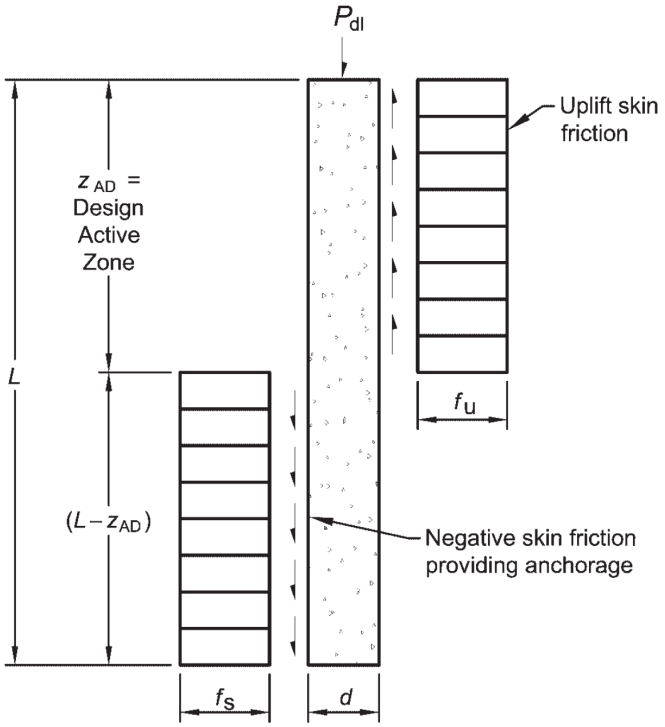

Figure 2.24. Forces acting on a pile in expansive soils (Nelson, 2015)

CHAPTER 3

FIELD AND LABORATORY STUDIES

This section describes each step of the study and the methods followed in detail. Initially, different soil samples were collected from various parts of Ankara. Quick laboratory experiments were carried out on these samples to determine their swelling potentials. Thus, the most critical clay was determined as the main material to be used in the study. The TMI value of the determined region was calculated, and its correspondence with the literature was investigated.

A considerable amount of soil samples taken from the region were brought to the laboratory and index tests, free swell, lateral swell, compaction, consolidation, X-ray Diffraction (XRD), scanning electron microscope (SEM), and methylene blue tests were performed to determine the mineralogical compositions and engineering parameters of the soil. In addition to these tests, unsaturated soil laboratory experiments, including filter paper, salt solution, and axis translation methods, were performed to determine the soil water retention curve (SWRC) of the clay.

The methodology of Kenanoglu and Toker (2023) was adopted to determine the engineering parameters required for the Barcelona Basic Method (BBM), which was chosen to simulate the soil behavior in RS-2. For this reason, a shrinkage curve was drawn by measuring the volume and unit weights of the specimens prepared with different water contents. The critical water content of the clay was determined by an evaporation test. Unsaturated triaxial and oedometer tests were performed on the samples prepared at the critical water content value and by increasing two and four percent from this value.

Chen's (1975) design methodology was used to determine safe design requirements for the clay and the parameters needed for the design were determined from

required laboratory tests. Undrained shear strength parameters of the clay to be used in Chen's method were determined by performing direct shear and unconfined compression tests. The shear strength between the clay and concrete block prepared at the same water/cement ratio as the pile was determined using direct shear tests. Therefore, adhesion factor (α) was determined. The swell pressure of the clay was determined using oedometer apparatuses and a small-scale laboratory set-up prepared to measure the uplift force applied on the pile. So, the uplift factor (β_u) is determined as it is the ratio of the swelling pressure of the soil to the uplift pressure.

3.1. Site selection

It is very common to name soils based on their region's name, such as London clay, Boston blue clay, Oslo clay, Ottawa sand, etc., although the properties and the behavior of the soil may vary significantly from location to location in the same region. Differences in environmental conditions and clay compositions play an important role in determining the behavior of the soil. Therefore, although the clay used in this study is generally referred to as Ankara expansive clay, it should be known that the engineering properties of the Ankara clay vary over the city.

At this stage of the study, two selection criteria were used to determine from where to take the soil samples to be used in this study. The first, chosen soil should have high expansive potential, therefore, the effects of the soil swelling on the pile can be measured clearly. Second, considering the quantity of soil needed for many laboratory tests, the site should be available for excavation and the collection of more clay samples.

Eight different disturbed soil samples were collected from different regions of Ankara. Three from Yuvakoy, one from Batikent, two from Cubuk, and two from Golbasi. Samples were taken after excavating approximately 50 cm of soil at each location, to avoid vegetation and organic materials. Some quick laboratory tests such as free and modified free swell, and Atterberg limit tests were conducted for each of them to decide which one to proceed with for the rest of this study. The

following figures from Figure 3.1 to Figure 3.5 show the soil samples and quick laboratory tests performed to determine their swelling potentials.

Figure 3.1. Golbasi Clay Sample-1

Figure 3.2. Golbasi Clay Sample-2 and MFSI Test

Figure 3.3. Cubuk Clay Sample-1 and Free Swell Test

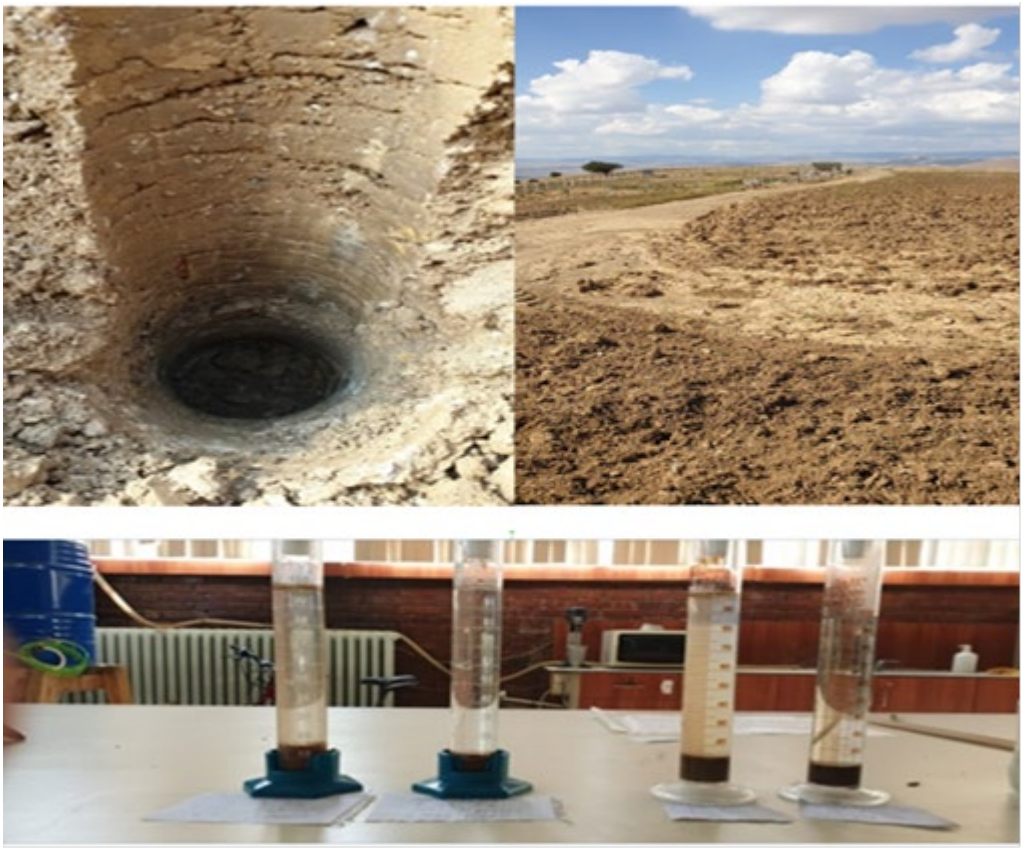

Figure 3.4. Cubuk Clay Sample-2 and Modified Free Swell Tests

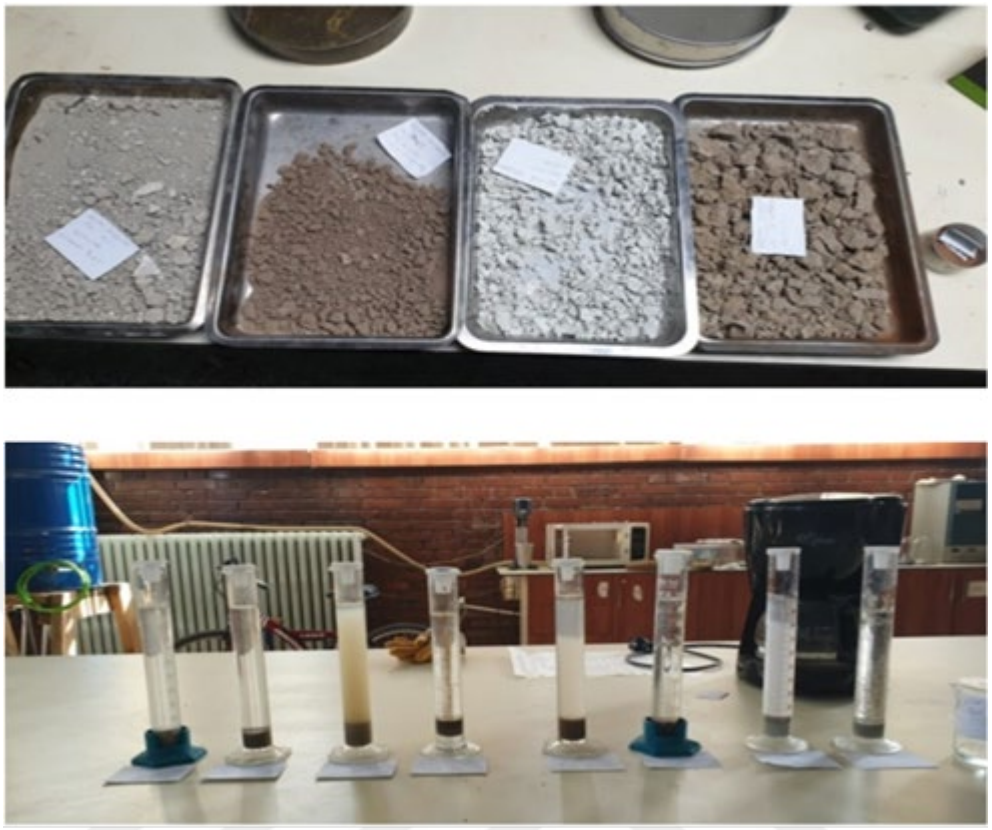

Figure 3.5. Batikent and Yuvakoy soil samples and Modified Free Swell Tests

3.2. Determination of Thornthwaite Moisture Index (TMI)

The Thornthwaite Moisture Index (TMI) can be used to relate the effect of climate conditions on the variation of the soil moisture profile. Monthly average temperature and rainfall data from 1927 to 2003 (t) were taken from the Republic of Türkiye Ministry of Environment, Urbanisation and Climate Change, General Directorate of Meteorology website to estimate Ankara's potential evapotranspiration (PE). The equations provided by Thornthwaite (1948) are used to calculate potential evapotranspiration (PE), adjustment factor (a), heat index (I), water balance, storage, deficit, and surplus. Each month's latitude correction factors were taken from the state hydraulic work (DSI) technical bulletin #105. Then TMI is calculated as it is a function of potential evaporation, deficit, and surplus.

3.3. Soil Collection and Preparation Process

3.3.1. Soil Collection Process

An excavation pit was opened at a depth of approximately 4 meters in Cubuk Akkuzulu, Ankara to determine the variation of water content with depth and to avoid plant or organic materials. Approximately 3 tons of disturbed soil samples were collected for this study. The exact location (40°11'48"N 33°08'32" E) of the pit excavation is marked as a red star in Figure 3.6.

Figure 3.6. Location of the Soil Sample

The excavation process of the pit excavation, collection of soil samples to determine the water content, measuring the depth of soil samples from the ground surface, and filling the samples into the bags are shown in Figure 3.7.

Figure 3.7. Soil Collection Process

After a pit excavation, 8 disturbed soil samples from each of three different profiles were taken from depths of 0.5, 1, 1.5, 2, 2.5, 3, 3.5, and 4 meters to measure water content change over the depth. All soil samples are packed in 3 plastic bags to make sure that no moisture loss would occur. Figure 3.8 shows the collected clay samples in the bags and a sufficient amount of them in a tare to oven-dry for water content measurements.

Figure 3.8. Disturbed Soil samples taken from different depths and water content measurements

3.3.2. Preparation of Soil Samples for the Laboratory Tests

Approximately 3 tonnes of disturbed soil samples were collected for this study. All experiments throughout this study used the material passing through sieve #40 (425 microns). Manual pulverization of these samples is very challenging, as all samples are flocculent and gain very high strengths due to the drying. The hammer was used to break the large blocks of clay into smaller pieces. Then, the smaller pieces were put into the jaw crusher to gain further smaller pieces. They were then thrown into the soil pulverizer, which is capable of separating the soil blocks into much smaller diameters. Then they were collected and tried to be grinded by hand using a piece of wood. After going through all these steps, the material was sieved through a #40 sieve and the soil was ready to be used in the soil laboratory tests. They are packed in a double plastic bag and stored. All soil preparation processes can be seen in Figure 3.9.

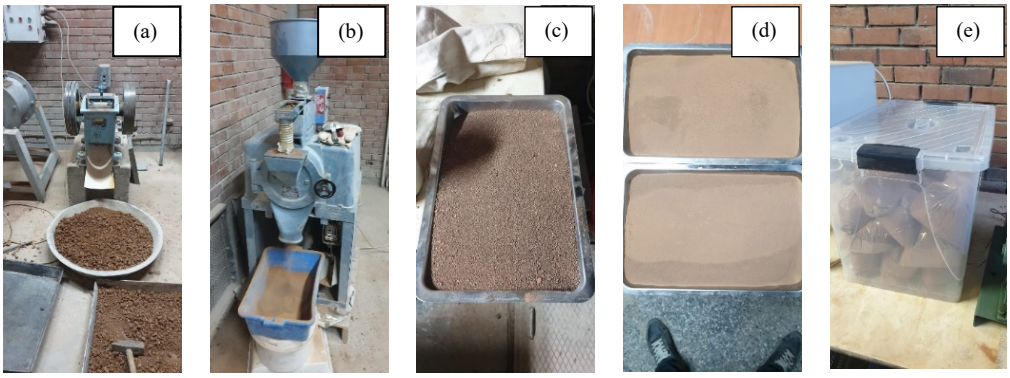

Figure 3.9. Soil Preparation stages before the laboratory tests

3.4. Laboratory Tests

3.4.1. Atterberg Limit Tests

Atterberg limit tests are one of the most common soil laboratory tests that were used to classify the clay. The plastic limit and liquid limit of the clay were determined using the ASTM D4318 standard Fig.3.10. The Casagrande cup method was chosen for liquid limit determination.

Figure 3.10. Atterberg Limits LL and PL Tests

3.4.1.1. Shrinkage Limit Tests

3 different methods were used to determine the shrinkage limit for the clay.

Linear Soil Shrinkage Test

The test was performed according to AS 1289.C4.1-1977. The linear shrinkage bar mold as shown in Figure 3. 11, was cleaned and the inner surface was slightly greased. The soil, prepared with a consistency two percent higher than the liquid limit, was carefully placed in the mold. Special care was taken to ensure that the soil placed in the mold was homogeneous and no air bubbles remained in the mold. The mold was left at room temperature for 1 day to dry slowly. It was then placed on the top of the working oven for another 1 day (to provide a warmer environment than room temperature). Finally, the experiment was completed by keeping it in a 104-degree oven for another 24 hours. The linear shrinkage (LS) is calculated as it is the ratio of the length difference of the soil before and after drying to the initial length.

Figure 3.11. Linear shrinkage limit test

Shrinkage limit determination by using mercury

Soil with a consistency of 2 percent higher than the liquid limit was used for the test. Shrinkage dishes as shown in Figure 3.12, were cleaned and the inside surfaces of the dishes were greased with a thin layer. The soil is gradually placed in a dish and compacted by tapping the dish after each addition of the soil until the

dish is completely full. Thus, entrapping air bubbles during the process was prevented. Similar to the drying process used for the linear shrinkage test, the shrinkage dishes were left at room temperature for 1 day to dry slowly. Then, they were placed on top of the working oven for another day. Then they were placed in a 104-degree oven to dry.

The volume of the shrinkage dishes and the dry samples were determined using mercury. First, the mass of an empty shrinkage dish was measured. The dish was then filled to the top with mercury. Excess mercury was removed from the top surface of the dish by using a plexiglass apparatus. The dish was then completely filled with mercury so that the top surface was completely flat. The weight of the dish filled with mercury was measured. Thus, the volume was found with mercury with a known density and measured weight. The same process was repeated for all four containers separately.

The volume of the dry soil specimen was also determined using a container filled to the top with mercury. The dry soil specimen was carefully placed on the mercury-filled container. It was then slowly pushed into the mercury-filled container with the help of the plexiglass so that it submerged completely. Therefore, the mercury with the same volume as the dry soil specimen was ejected out of the container. This mercury was collected and weighed. The volume of the dry soil was then determined using mercury of known density and weight.

Figure 3.12. Shrinkage limit determination by using mercury

Water submersion technique

The same specimens used to determine the shrinkage limit with mercury were also used for this method. Mercury is a very toxic material and using it without caution can cause serious health damage. Therefore, ASTM D4943-18 suggests using the submersion technique to determine the volume of the dry soil specimens. The test was performed according to this standard. The dry soils were covered with a thin layer of wax by dipping them into the melted wax. Then the volume of each soil was determined by using the submersion technique explained in detail in the shrinkage curve test.

3.4.2. Specific Gravity Test

The test was conducted to determine the specific gravity (G_s) of the clay. The method suggested for the plastic materials by ASTM D854 was used. Three tests were performed as it is the minimum number of required tests according to the standard, and specific gravity was calculated as the mean value of these three tests.

Figure 3.13. Specific gravity (G_S) photos

3.4.3. Sieve and Hydrometer Tests

Both tests were performed to derive the grain size distribution and determine the clay content of the soil. The sieve and hydrometer analyses were performed according to ASTM D6913 and ASTM D7928 standards, respectively. For the particles larger than No. 200 (75 microns) sieve analysis and the particles smaller than 75 microns hydrometer analysis was performed and grain size distribution was drawn by combining both. Grains smaller than 2 microns are defined as clay.

3.4.4. Compaction Test

The standard proctor method was used to conduct the compaction test according to ASTM D698 standard. The purpose of this test is the determine the relationship between water content and the dry unit weight of the clay under standard energy. The test result provides the optimum water content, which is the water content corresponding to the maximum dry density. In other words, it can provide a specific water content that, when clay is compacted under a standard energy, the maximum amount of soil particles can be packed in a unit volume.

The very common and fast way to perform this test is to begin the test with relatively dry soil and take a sufficient amount of soil to measure the water content. Then, continue for the next data point measurement by wetting the soil a little more than the previous data points. Another and more appropriate approach to drawing a compaction curve is to prepare clay samples for each data point can be prepared before performing the test and leave them for tempering for 24 hours. This approach requires more soil samples, but it is much more appropriate than the first one because the tempering period ensures that the water is evenly distributed in clay samples. This approach was used in this study and clay samples with different water contents were prepared and left for tempering for a day, as can be seen in Figure 3.12. The dry density corresponds to two percent less than the optimum dry density is found and used as an initial condition of the soil sample for the rest of the tests.

Figure 3.14. Compaction test photos

Figure 3.15. Tempering of the clay samples for compaction test

3.4.5. Modified Free Swell Test

The modified free swell test is a quick and easy test to predict the swelling potential of soil. The test is performed according to the Bureau of Indian Standards (1977) IS 2720. The soil passing through sieve 40 was dried in an oven for 24 hours. Two 10 grams of dry clay were placed in two graduated cylinders (10 grams for each cylinder). One of the graduated cylinders was filled until 100 mL with water and the other was filled until 100 mL with kerosene oil. Both graduated cylinders were sealed and left for 24 hours. Kerosene prevents swelling of the clay in the first graduated cylinder while the clay in the water swells. Then the Modified free swell was calculated as it is the ratio of the volumetric increase of swollen soil to the volume of soil in the tube filled with kerosene.

3.4.6. Swelling Potential and Swelling Pressure Tests

ASTM D4546 standard was used to perform this test. According to the standard, there are different methods to perform a swell test. A very low load (around 5 kPa) can be applied to a specimen and then by adding distilled water to the specimen, it can be allowed to swell freely. So, swelling potential can be found as it is the ratio of the change in volume over the initial specimen volume. Because the diameter of the oedometer ring is constant, it can also be simply defined as the ratio of the height difference to the initial height.

One of the most common ASTM methods to determine the swelling pressure is the constant volume method. In this method, some additional loads are applied to the specimen after adding distilled water, to prevent the swelling and keep the initial volume constant. The swelling pressure is the stress applied on the specimen such that no volumetric changes can be observed due to swelling.

One of the other ASTM methods allows to measurement of both swelling potential and pressure. The soil specimen can be allowed to swell freely until no swelling can be measured. So, swelling potential can be calculated as it was mentioned for the first method. Then, some stress can be applied to the specimen to make it return to its original initial height. So, that amount of the applied stress would be swelling pressure.

In this study, an oedometer set-up as shown in Figure 3.16 was used to perform the test.

The specimen is compacted in the oedometer ring to have water of 23 percent and a dry density of 1.462 g/cm^3. A filter paper was placed at the bottom and top of the specimen. Then, the ring was placed in the oedometer device and the top cap was placed at the top of the specimen. Approximately 7 kPa vertical pressure was applied to the specimen. Then water is added to let the soil free swell for 24 hours. When free swell was completed, stresses were applied to the specimen by degrees. So, the variety of swelling pressures for corresponding swelling potentials are measured.

Figure 3.16. Apparatus to measure swelling potential and swelling pressure

3.4.7. One-Dimensional Consolidation Test Using Incremental Loading

The test was performed according to ASTM D2435 to determine the coefficient of consolidation (c_v), compression index (c_c), and recompression index (c_r) to estimate the magnitude and rate of consolidation.

The soil sample with a water content of 23 percent was prepared and left in a humidity room for tempering for 48 hours. It is compacted in an oedometer ring with a diameter and height of 6.3 and 1.9 cm, respectively. Approximately 7 kPa surcharge pressure was applied to the specimen and the test started with the free swell stage by filling the cell with water. Vertical displacements versus time are recorded immediately after adding the water. Time intervals to record displacements were chosen as the squares of multiples of 0.5 in minutes up to 5 (corresponds to a reading at 25 minutes) as suggested in the standard to have better-looking time- displacement plots. In general, displacement readings were recorded at the times of 15 sec, 1 min, 2, 4, 6, 9, 12, 16, 20, 25; 36, 49, 64, 81, 100, 121; and 24 hours. Extra readings between 121 minutes and 24 hours were tried to record.

After the free swell stage of the test, load increments started and the same procedures were followed to draw a time-displacement plot for each load increment. Each load increment was adjusted to double the previous load. To determine the slope of the unloading-reloading line (c_r), two times applied loads decreased as ¼ of the previous loads. At the end of the test, the specimen was extruded and water content measurement was taken. The same oedometer equipment as shown in Figure 3.16 was used to perform the test.

3.4.8. Direct Shear Tests

The direct shear tests were performed to determine the shear strength of the soil under both drained and undrained conditions using square and circular shear boxes.

The drained direct shear test was performed according to the ASTM D3080 standard.

The soil specimen with 34.56 mm (it should be higher than approximately 12 mm according to the standard), a 23 percent water content, and 1.462 gr/cm^3 dry density (corresponding dry density for 23 percent of water content from compaction curve) was compacted in a square direct shear box with dimensions of 59.5 mm by 59.5 mm. Similar to the 1-D consolidation tests, a small surcharge load was applied to the specimen, the cell was filled with water, and swelling versus time was plotted. After the swelling is completed (at least 24 hours), the determined load is applied to the specimen, and consolidation under the applied load is recorded over time. Then the shearing rate is decided based on the consolidation characteristic of the soil, the minimum time to failure, and the estimated displacement at the failure.

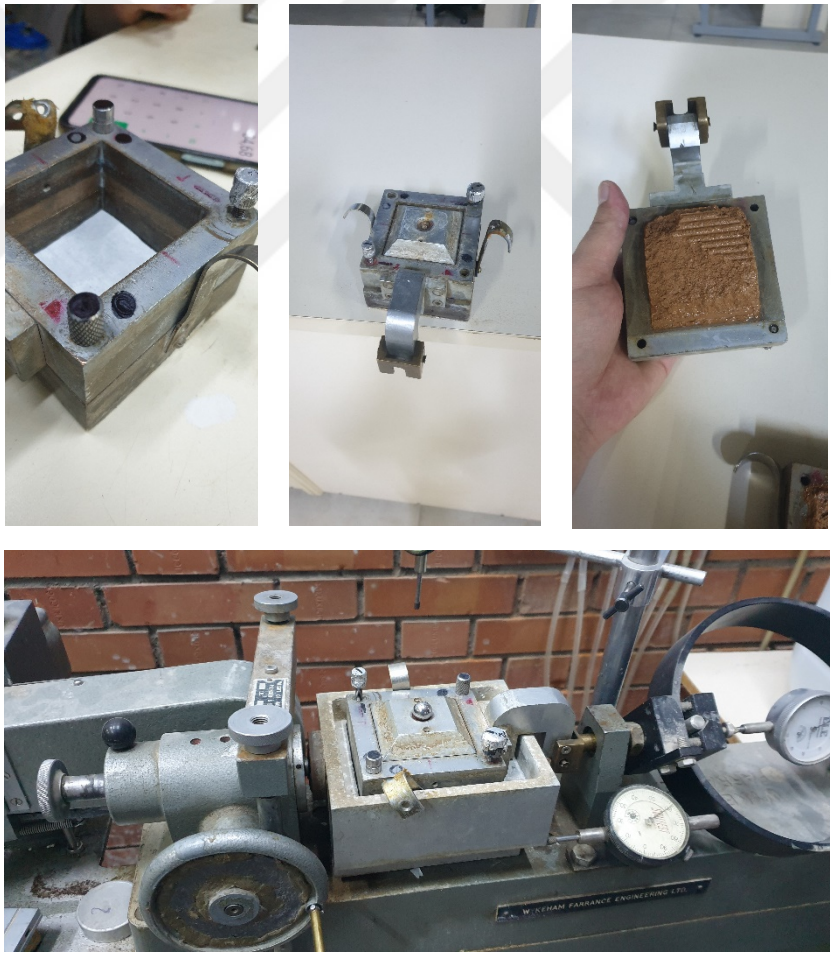

Figure 3.17. Direct Shear Test Apparatus

The undrained direct shear tests were performed using a circular shear box with a diameter of 60 mm. The tests were performed for soil specimens with water content of 17, 19, 21, 23, 25, 28 and 31 percent. The dry density that corresponds to each water content, was taken from the compaction curve. Soil samples were prepared for each different water content and placed in two plastic bags to prevent water loss. Then, all plastic bags were kept in a humidity room for 48 hours for tempering. Soil samples of each different water content were compacted in a shear box at a height of 34.1 mm. 0.06 mm/sec of shearing rate was chosen as ASTM D4767-11 suggests using 1 percent of the specimen height per minute. The soil samples, compacted soil samples, and the testing device can be seen in Figure 3.17 and 3.18.

Figure 3.18. Direct Shear Testing Procedures

The direct shear apparatus is also used to determine undrained interface shear strength between the soil and the concrete block. The same procedures were applied to prepare soil specimens with different water contents. The soils were compacted in the upper part of the shear box, and the concrete block was located at the bottom of the cell.

The concrete was produced using fine sand with a maximum grain size of 0.425 mm, using a water-cement ratio of 0.75, and a sand-cement ratio of 2.5. The same concrete is used that will be used in the following part of the study to produce

small concrete piles. The surface of the concrete block was sanded with P40-type sandpaper and adjusted to exactly match the cutting surface in the direct cutting cell. The same sandpaper was also used for concrete piles to have the same surface friction. Figure 3.19 shows the prepared concrete block and the test set-up for the interface shear strength tests.

Figure 3.19. Interface Direct Shear Test Apparatus

3.4.9. Unconfined Compression Tests

The unconfined compression test is one of the quickest tests to determine the unconfined compression strength (q_u) of cohesive soils. Therefore, it is widely being used by geotechnical engineers.

The tests were performed to determine the unconfined compression strength (q_u) of the soil with different water contents and dry unit weights to define the change in soil strength.

First, similar to the previous soil specimen preparation, the soils with water content of 17, 19, 21, 23, 25, 28, and 31 were prepared and left in the humidity room for tempering for 48 hours. The dry densities that correspond to each water content from the compaction curve were determined. The soil was compacted in 5 equal layers in the mold shown in Figure 3.20. The previous surface of the soil layers was scarred by a spatula to gain interlocking between each layer. 7 specimens with different water contents were prepared and the unconfined compression strength of each of them was determined.

Figure 3.20. Unconfined Compression Specimen Preparation

Second, instead of taking the dry densities for each specimen from the compaction curve, 7 identical specimens were prepared with a water content of 23 percent and corresponding dry density from the compaction curve. Then, three of these samples were air-dried according to Kenanoglu and Toker (2018) until the water content dropped to 17, 19, and 21. Each specimen was weighed from time to time to check if the water content dropped to the required final water content. The specimens reaching the desired water content were placed in two layers of plastic bags to prevent any water loss. The water contents of the other 3 specimens were increased using the water spraying method described by Kenanoğlu and Toker (2018) until they reached values of 25, 28, and 31. Wetted specimens were covered by a bigger mold to prevent direct contact with plastic bags. All prepared specimens were placed in a humidity room for 48 hours of tempering, before starting the test.

Figure 3.21. Tempering Unconfined Compression Test Specimens

The tests were performed with a strain rate of 1 percent of the specimen height (mm) per minute, as 0.72 mm/min. The testing device used for this study can be seen in Figure 3.21.

3.4.10. X-Ray Diffraction (XRD) Test

X-ray diffraction test provides the composition of all different minerals in the clay. The test was performed by the X-ray Diffraction Laboratory in Middle East Technical University's (METU) Central Laboratory.

The clay samples passing through a No. 40 sieve were dried in an oven at 50° for 48 hours. 2θ angle was required to cover a wide range of scanning from 5° to 60° to make sure that the test could contain all types of possible minerals in the clay. The scan speed was chosen as 5° per minute which was the slowest speed of the equipment. Table 3.1 shows the equipment and the measurement condition of the test.

Table 3.1.Measurement Conditions for the XRD Test

Types of equipment		Measurement Condition	
X-Ray Generator	40 kV, 15 mA	Scan Axis	θ / 2θ
Goniometer	MiniFlex 300/600	Scan Range	5° to 60°
Detector	D/teX Ultra2	Scan Speed	5.00° / min
Attachment	ASC-8, 1D scan mode	Step Width	0.02°

3.4.11. Scanning Electron Microscope (SEM)

QUANTA 400F Field Emission SEM instrument with a 1.2 nm resolution, as shown in Figure 3.22, in the Middle East Technical University central laboratory, was used for the test to observe the microstructure and Energy Dispersive X-ray Spectroscopy (EDX) technique used to determine the elemental composition of the soil.

A sample sieved through a No. 40 sieve and dried in a 55-degree oven for 2 days was used for the test. In order to obtain micro images of the specimen, images were taken from various parts of the specimen with x1000 to x25000 magnification. The elements contained in the sample and their amounts were determined by the EDS technique from 5 different parts of the sample.

Figure 3.22. QUANTA 400F Field Emission SEM

3.4.12. Methylene Blue Test

Clay content and the type of clay mineral have a significant effect on soil swelling potential and behavior. Determining the cation exchange capacity (CEC) of the clay is significant and it can be correlated with the soil behavior. The clays with higher CEC are likely to adsorb more methylene blue solution. Also, the adsorbed amount of methylene blue solution is directly related to the grain size distribution of the soil. It is known that decreasing the size of the soil increases the specific surface area (SSA) of the soil, and the amount of solution needed to be absorbed by the soil increases. The following procedure is followed to perform a methylene blue test and determine CEC and SSA.

10 gr methylene blue powder and 1 liter of distilled water were mixed in a beaker for one hour to prepare the methylene blue solution. 30 gr of dry clay and 200 mL of distilled water were mixed for 5 min at a speed of 700 rpm (Çokça,1991). Then the chart in Figure 2.13 was used to perform the test. Figure 3.23 shows the test apparatus, methylene blue solution, and soil solution.

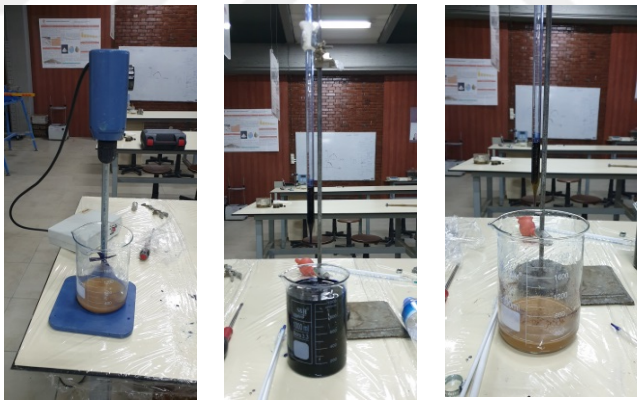

Figure 3.23. Methylene blue test apparatuses

3.4.13. Shrinkage Curve

The shrinkage curve is determined to obtain void ratio change when the soil expands or shrinks with the water content change. 10 specimens of 1 cm in height and 5 cm in diameter were prepared by compaction, using the dry unit weight corresponding optimum water content minus 2% on the compaction curve.

All prepared specimens were carefully covered with membrane, saturated, and placed in a humidity room for 2 days of tempering. The specimens were then taken from the humidity room and allowed to dry slowly at air temperature. After a certain amount of drying, the weights of the specimens were determined when the water content dropped to 39, 30, 25, 21, 18, 15, 12, 10, 7, or 4 percent. For this reason, each sample was weighed continuously to check whether it had dropped to the target weight. Specimens with the desired water content were carefully cut into two pieces; one piece was placed in a 104-degree oven to measure the water content, while the other piece was used for volume measurement.

The submersion technique was used for volume measurements. The portion of the specimen taken for volume measurements was weighed. It was then carefully submerged in melted wax and the entire surface was covered with a thin layer of wax. The wax was allowed to cool to room temperature for a few minutes and the wax-coated specimen was weighed again. The weight measurement in water was carried out with the help of the apparatus with an attached small tray (large enough to hold the wax-coated specimen) as shown in Figure 3.24. Then the beaker, which was more than half full of water, was placed on the scale and the small tray was slowly immersed in the water. Since small air bubbles that may be trapped under the tray may affect the calculations, after the tray was submerged, it was tapped gently with a thin spatula to remove any possible air bubbles. Then the weight of the set-up with the empty tray in the beaker was measured. The wax-coated sample, previously left to cool at room temperature, was then carefully placed on the tray in water, again making sure that no air bubbles were trapped. Then the weight of the set-up with the wax-coated sample on the tray was measured. At the end of the experiment, the temperature of the water was measured with a thermometer to determine the exact density of the water in the beaker. The test was completed after repeating the same process for all 10 specimens.

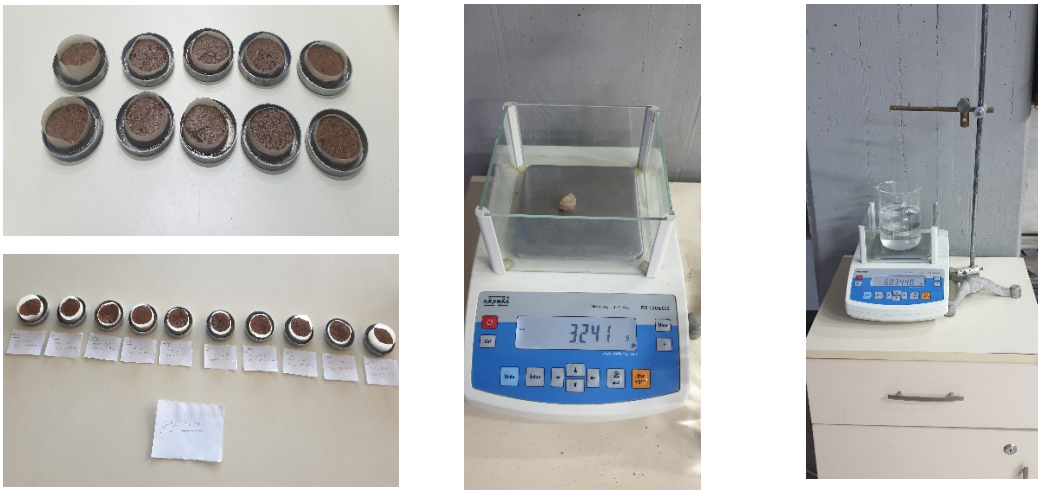

Figure 3.24. Shrinkage curve test process

3.5. Soil Water Retention Curve (SWRC) Development Tests

The soil water retention curve (SWRC) of the soil was developed to determine water content change with suction. SWRC was determined by combining the water content vs suction data obtained using 3 different methods and fitting them with the Van Genuchten fitting method. As mentioned in the relevant sections of the literature review, there are certain ranges in which different methods can provide data points. It is thought that using data points from the suction ranges that each method will provide the best result will help to create a more accurate curve in this context. Therefore, the salt solution method, the filter paper method, and the axis translation method were used to develop the SWRC of the soil.

3.5.1. Vapor Equilibrium Method

The test was carried out using 5 jars, each containing salt solutions of Potassium sulfate (K_2SO_4), potassium nitrate (KNO_3), potassium chloride (KCl), sodium chloride (NaCl), and sodium bromide (NaBr). 10 specimens, 1 cm in height and 3.57 cm in diameter were prepared using the compaction method with a water content of 23 percent and a dry density of 1.462 g/cm^3. 2 specimens were placed in each of 5 different salt solution jars using 2 layers of wire net apparatus as shown in Figure 3.25. A plastic apparatus was placed under each wire net to prevent direct contact of the specimens with the salt solution. Then, as shown in Figure 3.25, the

jars were tightly closed and left for 2 months to reach vapor equilibrium. During the testing process, it was confirmed that these salt solutions contained undissolved salt in solid form.

Figure 3.25. Salt solution test preparations

After 2 months, the cap of each jar was opened and the specimens were taken out. The two specimens were cut in half and one piece of each was placed in a 104-degree oven to measure the water content. The other parts were waxed using the submersion technique (explained under the shrinkage curve section) to measure the volume. The same process was followed for the specimens in all the jars as illustrated in Figure 3.26.

Figure 3.26. Salt solution specimens for water content and volume measurements

3.5.2. Filter Paper Method

The filter paper method was used to measure both matric suction by putting a filter paper between two specimens with direct contact and total suction by putting one filter paper at the top of the specimens with no direct contact. 26 specimens, 1 cm in height and 3.57 in diameter were prepared using the compaction method with a water content of 23 percent and a dry density of 1.462 g/cm^3. 6 specimens were air-dried to reduce the water content to 8, 13, and 19 percent (2 specimens at each water content) by continuously measuring and controlling their weights. 18 specimens 18 specimens were sprayed with water so that their water content increased to 25, 27, 29, 31, 33, 35, 37, 39, and 41 percent (2 specimens at each water content). All specimens were then placed in 3 layers of plastic bags and kept in a humidity room for 2 days for tempering. After two days the samples were taken out of the humidity room. Two samples with the same water content were placed on top of each other with two protective standard filter papers between them and the Whatman No. 42 type of filter paper in the middle. The specimen was taped tightly around the perimeter. Another Whatman No. 42 type filter paper was placed on the specimens after placing a plastic O-ring in between to prevent direct contact. Then the cap of the jar was tightly closed and taped. The same process was done for all samples and a 3-month wait for moisture equilibrium. All test phases can be seen in Figure 3.27.

Figure 3.27. Filter paper test preparations

After the 3-month waiting period, each jar was uncapped, and immediately the filter paper was taken out with tweezers and weighed. It was then placed in a 104-degree oven for water content measurements. The volumes of the specimens were measured both by waxing and submersion techniques and manually using a vernier caliper. First, each specimen was placed on a flat surface of plexiglass. A piece of metal with a known height was placed on it for easy measurement with the caliper. Next, a mold with a pre-calculated diameter and length was placed over the specimen and pushed at a right angle to get the part of the specimen into the mold. The specimen pieces outside the mold were collected and placed in a 104-degree oven for water content measurement. The height of the specimen pieces that remained inside the mold and thus had a diameter equal to the inner diameter of the mold was measured using a caliper. Then, these pieces were covered with melted wax and their volumes were measured using the submersion technique.

Finally, the filter papers were taken out of the oven and weighed twice, once immediately and again after the containers in which they were placed had cooled down. Thus, both total and matric suction were calculated using equations from equations 2.11 to 2.17.

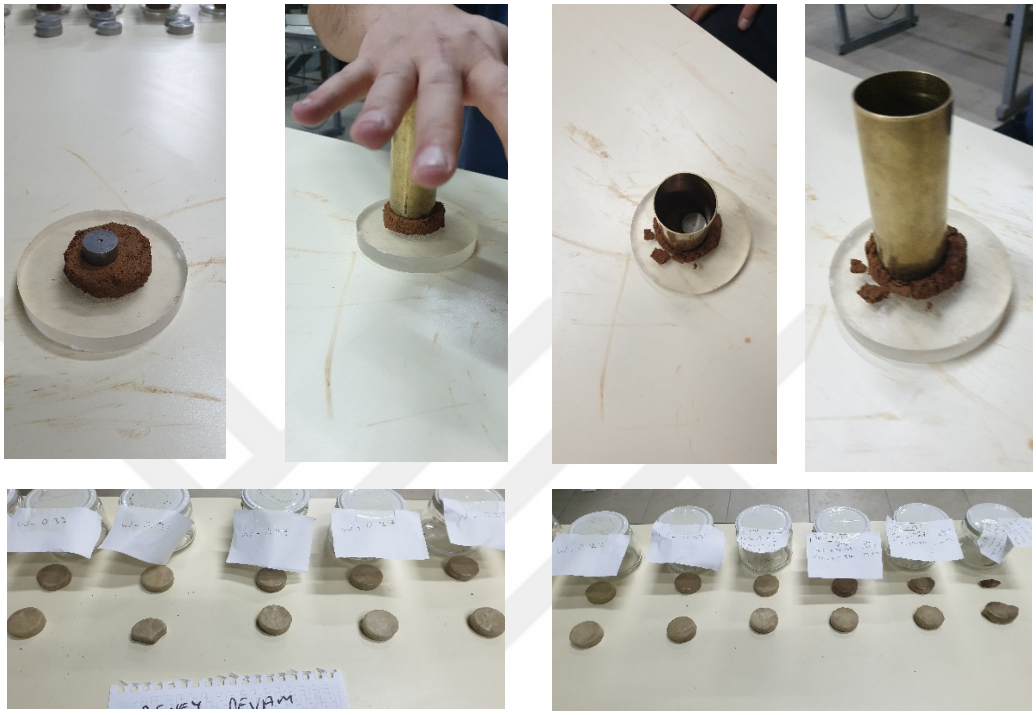

Figure 3.28. Filter paper method volume measurements at the end of the test

3.5.3. Axis Translation Method

The most popular suction method, the axis translation method, was used to measure the gravimetric and volumetric water content of the specimen under different suctions. For the test, an odometer setup with a high air entry ceramic with a capacity of 15 bar at the bottom was used. First, the setup was completely filled with de-aired water and kept under a pressure of 900 kPa for 24 hours to ensure that the ceramic was completely saturated with water. A mold with an inner diameter of 3.57 cm was weighed in which the sample would be compacted. The soil specimen was prepared by compaction in a mold with a height of 0.8 cm, a water content of 23 percent, and a dry density of 1.462 g/cm^3. The mold with the specimen was weighed and then carefully placed on the ceramic disk. To ensure

that no specimen parts would fall out of the mold each time the mold was placed in the setup or removed for weighing, this process was done with the setup lying on its side as shown in Figure 3.29 (e). After the mold was placed in the setup, the soil was gently pressed against the ceramic with an apparatus to ensure that the specimen and the ceramic disc were in contact. A suction was applied to the specimen and the specimen was allowed to equilibrate under this suction for 3 weeks. During this waiting phase, high-pressure air can diffuse in the water and form air bubbles in the low-pressure areas under the ceramic. (Kenanoglu, 2023). To prevent this, the setup was flushed daily with vacuumed de-aired water to remove any air bubbles from the system. After equilibrium was achieved, the specimen was removed, and its height was measured and weighed. The water content and volumetric change of the sample with known initial weight and height were determined. The same process was repeated for 5 different suction values, decreasing the applied suction each time. Then it was increased each time until the first applied suction value was reached again. Data points for SWRC were created by measuring the water content and volume change of the specimen for the corresponding suctions.

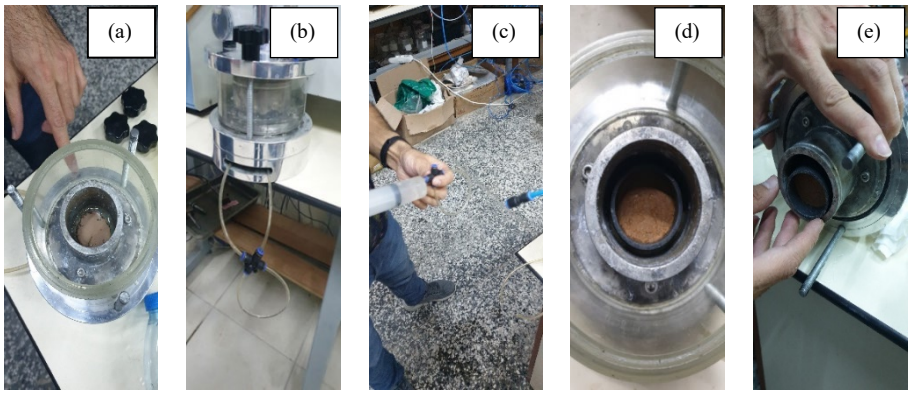

Figure 3.29. Axis translation method, test preparation

3.6. Determination of Barcelona Basic Model Parameters

The BBM model can be used to predict the complex behavior of expansive clays since it takes into account the effects of suction on strength and deformation in addition to the engineering parameters of other conventional constitutive models.

On the other hand, determining BBM parameters requires long, complex, and expensive controlled suction experiments. For this reason, the methodology proposed by Kenanoglu and Toker (2023), which offers an easier and more practical solution for determining the BBM parameters, was used in this study. All BBM parameters in Table 2.20 were determined by performing the following additional experiments and using the calibration methodology.

3.6.1. Additional Laboratory Tests to Determine Barcelona Basic Model Parameters

Kenanoglu and Toker (2024) state that, soil laboratory testing for unsaturated soils requires costly equipment and long testing time. Therefore, they proposed a practical framework to determine BBM parameters using a straightforward and rapid process rather than suction-controlled tests, which are complex and require a long testing time. Their proposed approach for determining BBM parameters and tests done in this study are presented in Table 3.2.

Table 3.2. Kenanoglu and Toker (2024) proposal for determining BBM parameters and tests done in this study

Kenanoglu and Toker (2024) proposal	**Test done in this study**
1 standard oedometer test	One saturated 1-d consolidation test
3 unsaturated K_0 tests	Three unsaturated quick consolidation tests with the water content of 19, 21, and 23 percent
2 triaxial CD tests	Two triaxial CD tests under 100 and 400 kPa confining pressure
Evaporation tests	Evaporation test to determine critical water content
Soil water retention curve	Axis translation method, filter paper method, salt solution method

3.6.1.1. Evaporation Test to Determine Critical Water Content

A soil specimen of 1 cm in height and 4.3 cm in diameter was compacted in a mold with an initial water content of 23 percent and a dry density of 1.462 g/cm^3 and saturated. The saturated specimen in the mold was placed on a digital scale and allowed to air-dry. The decrease in specimen weight was noted by taking readings at 2-hour intervals. The corresponding water content values for each reading were calculated. Water content change over time is plotted on a graph and critical water content is determined from the rate of mass decrease by using Knight et al. (1995) method Figure 3.30.

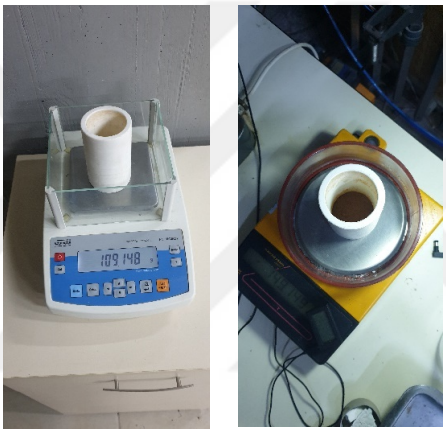

Figure 3.30. Evaporation test measurements

3.6.1.2. Unsaturated 1-D Consolidation Test

The unsaturated 1-D consolidation test was performed following the standard consolidation test procedure but without the water saturation step. The experiment was carried out on 3 specimens with an initial water content of 23 percent and a dry density of 1.462 g/cm^3 which were allowed to air dry to critical water content, critical water content +2% and +4%. Unlike the standard consolidation experiment, there was no waiting 24 hours at each load increment. The experiment was completed quickly as the vertical deformations of the specimen under load usually stopped after a few minutes. To prevent the specimen from drying out during the experiment and to keep the water content constant, the oedometer ring containing the specimen was covered with a nylon bag.

3.6.1.3. Simplified Unsaturated Triaxial Tests

Six specimens of approximately 3.6 cm and 7.2 cm in diameter and height, with a water content of 23 percent and a dry density of 1.462 g/cm^3 were prepared by compacting in 5 layers. 2 samples were air dried to w_{crt}, 2 samples were air dried to w_{crt} +2 and 2 samples were air dried to w_{crt} +4. Samples reaching the desired water content were wrapped in two layers of nylon bags and placed in a humidity room for tempering as shown in Figure 3.31. One of the samples prepared for each water content was sheared under 100 kPa and the other under 400 kPa confinement pressure with a strain range of 1 percent. The triaxial test setup and the deformed shape of some specimens after the test can be seen in Figure 3.32.

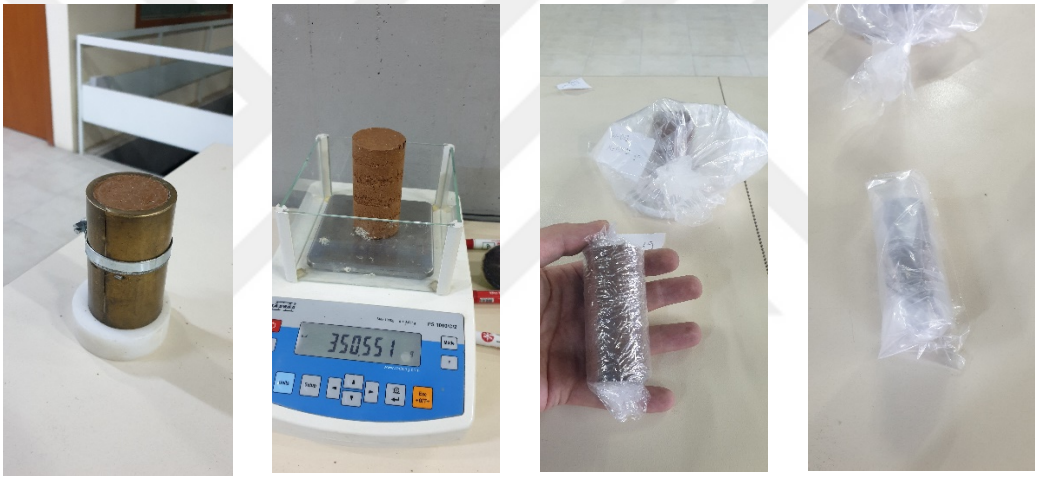

Figure 3.31. Specimen preparation for unsaturated triaxial tests

Figure 3.32. Unsaturated triaxial testing process

3.6.1.4. Saturated Triaxial CD Tests

2 specimens of approximately 3.6 cm in diameter and 7.2 cm in length were prepared with a water content of 23 percent and a dry density of 1.462 g/cm^3. The test was performed according to the ASTM D7181 standard. The test was performed for 100 kPa and 400kPa effective confining pressure. The strain rate was chosen to ensure drainage during the experiment Figure 3.33.

Figure 3.33. Triaxial CD test setup

3.6.2. Calibration of Barcelona Basic Model Parameters

One saturated 1-D consolidation test, two triaxial CD tests under 100 and 400 kPa confining pressure, three unsaturated quick consolidation tests with the water content of 19, 21, and 23 percent, three unsaturated quick triaxial tests with the initial water content of 19, 21 and 23 percent under 100 kPa, three quick triaxial tests with the initial water content of 19, 21 and 23 percent under 400 kPa, evaporation test and the soil water retention curve dataset were used for the calibration of the Barcelona Basic Model parameters according to methodology provided by Kenanoglu and Toker (2023).

3.6.2.1. The slope of elastic compression line (κ)

The stress-strain plot from the saturated and unsaturated quick 1-D consolidation and triaxial CD tests was used to determine the parameter κ. The slope of the

recompression lines (C_r) from the unloading and reloading portion of the stress-strain plot was determined. Then, the C_r was converted to the slope of the elastic compression line (κ). K_0 is assumed to be equal to 1- sinϕ.

3.6.2.2. The slope of the critical state line (M)

The slope of the critical state line was determined using the triaxial CD tests. The deviatoric stress (q) and the mean effective stress (p`) at the failure were determined for each test conducted with 100 kPa and 400 kPa confining pressure. A straight line is fitted to the two data points corresponding to these points. The slope of the line was calculated to determine the parameter M.

3.6.2.3. The Slope of the Saturated Virgin Compression Line (λ(0))

The Barcelona Basic Model with previously determined parameters of the slope of the elastic compression line (κ) and the slope of the critical state line (M), was used to obtain the best fit for the experimental triaxial CD data by changing the λ(0). The λ(0) value that would give the least sum of squares of differences between the BBM fitting and the actual experimental results was determined using the Excel goal seek function.

3.6.2.4. Slope of Apparent Tensile Strength vs. Suction (k)

1-D quick unsaturated consolidation tests were used to determine the initial parameter of k before the optimization process. The apparent cohesion of the soil according to the experimental data were calculated. Then the apparent cohesion value was used to determine the suction contribution to the cohesion. The suction values (s) were determined from the soil water retention curve. The p_s values against the suction were plotted and the k parameter to have a linear fit determined.

3.6.2.5. Loading-Collapse (LC) Parameters (r, β)

The parameter of the r was determined using the unsaturated 1-D consolidation test with the lowest water content and the 1-D saturated consolidation test. The slope of the virgin lines (C_c) was determined for both tests and the value of r was

determined as it is the ratio of the slope of the virgin lines. This value is used as the initial value for the parameter of r before the general optimization process.

All 1-D consolidation tests performed at the different initial water contents were used to determine the parameter of β. The slope of the virgin lines (C_c) for each test was determined. Then they were converted to the mean stress axis to determine λ(s). The suction values were taken from the soil water retention curve for the corresponding water contents.

3.6.2.6. The preconsolidation pressure (p_0*)

The preconsolidation pressures (p_0) were determined for each unsaturated 1-D consolidation test. The saturated preconsolidation pressure (p_0*) was determined using the predefined p_0 values found for each unsaturated 1-D consolidation test. The reference stress (p_c) was defined as an arbitrary value of 30 kPa, which provides a reasonable shape of shear curves for the quick triaxial tests before the optimization process.

3.6.2.7. General optimization process for BBM parameters

All BBM parameters were determined by optimizing for r, β, p_c, p_0*, and k by keeping κ, λ(0), and M fixed. The optimization aimed to determine the BBM parameters that would give the closest approximation to the results of all unsaturated 1-D consolidation and quick triaxial experiments. Summing the square of the differences between all predicted results and the experimental results, the parameters required to minimize this value were determined with the help of the Microsoft Excel goal seek function.

CHAPTER 4

TEST RESULTS AND DISCUSSION

4.1. Soil Collection

As can be seen from the literature, expansive soils are defined as problematic soils, and the prediction of the behavior of soils with a high percentage of swelling under different conditions can be more challenging than soils with a low percentage of swelling. Soil samples were collected from 10 different regions of Ankara province for this study. In addition, since soils with high swelling potential and pressure will have higher effects on pile foundations placed in them, the effect of soil swelling on pile foundations can be more easily measured in experiments to be conducted in the later stages of this study. Accordingly, soil samples were collected from various areas of Ankara. Modified free swell tests and Atterberg tests, which are commonly associated with the degree of swelling in the literature, were performed to determine the degree of swelling of each soil sample collected. The modified free swell index (MFI) and Atterberg test results for each soil sample collected can be seen in Table 4.1.

Table 4.1. Results of some rapid tests on the collected soils

	Coordinates (Lat (N), Lon (E))	Liquid Limit (%)	Plastic Limit (%)	Plasticity Index (%)	USCS Classification	Modified Free Swell Test (%)	Swelling Potential (%)
Golbasi-1	39°47'09"N 32°50'18"E	61	25	36	CH	50	X
Golbasi-2	39°47'01"N 32°50'19"E	66	26	40	CH	50	7
Batikent	39°56'53"N 32°44'01"E	X	X	X	X	25	X

Table 4.1. (continued)

Yuvakoy	40°00'44"N 32°44'07"E	74	30	44	CH	55	X
Yuvakoy-2	40°00'56"N 32°44'37"E	X	X	X	X	10	X
ODTU	39°53′10″N 32°47′02″E	X	X	X	X	17	X
Cubuk-1	40°11'48"N 33°08'32"E	73	30	43	CH	50	10
Cubuk-2	40°11'21"N 33°08'44"E	42	22	20	CL	20	X
Botanic Garden	39°53'25"N 32°44'27"E	47	24	23	CL	33	X
Etimesgut Gulyurt	39°47'49"N 32°33'05"E	46	22	26	CL	33	X

According to the modified free swell test and plasticity index values, the highest degree of swelling was observed in soil samples from Yuvakoy and Cubuk. The non-swelling behavior of the second soil sample taken from the Yuvakoy area was interpreted as a sign of changing geology in the region. Therefore, it was decided to work with clays from the Cubuk region to be used in the rest of the study.

After 4 meters of excavation in the area, soil samples were taken from 3 different profiles at 50 cm intervals to determine the water content change over depth. Figure 4.1 shows the variation of water content with depth, according to water content measurements conducted in the soil laboratory.

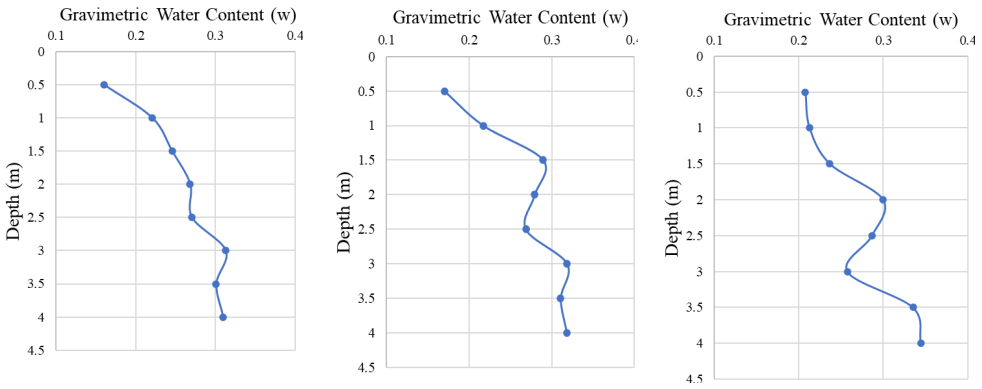

Figure 4.1. Water content change with depths in Cubuk, Ankara

4.2. Thornthwaite Moisture Index (TMI) Determination for Cubuk-Ankara

It was stated in the literature that the swelling behavior of soils is mostly observed in arid and semi-arid climate zones. Accordingly, the TMI value was calculated to determine the climate zone of the Cubuk region where the soil samples were taken. Monthly average temperature data (t) are taken from the Turkish State Meteorological Service website to estimate Ankara's potential evapotranspiration (PE). The equations from Eq 4.1 to Eq 4.5 are used to calculate PE, adjacement factor (a), heat index (I), water balance, storage, deficit, surplus, and TMI. Each month's latitude correction factors are taken from the state hydraulic work (DSI) technical bulletin #105 as can be seen in Appendix B.

The Thornthwaite Moisture Index (TMI) is calculated from the following Equations from 4.1 to 4.9. Table 2.1 shows different types of climate types according to the TMI.

$$PE = 16\left(\frac{10t}{I}\right)^{a} \times Latitude\ correction\ factor \qquad \textit{(Eq. 4.1)}$$

$$a = 0.000000675 \times I^3 - 0.0000771 \times I^2 + 0.49239 \qquad \textit{(Eq. 4.2)}$$

$$I = \sum_{i=1}^{12} i\ , where\ i = ({}^{t}/_{5})^{1.514} \qquad \textit{(Eq. 4.3)}$$

$$i = ({}^{t}/_{5})^{1.514} \qquad \textit{(Eq. 4.4)}$$

$$TMI = \frac{100(\sum Surplus) - 60(\sum Deficit)}{\sum PE} \qquad \textit{(Eq. 4.5)}$$

$$Water\ Balance = Rainfall - PE \qquad \textit{(Eq. 4.6)}$$

$$Storage = Storage\ of\ previous\ month + Water\ Balance\ for\ month \qquad \textit{(Eq. 4.7)}$$

Storage=0 if result is less than 0, =100 if result ≥ 100 mm

$$Deficit = |Water\ Balance| - Storage\ of\ previous\ month \qquad \textit{(Eq. 4.8)}$$

If storage for month = 0

$$Surplus = Water\ Balance + Storage\ of\ previous\ month - 100 \quad (Eq.\ 4.9)$$

If storage for month = 100

As a result, TMI was found as -22.4 and the site is considered a semiarid climatic type according to Table 2.1

Table 4.2. TMI calculation spreadsheet for the Cubuk region

	January	February	March	April	May	June	July	August	September	October	November	December	TOTAL
t (Average Temperature Data, °C)	0.300	1.700	5.700	11.300	16.100	20.000	23.400	23.500	19.000	13.200	7.300	2.600	
I (Heat Index)	0.014	0.195	1.219	3.437	5.873	8.157	10.346	10.413	7.547	4.348	1.773	0.372	53.694
a (Adjusment Factor)													1.337
Latitude Correction Factor for 40 N	0.840	0.830	1.030	1.110	1.240	1.250	1.270	1.180	1.040	0.960	0.830	0.810	
PE (Potential Evapotranspiration)	0.284	2.854	17.850	48.023	86.116	116.014	145.398	135.866	90.127	51.124	20.023	4.915	718.595
Rainfall (mm)	39.900	35.100	39.700	41.800	51.400	36.700	14.100	12.700	17.900	27.100	31.800	44.200	392.400
Water Balance	39.616	32.246	21.850	-6.223	-34.716	-79.314	-131.298	-123.166	-72.227	-24.024	11.777	39.285	
Storage	90.677	100.000	100.000	93.777	59.061	0.000	0.000	0.000	0.000	0.000	11.777	51.062	
Deficit	-	-	-	-	-	20.253	131.298	123.166	72.227	24.024	-	-	370.968
Surplus	-	22.923	21.850	-	-	-	-	-	-	-	-	-	44.773

4.3. Soil Index and Classification Tests

4.3.1. Atterberg Limit Tests

Liquid limit (LL) and plastic limit (PL) were found as 76 and 24 percent respectively. The plasticity index (PI) which is the difference between LL and PL, was found as 52. The soil is classified as high-plasticity clay according to the USBR classification system using the plasticity index and liquid limit as shown in Figure 4.2.

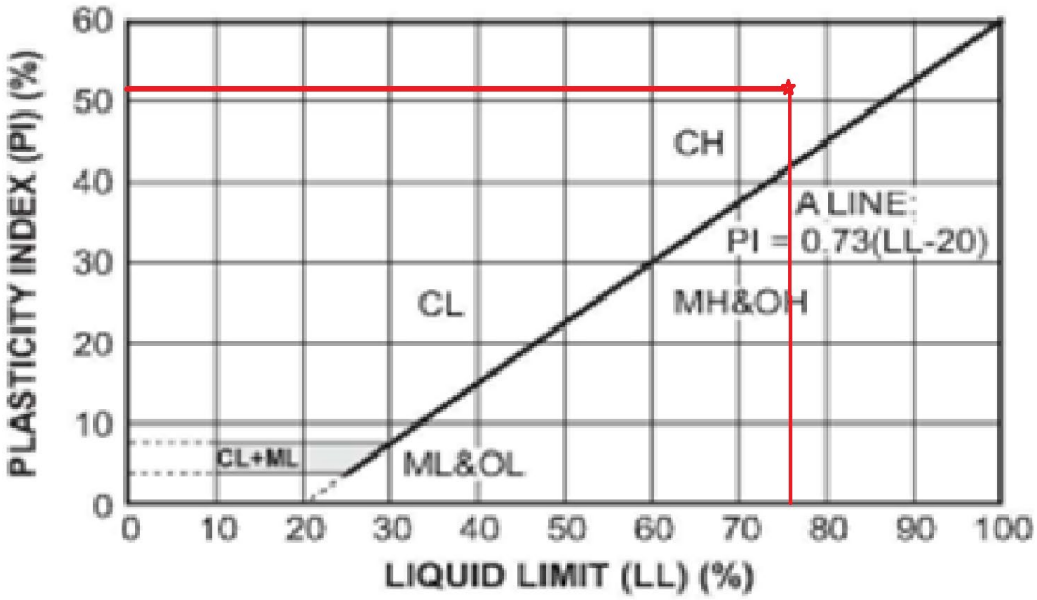

Figure 4.2. USBR plasticity chart

4.3.2. Shrinkage Limit Tests

According to the linear soil shrinkage test result, the shrinkage limit value was found to be 11%. The shrinkage limit was found to be 12% using mercury technique. Finally, the shrinkage limit was calculated as 12% using the water submersion technique recommended by ASTM D4913-18 standard. By evaluating all test results, the shrinkage limit of Ankara Cubuk clay was determined as 12%.

4.3.3. Specific Gravity

The specific gravity was found to be 2.778 after 3 experiments and averaging the results. The standard deviation was found to be 0.004, within acceptable limits according to relevant ASTM standards.

4.3.4. Grain Size Distribution

Sieve analysis to determine the coarse grain size and hydrometer analysis to determine the fine grain size of the soil were performed and matched up to draw the entire grain size distribution of the soil as shown in Figure 4.3. According to the USCS classification, clay content (particle size less than 0.002 mm) is found as 61 percent.

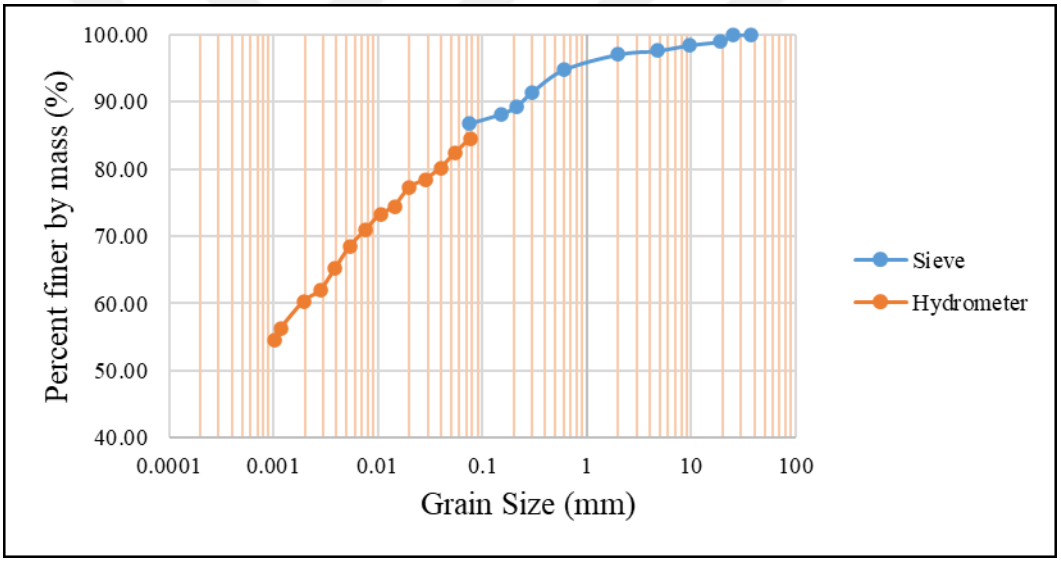

Figure 4.3. Grain size distribution

4.3.5. Activity of the soil

The activity of the soil is calculated as 0.85 as it is the ratio of the plasticity index (PI) to the clay content. According to Table 2.9, the soil with an activity of 0.85 can be classified as normal. According to Table 2.10, the soil has an activity close to the illite type of clays.

4.3.6. Compaction Test

The standard compaction test was performed to determine the compaction curve as shown in Figure 4.4. The optimum water content and maximum dry density found from the curve as 25 percent and 1.498 gr/cm^3 respectively. The degree of saturation at the optimum water content and the maximum dry density was found to be 84 percent.

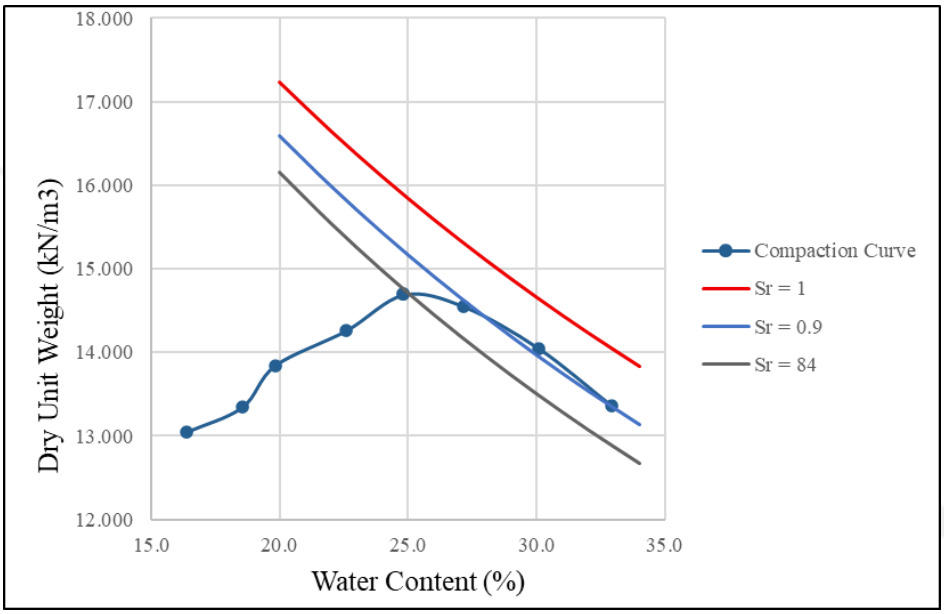

Figure 4.4. Compaction curve

4.4. Swell Potential-Pressure

In the experiment performed in the oedometer setup, at the beginning, the Cubuk clay was allowed to swell in water until it was completely saturated and no further swelling of the clay was observed. The swelling potential of the clay was thus found to be 9.4 %. Then, a pressure of approximately 32 kPa was applied to the sample and allowed to stabilize the vertical movement of the sample and then the swelling potential of the sample under this pressure was determined. The same procedure was repeated with pressure of 64, 96, 126, 142 and 157 kPa as shown in Figure 4.5. The pressure value that returns the sample to its initial volume (height) before it is allowed to free-swell was defined as 157 kPa as the swelling pressure of the Cubuk clay.

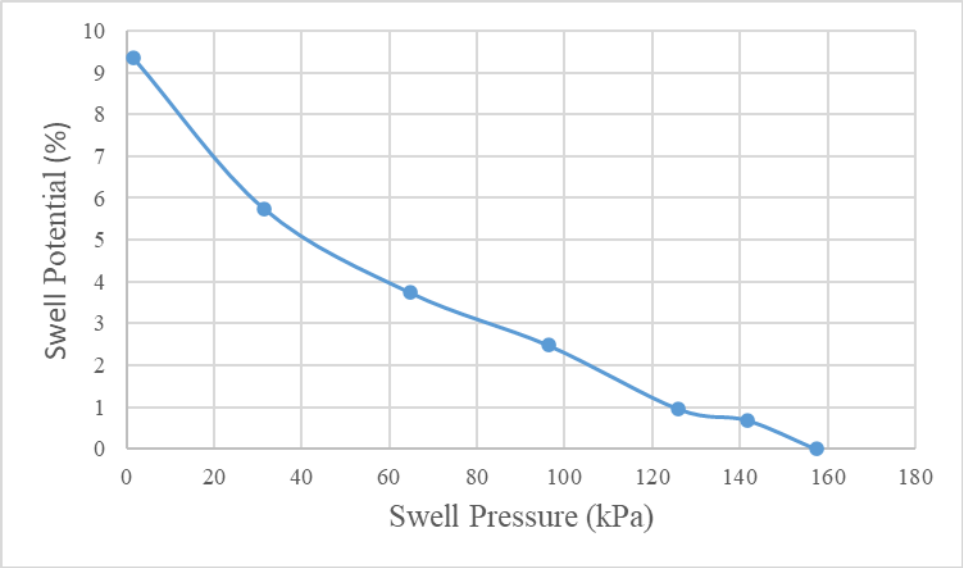

Figure 4.5. Swelling Potential vs Pressure

4.5. Hydraulic Tests

4.5.1. Shrinkage Curve

Saturated samples were air dried to different water contents. The volume, the unit weight, and the void ratio of the samples at each water content were determined. Then Equation 4.10 proposed by Fredlund et al. (2002), was used to fit the void ratio versus water content graph as shown in Figure 4. 6.

$$e(w) = a\left(\left(\frac{w}{b}\right)^{c} + 1\right)^{1/c} \qquad \textit{(Eq. 4.10)}$$

Where:

a ,b, c : fitting parameters

w : gravimetric water content

For each water content, the squares of the difference between the actual void ratio and the predicted void ratio were summed to find the total error. The constant fitting parameters that can give the minimum total error are found by using Excel's goal seek function. The fitting parameters of a, b, and c were found to be 0.55, 0.179, and 1.7 respectively.

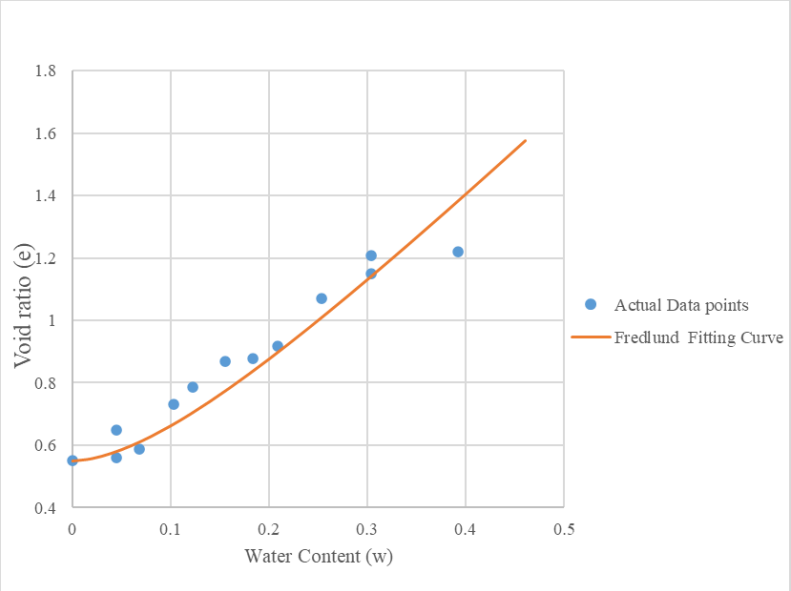

Figure 4.6. Shrinkage curve

4.4.2. Evaporation Test

The evaporation rate of a saturated sample on a digital scale is determined by taking a weight measurement at 2-hour intervals. Then, the water content values over time were plotted as shown in Figure 4.6.

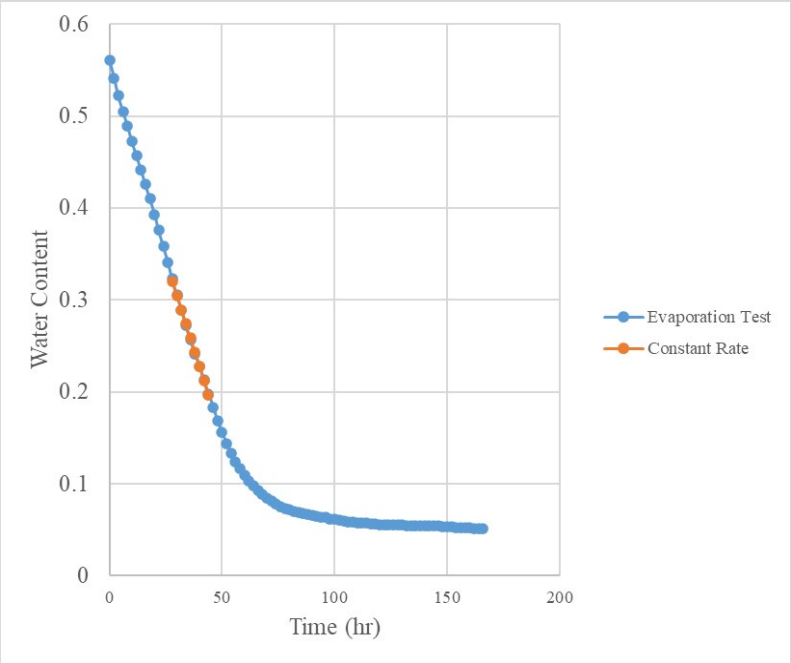

Figure 4.7. Evaporation test

The orange line in Figure 4.7 shows the region where the evaporation rate is approximately constant. The linear section was extended, and the deviation from the normal data was found to be as critical water content (w_{crt}) when it was 1 percent. The w_{crt} was assigned as 19.1 percent. Additionally, the water content of the sample, which was left to air-dry for about 7 days, was calculated as 5 percent at the end of the experiment.

4.4.3. Soil Water Retention Curve

Soil water retention curve (SWRC) was obtained by combining water content and suction values obtained using axis translation, filter paper, and salt solution methods.

4.4.3.1. Axis Translation Method

The axis translation method was used to generate both the wetting curve and the drying curve. The test was conducted for a specimen with an initial water content of 23 percent and a dry density of 1.462 g/cm^3. After several trials, it was found that the suction value at which the initial water content of the specimen would not change was 900 kPa. Then, the test started by applying 900 kPa suction to the specimen and sealed it for 1 month to ensure that the specimen had reached equilibrium. The specimen was then taken out for water content and volume measurements. The same procedure was followed for 500 kPa, 200 kPa, 100 kPa, and 50 kPa suctions. Decreasing the suction increased the water content of the specimen and 5 data points for the wetting curve were obtained. Then, the same procedure was applied from 50 kPa to 900 kPa for the drying curve. A graph in Figure 4.8 shows the data points obtained from both the wetting and drying portion of the test. These are the scanning curves between 50 kPa and 900 kPa. Both data sets from the wetting and drying curves found using this method were then used to obtain the main curve.

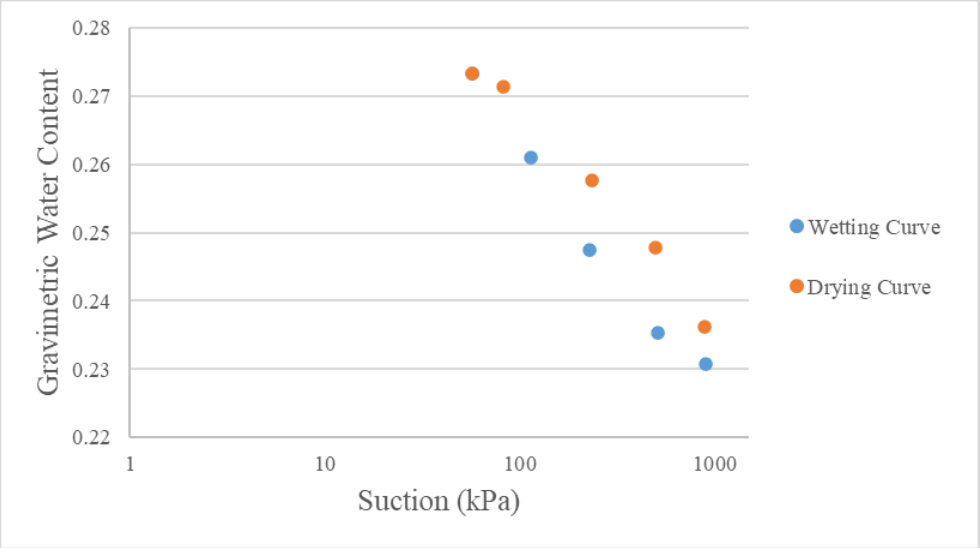

Figure 4.8. SWRC data points gained from the axis translation method

4.4.3.2. Filter Paper Method

The test was used to determine both matric suction and total suction with vapor equilibrium. Total suction values were obtained from filter paper placed over the specimens without direct contact with the specimens. Matric suction values were obtained from the filter paper placed between the samples. Suction values were calculated from the water contents of the filter papers using Equation 4.11 and 4.12 specified in ASTM D5298 for the Whatman No.42 filter paper. If the measured water content of the filter paper was less than 45.3 percent, Equation 4.11 was used, whereas if it was greater than 45.3 percent, Equation 4.11 was used.

$$\Psi = 5.327 - 0.0779 w_f \qquad \textit{(Eq. 4.11)}$$

$$\Psi = 2.412 - 0.0135 w_f \qquad \textit{(Eq. 4.12)}$$

Where;

Ψ : Suction (kPa)

w_f : Water content of the filter paper

The water content of each filter paper (w_f) was calculated using Equations 4.13 and 4.14.

$$M_f = M_2 - T_h \quad \textit{(Eq 4. 13)}$$

$$M_w = M_1 - M_2 + T_h - T_c \quad \textit{(Eq 4. 14)}$$

Where;

M_f : Mass of dry filter paper (g)

M_2 : Dry total mass (g)

T_h : Mass of the hot container (g)

M_w : Mass of the water in the filter paper (g)

T_c : Mass of the cold container (g)

The SWRC data points obtained according to the matric and total suction measurements obtained using the filter paper method are shown in Figure 4.9. As can be seen from the figure, the data points obtained with the filter paper method show a general trend, but some deviations from the general trend are obvious in some tests. The high sensitivity of the experiment is one of the major challenges to performing this experiment. However, these points showing a clear deviation from the trend were not used later when all the data points were collected and the SWRC was generated.

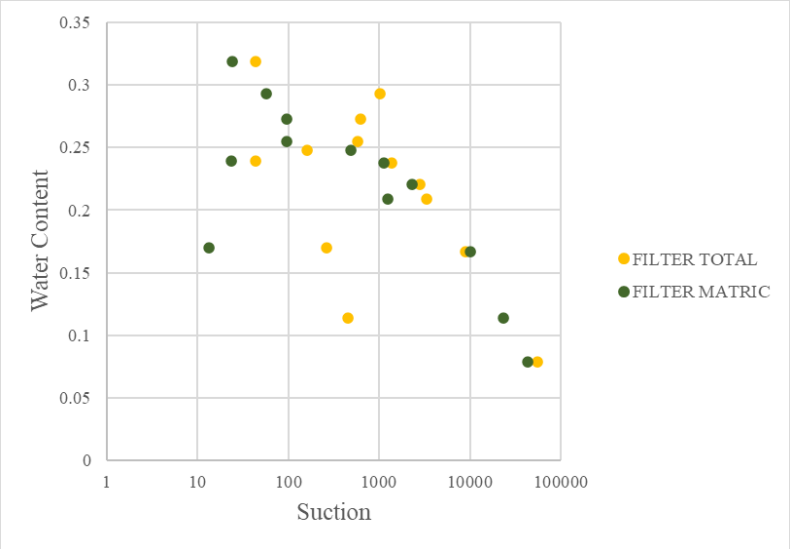

Figure 4.9. SWRC data points gained from the filter paper method

4.4.3.3. Salt Solution Method

5 data points at high suction values for SWRC were obtained by using 5 different salt solutions Fig 4.10. Since the amount of suction varies with the relative humidity, the relative humidity of each sample concerning temperature was found from Greenspan's (1977) tables, and the suction values were calculated using Equation 4.15 according to ASTM D5298.

$$\Psi = \frac{-\gamma_w RT}{v} \ln(RH) \qquad \textit{(Eq 4.15)}$$

Where;

Ψ : Suction (kPa)

R : Ideal gas constant (8.31432 Joules/mole·K)

T : Absolute temperature (Kelvin)

v : Volume of 1000 moles of liquid water (0.018 m^3)

RH : Relative humidity

Table 4.3. Relative humidity of salts and corresponding total suctions (ASTM E104.02, Kenanoğlu, 2023)

Salts	Relative Humidity	Suction (kPa)
KNO_3	93.6	8932
KCl	84.2	23226
K_2SO_4	97.3	3697
NaCl	75.3	38313
N_2Br	57.6	74502

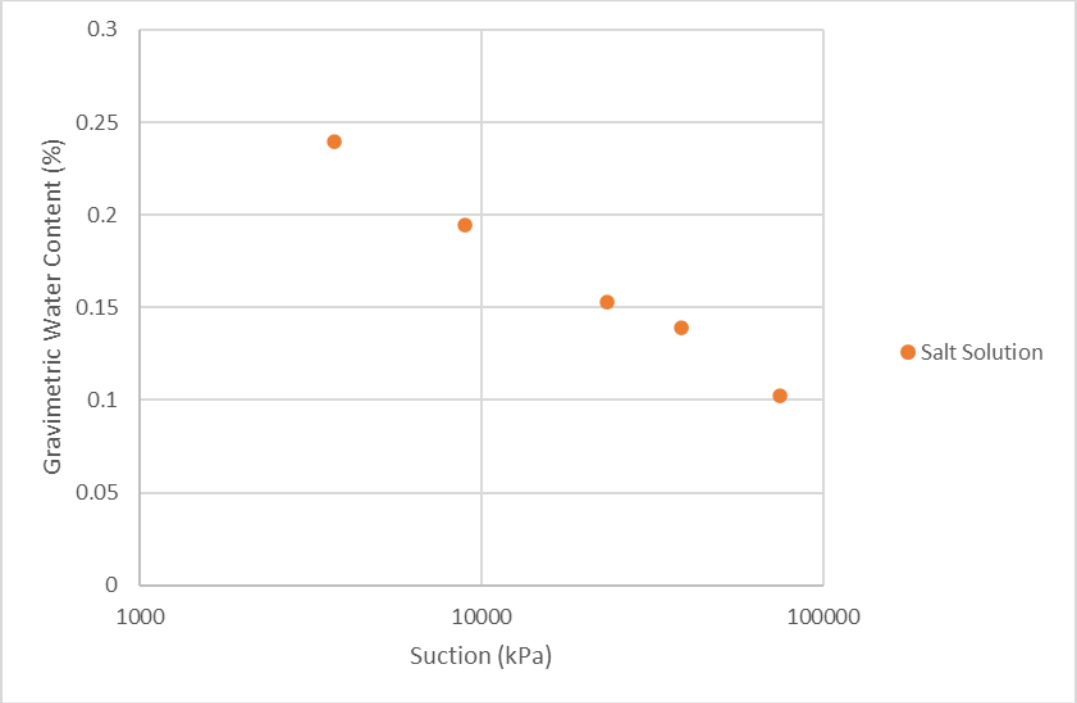

Figure 4.10.SWRC data points gained from the salt solution

4.4.3.4. SWRC Determination

All data obtained using the axis translation, filter paper, and salt solution methods mentioned above were combined as shown in Figure 4.11. As can be seen from the figure, some data points (obtained from the filter paper method) distort the trend. These points (shown with red cross) were removed from the data set and Figure 4.12 was created showing all data points obtained for the Ankara-Cubuk clay. To obtain a better fit, the point where the water content in the saturated state is 32% and the suction is 0 was manually added to Figure 4.12. Then, Figure 4.13 shows the variation with volumetric water content and Figure 4.14 shows the variation of the degree of saturation with suction.

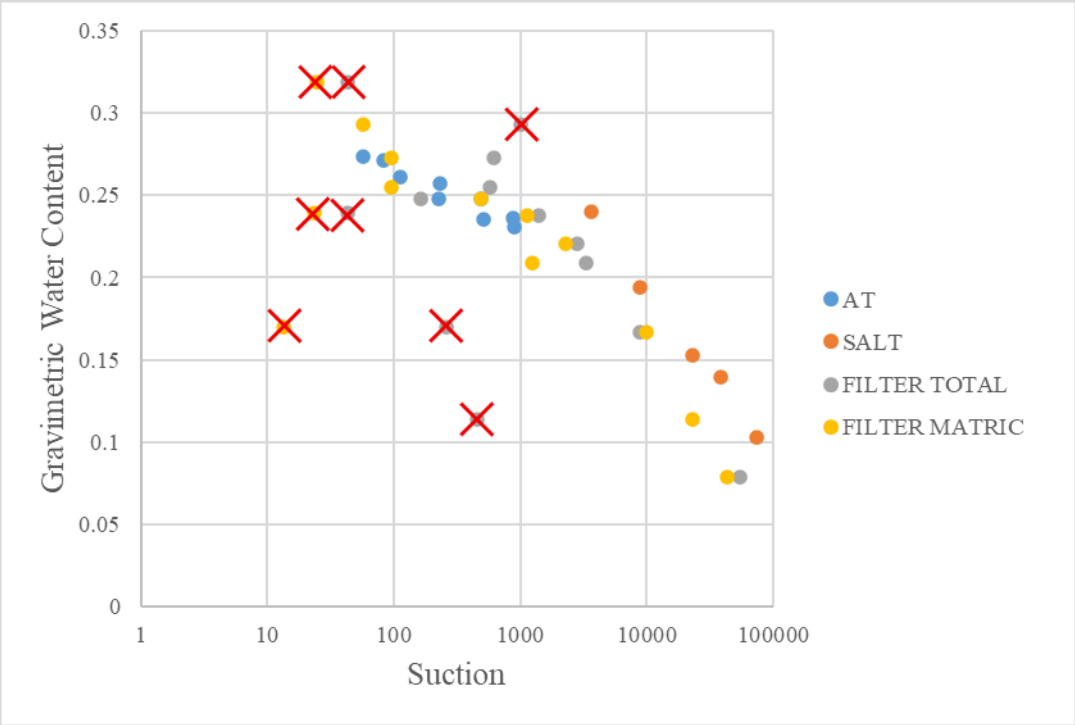

Figure 4.11. SWRC all data points

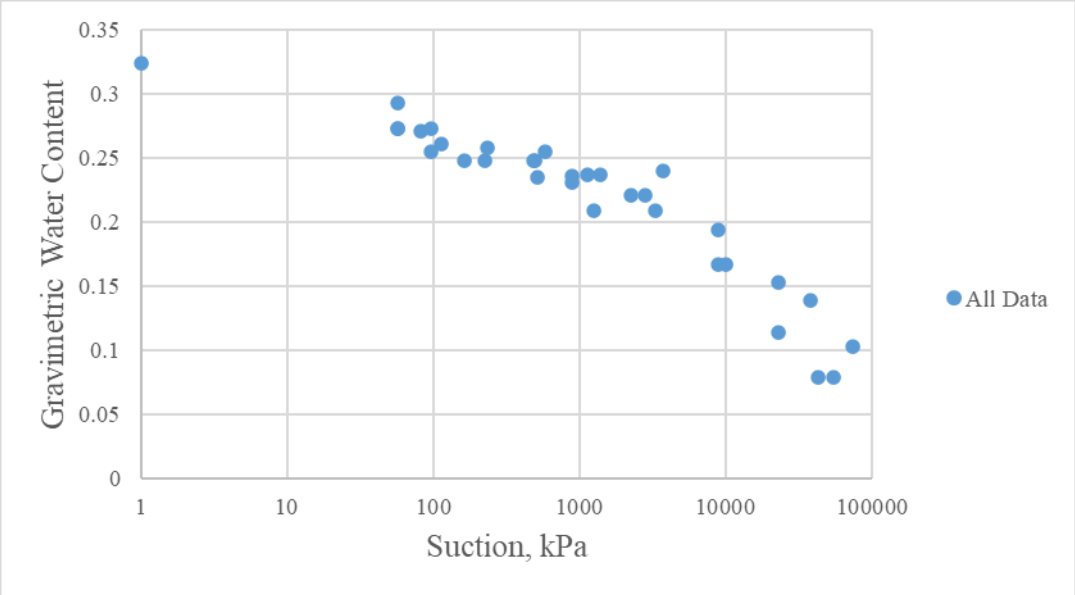

Figure 4.12. Ankara-Cubuk clay SWRC all data points

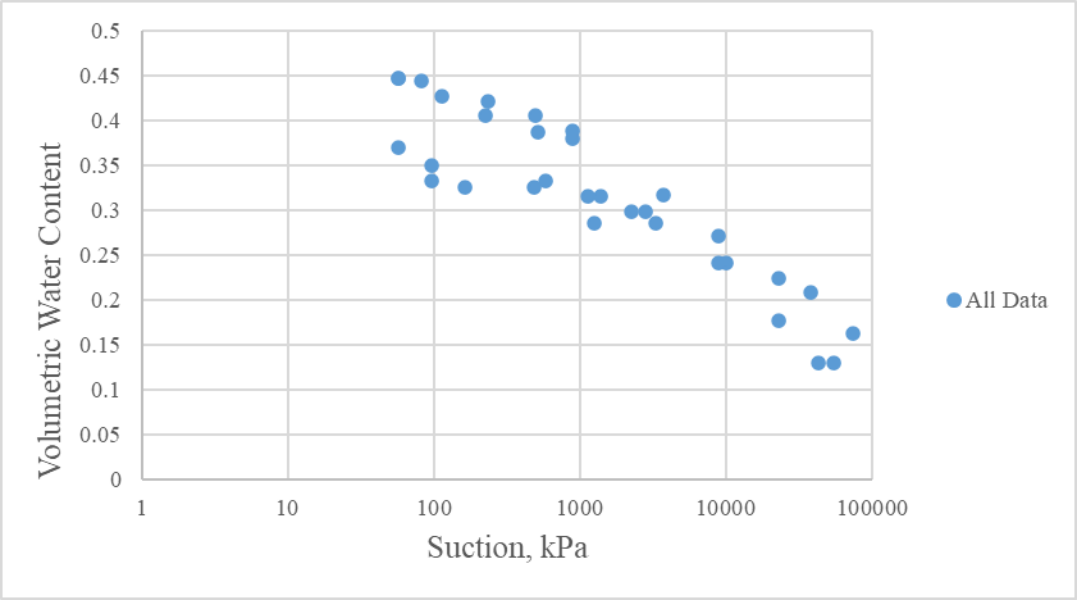

Figure 4.13. Ankara-Cubuk clay SWRC all data points with volumetric water content

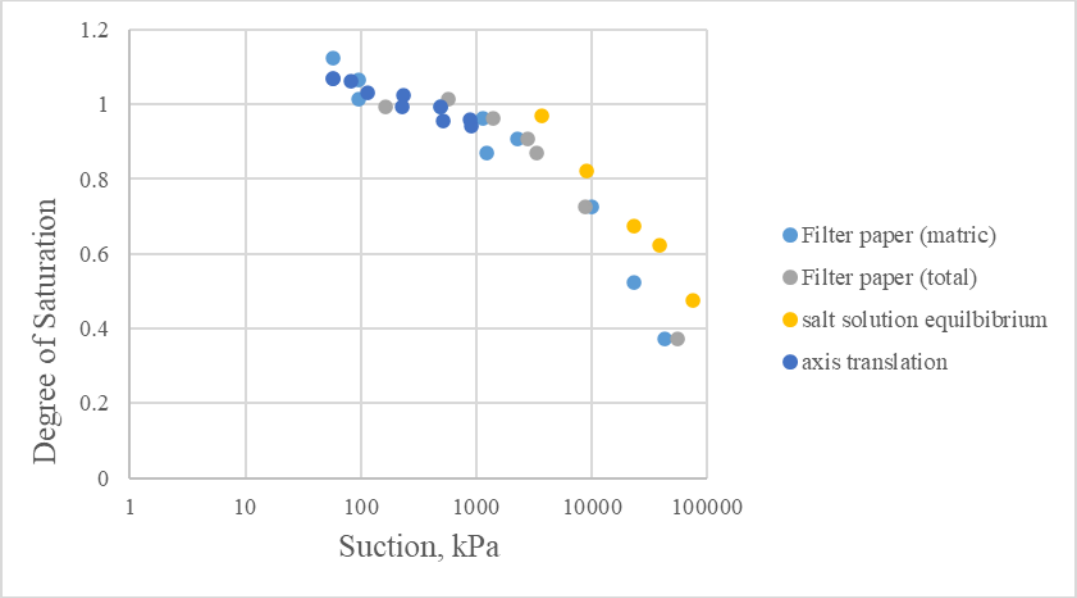

Figure 4.14. Ankara-Cubuk clay SWRC all data points with the degree of saturation

Using the Van Genuchten fitting method, the gravimetric water content, volumetric water content, and degree of saturation in suction obtained by using the Van Genuchten fitting method are fitted and given in Figures 4.15 to 4.18.

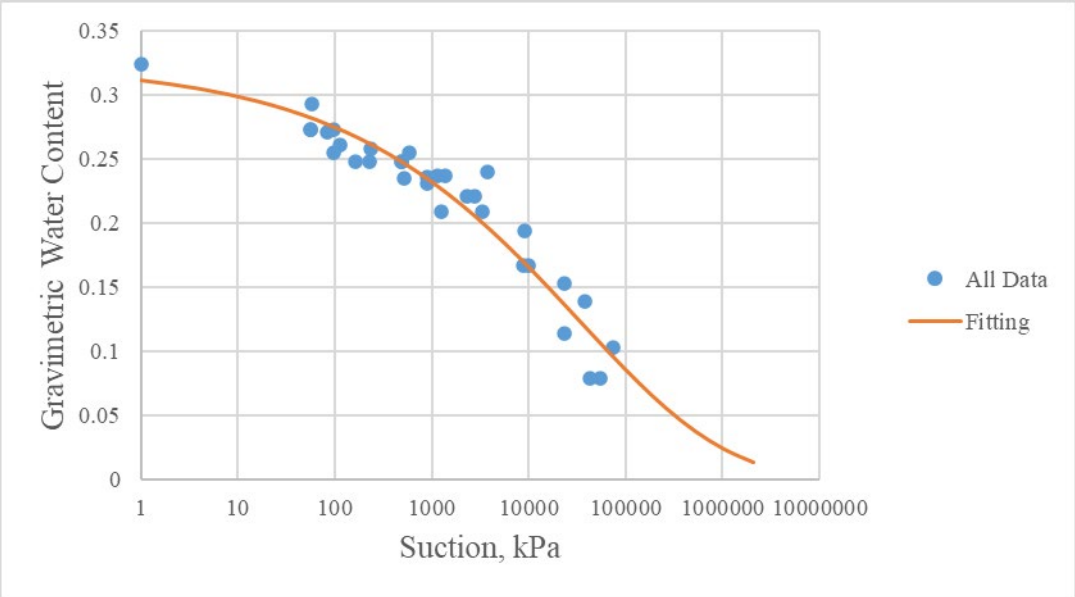

Figure 4.15. Ankara-Cubuk clay SWRC with Van Genuchten fitting

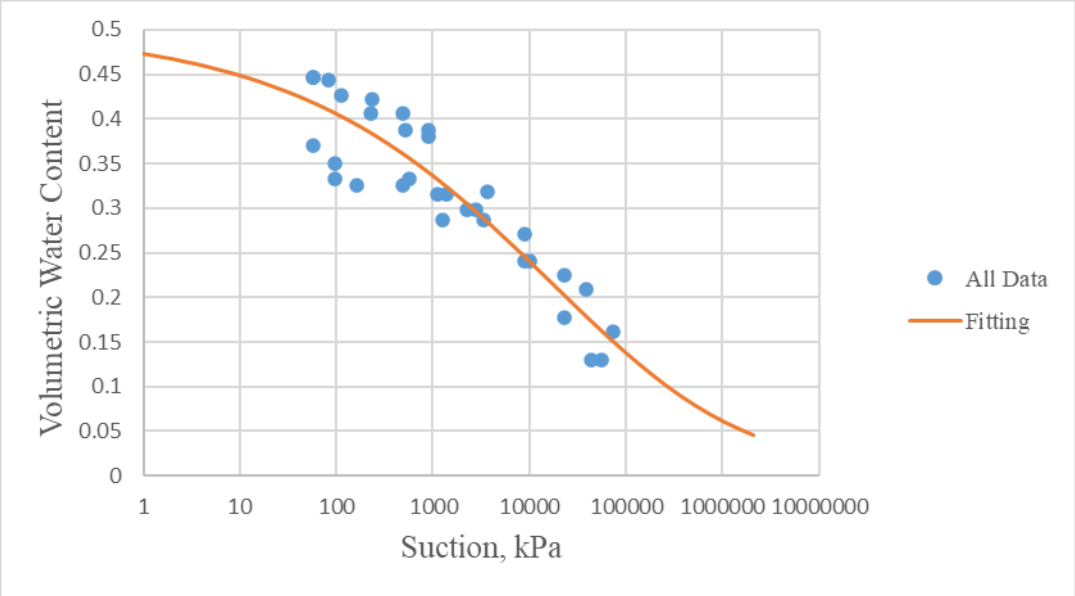

Figure 4.16. Ankara-Cubuk clay SWRC with volumetric water content (Van Genuchten fitting)

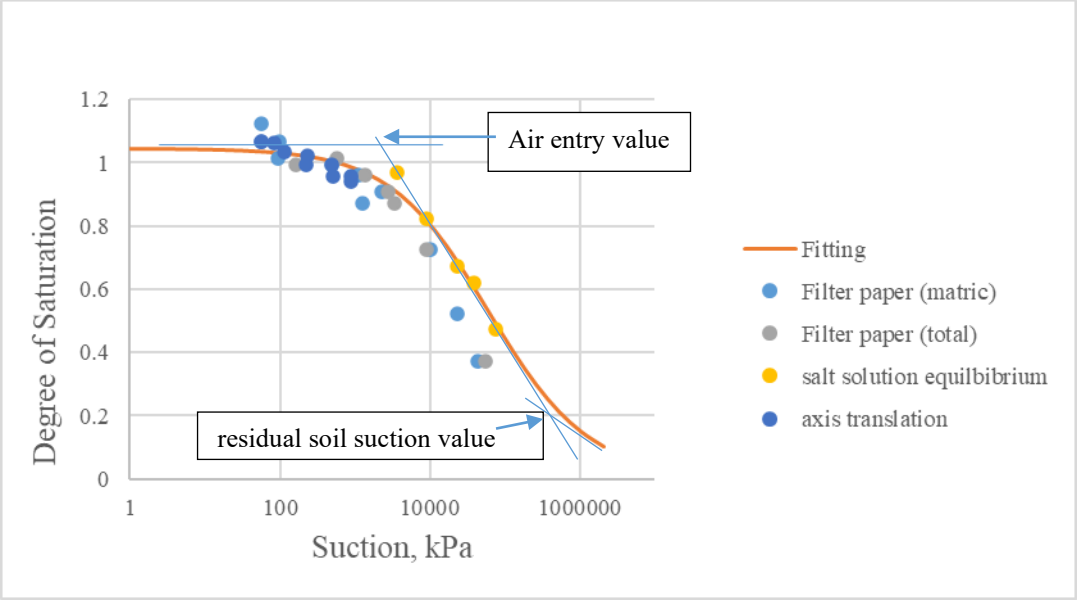

Figure 4.17. Ankara-Cubuk clay SWRC with degree of saturation (Van Genuchten fitting)

4.5. Mechanical Tests

4.5.1. Unconfined Compression Test

Undrained Shear Strength (cu) values of Ankara clay in different water contents were found by performing unconfined compression tests. Dry densities corresponding to different water contents were obtained from both the compression curve and the shrinkage curve.

The unconfined compression tests were performed on specimens prepared according to 7 different water content values (15, 17, 21, 23, 25, 28, and 31 percent) and corresponding dry density from the compaction curve as shown in Figure 4.18 (a). Figure 4.18 (b) shows the variation of undrained shear strength values determined for different dry density values. Figure 4.18 (c) shows the variation of undrained shear strength with respect to dry densities obtained from the compaction curve.

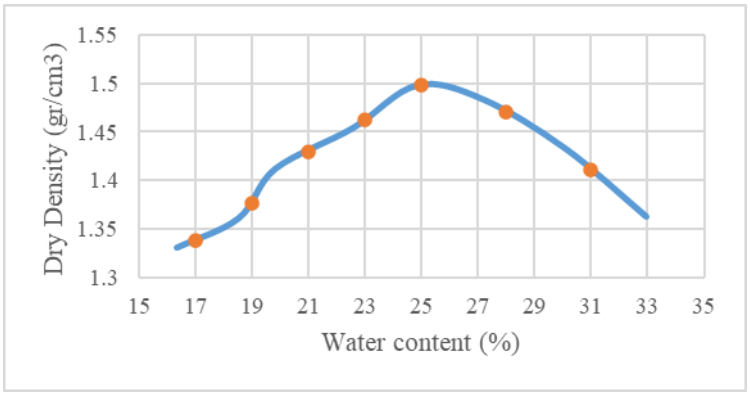

(a)

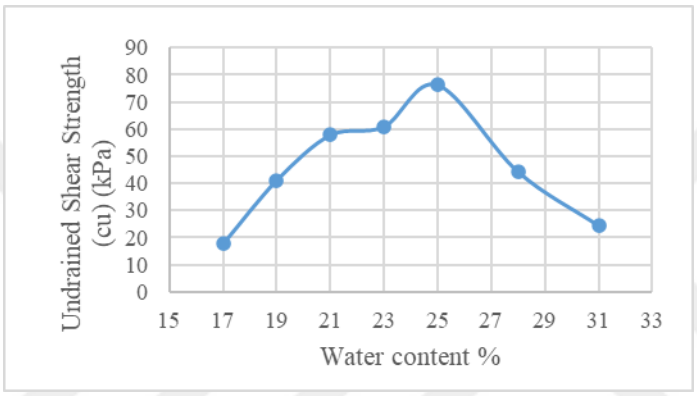

(b)

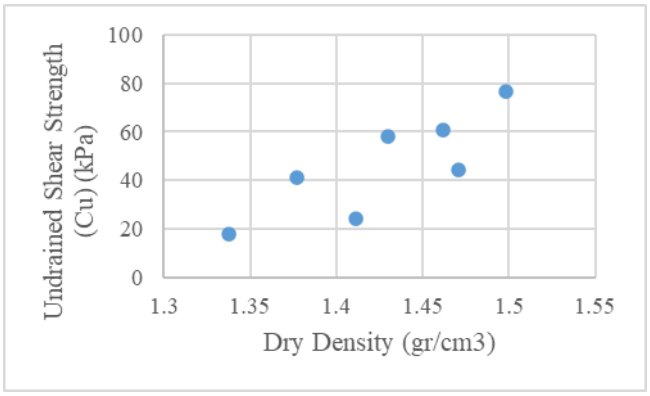

(c)

Figure 4.18. Undrained Shear Strength (cu) values for different compaction curve points

Similarly, Figure 4.19 (a) shows the dry densities obtained from the shrinkage curve corresponding to 7 different water content values (15, 17, 21, 23, 25, 28, and 31 percent). The distribution of undrained shear strength of the specimens prepared

according to these values is shown in Figure 4.19 (b). Figure 4.19 (c) shows the variation of undrained shear strength with respect to dry densities obtained from the shrinkage curve.

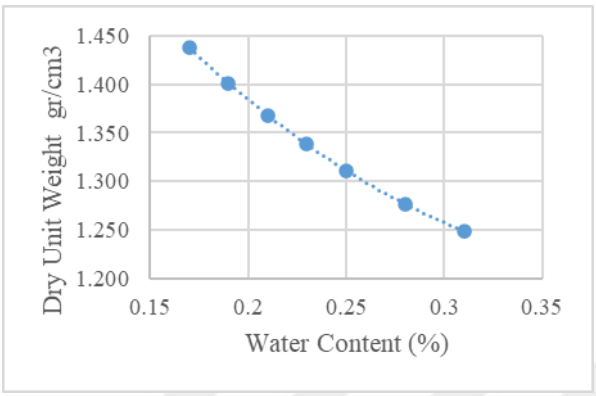

(a)

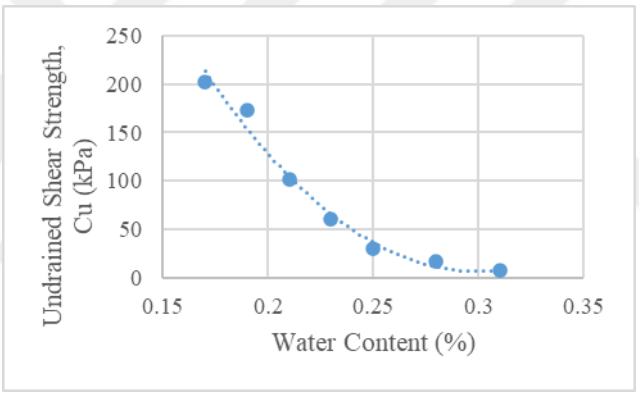

(b)

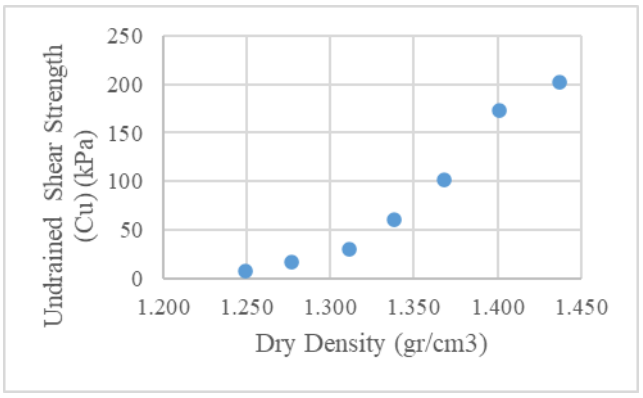

(c)

Figure 4.19. Undrained Shear Strength (c_u) values for different shrinkage curve points

4.5.2. Direct Shear Test

Direct shear test was performed to determine the adhesion factor between clay and pile foundation within the anchorage zone. Since there was no volume change in the clay within the anchorage zone, in the direct shear test, the clay specimen was sheared by applying normal pressure equivalent to the swelling pressure of approximately 150 kPa. Figure 4.20 (a) shows the undrained shear strength of the clay prepared with a water content of 23 percent, while Figure 4.20 (b) shows the interface shear strength between the clay and the concrete block with the same surface roughness as the pile foundation. The ratio of the strength of the clay to clay-concrete interfacial strength was found to be 0.62 from the ratio of the maximum shear stresses (56.3 kPa / 35.1 kPa).

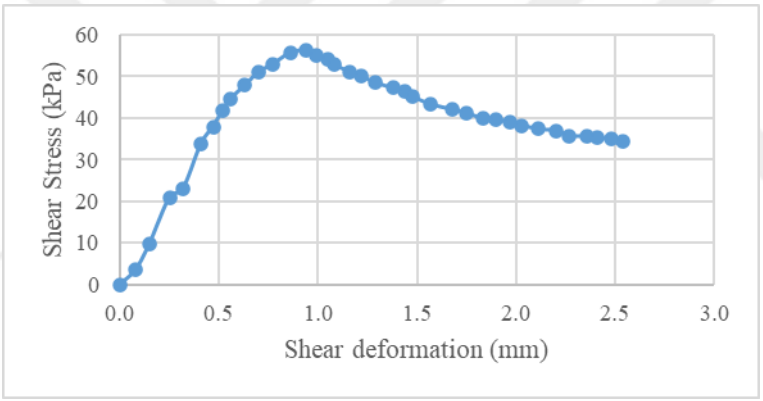

(a)

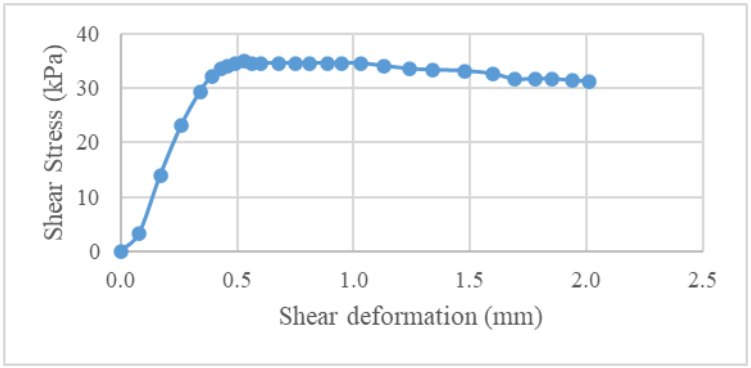

(b)

Figure 4.20. Direct shear test results of (a) clay, (b) concrete-clay interface

4.6. Investigation of the Mineralogy of Ankara Expansive Clay

The soil samples taken from the Cubuk district of Ankara were natural clay and therefore were expected to contain more than one mineral. It is known from the literature that each of the different clay minerals and the amount of each of them has a significant effect on soil behavior. For this reason, different laboratory experiments were used to determine the mineralogy of Cubuk clay.

4.6.1. Methylene Blue Test Results

The Methylene Blue Test was performed using the chart provided by Cokca (2002) shown in Figure 2.13 in the Literature Review chapter. As can be seen from Figure 4.21, when 275 ml of Methylene Blue solution was mixed with the soil solution, 5 light blue halos were observed, and the test was ended.

Figure 4.21. Methylene blue test result

In the literature review section, cation exchange capacity (CEC) and specific surface area (SSA) values associated with clay mineralogy and behavior were calculated using Equations 4.16 to 4.18 according to NF P 94-068 standard.

$$VB\ (cc) = VMB \times 0.01 \times WS \qquad \textit{(Eq. 4.16)}$$

Where;

VMB : The volume of methylene blue added until the endpoint is reached

WS : The weight of the dry sample used in this test

$$CEC\left(\frac{meq}{100g}\right) = \left(\frac{100}{WS}\right) \times WMB \times NBM \qquad \textit{(Eq. 4.17)}$$

Where;

WMB : The weight of dry methylene blue used for methylene blue solution

NMB : The normality of methylene blue

The molecular weight of methylene blue used for methylene blue solution was 320g.

$$SSA\left(\frac{m^2}{g}\right) = \left(\frac{VB}{100}\right) \times \left(\frac{AN}{WMN}\right) \times (AMB) \qquad \textit{Eq (4.18)}$$

Where;

AN : Avogadro's Number (6.02×10^{23}/mol)

AMB : The area covered by one methylene blue molecule ($130 \times 10^{-20} m^2$ according to Hang and Brindley, 1970)

As a result, SSA and CEC are calculated as 224.2 m^2 and 28.6 meq/100g, respectively for the Cubuk-Ankara clay.

In general, Mitchell and Soga, 2005 gave CEC values of 15 to 50 meq/100g for Illite-type clays and 80 to 150 meq/100g for Montmorillonite-type clays. Based on these ranges, it can be concluded that the Cubuk-Ankara clay with a CEC of 28.6 meq/100g can be considered an Illite-type clay. On the other hand, Mitchell and Soga, 2005 stated that the SSA value of Illite-type clays is generally between 80 and 120 m^2/g and the SSA value of Montmorillonite-type clays is between 600 and 800 m^2/g. For this reason, the SSA value of 224.2 m^2 found for the Cubuk-Ankara clay indicates that the clay may contain both illite and montmorillonite and may exhibit a behavior between these clay types.

4.6.2. Scanning Electron Microscope (SEM)

SEM and EDX analyses for Cubuk-Ankara clay were performed at the central laboratory of METU. The SEM images with magnifications ranging from 1000x to 25000x were taken from different sections of the clay sample. The EDX report results, showing each element and its amount in selected parts of the clay sample, were interpreted together with the SEM images to make inferences about clay mineralogy.

Figure 4.22 shows a large clay aggregate, approximately 300 µm wide, imaged using 1,000× magnification. This aggregate has a rough and fragmented surface and is composed of many small plate-like particles. The clay at this scale looks like a sticky lump with irregular, rough edges. These types of macroscopic blocky masses of clay aggregate can be formed by the interparticle attraction of montmorillonite or illite type of clay minerals.

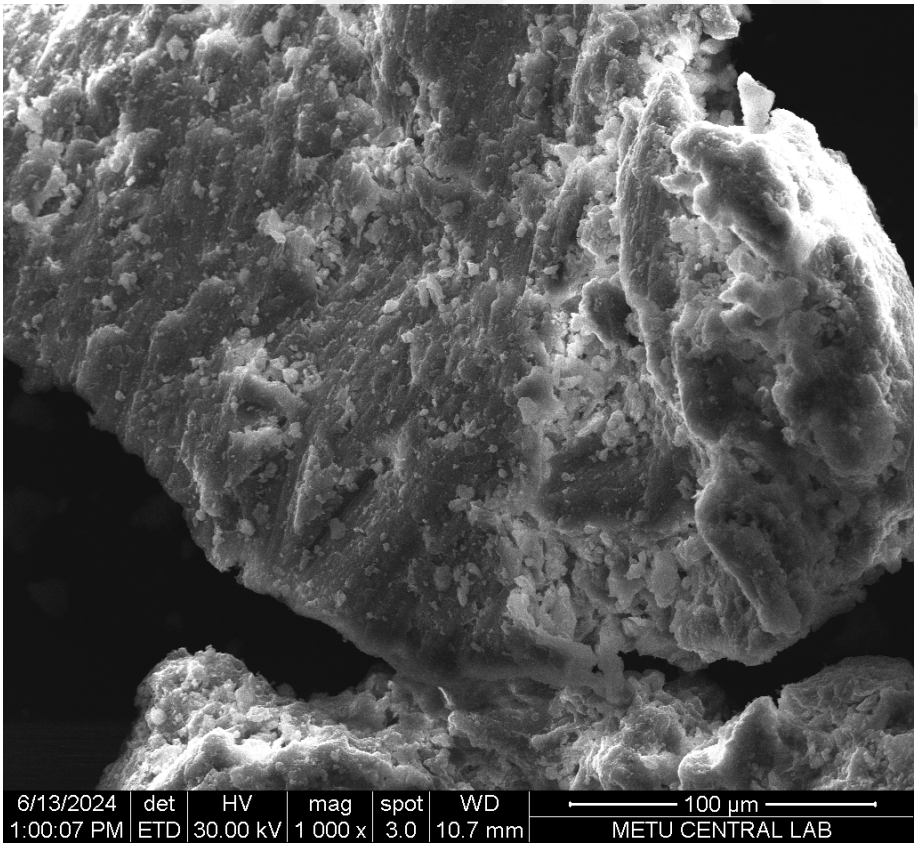

Figure 4.22. SEM image with 1000x magnification

The 25000x magnification image shown in Figure 4.23 shows the fine-scale morphology of the clay. This image shows generally less than 1 μm in size thin, flaky platelets with irregular shapes and ragged edges. This feature can be interpreted as a smectite-type clay mineral. In addition, irregularly shaped and poorly stacked clay minerals cause porous formation as seen in the figure and this can be interpreted as a characteristic appearance of the expansive clays. The large light-colored grain at the bottom of the figure is very likely a quartz mineral in a clay matrix.

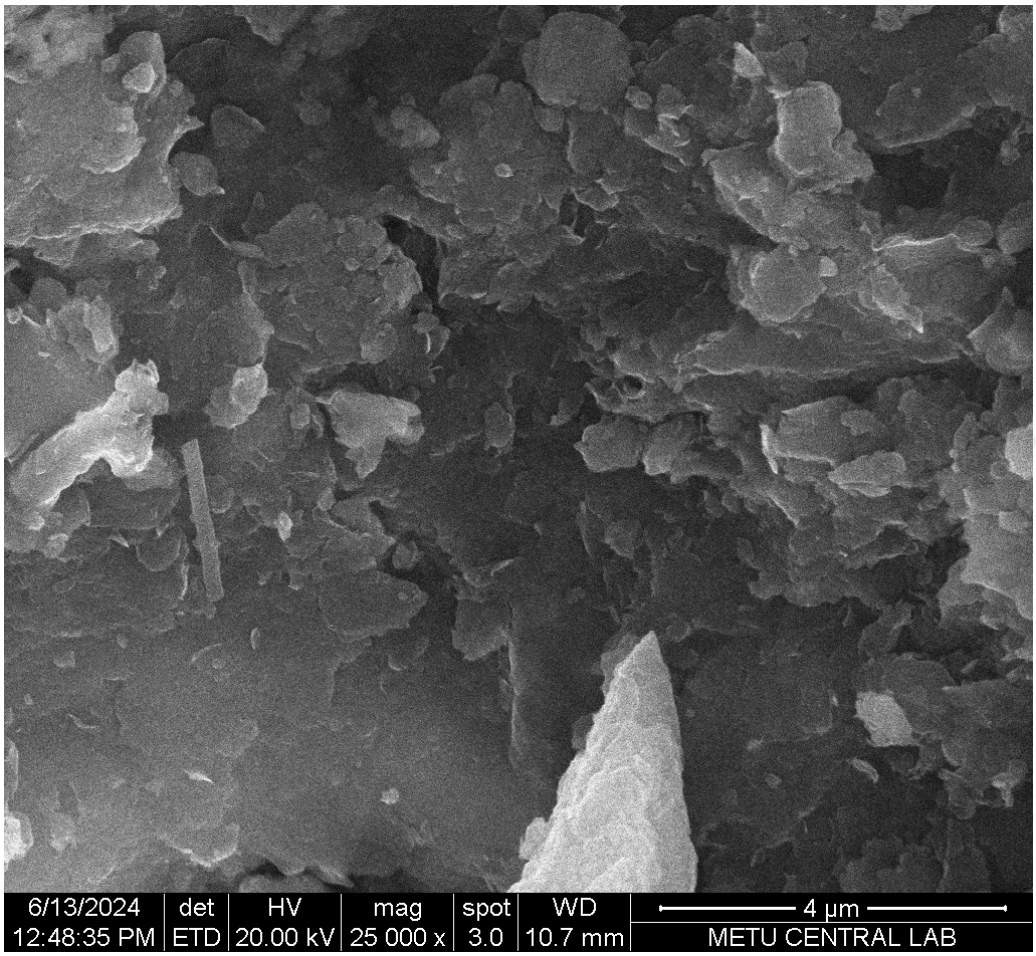

Figure 4.23. SEM image with 25000x magnification

An additional 24 images taken from different parts of the clay sample and at different magnifications are shown in Appendix D. Similarly, irregular fine flake-

shaped particles with platy morphology of the clay sample in the images were interpreted as illite-smectite type clay minerals.

4.6.3. Energy-Dispersive X-ray Spectroscopy (EDX) Analysis of Cubuk-Ankara Clay

EDX analysis was performed to determine the elements present in the clay sample. The results of EDX analysis in different parts of the clay sample are shown in Appendix E. In general, when the EDX analysis results are evaluated, it is seen that the clay sample contains high proportions of Si and Al elements and O^{-2} as a major anion. In addition, the clay sample also contains the elements Mg, Ca, K, and Fe in lower proportions. The presence of Si, Al, O, Mg, and Ca contains all the elements required for Montmorillonite's chemical formula. As mentioned in the literature review chapter in the clay mineralogy Section 2.1, the detection of the K is a very strong indicator of the presence of Illite mineral. The element Fe, which gives the clay its reddish-brown color, which is often noted in the literature and in this study to identify Ankara clay, was also detected in the EDX results.

In addition, in the literature review chapter, Figure 2.1 provided by Mitchell and Soga (2005) shows the components of a variety of clay minerals. Montmorillonite and Illite minerals have 2:1 semi-basic units (two silicate sheets to one alumina sheet). When the EDX analysis results are investigated, it is seen that the Si/Al atomic ratio is approximately two, and therefore it is interpreted that the clay mineral analyzed has 2:1 semibasic units. Thus, the presence of Ca, Na, or Mg elements between adjacent units is considered as smectite-type clay mineral and the presence of K cation is considered as illite mineral. The findings of this evaluation are in parallel with the findings obtained from SEM images.

4.6.4. X-Ray Diffraction (XRD) Result

The test was conducted at METU Central Laboratory to determine the main minerals in Cubuk-Ankara clay. Figure 4.24 shows the minerals detected in the clay corresponding to 2θ angles of 5 to 60 degrees.

Phase name	Chemical formula	FOM	Phase reg. detail	Space Group	DB Card Number
Quartz, syn	Si O2	0.460	S/M:PDF-4+ 2023	154 : P3221	00-033-1161
Calcite, syn	Ca (C O3)	0.770	S/M:PDF-4+ 2023	167 : R-3c:H	01-085-0849
montmorillonite	Na0.37 Ca0.16 K0.03 (Al3.05 Fe0.41 +3 Mg0.55 Ti0.01) (Si7.77 Al0.23) O20 (O H)4 ·x H2 O	1.170	S/M:PDF-4+ 2023		00-072-0370

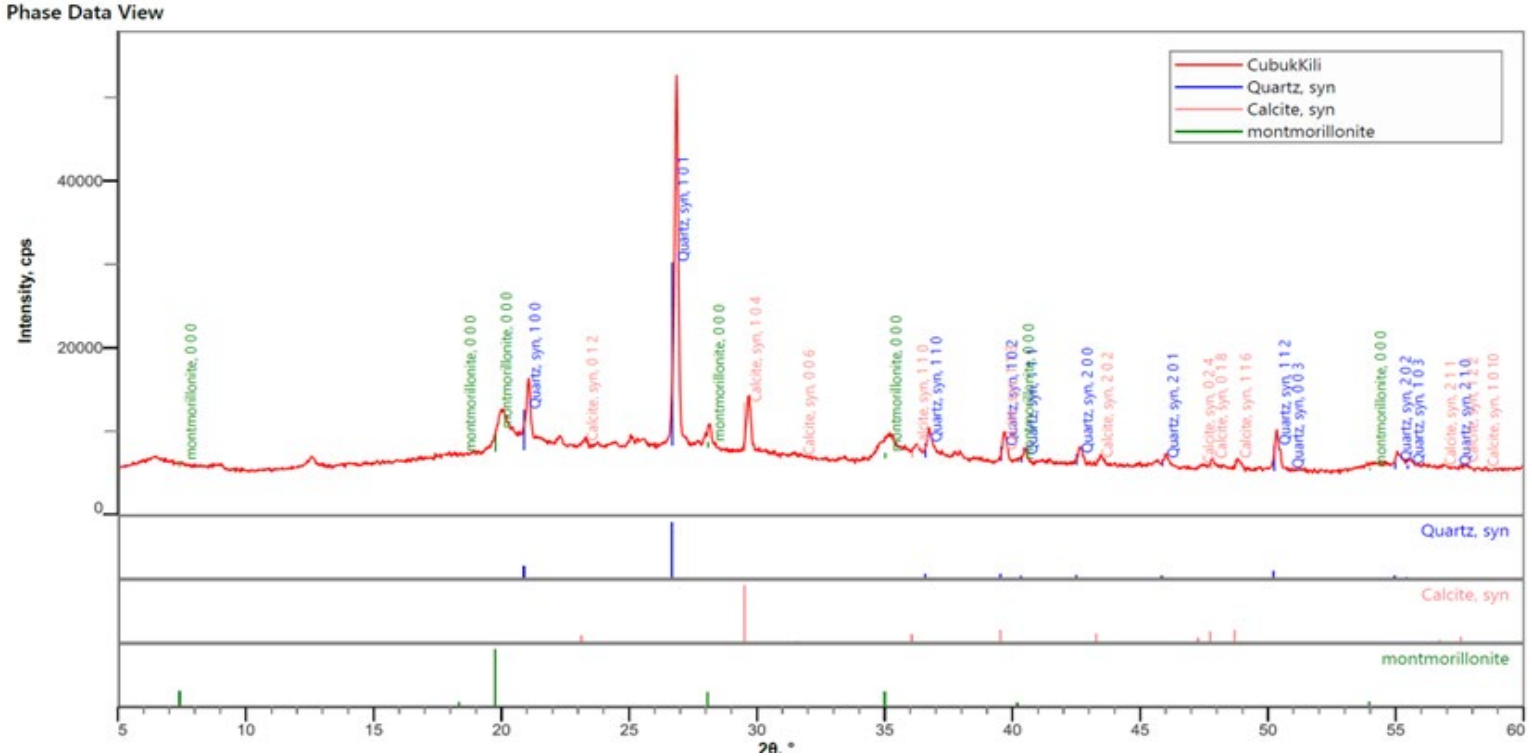

Figure 4.24. X-Ray Diffraction (XRD) Result for the Cubuk-Ankara clay

According to the results of the analysis, montmorillonite is the main clay mineral in the Cubuk clay. In addition to the clay mineral, quartz (SiO_2) and calcite ($CaCO_3$) minerals known as nonexpansive material are also present in the sample to a significant extent. A detailed report for the XRD can be seen in Appendix C.

4.7. Determination of Barcelona Basic Model Parameters

4.7.1 The slope of the elastic compression line (κ)

The slope of the recompression lines (C_r) was determined from the unsaturated 1-D compression test on specimens prepared with 19, 21, and 23 percent water content. Figure 4.25 to 4.27 shows the results of the tests. Then determined C_r values were converted to the slope of the elastic compression line (κ) using Equation 4.19. The slope of elastic compression lines for specimens with 19, 21, and 23 percent water content were found as 0.203, 0.194, and 0.195, respectively. The mean value of κ was taken as 0.0198.

$$\kappa = C_r \log \frac{1 + 2K_0}{3} \qquad \textit{(Eq. 4.19)}$$

Where;

c_r : The slope of the recompression line in the vertical stress (σ_v) vs. void ratio (e) space;

K_0 : The lateral earth pressure coefficient

Assuming that Jaky's formula is valid, the K_0 was calculated using Equation 4.20. Internal friction angle (Φ') is determined from 2 triaxial CD tests that were performed for 100 kPa and 400 kPa confinement pressure. Therefore, consolidation and triaxial CD tests data were used to obtain the parameter κ.

$$K_0 = 1 - \sin(\Phi') \qquad \textit{(Eq. 4.20)}$$

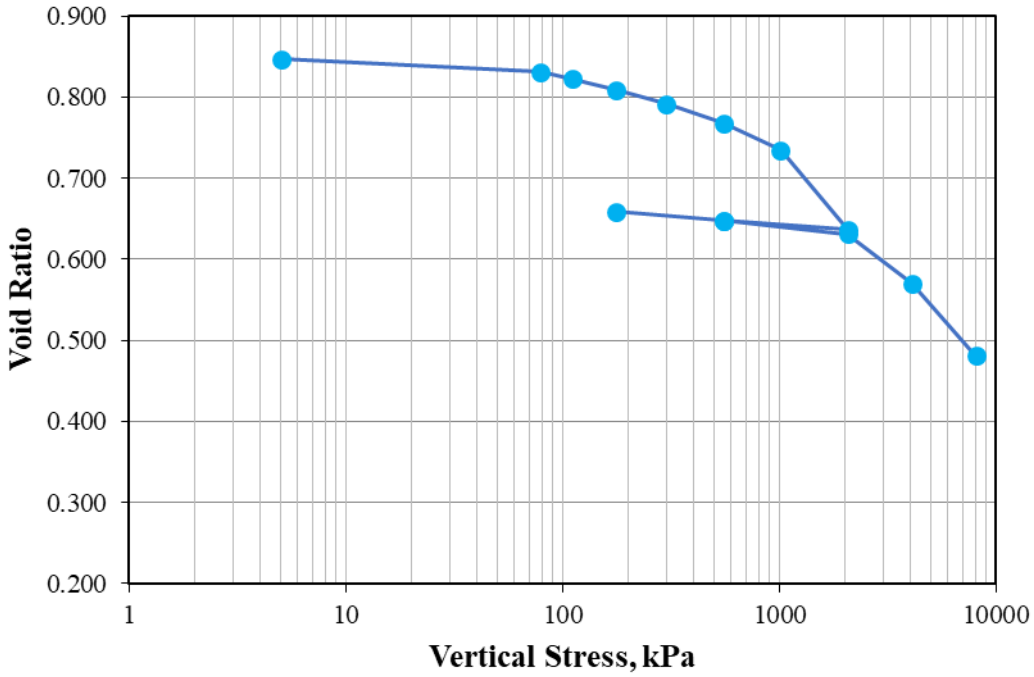

Figure 4.25. Unsaturated 1-D compression test result for specimen with the water content of 19 percent

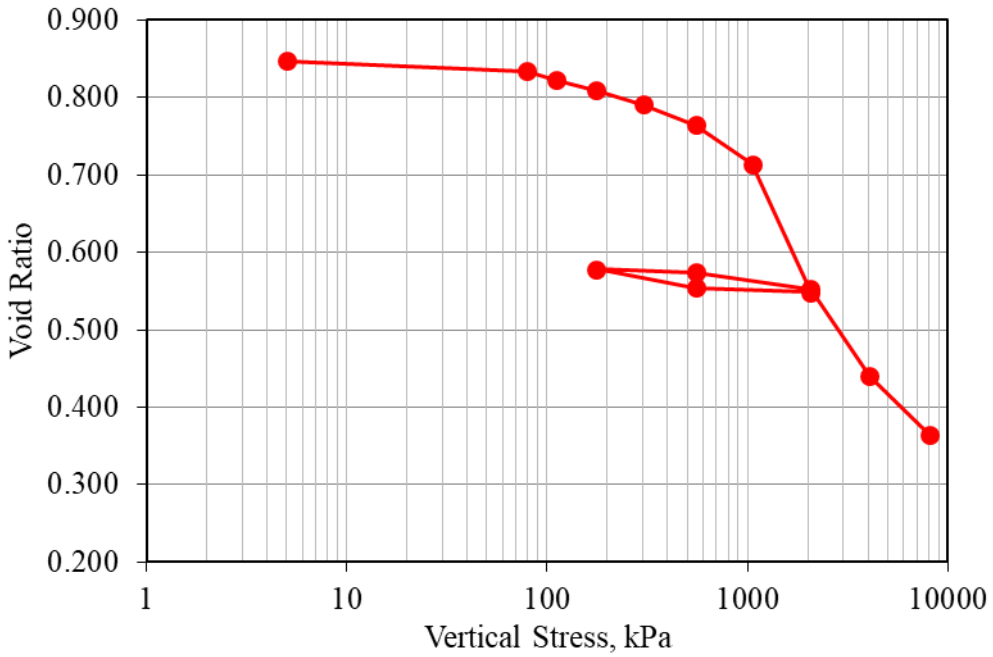

Figure 4.26. Unsaturated 1-D compression test result for specimen with the water content of 21 percent

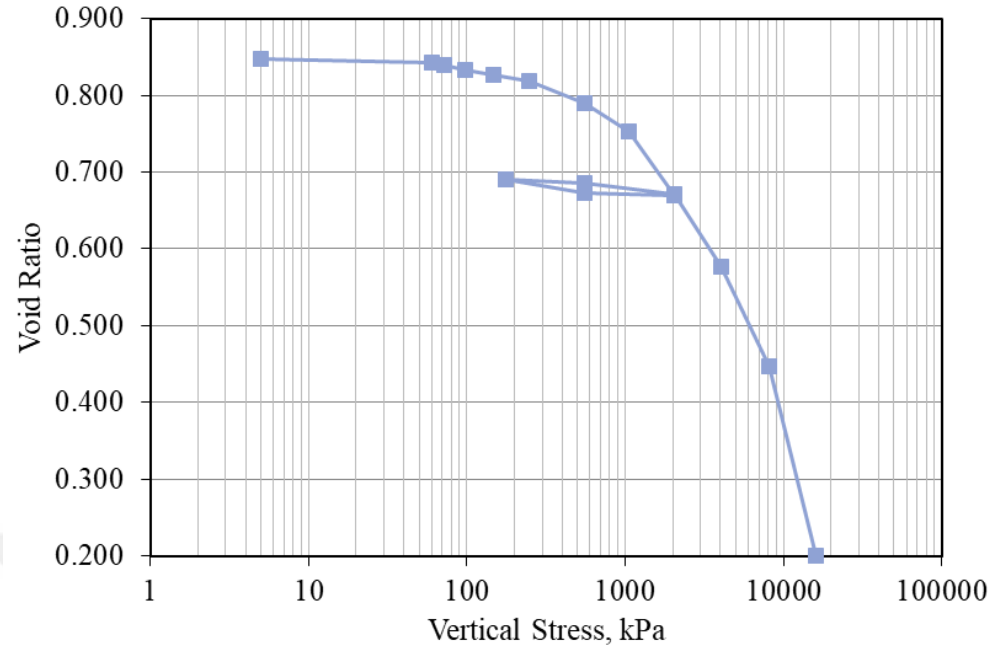

Figure 4.27. Unsaturated 1-D compression test result for specimen with the water content of 23 percent

4.7.2. The slope of the critical state line (M)

The deviatoric stress (q) and the mean effective stress (p`) at failure under 100 kPa and 400 kPa effective confining pressure are shown in Figure 4.28. The slope of the straight line fitted to the two data points is determined as 0.67, which is the slope of the critical state line (M).

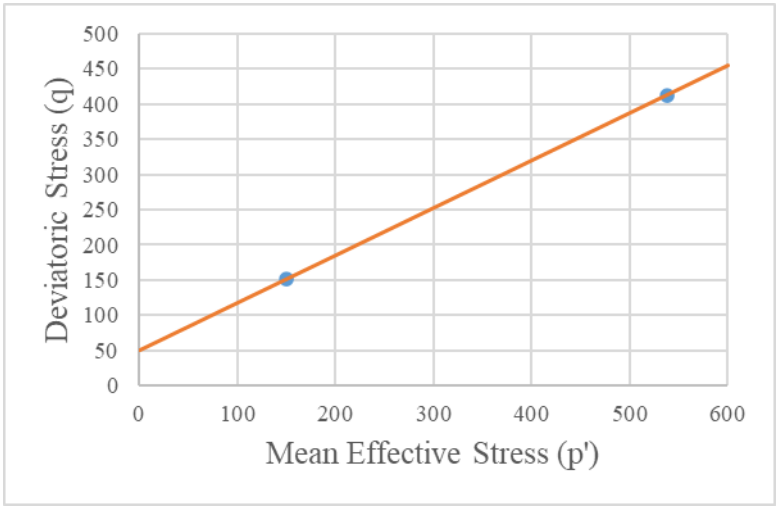

Figure 4.28. The slope of the critical state line (M)

4.7.3. The slope of the saturated virgin line (λ(0))

The previously determined values of 0.0198 for the slope of the elastic compression line (κ) and 0.67 for the slope of the critical state line (M), were used to determine the best fit for the experimental saturated triaxial CD data by changing the λ(0). The λ(0) value is optimized by using the Excel solver function to find the square of the least square difference between the BBM prediction and the actual experimental results. Figure 4.29 shows the results of triaxial CD experiments under 100 kPa and 400 kPa confining pressure and the BBM prediction with the minimum deviation. Thus, the value of λ(0) that would give this minimum deviation was found to be 0.084.

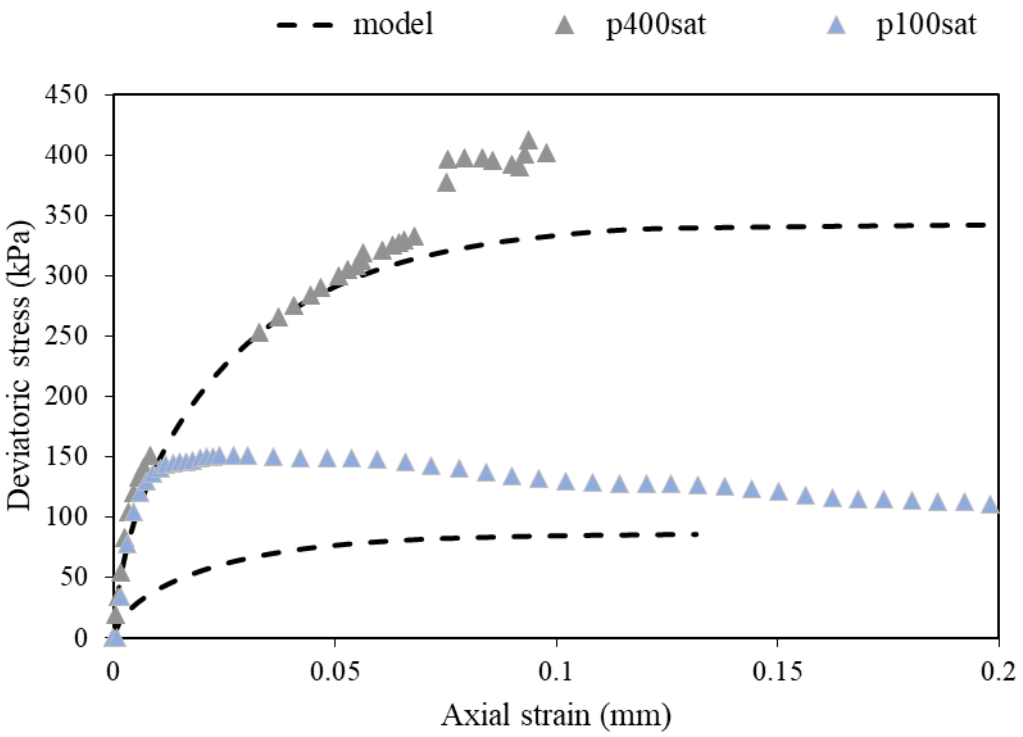

Figure 4.29. BBM prediction of triaxial CD tests with the minimum deviation

4.7.4. Suction Contribution to Apparent Cohesion (k)

The parameters of apparent cohesion (c") and cohesion increased due to suction (p_s) values calculated using Equations 4.21 and 4.22 for each quick triaxial

unsaturated test result as shown in Table 4.6. The suction values corresponding to the relevant water contents were determined from the soil water retention curve.

$$c'' = \frac{\frac{\sigma_{d,e}}{2}(1 - sin\Phi) - \sigma_c sin\Phi}{cos\Phi} \quad \textit{(Eq. 4.21)}$$

$$p_s = k \times s = \frac{c''}{tan\Phi} \quad \textit{(Eq. 4.22)}$$

Table 4.4. Determination of p_s

Confining Pressure (kPa)	Water Content (%)	Suction, s (kPa)	Deviatoric Stress, q (kPa)	Apparent Cohesion, c`` (kPa)	Increased Cohesion with suction, p_s (kPa)
100	19	4764	1521	524	1648
100	21	2400	852	280	879
100	23	1106	587	183	576
400	19	4764	1578	450	1415
400	21	2400	1094	273	859
400	23	1106	685	123	387

The calculated p_s values against the suction were plotted and the k parameter that provides a linear best fit as shown in Figure 4.30 is determined as 0.29. This value was used as an initial value of the parameter k before the general optimization process.

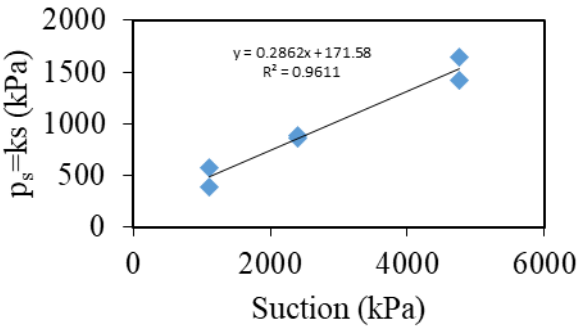

Figure 4.30. Determination of suction contribution to apparent cohesion (k)

4.7.5. Loading-Collapse (LC) Parameters (r, β)

The slope of the virgin lines (C_c) was calculated for both saturated and quick unsaturated 1-D consolidation tests. Suction for the saturated condition was taken as zero and the suction for the water content of 19, 21, and 23 percent were determined from the soil water retention curve. Then using Equation 4.23 all c_c values were converted to mean stress axis to determine λ(s). Table 4.7 shows the calculated C_c, λ(s) and the corresponding suction values.

$$\lambda(s) = C_c \log\left(\frac{1+2K_0}{3}\right) \qquad \textit{(Eq. 4.23)}$$

$$\lambda(s) = \lambda(0)((1-r)\exp(-\beta s) + r) \qquad \textit{(Eq. 4.24)}$$

Table 4.5. C_c and λ(s) values

Suction, s	The slope of the virgin compression lines (c_c)	The slope of the virgin compression line under constant suction, λ(s)
0	0.331	0.0324
4764	0.275	0.0270
2400	0.327	0.0270
1106	0.282	0.0271

The parameter of the r was found to be 0.831, as it is the ratio of λ(s) at the highest suction (lowest water content) and the λ(s) at the zero suction. The parameter β is derived using Equation 4.24 as 0.0031.

4.7.6. The preconsolidation pressure (p_0*)

The preconsolidation pressure (p_0) for each unsaturated 1-D consolidation test was determined from the experimental tests. According to the results of the experiments for 19, 21, and 23 percent water contents, the p_0 values were determined as 650,

351, and 295 kPa, respectively. The p_0* corresponding to the preconsolidation stress in the saturated state is then calculated using Equation 4.25 as 311, 194, and 192 kPa respectively.

$$p_0 = p_c(p_0^*/p_c)^{\frac{\lambda(0)-\kappa}{\lambda(s)-\kappa}} \qquad \textit{Eq (4.25)}$$

4.7.7. General optimization process for BBM parameters

The values of the slope of the elastic compression line (κ), the slope of the saturated virgin line (λ(0)), and the slope of the critical state line (M) parameters were taken as calculated above and were not changed during the overall optimization phase. The optimization aimed to determine the BBM parameters that would give the closest approximation to the results of all unsaturated 1-D consolidation and quick triaxial experiments. Summing the square differences between all predicted results and the experimental results, the parameters required to minimize this value were determined with the help of the Microsoft Excel solver. Table 4.8 shows the final BBM parameters obtained after optimization. Figure 4.32 through 4.37 shows the results of the unsaturated experiments performed in the laboratory and the results obtained according to the estimated BBM parameters.

Figures 4.38 and 4.39 show the k-line and loading collapse curves in the p-s plane for specimens with water contents of 19, 21, and 23 % under 100 kPa and 400 kPa confining pressure, respectively. Figures 4.40 and 4.41 show the stress paths, critical state lines, and yield surfaces in the p-q plane for specimens with water contents of 19, 21, and 23% under 100 kPa and 400 kPa confining pressure, respectively. Figures 4.42 and 4.43 show the critical state lines and yield surfaces in the three-dimensional p-q-s plane for specimens with water contents of 19, 21, and 23 % under 100 kPa and 400 kPa confining pressure, respectively. Figures 4.44 and 4.45 show the k lines, yield surfaces and LC curves in the three-dimensional p-q-s plane for samples with water contents of 19, 21, and 23 % under 100 kPa and

400 kPa confining pressure, respectively. The LC curves shown in the 2-D and 3-D figures are calculated based on the data obtained after deviatoric stress loading.

Table 4.6. Final BBM parameters after the optimization process

λ(0)	0.084
κ	0.0198
r	0.8909
β	0.0011
p_c	7.9
k	0.56
M	0.67

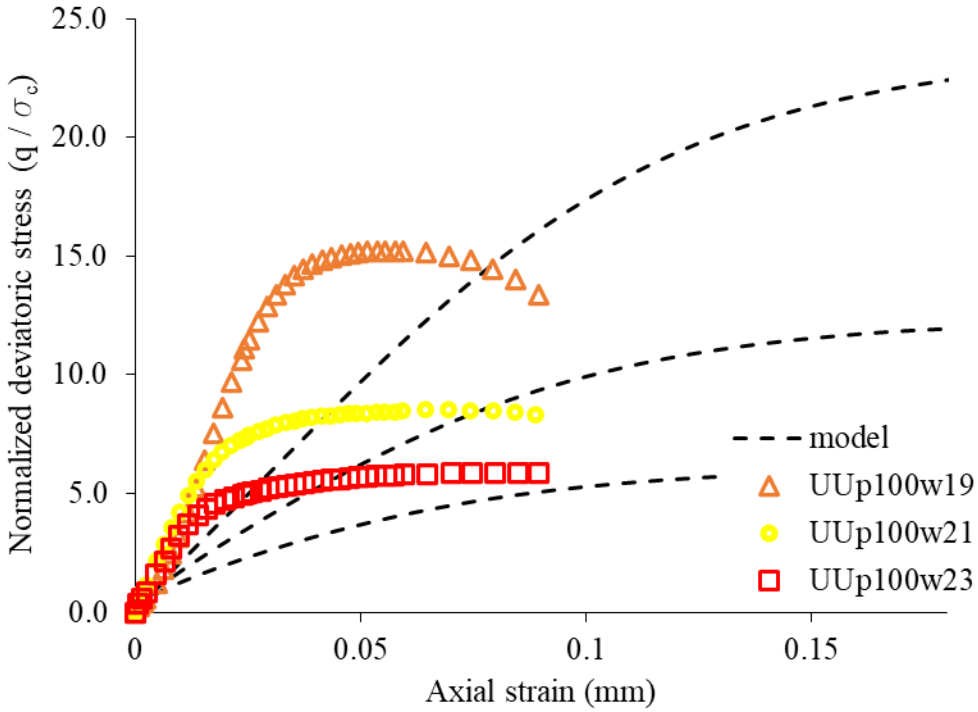

Figure 4.31. Model prediction curves for normalized deviatoric stress under 100 kPa confining pressure

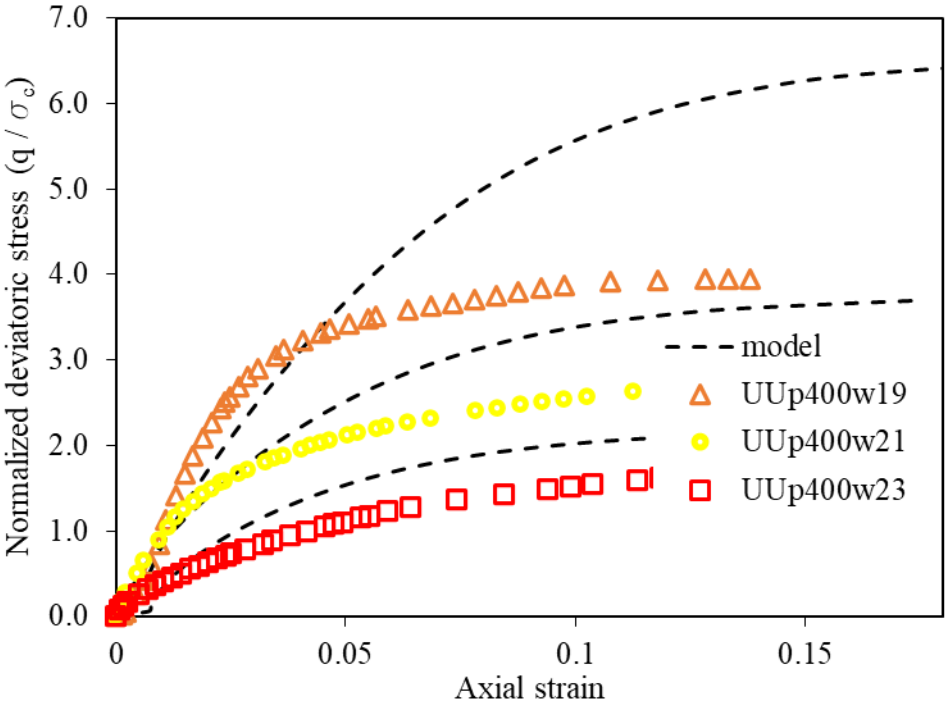

Figure 4.32. Model prediction curves for normalized deviatoric stress under 400 kPa confining pressure

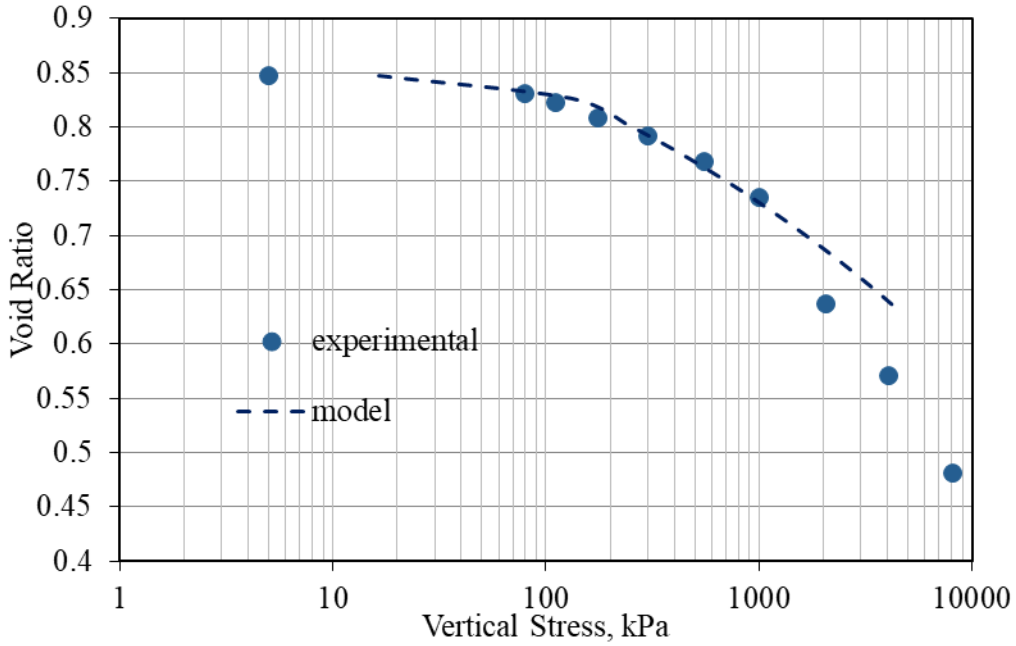

Figure 4.33. Experimental result vs BBM prediction for initial water content of 19%

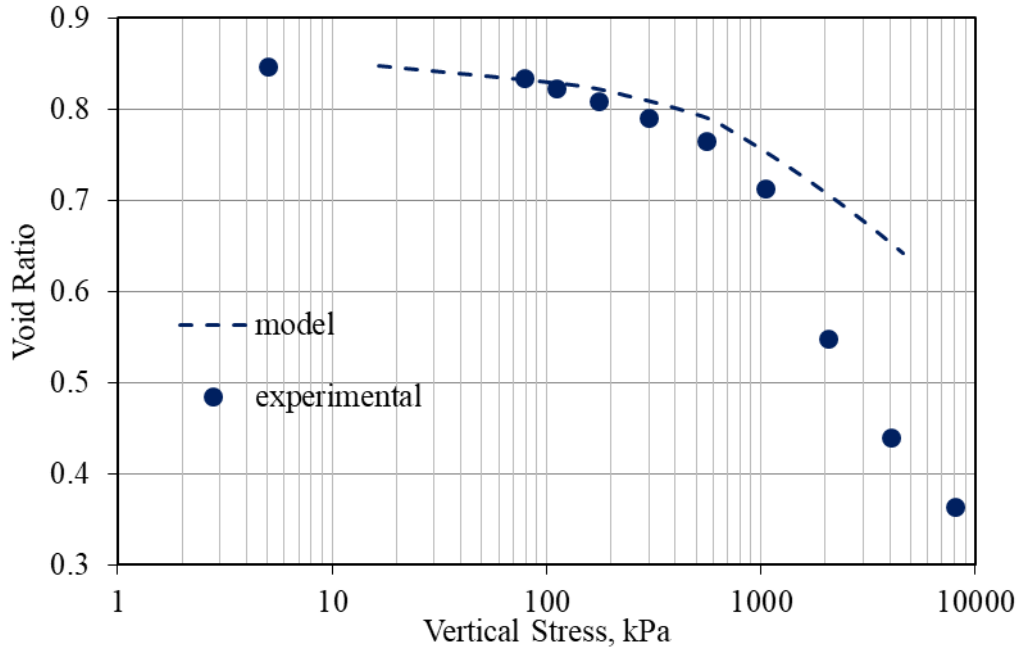

Figure 4.34. Experimental result vs BBM prediction for initial water content of 21%

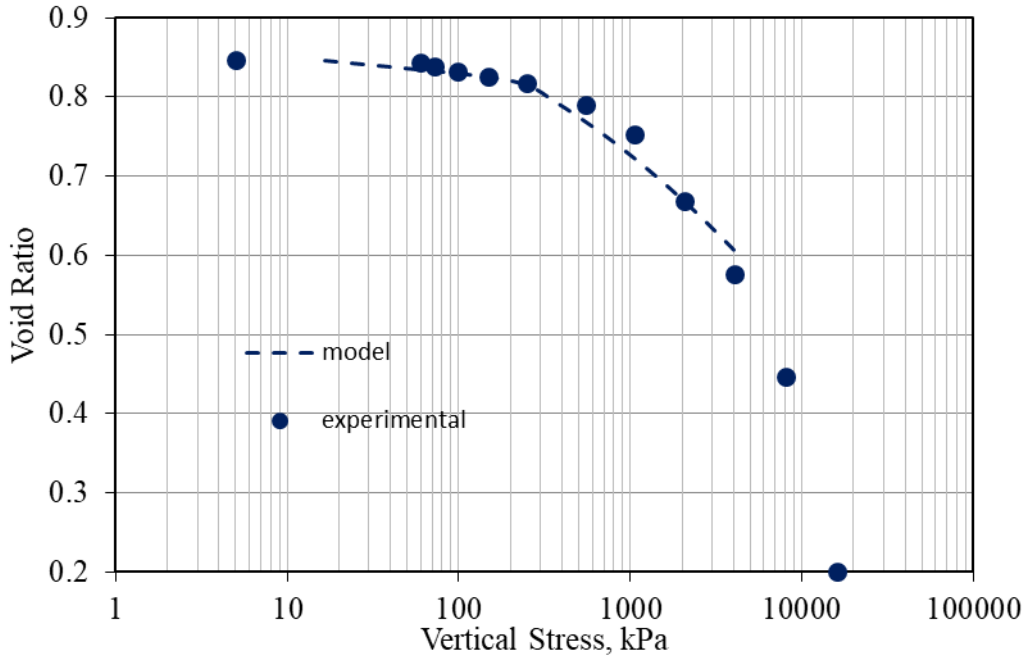

Figure 4.35. Experimental data vs BBM prediction for initial water content of 23%

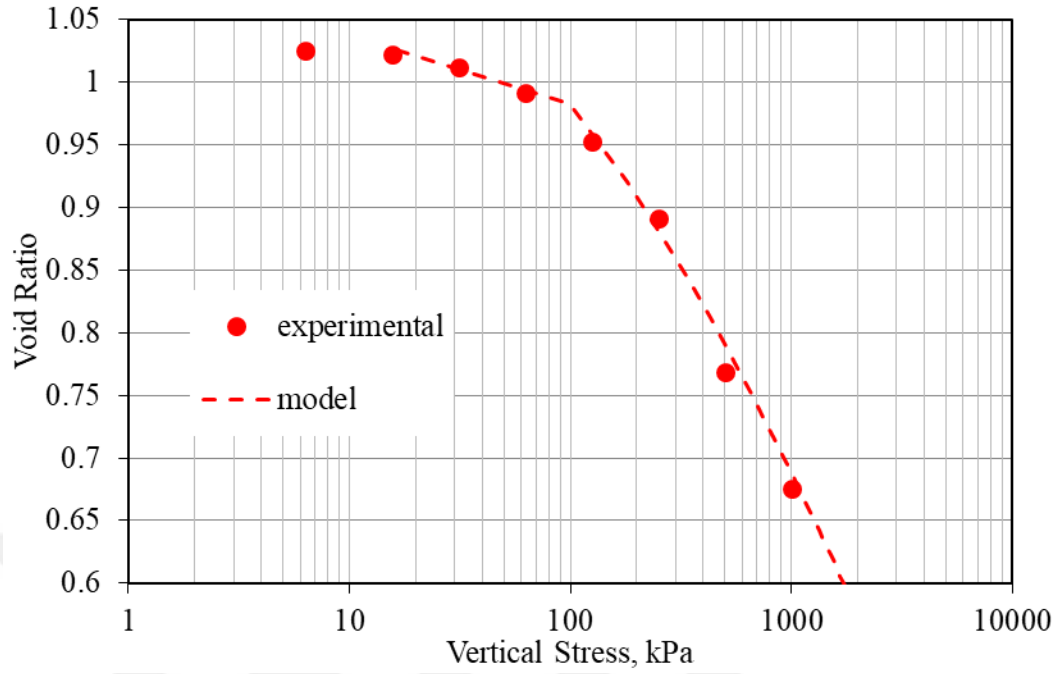

Figure 4.36. Experimental results vs BBM prediction for saturated condition

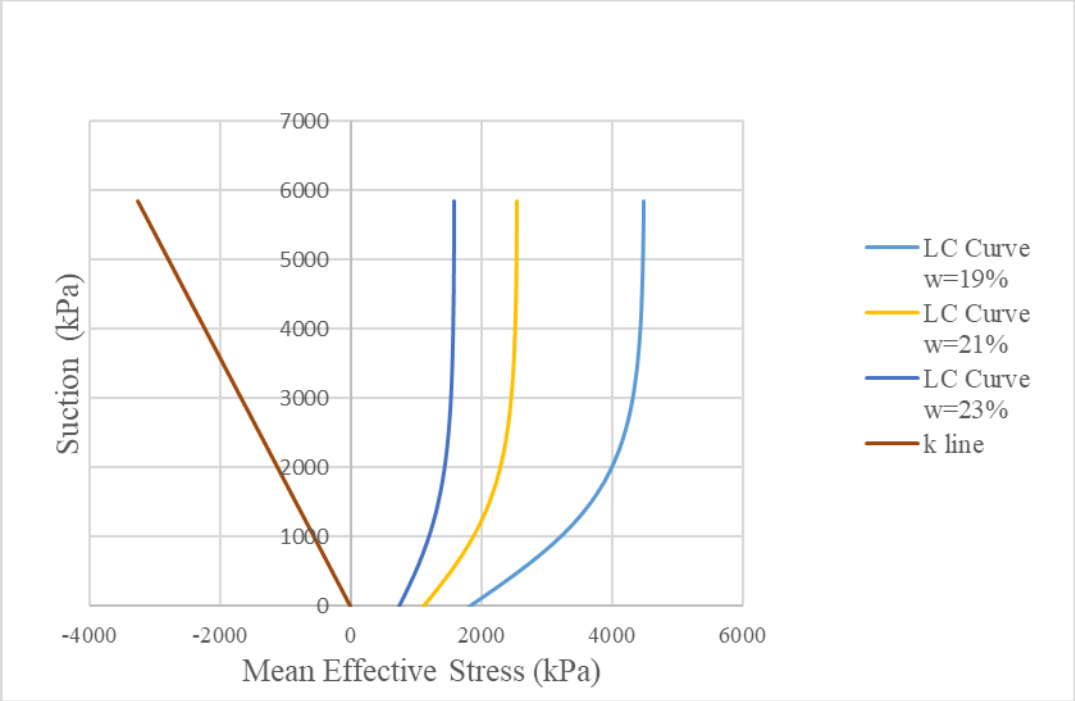

Figure 4.37. LC curves and k line for the clay with 19, 21, 23 % of water contents under 100 kPa confining pressure

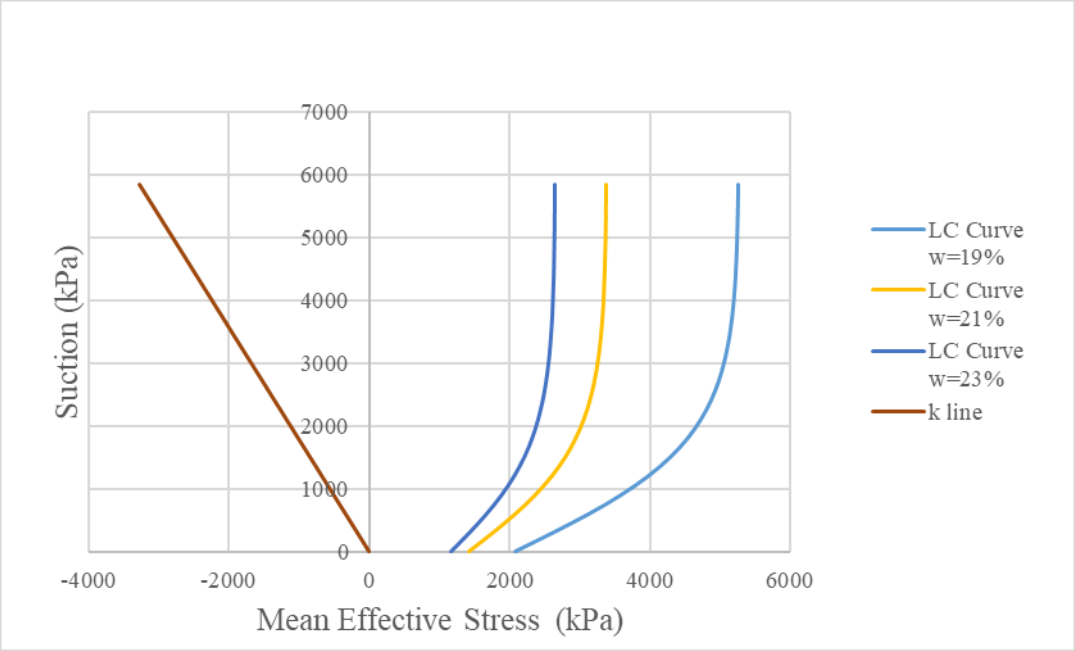

Figure 4.38. LC curves and k line for the clay with 19, 21, 23 % of water contents under 400 kPa confining pressure

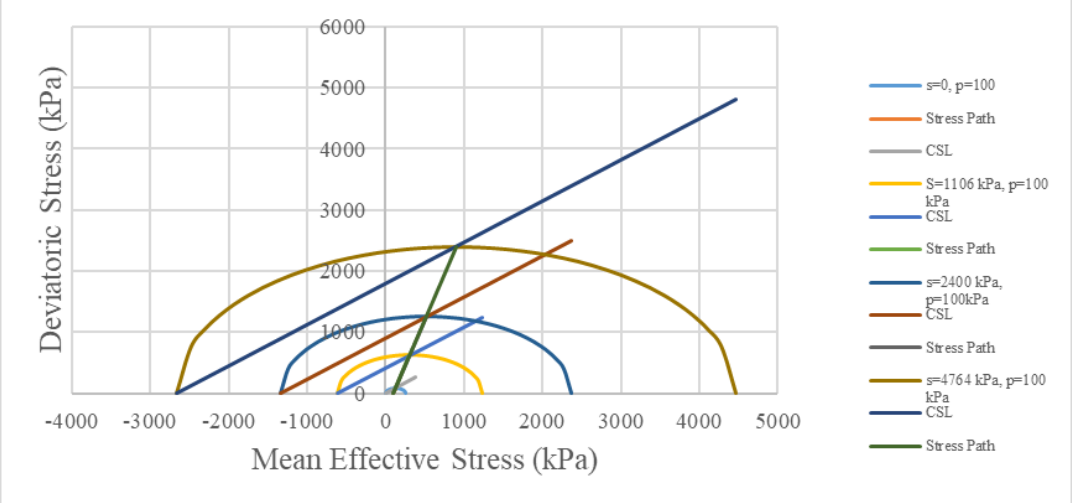

Figure 4.39. Stress paths, critical state lines, and yield surfaces in the p-q plane under 100 kPa confining pressure

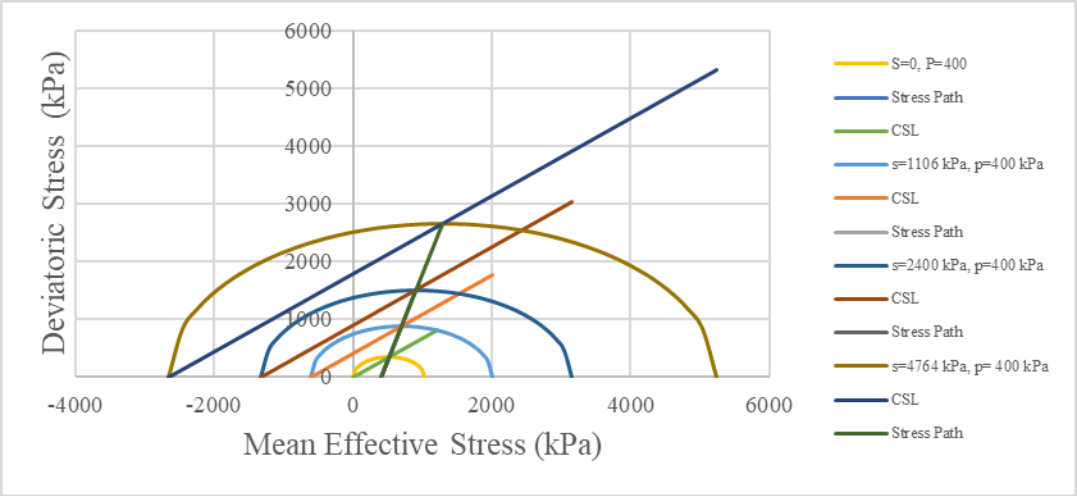

Figure 4.40. Stress paths, critical state lines, and yield surfaces in the p-q plane under 400 kPa confining pressure

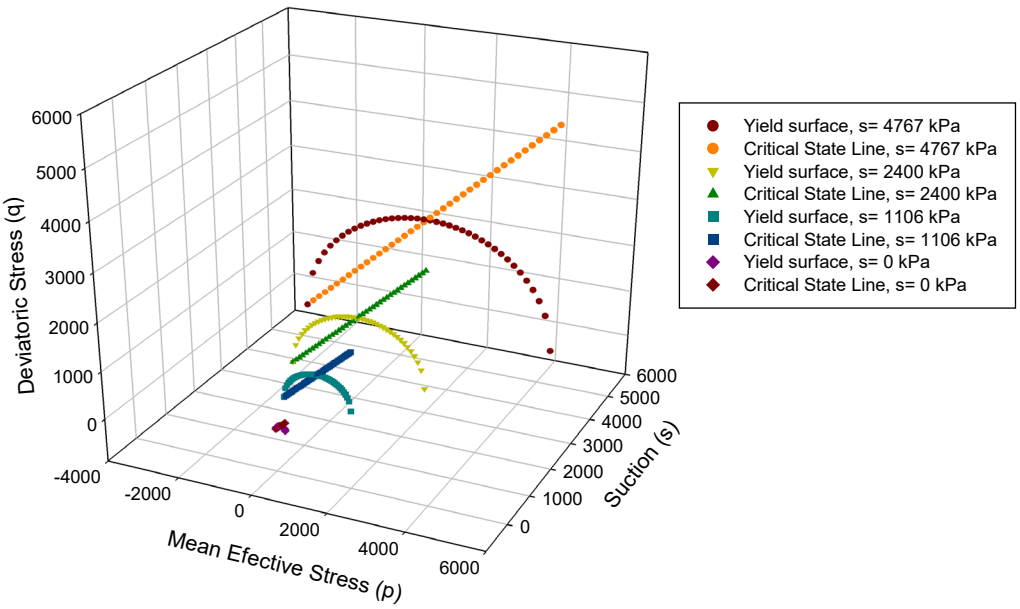

Figure 4.41. Critical state lines, and yield surfaces under 100 kPa confining pressure

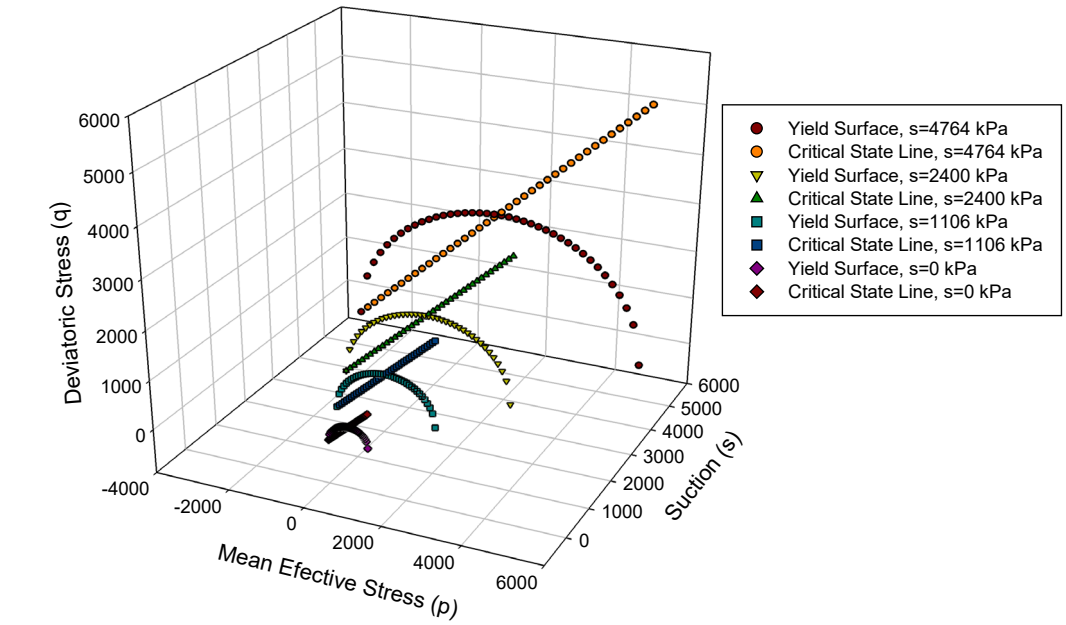

Figure 4.42. Critical state lines, and yield surfaces under 400 kPa confining pressure

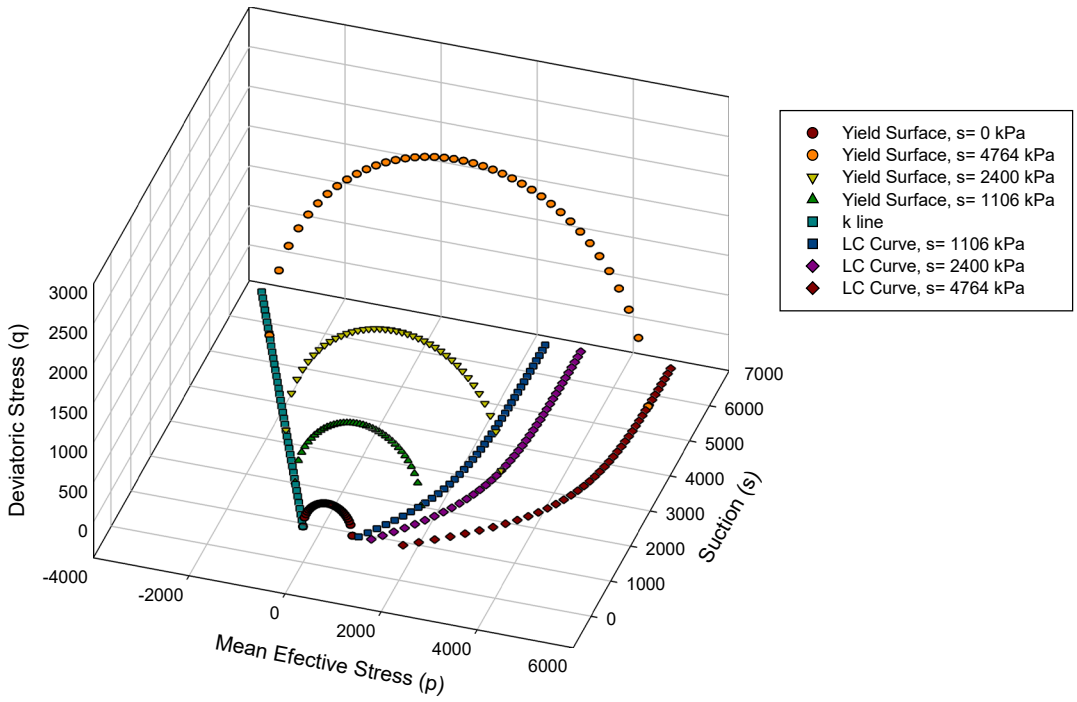

Figure 4.43. Yield surfaces, k line and LC curves under 100 kPa confining pressure

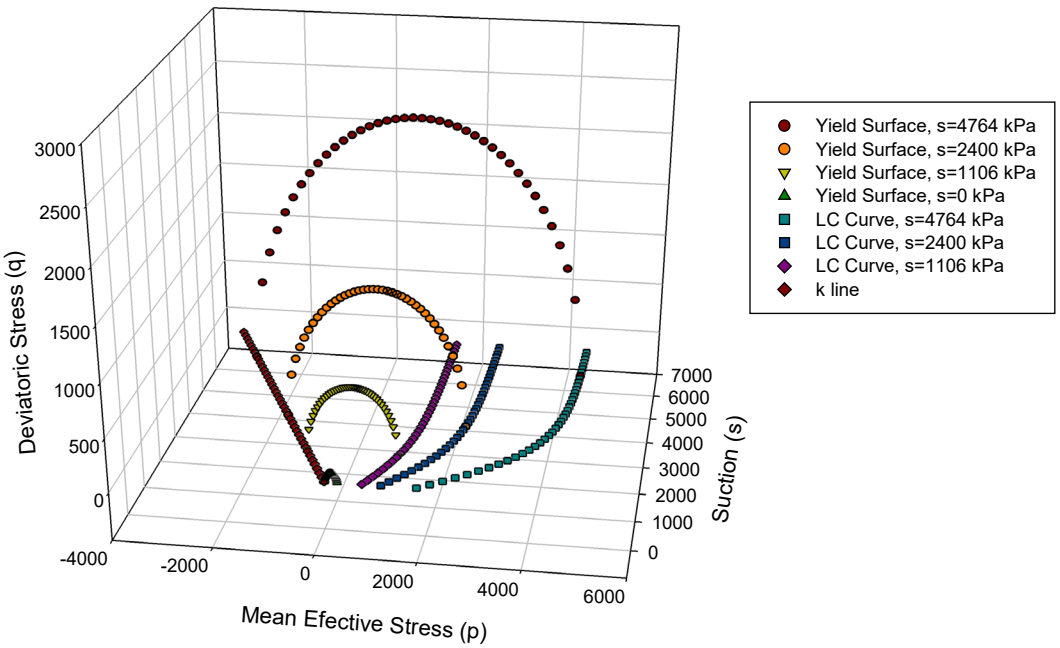

Figure 4.44. Yield surfaces, k line and LC curves under 400 kPa confining pressure

CHAPTER 5

LABORATORY MODEL TESTS

5.1. Model Tests in PVC Meter Test Set-up

PVC meter apparatus as shown in Figure 5.1 was used to perform small-scale lab experiments to determine the expansion of the clay and the upward movement of the pile driven into the soil. The test setup was chosen for its simplicity to determine if any movement on the pile could be observed in the pile before moving to larger larger-scale laboratory test.

Figure 5.1. PVC meter size laboratory test setup

5.2. Laboratory Size Model Tests in the 15.2 cm diameter, 5 cm height mold for Pile Foundation in Expansive Clay

5.2.1. Preparation of pile and drainage pipes

PVC pipes with an inner diameter of 1.5 cm were cut to make them 6.3 cm long. Then the pipes were cut into two longitudinal pieces so that the concrete to be poured into it could be easily removed from the pipe after setting without damage. Then it was put together, taped, and ready to be concreted.

A mixture ratio of 100 g of sand with a maximum grain size of 0.42 mm, 40 g of cement, and 30 g of water was used for the concrete used to make the piles. The mixture was kept in water for 30 seconds, then mixed for 1 minute, then left for 30 seconds, then mixed rapidly for 45 seconds and ready to be poured into the pipes as shown in Figure 5.2 (a). After waiting 2 days and making sure that the piles were solidified, the tapes around the pipes were removed and the pipe pieces were separated from the piles as shown in Figures 5.2 (b) and 5.2 (c).

In the experiment, PVC pipes with a diameter of 0.5 mm were cut to a length of approximately 6.3 mm to saturate the clay quickly and to reduce the waiting time. The pipes that would remain in the clay were holed at various points to allow water to pass through the clay as shown in Figure 5.2 (d). In this way, 8 pipes were prepared and got ready to be used in the experiment.

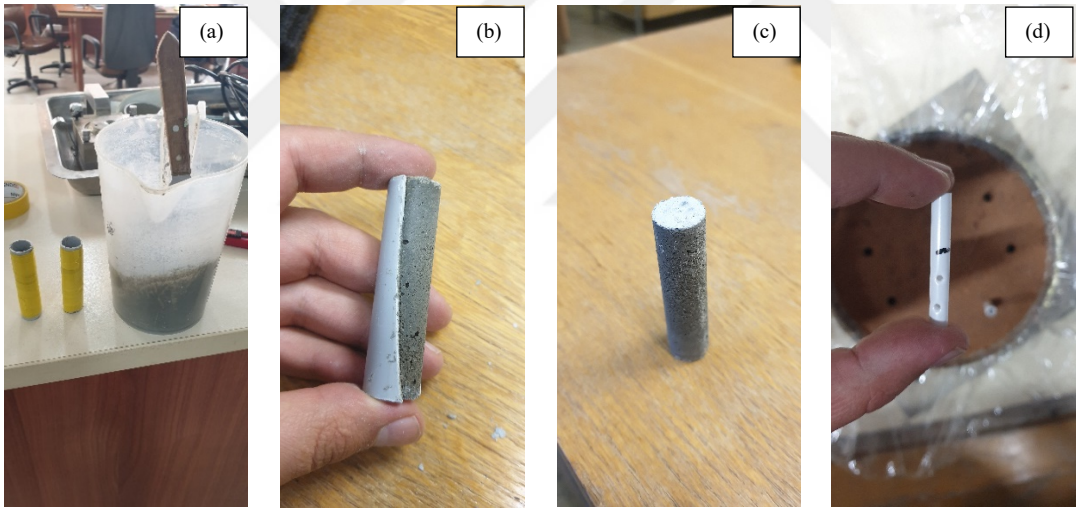

Figure 5.2. Preparation of piles

5.2.2. Preparation of the soil for the test

In this experimental setup, the 15.2 cm diameter mold shown in Figure 5.3 (a) was used. The clay sample was compacted into the mold with each layer at a height of 1 cm, for a total of 5 layers. To ensure adhesion between the next layer and the previously compacted layer, the surface of the previously compacted layer was scarified with a spatula as shown in Figure 5.3 (b).

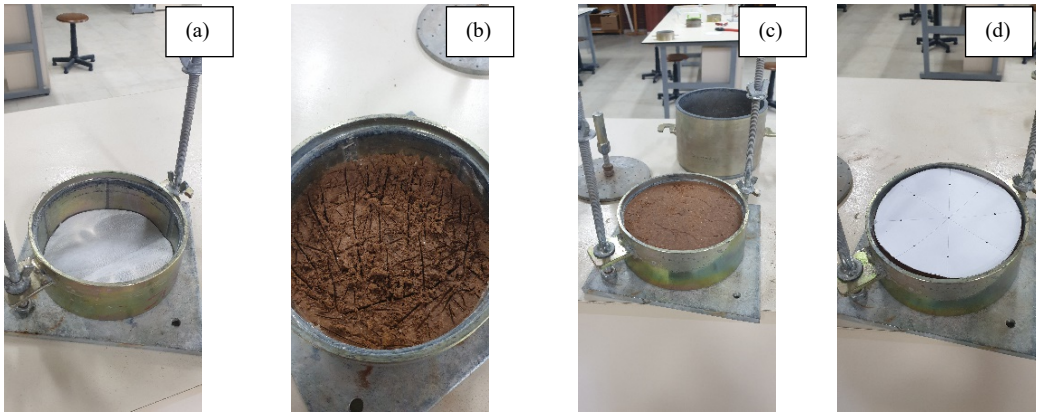

Figure 5.3. Preparation of clay for the lab size test setup

As shown in Figure 5.3 (d), the center points of the pile and the PVC pipes to be used as drainage channels were marked on the paper placed on the compacted clay. Then the 8 marked center points of the drainage channels were drilled using a vertical straight-down drill as shown in Figure 5.4 (a). The previously prepared PVC pipes were carefully inserted into the open holes with rotational movements.

So the setup became as shown in Figure 5.4 (b). To drill the hole for the previously prepared pile, a drill bit with a 1.32 cm diameter, slightly smaller than the diameter of the pile, as shown in Figure 5.4 (c), was selected. Then the hole for the pile was drilled with the selected drill bit as shown in Figure 5.4 (d). The pile diameter was then reduced to tightly fit into the drilled hole with sandpaper P40 with a maximum grain size of 0.425 mm. After recalculating the weight and diameter of the final pile, it was carefully inserted into the clay with rotational movements as shown in Figure 5.4 (e). The test setup was then ready to start the experiment.

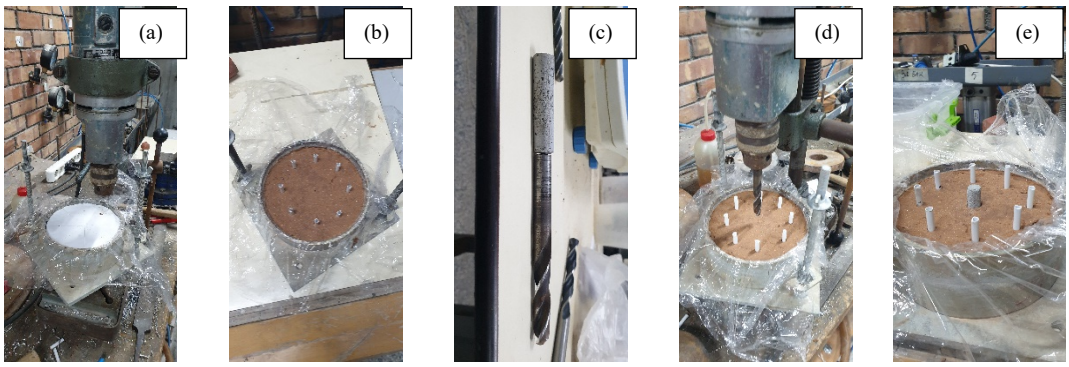

Figure 5.4. Installation of piles and drains in the test setup

5.2.3. Preparation of the soil for the test with anchorage zones

It is known that the change in water content in the active zone of expansive clays causes a volumetric change in the soil and therefore causes the pile to be moved. Pile dimensions should be designed so that enough of the pile is inserted into the anchorage zone to prevent it from moving. In this experimental setup, different anchorage zones and active zone depths were created to investigate how much of the pile length should be within the anchorage zone to prevent pile movement for safe pile design. Therefore, after compacting the clay at certain heights, an impermeable layer was formed and experimental setups were prepared for different anchorage zone depths.

First, the clay was compacted into the mold as shown in Figure 5.5 (a) and then the surface was leveled with a spatula. Thus, plastic thin rulers taped on the inside of the mold were used to monitor the exact level of compaction. After ensuring that the surface was completely flat as shown in Figure 5.5 (b), melted wax was poured over the clay to create an impermeable layer, and waited for it to cool down. Then, the surface was covered with thin stretch wrap as shown in Figure 5.5 (c). The apparatus in Figure 5.5 (d) was placed on the stretch wrap and the stretch wrap was gently stretched from all sides to prevent the forming of a fold. The remaining clay was then carefully compacted so that the wax and stretch wrap would not be damaged. Finally, the test setup was prepared by placing the piles and drainage pipes as described in detail above.

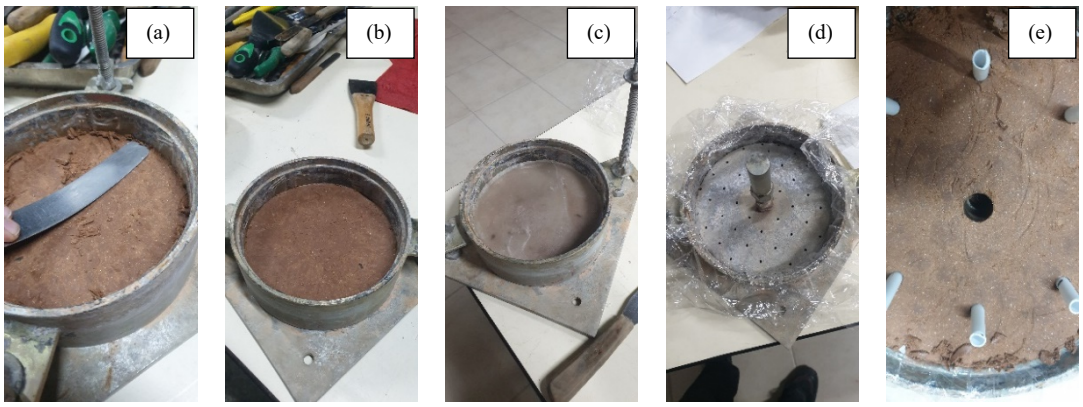

Figure 5.5. Preparation of test setup with anchorage zones

5.2.4. Saturating the test setup and measuring pile movement

The experimental setup, which was intended to be completely saturated, was placed in a plastic cabinet in which the mold could fit completely as shown in Figure 5.6 (a). To reduce the duration of the experiment, the container was filled with water so that the height of the water level did not exceed the height of the mold. Thus, water enters the experimental setup from under the mold. Water was also poured on the surface of the compacted clay, creating a ponding of about 1 cm. In this way, water entry was provided from the top of the clay. Finally, PVC pipes inserted into the clay were filled with water at regular intervals to allow the compacted clay to absorb water from the sides. Dial gages placed on the concrete pile were used to measure how much the pile moved upward as the clay saturated. The experiment was ended when the clay was completely saturated and no further movement of the pile was measured. The total movement of the clay and the pile was then recorded.

In experimental setups with a certain amount of anchorage zone, as shown in Figure 5.6 (b), water change in the anchorage zone and therefore water penetration is not desired. For this reason, water was only supplied from above and through drainage pipes in these setups. In these experiments, the anchoring zone depth required to prevent the movement of the concrete pile by the saturated clay was determined. Therefore, the experiment was repeated with different test setups until the anchorage zone depth was found at which no movement of the pile was observed. After all experiments, soils in the saturated and the anchorage zones were separated as shown in Figure 5.6 (c) and (d). The clay around the pile was checked to see if the clay was completely saturated. In addition, samples were taken from the clays in the anchorage zone for water content measurement and it was checked whether water leaked into this zone.

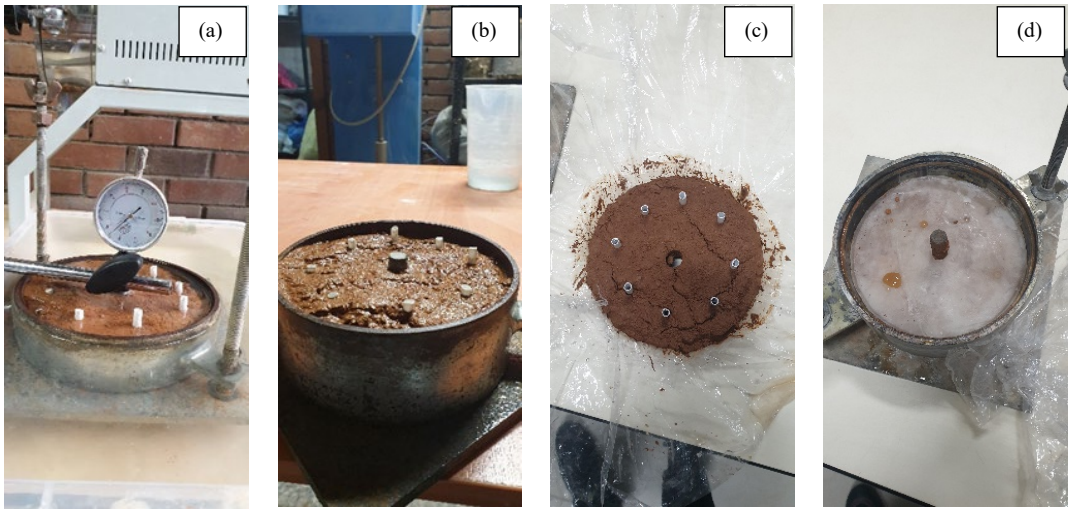

Figure 5.6. Test setup photos during and after the experiment

5.2.5. Laboratory Test Results

First, an experiment was carried out with the entire pile foundation in the Ankara-Cubuk expansive clay, as shown in Figure 5.7 (a), to determine how much upward movement of the pile was induced by heave. The maximum movement of the pile foundation over time was found to be 4.52 mm, as shown in 5.7 (b). At the end of the experiment, the amount of swelling measured at different points in the compacted clay was 5.8 mm on average.

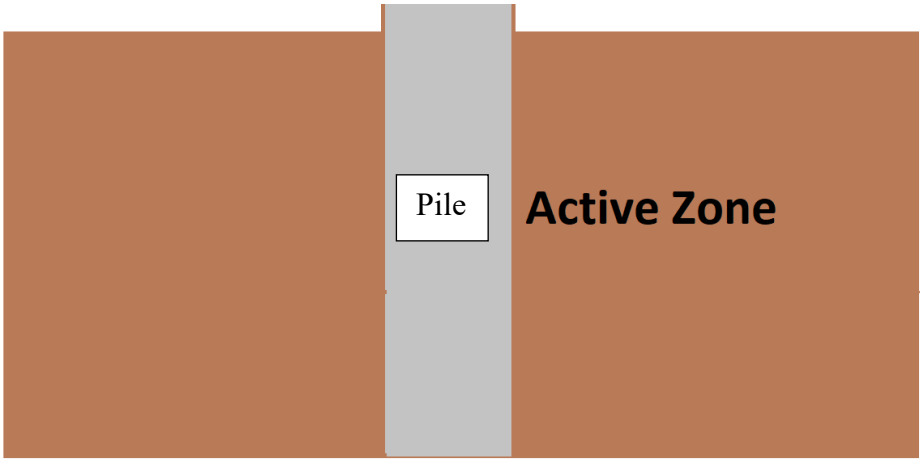

(a)

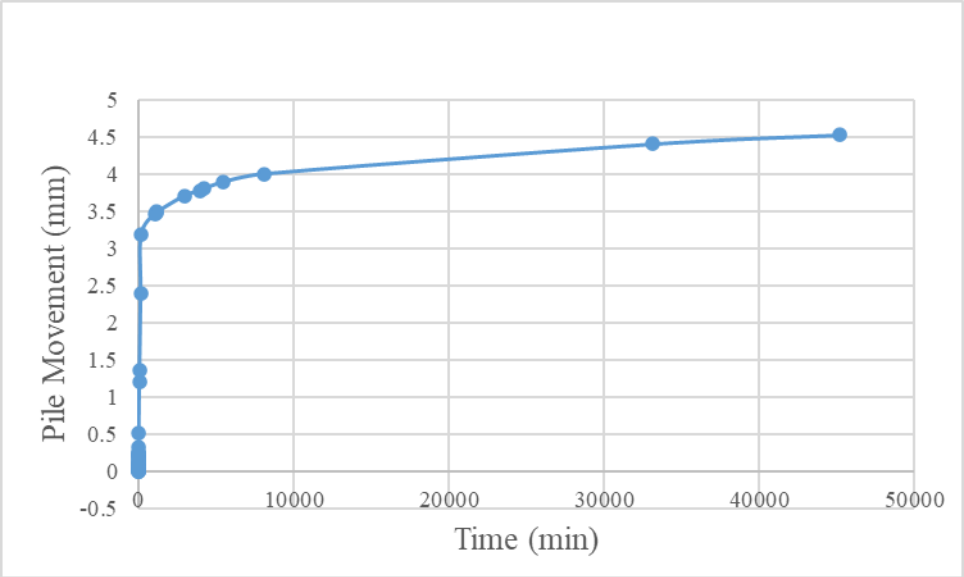

(b)

Figure 5.7. (a) Fully saturated set-up sketch, (b) Pile movement over time

Next, the experimental setup was prepared as shown in Figure 5.8 (a), with 2.5 cm as an anchorage zone with no water content change and 2.5 cm as the active zone where swelling will occur. Figure 5.8 (b) shows the upward movement of the pile measured over time. The experiment showed an average upward movement of 2.75 mm in the compacted clay and a maximum upward movement of 1.03 mm in the pile. This result shows that the amount of anchorage zone is not sufficient to prevent pile movement.

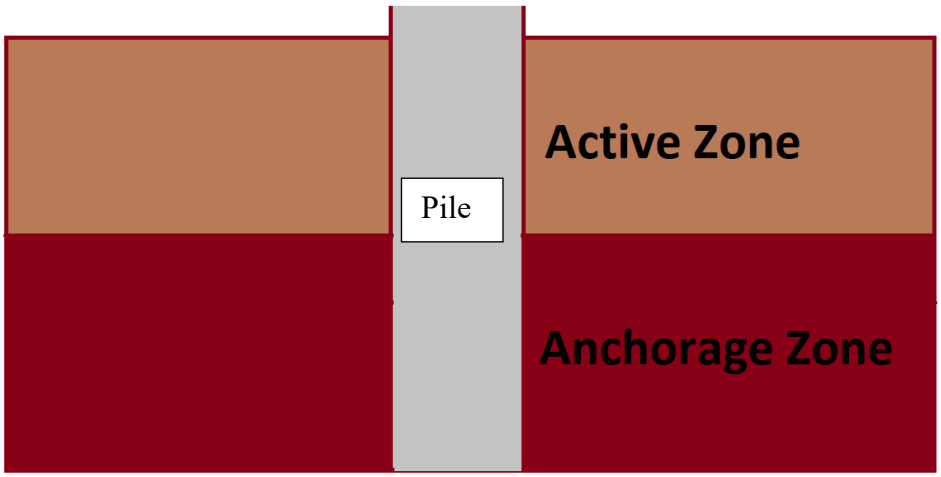

(a)

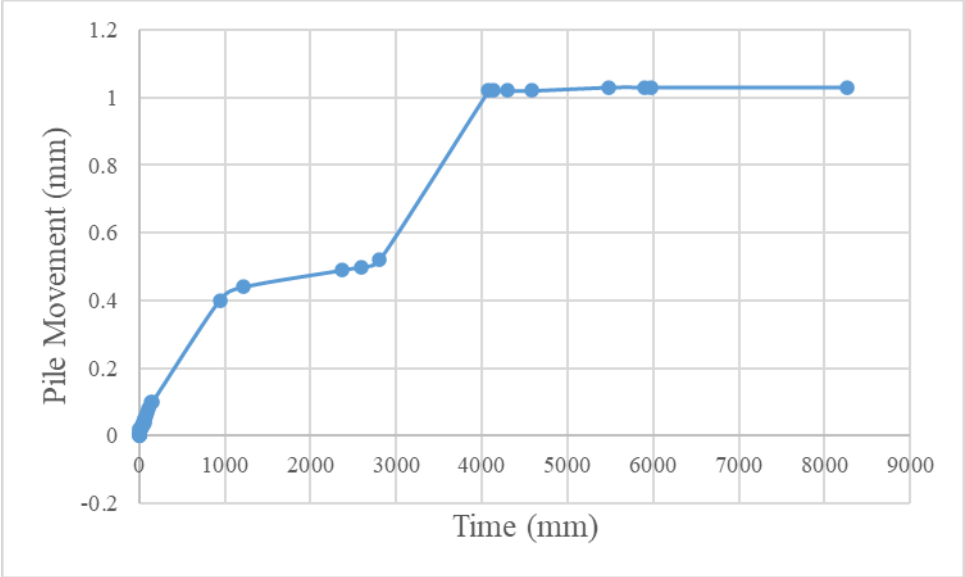

(b)

Figure 5.8. (a) 2.5 cm in active, 2.5 cm in anchor zone set-up, (b) Pile movement over time

Finally, the experimental setup was prepared as shown in Figure 5.9 (a)where the pile was placed in 5 cm of compacted clay with 2/5 (2 cm) of the pile in the active zone and 3/5 (3 cm) of the pile in the anchorage zone. Figure 5.9 (b) shows the upward movement of the pile over time. According to the graph in Figure 5.9 (b), which shows the upward movement of the pile over time, a negligibly low movement of 0.06 mm was observed when water was first introduced into the setup, but no movement was observed in the experiment, which continued for weeks. According to this result, it was found that in order to stabilize the single pile foundation movement in Ankara-Cubuk clay, the portion of the pile within the anchorage zone should be at least 1.5 times the portion within the active zone.

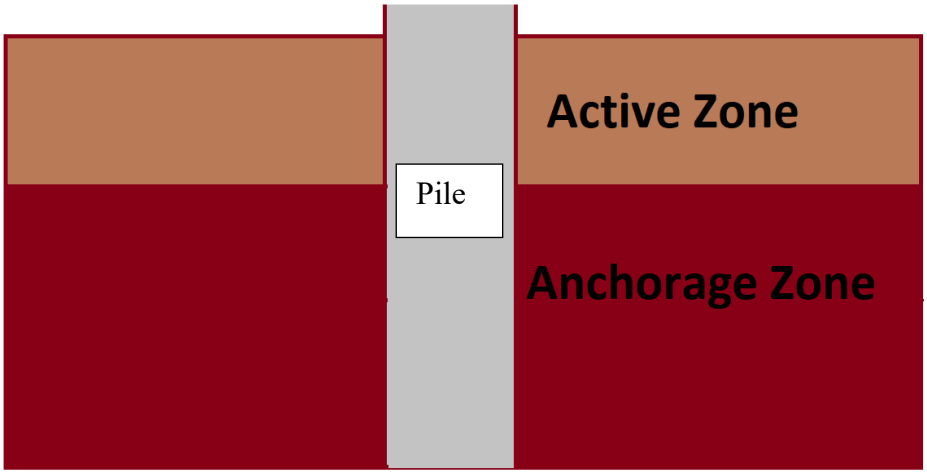

(a)

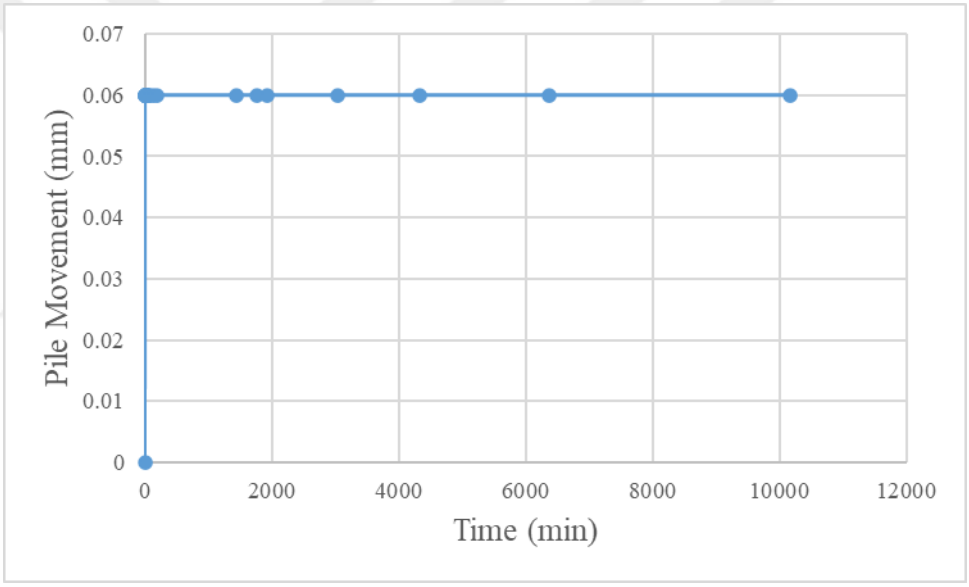

(b)

Figure 5.9. (a) 2 cm in active, 3 cm in anchor zone set-up, (b) Pile movement over time

5.3. Determination of Adhesion Factors

The adhesion factors of the undrained shear strengths of the specimens prepared from two different curves at different water contents and dry densities were found from the formulas recommended for driven piles in Table 5.1. The table shows that

when the undrained shear strength is low, the adhesion factor approaches 1 and when the undrained shear strength increases, the adhesion factor decreases.

Table 5.1. Determination of adhesion factor (α) from the undrained shear strength (c_u) (Coduto, 1994; modified from Cherubini and Vessia, 2008)

Pile Type	Undrained Shear Strength (c_u)	Adhesion Factor (α)
Bored piles	≤ 51 kPa	1
Bored piles	>51 kPa	$0.32 + 250c_u^{-1.5}$
Driven piles	≤ 32 kPa	1
Driven piles	> 32 kPa	$0.35 + 170c_u^{-1.6}$

The adhesion factors for different water contents and dry densities, calculated using the formulas given in Table 5.1, based on the unconfined compression test results, are shown in Table 5.2.

Table 5.2. Adhesion factor determination

Water Content (%)	Undrained Shear Strength from Compaction Curve	Undrained Shear Strength from Shrinkage Curve	Adhesion Factor (α) from Compaction Curve	Adhesion Factor (α) Shrinkage Curve
0.17	17.7	202.8	1	0.39
0.19	41.2	173.7	0.79	0.39
0.21	57.9	102.3	0.61	0.45
0.23	61.0	61.0	0.59	0.59
0.25	76.4	30.1	0.52	1
0.28	44.4	16.6	0.74	1
0.31	24.5	7.9	1	1

5.4. Determination of Adhesion Factors

For the safe pile design, as proposed by Chen, 1975 and commonly used in foundation design, the uplift forces acting on the pile in the active zone should not be higher than the witholding forces in the anchorage zone that would prevent the pile from moving. From the pile foundation movements measurements in the

Ankara-Cubuk clay described above, it was found that the minimum anchorage zone depth required for no movement in the pile, where the part of the pile foundation in the anchorage zone was 1.5 times the part in the active zone. In other words, this is the case where the uplift and the withholding forces acting on the pile are equal to each other. In Equation 5.1, the left side of the equation shows the uplift force acting on the pile in the active zone, and the right side shows the withholding forces acting on the pile in the anchorage zone.

$$\Pi\ d\ Z_a\ \beta\ P_s = \Pi\ d\ \alpha\ c_u(L - Z_a) \qquad Eq\ (5.1)$$

In previous chapters, swelling pressure (p_s) was found to be 157 kPa. The active zone depth (z_a) was found to be 2 cm, and the anchorage zone depth (L-z_a) was found to be 3 cm in the last experimental setup where the uplift forces were equal to the withholding forces. Adhesion factor (α) was found to be approximately 0.6 and undrained shear strength (c_u) 61 kPa from the unconfined compression test with a water content of 23. When all these values are substituted in Equation 5.1, the uplift factor (β_u) is determined to be approximately 0.35.

CHAPTER 6

NUMERICAL ANALYSIS RESULTS OF THE LABORATORY MODEL TEST

6.1. RS-2 Numerical Model

RS-2 is a powerful software created by Rocscience Inc. that is often used for geotechnical design using the finite element (FE) method. Since this software can be used to model stress distribution, deformation, and underground water flow, it is often used by geotechnical engineers for slope stability, tunnels, embankments, retaining walls, and foundation design analysis. While many constitutive models such as Mohr-Coulomb, Hoek-Brown, Modified Cam-Clay, and Hardening Soil Model can be used for soil and rock modeling, the Barcelona Basic Model (BBM) can be used to model the behavior of unsaturated soil.

The parameters of the Barcelona Basic Model, determined by the methodology of Kenanoglu and Toker, (2023), described in detail in the previous chapters, were assigned to the parameters of the Ankara Cubuk expansive clay in the RS-2 software. The experimental setup was modeled axisymetrically using the dimensions of the test setup in the laboratory as shown in Figure 6.1. Thus, it was tried to determine whether the numerical modeling of the experimentally determined BBM parameters could provide a similar amount of swelling and pile movement as the physical test setup (laboratory model) results in the laboratory.

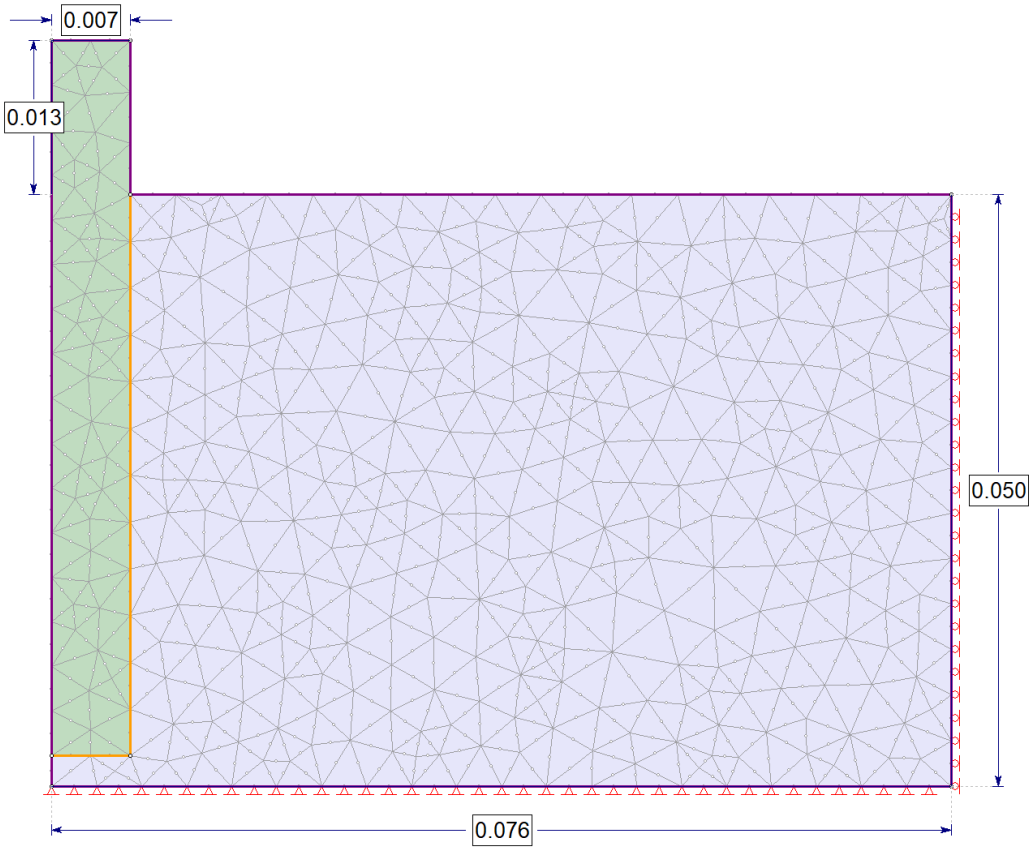

Figure 6.1. Axisymmetric RS-2 model

6.2. Boundary Conditions

In the Numerical RS-2 model shown in Figure 6.1, the boundary conditions were chosen to represent the experimental setup in the laboratory. The red triangular patterned boundary in the bottom part of the model represents the fixed boundary condition where there is no horizontal and vertical displacement. The red circular patterned boundary on the right side of the model represents the boundary condition that does not allow displacement horizontally but allows displacement vertically. No restrictive boundary condition is assigned to the top of the model and horizontal and vertical displacements are allowed in this part. The green area shown on the left side of the model represents the pile foundation and the lines shown in orange indicate the interactions between the pile and the clay.

6.3 Analysis Results

According to the results of the analysis performed using the BBM parameters shown in Table 6.1 and the results shown in Figure 6.2; it was found that an upward movement of 4.07 mm occurred in the concrete pile. The upward movement of the clay surface is minimum at the surface where the pile contacts the clay and maximum in the middle of the model. This behavior is similar to the clay movement observed in laboratory experiments. From the average of 10 different vertical movements taken at equal intervals from the clay surface, the upward movement of the clay was found to be approximately 5.41 mm.

Table 6.1. BBM parameters used in the RS-2 software

$\lambda(0)$	0.084
κ	0.0198
r	0.8909
β	0.0011
p_c	7.9
k	0.56
M	0.67

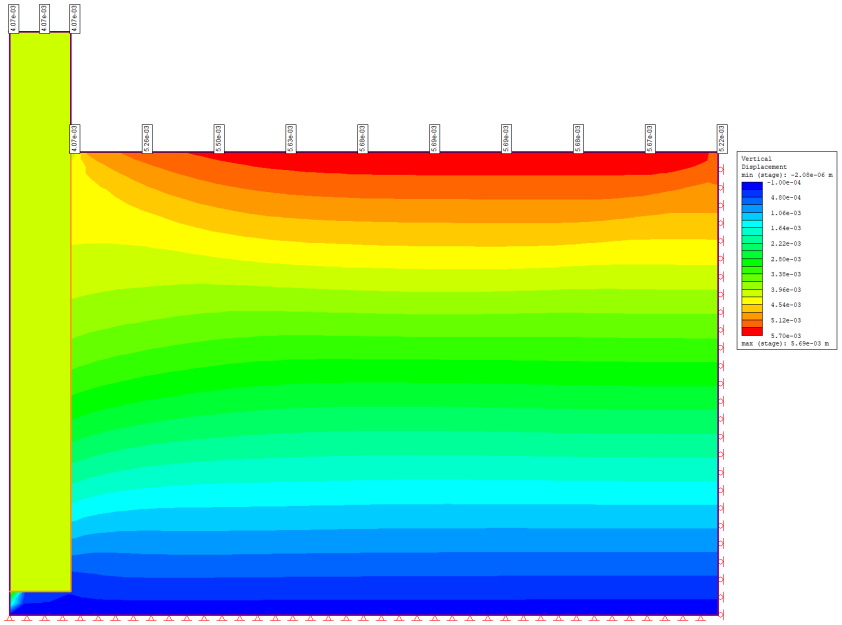

Figure 6.2. RS2 Analysis Results

6.4. Sensitivity Analysis for λ(0), κ, r, β, p_c, k and M parameters

Sensitivity analyses were performed for the parameters λ(0), κ, r, β, p_c, k and M to determine the effect of each of the BBM parameters used in the RS2 model on the upward movement of the pile. Figures 6.3 to 6.9 show the results of the sensitivity analysis for each parameter.

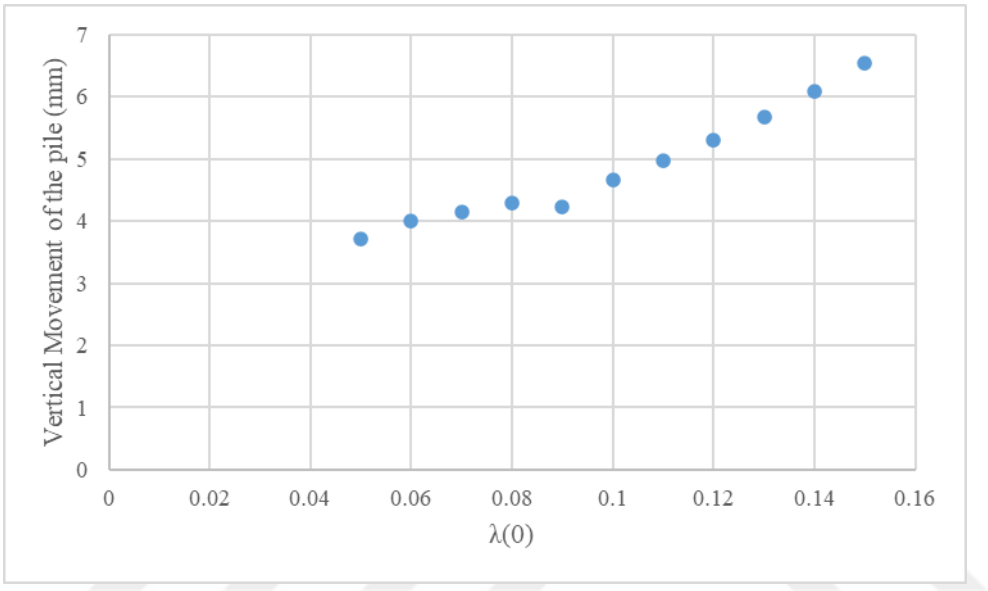

Figure 6.3. Sensitivity Analysis for λ(0)

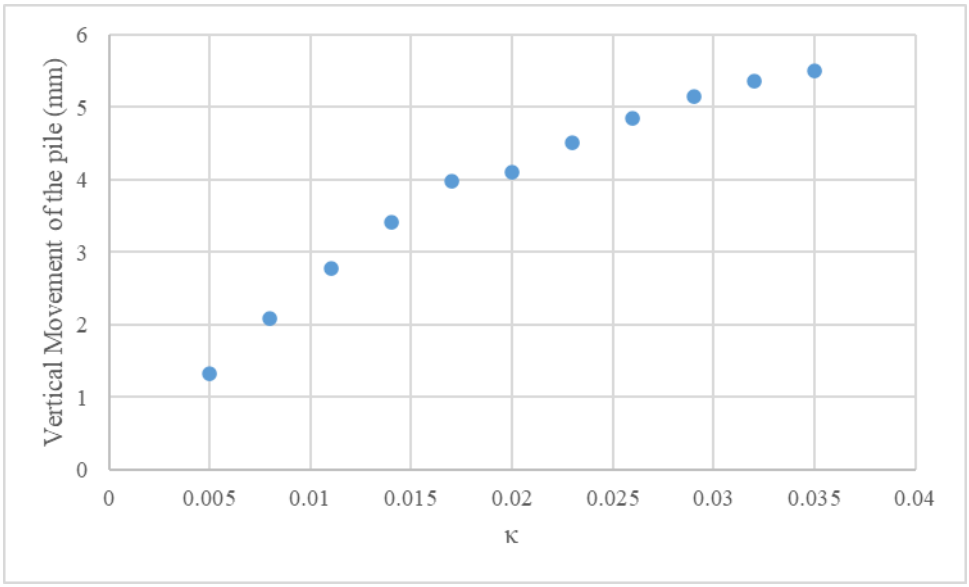

Figure 6.4. Sensitivity Analysis for κ

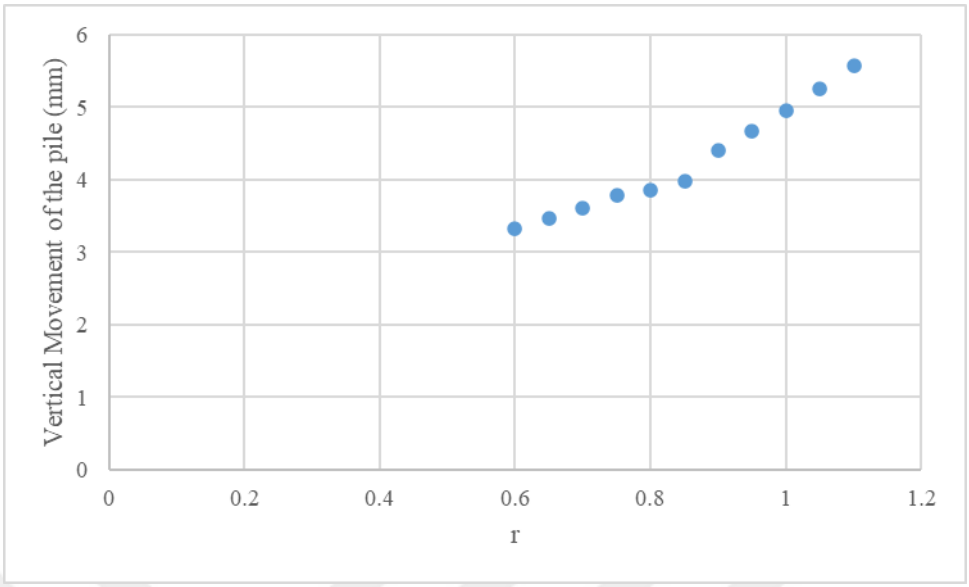

Figure 6.5. Sensitivity Analysis for r

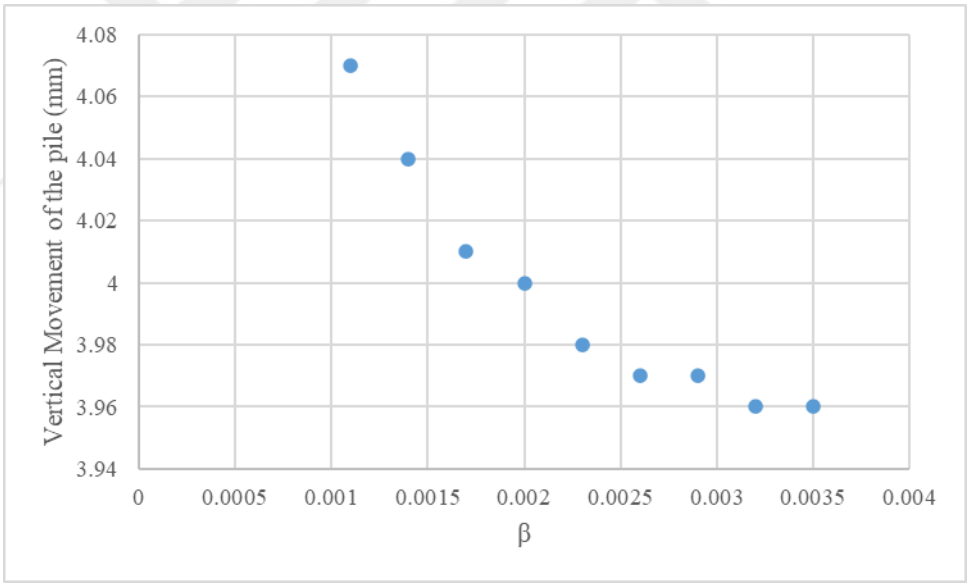

Figure 6.6. Sensitivity Analysis for β

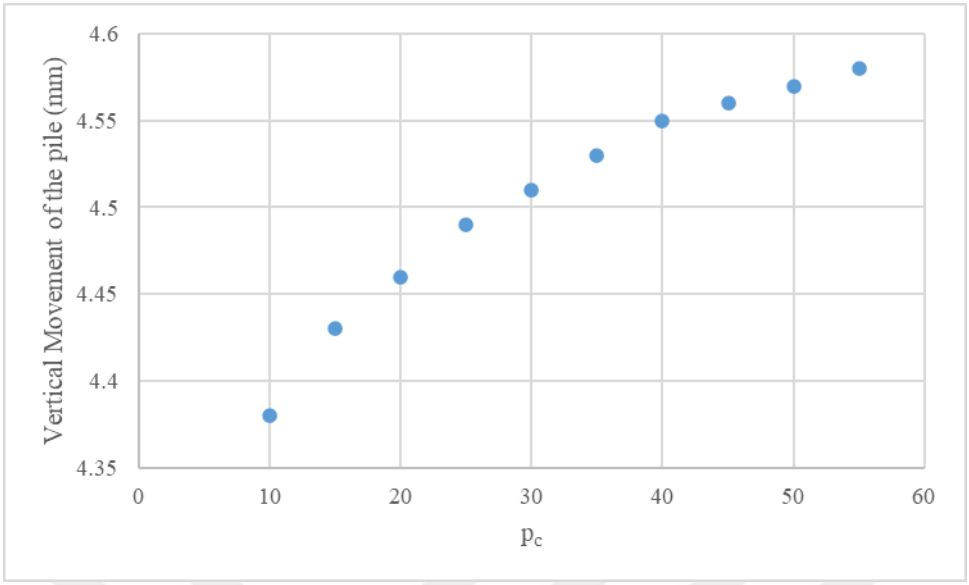

Figure 6.7. Sensitivity Analysis for p_c

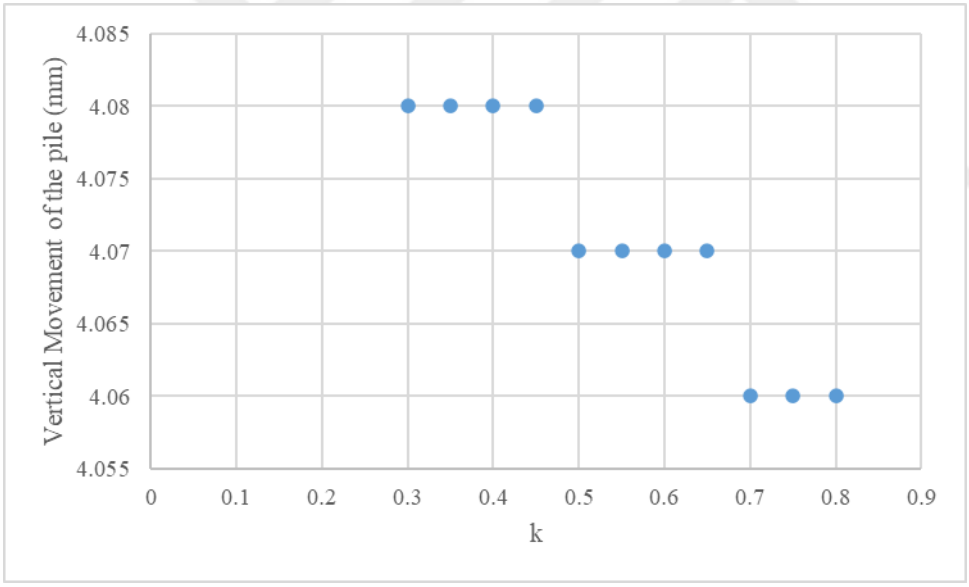

Figure 6.8. Sensitivity Analysis for k

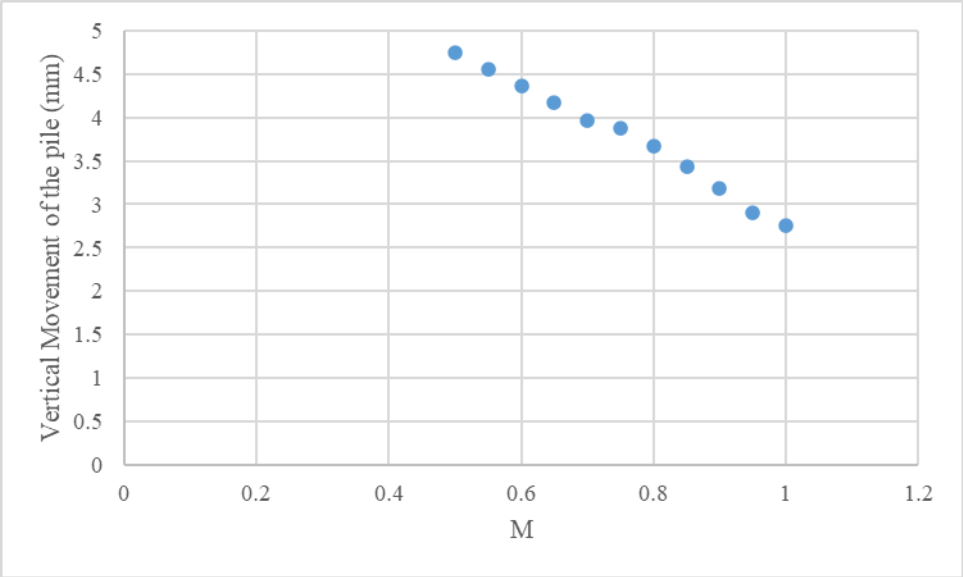

Figure 6.9. Sensitivity Analysis for M

The results of the analysis show that λ(0) (the slope of the virgin compression line) is the most sensitive parameter. An increase in this value leads to higher compressibility of the clay, which affects the movement of the concrete pile. Similarly, the parameter κ (slope of the unloading-reloading line) was found to be the most sensitive parameter after λ(0). In general, sensitivity analysis shows that when piles are designed in expansive clays, changes in these two parameters cause significant movements in the pile structure. Therefore, more care should be taken in determining these parameters.

CHAPTER 7

CONCLUSIONS AND RECOMMENDATIONS FOR FUTURE RESEARCH

7.1. Conclusion

Concrete pile foundations are frequently used throughout the world to prevent damage to superstructures from volumetric changes in expansive clays. This PhD thesis study provided guidelines for the design of single concrete piles in the expansive Ankara clay. Guidelines were given to estimate the uplift and adhesion forces of the piles in expansive Ankara clay.

First, a variety of clay samples were taken from various regions of Ankara. Quick laboratory tests were conducted to determine the swelling potential of different types of soils in various regions of Ankara province. The plasticity index of the high plasticity clay from the Cubuk region was found to be approximately 52% and was determined as the clay with the highest swelling capacity and was used for this study.

Subsequently, the climate of the Cubuk region was determined as semi-arid by Thornthwaite Moisture Index (TMI) analysis (TMI ≈ –22). This means that the water content of the soil in the region can show significant changes as a result of seasonal changes. Therefore, the presence of expansive clay in the region poses a significant threat to the structures to be built on it.

Grain size distribution was determined by combining the sieve and hydrometer test results. According to the obtained result, the clay content of the soil was determined as 61 %. Using the previously determined plasticity index of the clay, the activity of the Cubuk clay was determined as 0.85.

Specific Gravity of the ground was found to be 2.778. Using linear soil shrinkage test, mercury and water submersion techniques, the shrinkage limit of the soil was found to be 12%.

According to the compaction test results, the optimum water content of the clay was found to be 25%, and the maximum dry density at the optimum water content was 1.498 g/cm^3.

The change in volume and dry density values due to the change in the water content of the soil was determined by drawing shrinkage curve.

Soil water retention curve was derived by combining the data obtained from axis translation, salt solution and filter paper methods.

Mechanical and mineralogical laboratory experiments have shown that the Cubuk clay soil contains a significant amount of Montmorillonite-type clay minerals with a swelling pressure of approximately 150 kPa.

According to the methylene blue test results, the specific surface area of the soil was 224.2 m^2/g and the cation exchange capacity was 18.6 meq/100 g.

The undrained shear strengths of the soil specimens prepared at 7 different water contents and dry densities chosen from shrinkage and compaction curve were determined and the adhesion factor of the soil was calculated using these measurements. The adhesion factor was approximately 0.6 for the soil with a water content of 23 % and a dry density of 1.462 g/cm^3.

According to the results of the experiments carried out in the laboratory, it was observed that if 3/5 of the total length of the single piles is placed in the anchor zone in the Ankara clay, there will be no movement of the pile. Thus, from the equality of uplift forces and withholding forces acting on the pile, the uplift factor was found to be 0.38.

In addition, the Barcelona Basic Model parameters were calibrated using the numerous saturated, unsaturated experimental results and the defined soil water

retention curve of Cubuk clay. The laboratory experiment was simulated using the RS-2 software with the calibrated BBM parameters. It was observed that the numerical RS-2 analysis using the BBM soil model gave a similar estimation of upward pile movement as found in the laboratory experiments.

From the sensitivity analysis, it was determined that $\lambda(0)$ (slope of the compression line) and κ (slope of the unloading-reloading line) were the most sensitive parameters for the movement of the pile foundation in expansive clay.

In general, this study is significant in understanding the saturated and unsaturated behavior of Ankara-Cubuk clay while describing it with comprehensive laboratory experiments. The adhesion and uplift factors required for safe pile design in expansive clays were found for Ankara-Cubuk clay and the anchoring zone depth required for safe pile design was found to be 1.5 times the active zone depth, which is one of the major results of the study. This knowledge is an important reference for pile foundations to be designed especially in arid and semi-arid climates like Ankara where expansive clay distribution is widespread and climatic conditions can cause a significant change in the water content in the soil. In addition, this study shows that Ankara-Cubuk clay, which is very difficult to predict the behavior and model because of the change in material properties depending on the water content, can be modeled using the BBM method.

7.2. Recommendations For Future Research

Although this is a comprehensive study in describing the behavior of the Ankara-Cubuk expansive clay and modeling its interaction with a concrete pile foundation, it is recommended to validate the findings in by additional future studies.

First, the study can be repeated with different sized piles and laboratory setups and the results can be compared with the obtained findings. Ideally, instead of a small scaled setup artificially prepared in the laboratory, full scaled measurements in the field may give more realistic results.

Different types of expansive clays can be taken from different locations in Ankara or Türkiye for testing.

In addition to structures that require the use of single pile foundations such as wind panels, electric poles, etc., experiments can also be extended by using pile groups for situations where group pile foundations are required.

The behavior of piles used in slopes can be studied by performing slope stability analyses.

The behavior of pile types that may have different interface shear strengths, such as steel piles, can be evaluated by conducting similar studies.

The effect of wetting and drying cycles on the pile can be studied.

Numerical analyses can be performed using different unsaturated soil models.

Effects of different structural loads on pile behavior can be studied.

The effect of reducing the friction between the clay and the pile by using a pile jacket in the active zone can be studied. This method will reduce the upward movement of the pile.

REFERENCES

AFNOR. (1993). *Mesure de la quantité et de l'activité de la fraction argileuse (Norme Française NF, pp. 68–94).* Association Française de Normalisation (AFNOR).

Ahmed, M. Y., Evans, R., & Imteaz, M. A. (2016, October). *Influence of roadside vegetation on roughness progression for pavements founded on expansive soils.* Paper presented at the 2nd IRF Asia Regional Congress & Exhibition, Kuala Lumpur, Malaysia.

Akgün, H., Türkmenoğlu, A. G., Met, İ., Yal, G. P., & Koçkar, M. K. (2017). The use of Ankara clay as a compacted clay liner for landfill sites. *Clay Minerals*, 52(3), 391–412. https://doi.org/10.1180/claymin.2017.052.3.08

Al-Mukhtar, M., Lasledj, A., & Alcover, J. (2010). Behaviour and mineralogy changes in lime-treated expansive soil at 20°C. *Applied Clay Science, 50*(2), 191–198. https://doi.org/10.1016/j.clay.2010.07.023

Alnmr, A., Ray, R. P., & Alsirawan, R. (2023). A state-of-the-art review and numerical study of reinforced expansive soil with granular anchor piles and helical piles. *Sustainability, 15*(3), 2802. https://doi.org/10.3390/su15032802

Alonso, E. E., Vaunat, J., & Gens, A. (1999). Modelling the mechanical behaviour of expansive clays. *Engineering Geology, 54*(1–2), 173–183.

Al-Rawas, A. A., Hago, A. W., & Al-Sarmi, H. (2005). Effect of lime, cement and Sarooj (artificial pozzolan) on the swelling potential of an expansive soil from Oman. *Building and Environment, 40*(5), 681–687. https://doi.org/10.1016/j.buildenv.2004.08.028

ASTM D4318-17e1. (2017). *Standard test methods for liquid limit, plastic limit, and plasticity index of soils.* ASTM International. https://doi.org/10.1520/D4318-17E01

ASTM International. (2003). *ASTM D5298-03: Standard test method for measurement of soil potential (suction) using filter paper*. https://doi.org/10.1520/D5298-03

ASTM International. (2004). *ASTM D3080/D3080M-04: Standard test method for direct shear test of soils under consolidated drained conditions*. https://doi.org/10.1520/D3080-04

ASTM International. (2006). *ASTM D854-06e1: Standard test methods for specific gravity of soil solids by water pycnometer*.

ASTM International. (2009). *ASTM D6913-04: Standard test methods for particle-size distribution (gradation) of soils using sieve analysis*. https://doi.org/10.1520/D6913-04

ASTM International. (2011). *ASTM D4767-11: Standard test method for consolidated undrained triaxial compression test for cohesive soils*. https://doi.org/10.1520/D4767-11

ASTM International. (2011). *ASTM D5890-11: Standard test method for swell index of clay mineral component of geosynthetic clay liners*. https://doi.org/10.1520/D5890-11

ASTM International. (2011). *ASTM D5890-11: Standard test method for swell index of clay mineral component of geosynthetic clay liners*. https://doi.org/10.1520/D5890-11

ASTM International. (2011). *ASTM D7181-11: Standard test method for consolidated drained triaxial compression test for soils*. https://doi.org/10.1520/D7181-11

ASTM International. (2012). *ASTM E104-02(2012): Standard practice for maintaining constant relative humidity by means of aqueous solutions*. https://doi.org/10.1520/E0104-02R12

ASTM International. (2014). *ASTM D4546-14: Standard test methods for one-dimensional swell or collapse of soils*. https://doi.org/10.1520/D4546-14

ASTM International. (2017). *ASTM D7928-17: Standard test method for particle-size distribution (gradation) of fine-grained soils using the sedimentation (hydrometer) analysis*. https://doi.org/10.1520/D7928-17

ASTM International. (2018). *ASTM D4943-18: Standard test method for shrinkage factors of soils by the wax method*. ASTM International. https://doi.org/10.1520/D4943-18

ASTM International. (2021). *ASTM D1557-12(2021): Standard test methods for laboratory compaction characteristics of soil using modified effort (56,000 ft-lbf/ft³ (2,700 kN-m/m³))*. https://doi.org/10.1520/D1557-12R21

ASTM International. (2021). *ASTM D698-12(2021): Standard test methods for laboratory compaction characteristics of soil using standard effort (12,400 ft-lbf/ft³ (600 kN-m/m³))*. https://doi.org/10.1520/D0698-12R21

Baker, M. L., Baas, J. H., Malarkey, J., Jacinto, R. S., Craig, M. J., Kane, I. A., & Barker, S. (2017). The effect of clay type on the properties of cohesive sediment gravity flows and their deposits. *Journal of Sedimentary Research, 87*(11), 1176–1195.

Basma, A. A., & Tuncer, E. R. (1991). Effect of lime on volume change and compressibility of expansive clays. *Transportation research record*, (1295).

Basma, A. A., Al-Homoud, A. S., & Husein, A. (1995). Laboratory assessment of swelling pressure of expansive soils. *Applied Clay Science, 9*(5), 355–368.

Benvenga, M. M. (2005). *Pier-soil adhesion factor for drilled shaft piers in expansive soil* (Master's thesis, Colorado State University). Colorado State University Libraries.

Bunaciu, A. A., Udriştioiu, E. G., & Aboul-Enein, H. Y. (2015). X-ray diffraction: Instrumentation and applications. *Critical Reviews in Analytical Chemistry, 45*(4), 289–299. https://doi.org/10.1080/10408347.2014.949616

Bureau of Indian Standards. (1986). *IS 2720 (Part XL): Methods of test for soils – Determination of free swell index of soils*. Bureau of Indian Standards.

Bureau of Indian Standards. (1987). *Standards India* (Vol. 1). Bureau of Indian Standards.

Chen, F. H. (1988). *Foundations on expansive soils*. Elsevier Science.

Chen, F. H. (2012). *Foundations on expansive soils* (Vol. 12). Elsevier.

Cherubini, C., & Vessia, G. (2007). Reliability approach for the side resistance of piles by means of the total stress analysis (α method). *Canadian Geotechnical Journal, 44*(11), 1378–1390.

Chittoori, B., & Puppala, A. J. (2011). Quantitative estimation of clay mineralogy in fine-grained soils. *Journal of Geotechnical and Geoenvironmental Engineering, 137*(11), 997–1008.

Coduto, D. P. (1994). *Foundation design: Principles and practices*. Prentice Hall.

Çokça, E. (1991). *Swelling potential of expansive soils with a critical appraisal of the identification of swelling of Ankara soils by methylene blue tests* (Doctoral dissertation, Middle East Technical University, Ankara, Türkiye).

Cokca, E. (2001). Use of class C fly ashes for the stabilization of an expansive soil. *Journal of Geotechnical and Geoenvironmental Engineering, 127*(7), 568–573. https://doi.org/10.1061/(ASCE)1090-0241(2001)127:7(568)

Çokça, E. (2002). Relationship between methylene blue value, initial soil suction and swell percent of expansive soils. *Turkish Journal of Engineering and Environmental Sciences, 26*, 521–529.

Dafalla, M. A., Al-Shamrani, M. A., Puppala, A. J., & Ali, H. E. (2012). Design guide for rigid foundation systems on expansive soils. *International Journal of Geomechanics, 12*(5), 528–536.

Das, B. M. (2011). *Principles of foundation engineering* (SI 7th ed.). Cengage Learning.

Deliktaş, C., & Çokça, E. (2020). Influence of swell on undrained shear strength of expansive Ankara clay. *Arabian Journal of Geosciences, 13*, Article 903. https://doi.org/10.1007/s12517-020-05767-z

Elsharief, A. M., Ahmed, E. O., & Mohamedzein, Y. E. A. (2016). Guidelines for the design of bored concrete piles in expansive soils of Sudan. *Journal of Building and Road Research, 8*(1).

Ergüler, Z. A., & Ulusay, R. (2003). A simple test and predictive models for assessing swell potential of Ankara (Türkiye) clay. *Engineering Geology, 67*(3–4), 331–352.

Ertekin, Y. (1991). *Measurement of lateral swell pressure with thin wall oedameter technique* (Master's thesis, Middle East Technical University).

Fityus, S., & Smith, D. W. (2000). The influence of fabric and mineralogy on the expansivity of an Australian residual clay. In H. Rahardjo & D. G. Toll (Eds.), *Unsaturated soils for Asia* (pp. 657–662).\

Fredlund, D. G., Rahardjo, H., & Fredlund, M. D. (2012). *Unsaturated soil mechanics in engineering practice*. John Wiley & Sons.

Gallipoli, D., D'Onza, F., & Wheeler, S. J. (2010). A sequential method for selecting parameter values in the Barcelona basic model. *Canadian Geotechnical Journal, 47*(11), 1175–1186.

Gardner, R. (1937). A method of measuring the capillary tension of soil moisture over a wide moisture range. *Soil Science, 43*(4), 277–284. https://doi.org/10.1097/00010694-193704000-00004

Gérmaine, J. T., & Gérmaine, A. V. (2009). *Geotechnical laboratory measurements for engineers*. John Wiley & Sons.

Greenspan, L. (1977). Humidity fixed points of binary saturated aqueous solutions. *Journal of Research of the National Bureau of Standards. Section A, Physics and Chemistry, 81A*(1), 89–96. https://doi.org/10.6028/jres.081A.011

Grim, R. E. (1959). Physico-chemical properties of soils: Clay minerals. *Journal of the Soil Mechanics and Foundations Division, 85*(2), 1–17.

Grim, R. E. (1962). Clay mineralogy: The clay mineral composition of soils and clays is providing an understanding of their properties. *Science, 135*(3507), 890–898. https://doi.org/10.1126/science.135.3507.890

Hamblin, A. P. (1981). Filter-paper method for routine measurement of field water potential. *Journal of Hydrology, 53*(3–4), 355–360.

Holtz, R. D., Kovacs, W. D., & Sheahan, T. C. (1981). *An introduction to geotechnical engineering* (Vol. 733). Prentice-Hall.

Holtz, R. D., Kovacs, W. D., & Sheahan, T. C. (2011). *An introduction to geotechnical engineering* (2nd ed.). Prentice Hall.

Holtz, W. G., & Gibbs, J. J. (1956). Engineering properties of expansive clays. *ASCE Transactions, 121*, Paper No. 2814. https://doi.org/10.1061/(ASCE)0733-9410(1993)119:2(374).

Ikizler, S. B. (2018). A moisture index map of Türkiye for design of slabs resting on expansive soils by GIS approach. *Teknik Dergi, 29*(6), 8731–8751.

Ito, M., & Azam, S. (2013). Engineering properties of a vertisolic expansive soil deposit. *Engineering Geology, 152*, 10–16.

Jalal, F. E., Xu, Y., Iqbal, M., Jamhiri, B., & Javed, M. F. (2021). Predicting the compaction characteristics of expansive soils using two genetic

programming-based algorithms. *Transportation Geotechnics, 30*, 100608. https://doi.org/10.1016/j.trgeo.2021.100608

Jury, W. A., Gardner, W. R., & Gardner, W. H. (1991). *Soil physics* (5th ed.). John Wiley & Sons.

Kalkan, E., & Bayraktutan, M. S. (2007). Geotechnical evaluation of Turkish clay deposits: A case study in Northern Türkiye. *Environmental Geology, 55*(5), 937–950. https://doi.org/10.1007/s00254-007-1044-8

Kenanoğlu, M. B. (2023). *Determination of unsaturated soil properties from simplified experimental procedures* (Doctoral dissertation, Middle East Technical University).

Kenanoğlu, M. B., & Toker, N. K. (2018, August). *Changing and equilibrating water content of triaxial test specimens without suction control* [Conference paper]. Middle East Technical University. https://www.researchgate.net/publication/343295809

Knight, R. J., Tercier, P., & Georgi, D. T. (1995, June). *A laboratory procedure for estimating irreducible water saturation from cuttings*. Paper presented at the SPWLA 36th Annual Logging Symposium, Paris, France.

Leong, E. C., & Wijaya, M. (2023). *Laboratory tests for unsaturated soils*. CRC Press.

Likos, W. J., & Lu, N. (2002). Filter paper technique for measuring total soil suction. *Transportation Research Record, 1786*(1), 120–128.

Lu, N., & Likos, W. J. (2004). *Unsaturated soil mechanics*. John Wiley & Sons.

Lucian, C. H. (2011). Geotechnology to determine the depth of active zone in expansive soils in Kibaha, Tanzania. *Global Journal of Pure and Applied Sciences, 17*(2), 189–195.

Lyons, S. E., & Ross, R. M. (2015). Earth hazards of the South Central US. In *Earth hazards in the South Central US* (pp. 301–334).

Mabirizi, D., & Bulut, R. (2009). A comparison of total suction measurements with thermocouple psychrometer, filter paper technique, and chilled-mirror device. In *Characterization, modeling, and performance of geomaterials: Selected papers from the 2009 GeoHunan International Conference* (pp. 1–6). American Society of Civil Engineers.

Mitchell, J. K., & Soga, K. (2005). *Fundamentals of soil behavior* (3rd ed.). John Wiley & Sons.

Mitchell, P. W. (2013). Climate change effects on expansive soil movements. In *Proceedings of the 18th International Conference on Soil Mechanics and Geotechnical Engineering, Paris 2013* (pp. 1159–1162).

Mittal, V., Samanta, M., & Maurya, M. C. (2025). Effect of soil constitutive models and slenderness ratios of piles on seismic performance of moment-resisting frames supported on pile foundation considering soil–pile–structure interaction. *Journal of Structural Design and Construction Practice, 30*(2), 04025004.

Mohan, D., & Chandra, S. (1961). Frictional resistance of bored piles in expansive clays. *Géotechnique, 11*(4), 294–301. https://doi.org/10.1680/geot.1961.11.4.294

Mollamahmutoğlu, M., Yılmaz, Y., & Güngör, A. G. (2005). Stabilization of expansive soils of Bursa (Türkiye) region highway fills using fly ash. In *Proceedings of the International Conference on Problematic Soils* (pp. 1–8). Eastern Mediterranean University.

Murray, H. H. (2007). *Applied clay mineralogy: Occurrences, processing and application of kaolins, bentonites, palygorskite-sepiolite, and common clays*. Elsevier.

Nalbantoglu, Z., & Gucbilmez, E. (2001). Improvement of calcareous expansive soils in semi-arid environments. *Journal of Arid Environments, 47*(4), 453–463. https://doi.org/10.1006/jare.2000.0726

Nalbantoglu, Z., & Tawfiq, S. (2006). Evaluation of the effectiveness of olive cake residue as an expansive soil stabilizer. *Environmental Geology, 50*(6), 803–807. https://doi.org/10.1007/s00254-006-0252-y

Naval Facilities Engineering Command. (1986). *Foundations and earth structures (Design Manual 7.02)*. Alexandria, VA: Naval Facilities Engineering Command.

Nelson, J. D., & Miller, D. J. (1992). *Expansive soils: Problems and practice in foundation and pavement engineering*. John Wiley & Sons.

Nelson, J. D., & Miller, D. J. (1997). *Expansive soils: Problems and practice in foundation and pavement engineering*. John Wiley & Sons.

Nelson, J. D., Chao, K. C., Overton, D. D., & Nelson, E. J. (2015). *Foundation engineering for expansive soils*. John Wiley & Sons.

Öncü, Ş., & Bilsel, H. (2018). Utilization of waste marble to enhance volume change and strength characteristics of sand-stabilized expansive soil. *Environmental Earth Sciences, 77*(461), 1–13. https://doi.org/10.1007/s12665-018-7638-5

Özdemir, A., Kalkan, E., & Turhan, D. (2024). Geotechnical investigation for a damaged light building erected on a fill material-rich in expansive soil. *International Journal of Earth Sciences Knowledge and Applications*, *6*(2), 143–157.

Ozer, M., Ulusay, R., & Isik, N. S. (2011). Evaluation of damage to light structures erected on a fill material rich in expansive soil. *Bulletin of Engineering Geology and the Environment, 71*(1), 21–36. https://doi.org/10.1007/s10064-011-0395-2

Poulos, H. G. (1993). Piled rafts in swelling or consolidating soils. *Journal of Geotechnical Engineering, 119*(2), 374–380. https://doi.org/10.1061/(ASCE)0733-9410(1993)119:2(374)

Prakash, S., & Sharma, H. D. (1991). *Pile foundations in engineering practice*. John Wiley & Sons.

Pruška, J., & Šedivý, M. (2017, September). Swelling soils in the road structures. *IOP Conference Series: Materials Science and Engineering, 236*(1), 012037. https://doi.org/10.1088/1757-899X/236/1/012037

Radevsky, R. (2001). Expansive clay problems—How are they dealt with outside the USA In *Expansive clay soils and vegetative influence on shallow foundations* (pp. 172–191). American Society of Civil Engineers.

Rajesh, S., Roy, S., & Madhav, S. (2017). Study of measured and fitted SWCC accounting the irregularity in the measured dataset. *International Journal of Geotechnical Engineering, 11*(4), 321–331.

Rao, R. R., Rahardjo, H., & Fredlund, D. G. (1988). Closed-form heave solutions for expansive soils. *Journal of Geotechnical Engineering, 114*(5), 573–588. https://doi.org/10.1061/(ASCE)0733-9410(1988)114:5(573)

Rehman, A. (2017). *Swelling correlations* [SlideShare presentation]. SlideShare. Retrieved November 16, 2024, from https://www.slideshare.net/slideshow/swelling-correlations/71847097

Richards, B. G., Peter, P., & Emerson, W. W. (1983). The effects of vegetation on the swelling and shrinking of soils in Australia. *Geotechnique*, *33*(2), 127–139. https://doi.org/10.1680/geot.1983.33.2.127

Ridley, A. M., Dineen, K., Burland, J. B., & Vaughan, P. R. (2003). Soil matrix suction: Some examples of its measurement and application in geotechnical engineering. *Géotechnique*, *53*(2), 241–253. https://doi.org/10.1680/geot.2003.53.2.241

Rosenbalm, D., & Zapata, C. E. (2017). Effect of wetting and drying cycles on the behavior of compacted expansive soils. *Journal of Materials in Civil Engineering, 29*(1), 04016191.

Sapaz, B. (2004). *Lateral versus vertical swell pressures in expansive soils* (Doctoral dissertation, Middle East Technical University). Middle East Technical University Institutional Repository.

Seed, H. B., Woodward, R. J., & Lundgren, R. (1962). Prediction of swelling potential for compacted clays. *Journal of the Soil Mechanics and Foundations Division, ASCE*, *88*(SM3), 53–87.

Sharma, R., Bisen, D. P., Shukla, U., & Sharma, B. G. (2012). X-ray diffraction: A powerful method of characterizing nanomaterials. *Recent Research in Science and Technology*, *4*(8), 77–79.

Shen, M. F., Tan, X. H., Xin, Z. Y., Xie, Y., & Xu, Q. (2013). Laboratory research of soil water characteristic curve by osmotic method and filter paper method. *Electronic Journal of Geotechnical Engineering*, *18*(1), 5421–5434.

Shi, B., Jiang, H., Liu, Z., & Fang, H. Y. (2002). Engineering geological characteristics of expansive soils in China. *Engineering Geology, 67*(1–2), 63–71.

Skempton, A. W. (1953). The colloidal activity of clays. In *Selected papers on soil mechanics* (Vol. 1, pp. 57–61). London: Thomas Telford.

Skempton, A. W. (1959). Cast in-situ bored piles in London clay. *Geotechnique, 9*(4), 153–173. https://doi.org/10.1680/geot.1959.9.4.153

Soltani, A., Azimi, M., Deng, A., & Taheri, A. (2019). A simplified method for determination of the soil–water characteristic curve variables. *International Journal of Geotechnical Engineering, 13*(4), 316–325. https://doi.org/10.1080/19386362.2017.1344450

Sridharan, A., & Prakash, K. (2000). Classification procedures for expansive soils. *Proceedings of the Institution of Civil Engineers - Geotechnical Engineering*, *143*(4), 235–240. https://doi.org/10.1680/geng.2000.143.4.235

Standards Association of Australia. (1977). *AS 1289.C4.1-1977: Methods of testing soils for engineering purposes – Soil classification tests – Determination of the linear shrinkage of a soil – Standard method*. Standards Association of Australia.

Taylor, R. K. (1985). Cation exchange in clays and mudrocks by methylene blue. *Journal of Chemical Technology and Biotechnology. Chemical Technology*, *35*(4), 195–207.

Thornthwaite, C. W. (1948). An approach toward a rational classification of climate. *Geographical Review*, *38*(1), 55–94. https://doi.org/10.2307/210739

Tjandra, D., & Soemitro, R. A. A. (2013). The effects of water content variation on adhesion factor of pile foundation in expansive soil. *Civil Engineering Dimension*, *15*(2), 114–119.

Türköz, M., & Tosun, H. (2011). The use of methylene blue test for predicting swell parameters of natural clay soils. *Scientific Research and Essays, 6*(8), 1780–1792.

Ünver, İ. S., Lav, M. A., & Çokça, E. (2021). Improvement of an extremely highly plastic expansive clay with hydrated lime and fly ash. *Geotechnical and Geological Engineering, 39*(5), 4917–4932. https://doi.org/10.1007/s10706-021-01803-1

Verma, S. K., & Maru, S. (2013). Behaviourial study of expansive soils and its effect on structures–A review. *International Journal of Innovations in Engineering and Technology, 2*(2), 228–238.

Verruijt, A. (2001). *Soil mechanics* (p. 315). Delft University of Technology.

Wagner, S. (2002). *The effects of variable amounts of clay and organic matter on soil structural evolution* (Master's thesis). University of Sydney.

Wheeler, S. J., Gallipoli, D., & Karstunen, M. (2002). Comments on use of the Barcelona Basic Model for unsaturated soils. *International Journal for Numerical and Analytical Methods in Geomechanics, 26*(15), 1561–1571.

Wilson, S. D. (1970). Suggested method of test for moisture-density relations of soils using Harvard compaction apparatus. In *Special procedures for testing soil and rock for engineering purposes* (5th ed.). ASTM International.

Wise, J. R., & Hudson, W. R. (1971). *An examination of expansive clay problems in Texas* (No. 118-5). University of Texas at Austin.

Wu, X., & Vanapalli, S. K. (2022). Three-dimensional modeling of the mechanical behavior of a single pile in unsaturated expansive soils during infiltration. *Computers and Geotechnics, 145*, 104696. https://doi.org/10.1016/j.compgeo.2022.104696

Xiao, H.-B., Zhang, C.-S., Wang, Y.-h., & Fan, Z.-H. (2011). Pile-soil interaction in expansive soil foundation: Analytical solution and numerical simulation. *International Journal of Geomechanics, 11*(3), 159–166. https://doi.org/10.1061/(ASCE)GM.1943-5622.0000046

Ye, W. M., Bai, Y., Jin, Q., Chen, B., & Cui, Y. J. (2006). Lab experimental study on soil-water characteristics of Shanghai soft clay. *Chinese Journal of Geotechnical Engineering, 28*(2), 260–263. *(in Chinese).*

Yilmaz, I., & Karacan, E. (2002). Geotechnical properties of clayey alluvial soils in the Erbaa Basin, Türkiye. *International Geology Review, 44*(2), 179–190. https://doi.org/10.2747/0020-6814.44.2.179

Zhang, D., & Acosta-Martinez, H. (2023). *Climate change challenges for the geotechnical design of solar farm foundations*. In *Proceedings of the 14th*

Australia and New Zealand Conference on Geomechanics (ANZGeo 2023), Cairns, Australia.

Zhang, X., & Xiao, M. (2013). Using modified state surface approach to select parameter values in the Barcelona basic model. *International Journal for Numerical and Analytical Methods in Geomechanics, 37*(12), 1847–1866. https://doi.org/10.1002/nag.2112

Zhang, X., Alonso, E. E., & Casini, F. (2016). Explicit formulation of at-rest coefficient and its role in calibrating elasto-plastic models for unsaturated soils. *Computers and Geotechnics, 71*, 56–68.

Zheng, J. L., Zhang, R., & Yang, H. P. (2009). Highway subgrade construction in expansive soil areas. *Journal of Materials in Civil Engineering, 21*(4), 154–162. https://doi.org/10.1061/(ASCE)0899-1561(2009)21:4(154)

APPENDICES

A. FIGURES TO EXPLAIN THE PARAMETERS OF BBM FROM INTERNET

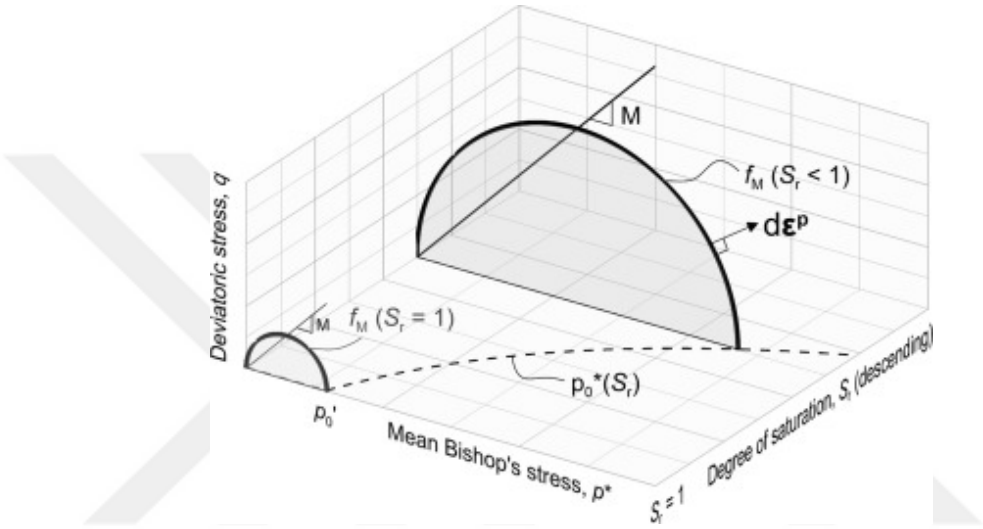

Figure A.1. *Comparison of p-q-Sr diagram and p-q-s diagram.*

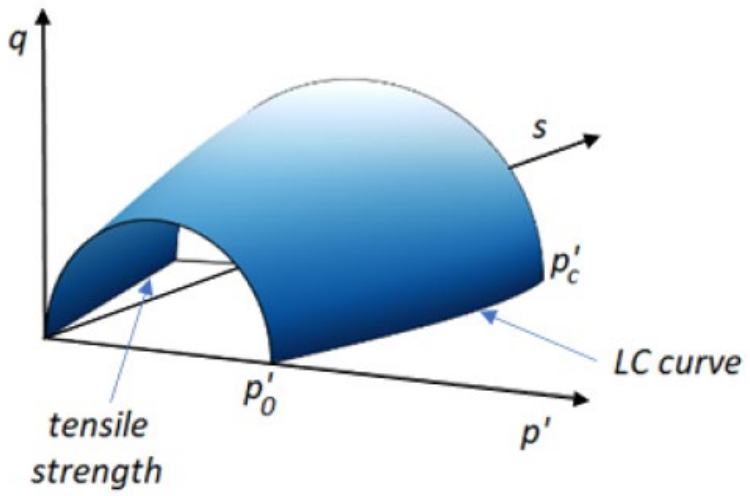

Figure A.2. BBM model demonstration

A.1. Parameters for BBM

$$\acute{\sigma} = (\sigma - u_a) + \chi(u_a - u_w)$$

$$f_1 = q^2 - M^2(p + p_s)(p_0 + p) = 0$$

$$f_2 = s - s_0 = 0$$

$$\frac{Po}{p_c} = \left(\frac{p_0^*}{p^c}\right)^{\left(\frac{\lambda(0)-\kappa}{\lambda(s)-\kappa}\right)}$$

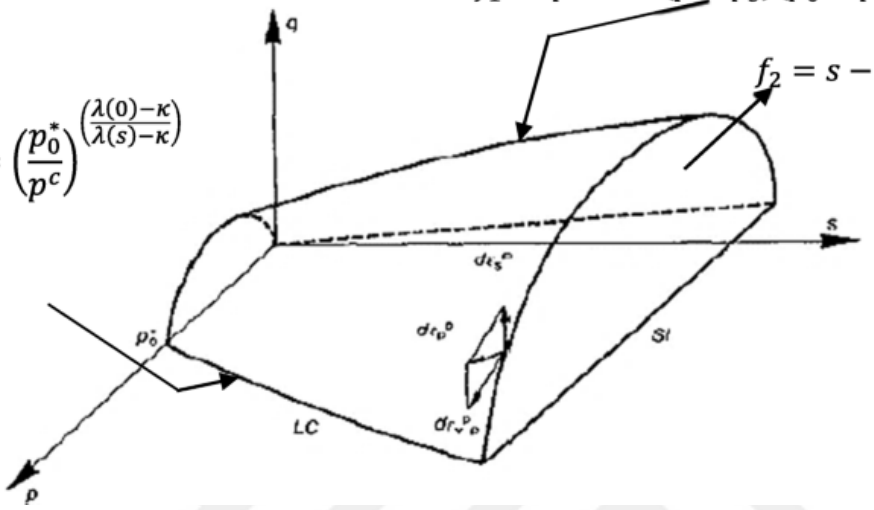

Figure A.3. Figure to explain the parameters of BBM yield surface

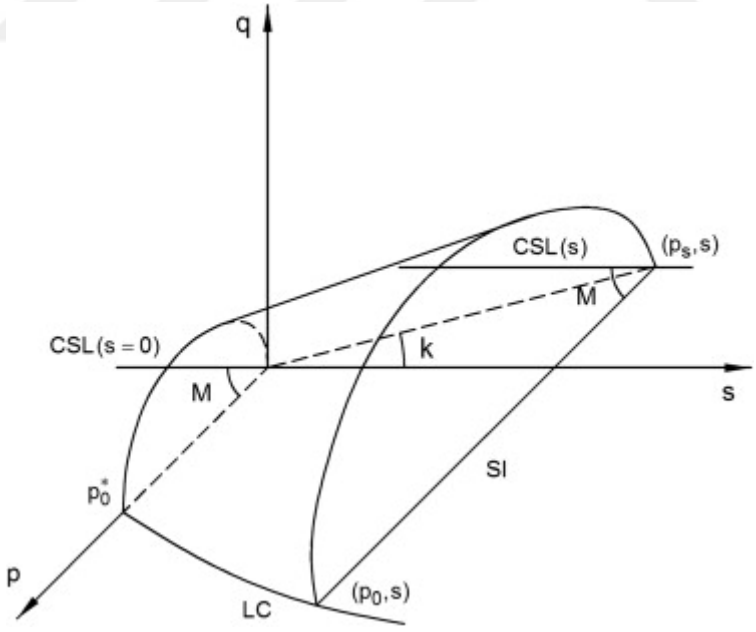

Figure A.4. Figure for BBM (yield surface)

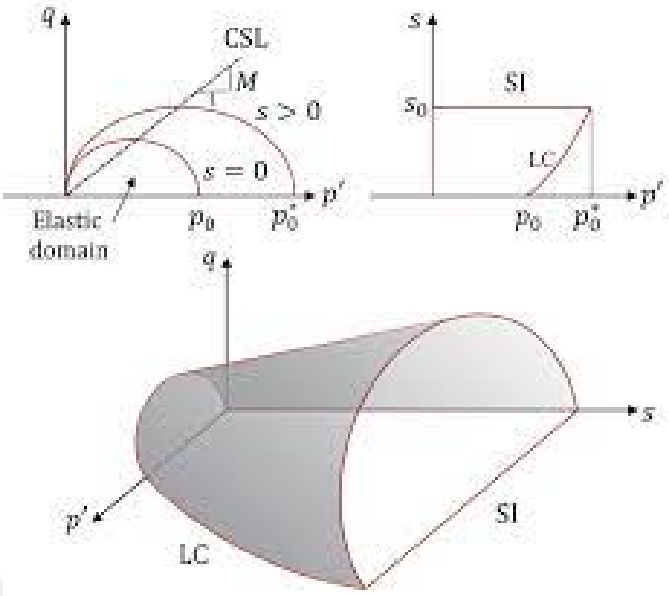

Figure A.5. Figure to explain the parameters of BBM

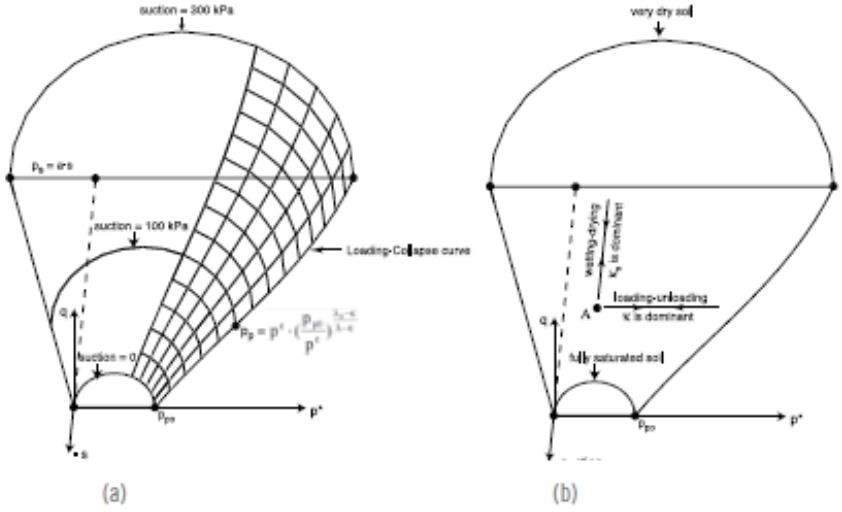

Figure A.6. Figure to explain the parameters of BBM yield surface

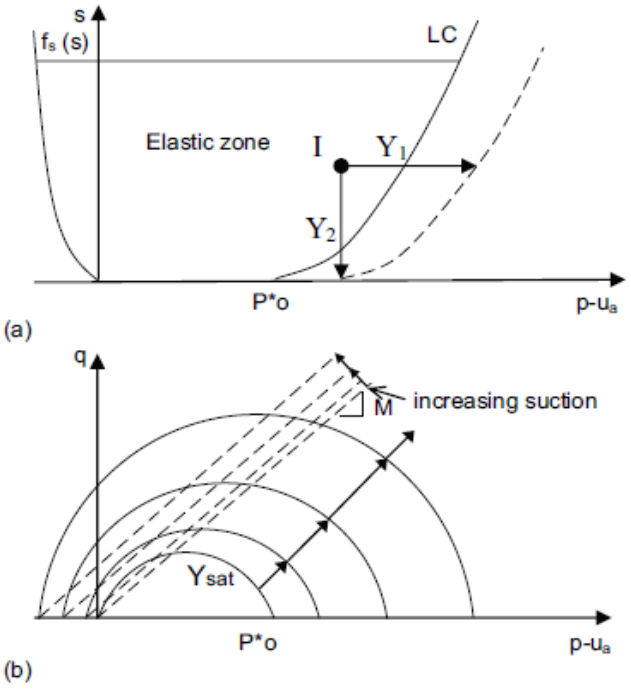

Figure A.7. Figure to explain the parameters of BBM (Alonso et al., 1990)

Figure 1. Limit state curves and elastic domains for unsaturated soils-BBM (after Alonso et al., 1990).

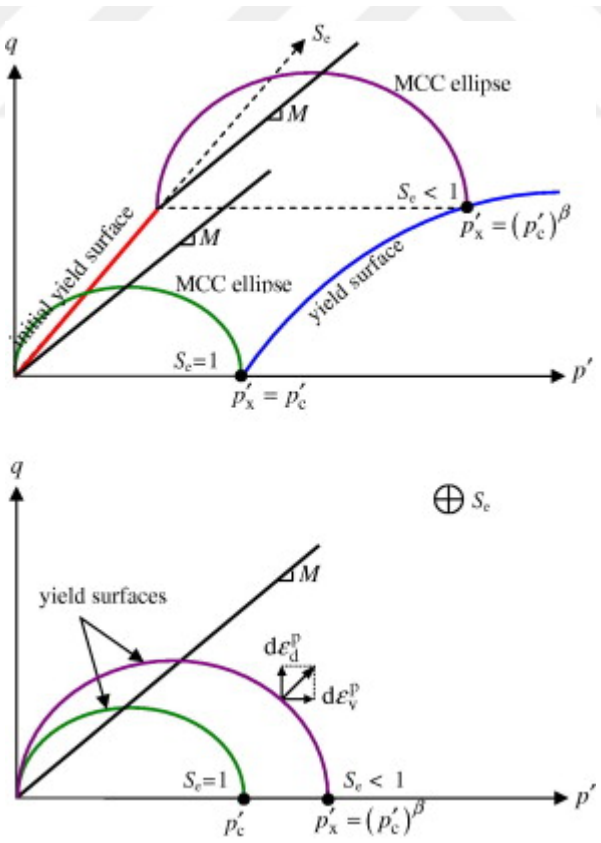

Figure A.8. Figure to explain the parameters of BBM yield surface

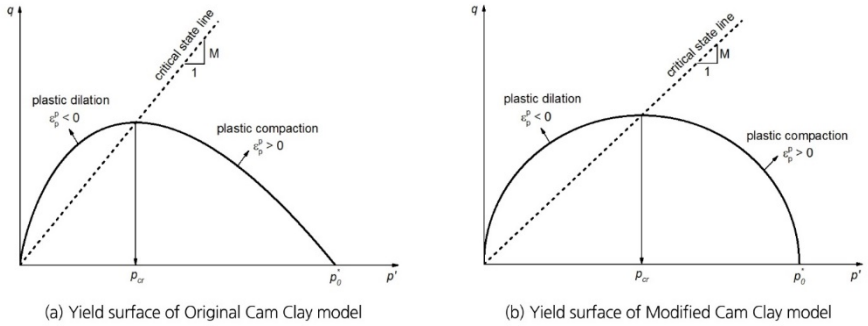

Figure A.9. Yield surface in the p´-q plane

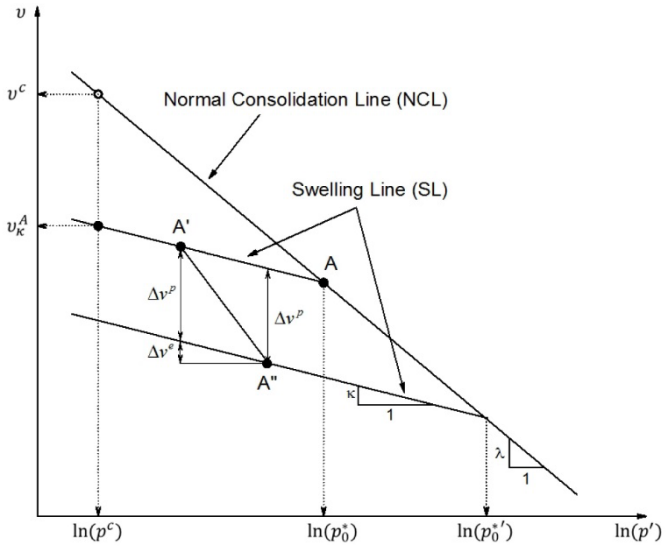

Figure A.10. Normal consolidation line and unloading-reloading (swelling) lines for an isotropic compression test

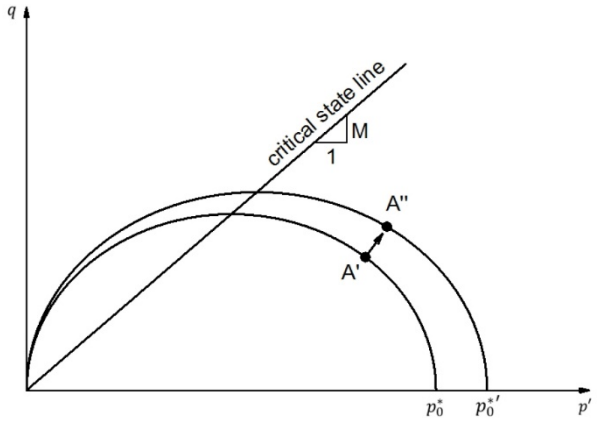

Figure A.11. An incremental consolidation pressure change due to movement of point from A´ to A´´

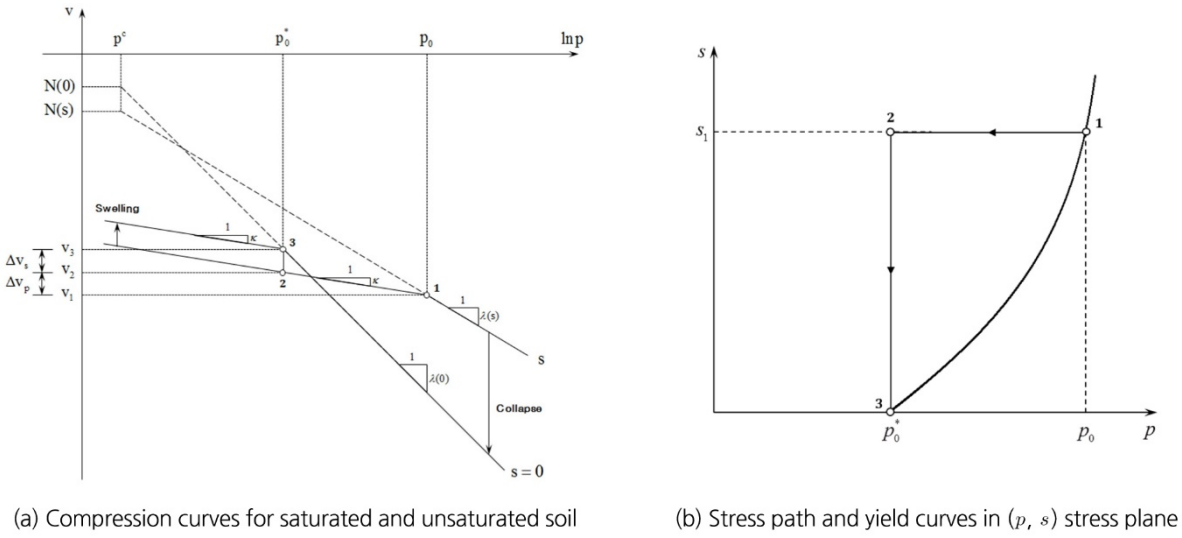

(a) Compression curves for saturated and unsaturated soil

(b) Stress path and yield curves in (p, s) stress plane

Figure A.12. Relationship between preconsolidation stresses p_0 and p_0* (Alonso et al., 1990)

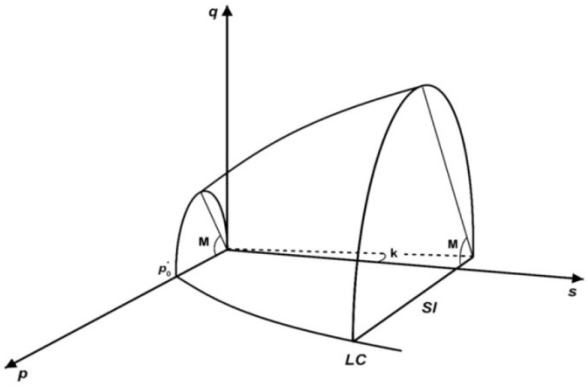

(a) Three-dimensional representation of the yield surface in the $p-q-s$ space

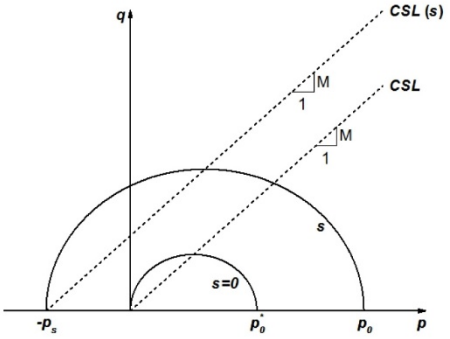

(b) Sections of the three-dimensional yield surface in the $p-q$ space by s=constant planes

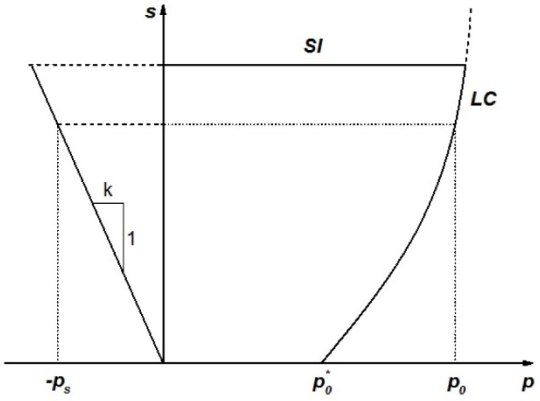

(c) Sections of the three-dimensional yield surface in the $p-s$ space by $q=0$ plane

Figure A.13. The yield surface in Barcelona Basic Model (modified after Gens, 1995)

B. TMI AND CLAY MINERALOGY IDENTIFICATION

Table B.1. Latitude degree and monthly correction coefficient values

Kuzey Enlemleri [a]	- A y l a r -											
	1	2	3	4	5	6	7	8	9	10	11	12
0°	1,04	0,94	1,04	1,01	1,04	1,01	1,04	1,04	1,01	1,04	1,01	1,04
5°	1,02	0,93	1,03	1,02	1,06	1,03	1,06	1,05	1,01	1,03	0,99	1,02
10°	1,00	0,91	1,03	1,03	1,08	1,06	1,08	1,07	1,02	1,02	0,98	0,99
15°	0,97	0,91	1,03	1,04	1,11	1,08	1,12	1,08	1,02	1,01	0,95	0,97
20°	0,95	0,90	1,03	1,05	1,13	1,11	1,14	1,11	1,02	1,00	0,93	0,94
25°	0,93	0,89	1,03	1,06	1,15	1,14	1,17	1,12	1,02	0,99	0,91	0,91
26°	0,92	0,88	1,03	1,06	1,15	1,15	1,17	1,12	1,02	0,99	0,91	0,91
27°	0,92	0,88	1,03	1,07	1,16	1,15	1,18	1,13	1,02	0,99	0,90	0,90
28°	0,91	0,88	1,03	1,07	1,16	1,16	1,18	1,13	1,02	0,98	0,90	0,90
29°	0,91	0,87	1,03	1,07	1,17	1,16	1,19	1,13	1,03	0,98	0,90	0,89
30°	0,90	0,87	1,03	1,08	1,18	1,17	1,20	1,14	1,03	0,98	0,89	0,88
31°	0,90	0,87	1,03	1,08	1,18	1,18	1,20	1,14	1,03	0,98	0,89	0,88
32°	0,89	0,86	1,03	1,08	1,19	1,19	1,21	1,15	1,03	0,98	0,88	0,87
33°	0,88	0,86	1,03	1,09	1,19	1,20	1,22	1,15	1,03	0,97	0,88	0,86
34°	0,88	0,85	1,03	1,09	1,20	1,20	1,22	1,16	1,03	0,97	0,87	0,86
35°	0,87	0,85	1,03	1,09	1,21	1,21	1,23	1,16	1,03	0,97	0,86	0,85
36°	0,87	0,85	1,03	1,10	1,21	1,22	1,24	1,16	1,03	0,97	0,86	0,84
37°	0,86	0,84	1,03	1,10	1,22	1,23	1,25	1,17	1,03	0,97	0,85	0,83
38°	0,85	0,84	1,03	1,10	1,23	1,24	1,25	1,17	1,04	0,96	0,84	0,83
39°	0,85	0,84	1,03	1,11	1,23	1,24	1,26	1,18	1,04	0,96	0,84	0,82
40°	0,84	0,83	1,03	1,11	1,24	1,25	1,27	1,18	1,04	0,96	0,83	0,81
41°	0,83	0,83	1,03	1,11	1,25	1,26	1,27	1,19	1,04	0,96	0,82	0,80
42°	0,82	0,83	1,03	1,12	1,26	1,27	1,28	1,19	1,04	0,95	0,82	0,79
43°	0,81	0,82	1,02	1,12	1,26	1,28	1,29	1,20	1,04	0,95	0,81	0,77
44°	0,81	0,82	1,02	1,13	1,27	1,29	1,30	1,20	1,04	0,95	0,80	0,76
45°	0,80	0,81	1,02	1,13	1,28	1,29	1,31	1,21	1,04	0,94	0,79	0,75
46°	0,79	0,81	1,02	1,13	1,29	1,31	1,32	1,22	1,04	0,94	0,79	0,74
47°	0,77	0,80	1,02	1,14	1,30	1,32	1,33	1,22	1,04	0,93	0,78	0,73
48°	0,76	0,80	1,02	1,14	1,31	1,33	1,34	1,23	1,05	0,93	0,77	0,72
49°	0,75	0,79	1,02	1,14	1,32	1,34	1,35	1,24	1,05	0,93	0,76	0,71
50°	0,74	0,78	1,02	1,15	1,33	1,36	1,37	1,25	1,06	0,92	0,76	0,70

(a) Türkiye, 36° - 42° kuzey enlemleri arasında yer almaktadır

Table B.2. Adjustment coefficient calculation equations

Aylar	F(λ)'yı Hesaplama Denklemi [a], [b]	R^2 [c]
1	$y = -7x10^{-5}x^2 - 0,0023x + 1,0312$	0,9938
2	$y = -4 x10^{-5}x^2 - 0,0010x + 0,9349$	0,9910
3	$x = 0 \rightarrow y = 1,04$; $0 < x < 43 \rightarrow y = 1,03$; $x \geq 43 \rightarrow y = 1,02$	-
4	$y = 3 x 10^{-5}x^2 + 0,0013x + 1,0119$	0,9943
5	$y = 6 x10^{-5}x^2 + 0,0025x + 1,0475$	0,9964
6	$y = 7 x10^{-5}x^2 + 0,0032x + 1,0147$	0,9984
7	$y = 6 x10^{-5}x^2 + 0,0033x + 1,0444$	0,9964
8	$y = 4 x10^{-5}x^2 + 0,0020x + 1,0427$	0,9935
9	$0 \leq x < 10 \rightarrow y = 1,01$; $10 \leq x < 29 \rightarrow y = 1,02$; $29 \leq x < 38 \rightarrow y = 1,03$ $38 \leq x < 48 \rightarrow y = 1,04$; $48 \leq x < 50 \rightarrow y = 1,05$; $x \geq 50 \rightarrow y = 1,06$	-
10	$y = -2 x10^{-5}x^2 - 0,0013x + 1,0363$	0,9855
11	$y = -6 x10^{-5}x^2 - 0,0022x + 1,004$	0,9958
12	$y = -8 x10^{-5}x^2 - 0,0024x + 1,0307$	0,9958

(a) $y = F(\lambda)$ ve x: Alanın enlem derecesi
(b) Denklemler Çizelge 1'deki değerler kullanılarak hesaplanmıştır.
(c) Regresyon katsayısı

C. XRD

General information

Analysis date	2024-05-30 16:22:53	Measurement start time	2024-05-30 15:34:54
Analyst	Administrator	Operator	Administrator
Sample name		Comment	
Measured data name	C:\Users\Rigaku\Desktop\SefaYildirim-Mayis2024-43608\Cu...	Memo	

Measurement Conditions

X-Ray generator	40 kV, 15 mA	Scan mode	1D(scan)
Incident primary	No unit	Scan speed/Duration time	5.00 °/min
Goniometer	MiniFlex 300/600	Step width	0.02 °
Attachment	ASC-8	Scan axis	θ/2θ
Filter	None	Scan range	5 ~ 60 °
Selection slit	None	DS	1.25deg
Diffracted beam mono	None	IHS	10 mm
Detector	D/teX Ultra2	SS	Open
Optics attribute	None	RS	Open

Measured profile view

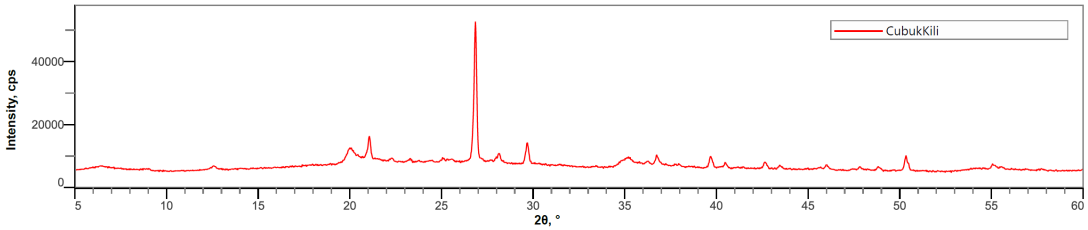

Figure C.1. XRD results from evaluatıon of Cubuk clay.

Peak profiling conditions

Peak search method	Second derivative method	σ cut	3.00		
Profile fitting	Run completed	Peak shape	Split pseudo-Voigt	Fitting condition	Auto(Refine background)

Peak Profile View

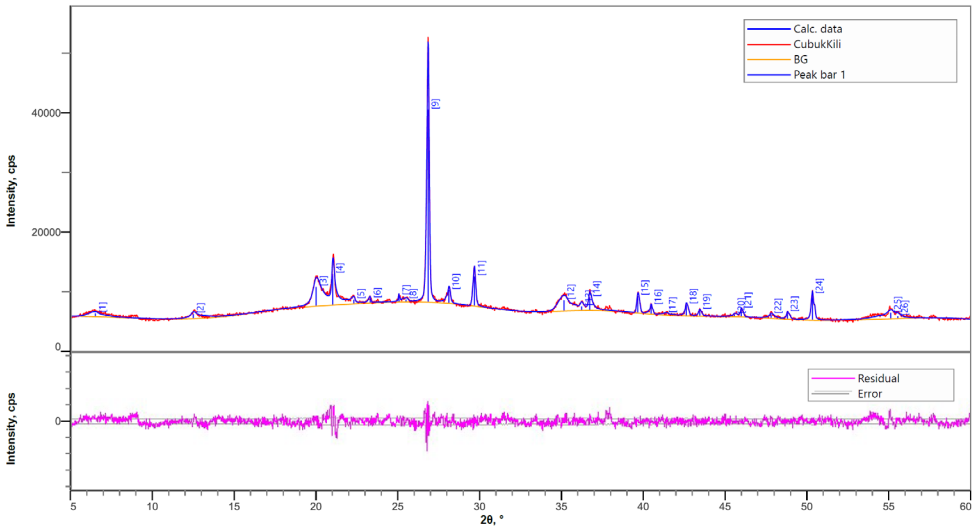

Figure C.2. XRD results from evaluation of Cubuk clay

Table C.1. XRD peak list for Cubuk clay

No.	2θ, °	d, Å	Height, cps	FWHM, °	Int. I., cps°	Int. W., °	Asymmetry	Decay(ηL/mL)	Decay(ηH/mH)	Size, Å
1	6.52(5)	13.55(10)	570(14)	0.83(7)	715(63)	1.25(14)	1.3(3)	0.0(6)	1.5(3)	100(9)
2	12.498(14)	7.077(8)	759(19)	0.59(7)	882(38)	1.16(8)	0.5(2)	1.21(18)	1.51(12)	141(16)
3	20.003(18)	4.435(4)	3217(58)	0.63(2)	3236(76)	1.01(4)	0.59(9)	0.79(12)	1.14(9)	133(5)
4	21.011(5)	4.2247(11)	5180(88)	0.175(11)	1443(48)	0.279(14)	0.59(9)	0.79(12)	1.14(9)	481(30)
5	22.31(2)	3.982(4)	693(14)	0.30(10)	393(57)	0.57(9)	4(6)	1.5(4)	0.6(12)	278(95)
6	23.303(5)	3.8142(9)	744(15)	0.14(2)	131(16)	0.18(3)	5(5)	0.5(4)	0.0(11)	592(92)
7	25.064(10)	3.5500(14)	1089(22)	0.056(13)	70(19)	0.065(19)	3(2)	0.3(6)	0.0(13)	1505(359)
8	25.49(8)	3.491(10)	423(9)	0.46(11)	223(34)	0.53(9)	3(2)	0.3(6)	0.0(13)	185(44)
9	26.845(3)	3.3184(3)	32256(281)	0.152(2)	6049(50)	0.188(3)	2.3(2)	0.30(3)	0.67(8)	561(9)
10	28.108(13)	3.1721(15)	2226(44)	0.16(2)	606(30)	0.272(19)	1.1(4)	1.5(2)	0.6(4)	548(79)
11	29.671(7)	3.0084(7)	4940(84)	0.164(7)	972(26)	0.197(9)	2.2(5)	0.00(12)	0.9(2)	522(22)
12	35.140(19)	2.5517(13)	1796(36)	0.79(3)	2200(63)	1.22(6)	1.19(14)	0.00(14)	1.55(8)	110(4)
13	36.220(15)	2.4781(10)	726(16)	0.19(4)	211(31)	0.29(5)	1.19(14)	0.00(14)	1.55(8)	466(99)
14	36.715(6)	2.4458(4)	2230(44)	0.166(12)	575(27)	0.258(17)	1.19(14)	0.00(14)	1.55(8)	525(38)
15	39.650(10)	2.2712(6)	2850(58)	0.155(10)	487(22)	0.171(11)	1.1(3)	0.0(2)	0.2(2)	567(35)
16	40.462(10)	2.2275(5)	1441(32)	0.124(15)	280(18)	0.194(17)	1.2(5)	1.4(3)	0.0(5)	714(85)
17	41.34(3)	2.1821(16)	315(8)	0.34(9)	222(29)	0.70(11)	0.8(10)	1.5(3)	1.4(5)	258(66)
18	42.612(11)	2.1200(5)	1889(43)	0.154(17)	428(19)	0.227(15)	1.0(3)	1.1(3)	0.6(3)	577(64)
19	43.436(19)	2.0817(9)	1001(24)	0.15(3)	223(18)	0.22(2)	1.4(9)	0.9(5)	1.0(6)	605(117)
20	45.544(18)	1.9901(7)	419(11)	0.22(7)	137(25)	0.33(7)	0.6(3)	1.5(2)	0.2(3)	411(126)
21	45.964(5)	1.97287(19)	1391(33)	0.119(14)	247(20)	0.178(19)	0.6(3)	1.5(2)	0.2(3)	755(90)
22	47.791(15)	1.9016(6)	682(17)	0.25(4)	330(26)	0.48(5)	1.1(8)	1.2(3)	1.5(4)	359(59)
23	48.790(17)	1.8650(6)	1125(28)	0.14(2)	240(19)	0.21(2)	0.9(6)	1.1(5)	0.7(5)	634(102)
24	50.318(5)	1.81191(17)	4284(86)	0.145(6)	863(19)	0.202(8)	1.8(3)	0.66(12)	0.86(17)	634(26)
25	55.10(3)	1.6655(7)	992(24)	0.65(8)	1374(174)	1.4(2)	2.1(10)	1.55(12)	1.5(2)	144(18)
26	55.53(4)	1.6536(11)	365(9)	0.23(19)	180(160)	0.5(5)	2.1(10)	1.55(12)	1.5(2)	405(338)

Phase name	Chemical formula	FOM	Phase reg. detail	Space Group	DB Card Number
Quartz, syn	Si O2	0.460	S/M:PDF-4+ 2023	154 : P3221	00-033-1161
Calcite, syn	Ca (C O3)	0.770	S/M:PDF-4+ 2023	167 : R-3c:H	01-085-0849
montmorillonite	Na0.37 Ca0.16 K0.03 (Al3.05 Fe0.41 +3 Mg0.55 Ti0.01) (Si7.77 Al0.23) O20 (O H)4 ·x H2 O	1.170	S/M:PDF-4+ 2023		00-072-0370

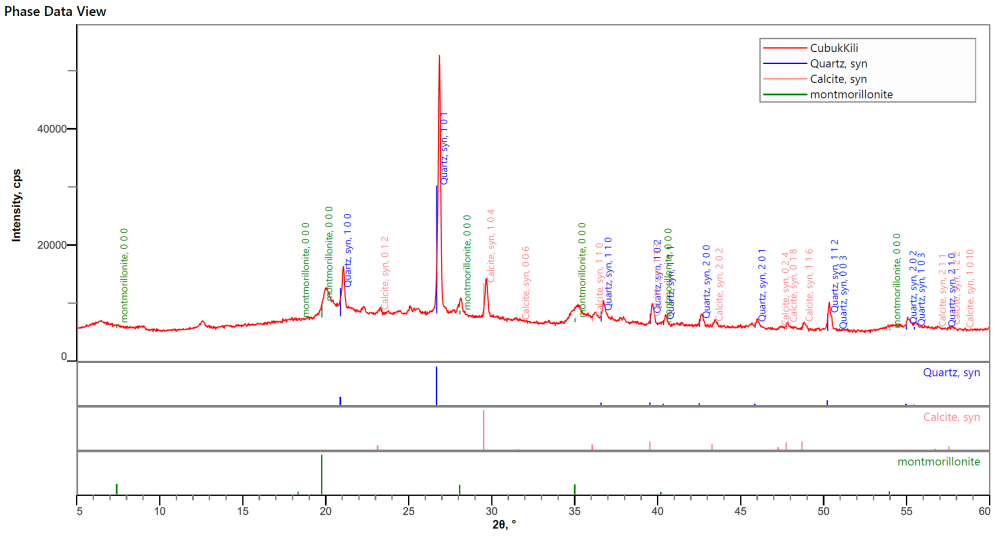

Figure C.3. Minerals determined in Cubuk clay from XRD test

D. SEM PHOTOS

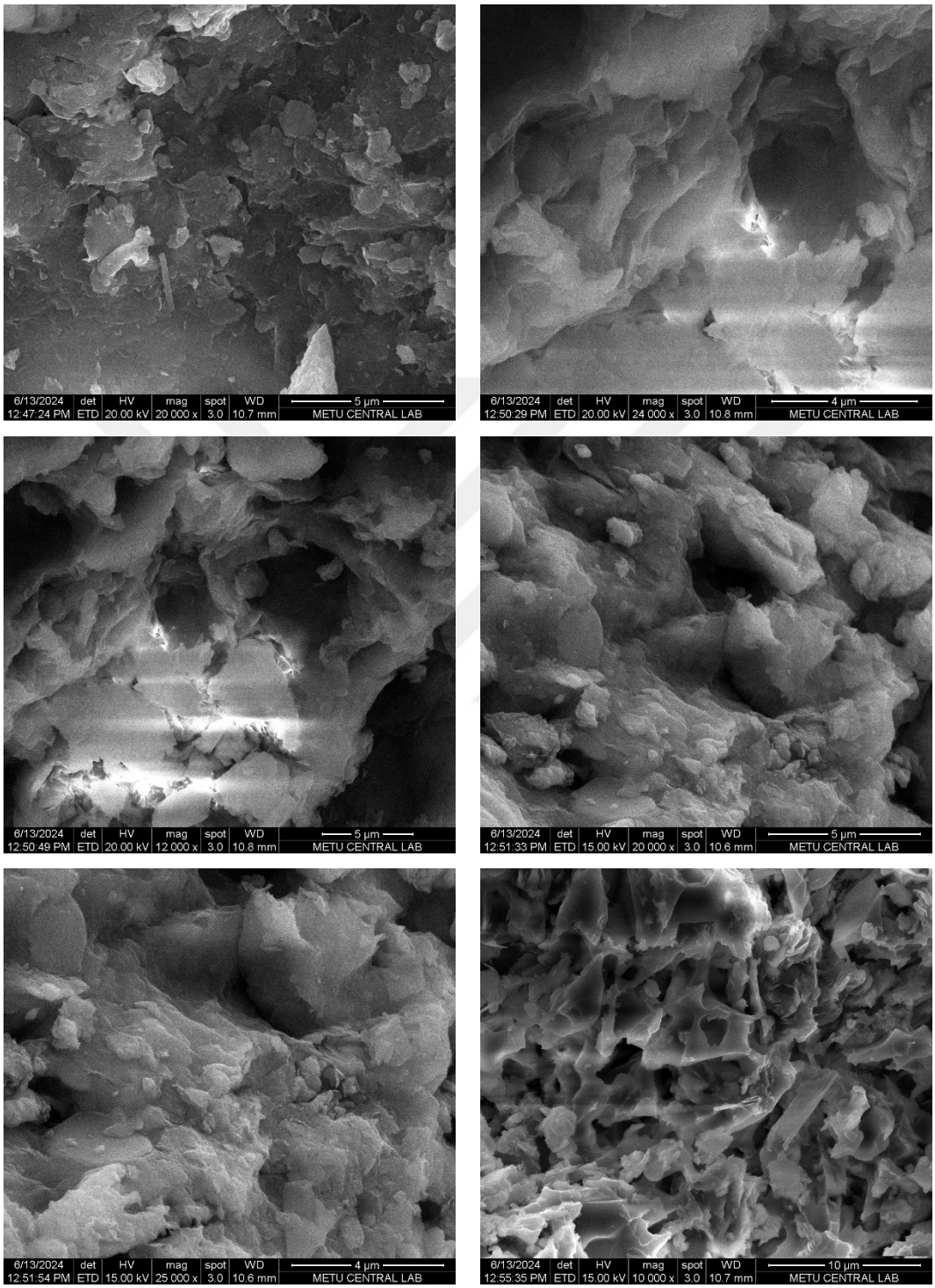

Figure D.1. SEM photos

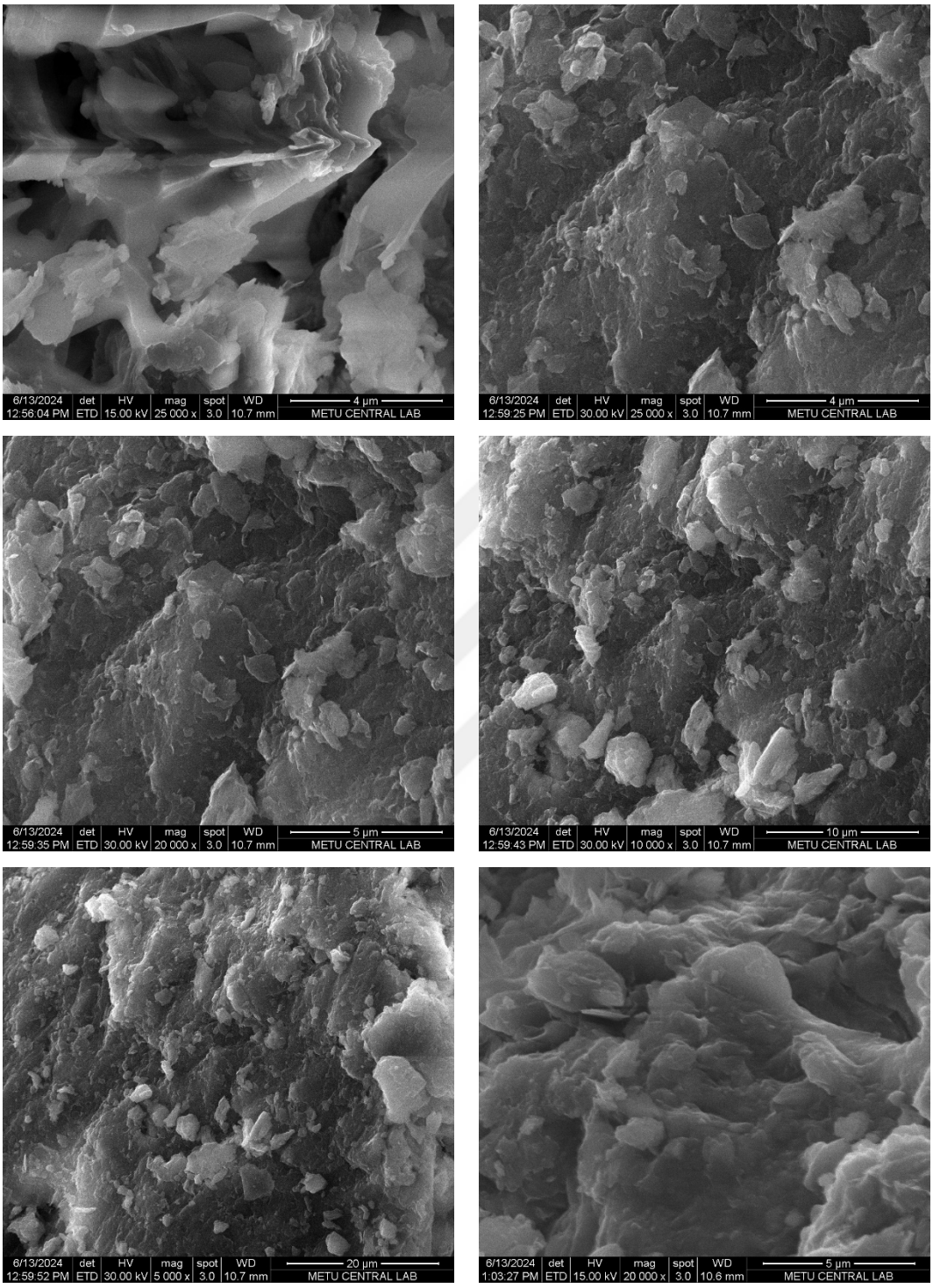

Figure D.2. SEM photos

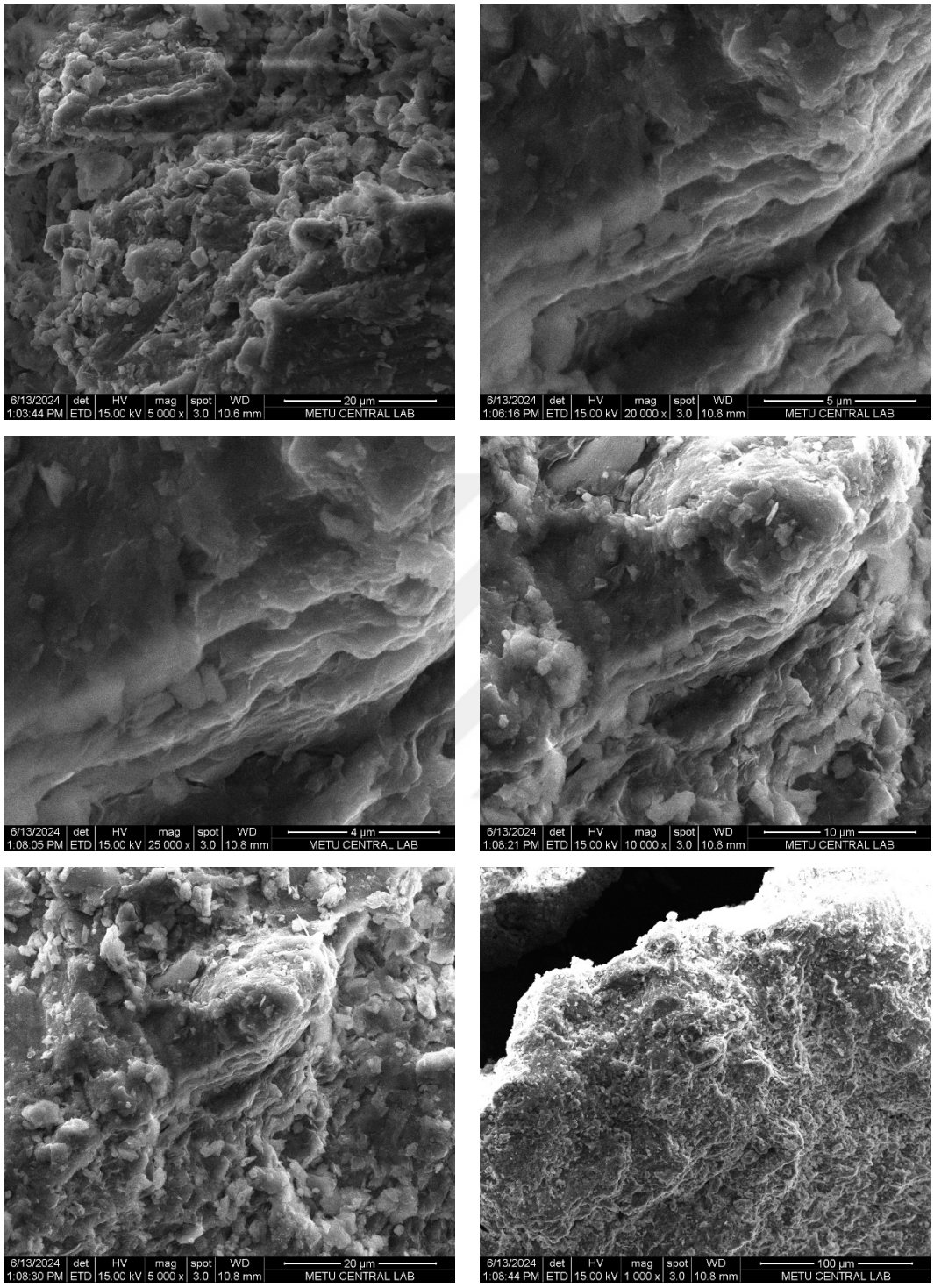

Figure D.3. SEM photos

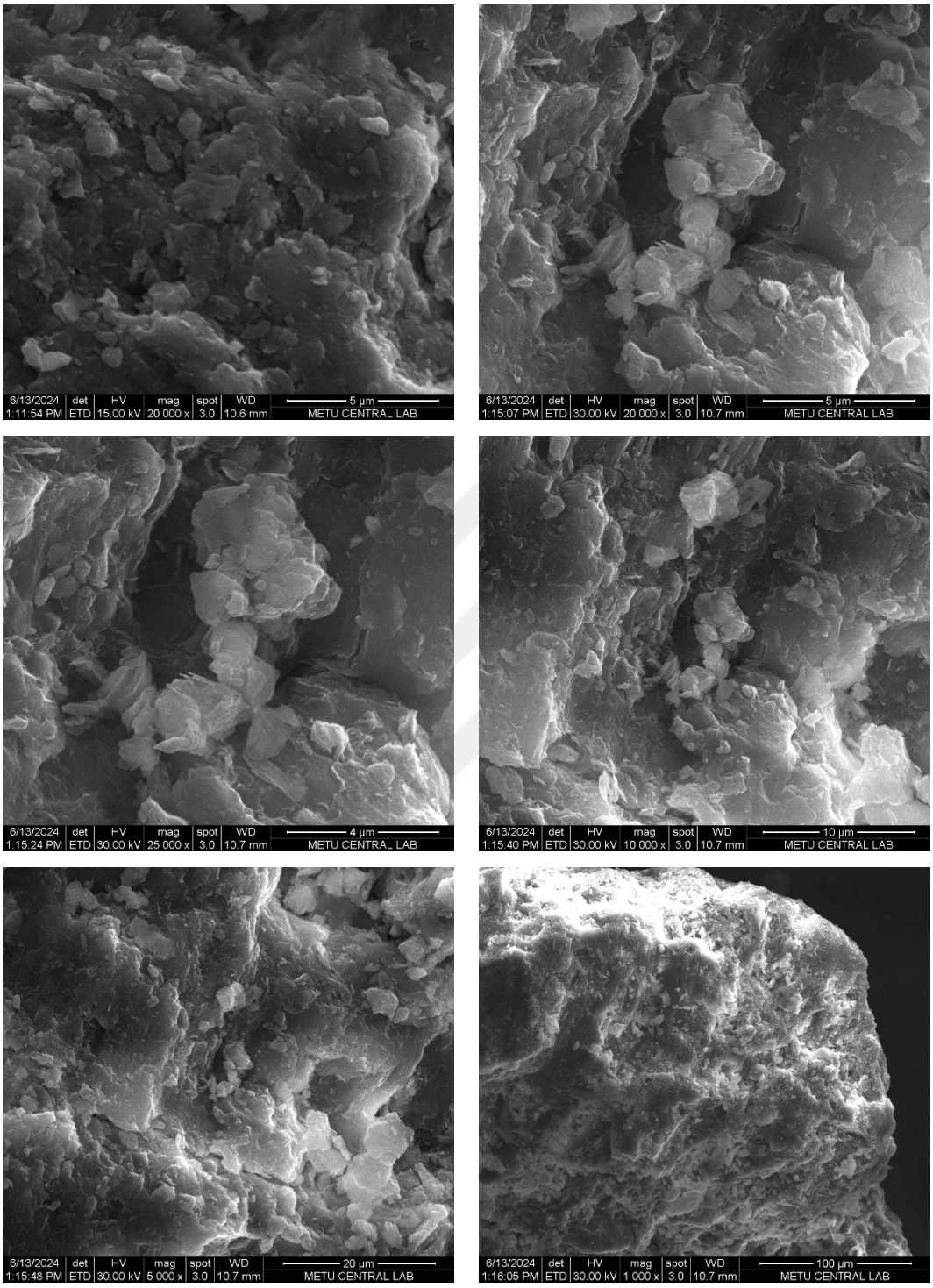

Figure D.4. SEM photos

E. EDX GRAPHS

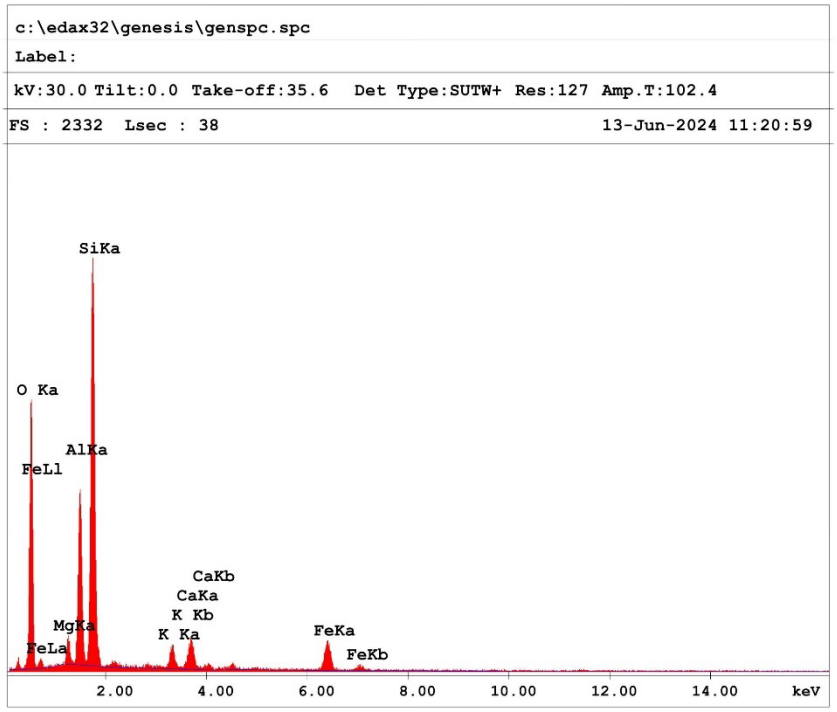

EDAX ZAF Quantification (Standardless)
Element Normalized
SEC Table : Default

Element	Wt %	At %	K-Ratio	Z	A	F
O K	49.09	63.92	0.1352	1.0256	0.2683	1.0006
MgK	2.28	1.95	0.0085	0.9888	0.3722	1.0098
AlK	11.55	8.91	0.0546	0.9607	0.4865	1.0120
SiK	29.35	21.76	0.1417	0.9897	0.4876	1.0007
K K	1.56	0.83	0.0114	0.9384	0.7755	1.0053
CaK	2.17	1.13	0.0174	0.9603	0.8301	1.0026
FeK	3.99	1.49	0.0353	0.8882	0.9942	1.0000
Total	100.00	100.00				

c:\edax32\genesis\genspc.spc

Element	Net Inte.	Bkgd Inte.	Inte. Error	P/B
O K	156.60	1.87	1.30	83.76
MgK	19.68	6.85	4.73	2.87
AlK	132.50	6.31	1.47	21.00
SiK	336.22	5.97	0.89	56.30
K K	22.54	3.27	3.86	6.89
CaK	32.09	2.86	3.09	11.24
FeK	37.44	1.45	2.73	25.75

Figure E.1. EDX Graphs

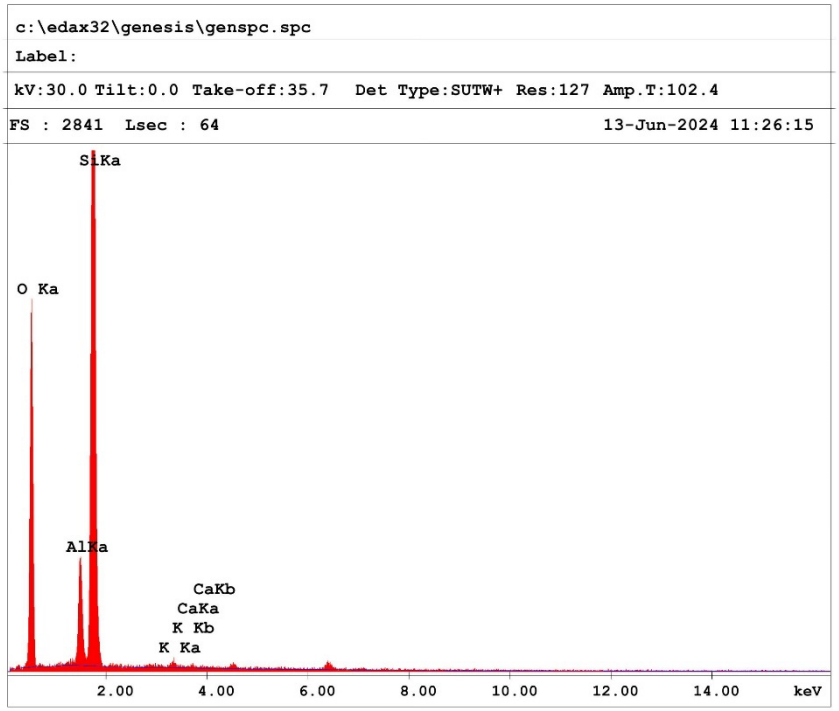

EDAX ZAF Quantification (Standardless)
Element Normalized
SEC Table : Default

Element	Wt %	At %	K-Ratio	Z	A	F
O K	53.10	66.49	0.1563	1.0182	0.2889	1.0006
AlK	5.47	4.06	0.0296	0.9538	0.5552	1.0203
SiK	40.90	29.17	0.2474	0.9826	0.6157	1.0001
K K	0.36	0.18	0.0025	0.9306	0.7589	1.0003
CaK	0.17	0.09	0.0014	0.9524	0.8261	1.0000
Total	100.00	100.00				

Element	Net Inte.	Bkgd Inte.	Inte. Error	P/B
O K	155.07	2.24	1.02	69.10
AlK	61.33	4.11	1.70	14.91
SiK	501.96	4.25	0.56	117.98
K K	4.25	3.21	9.59	1.33
CaK	2.14	3.26	17.20	0.66

Figure E.2. EDX Graphs

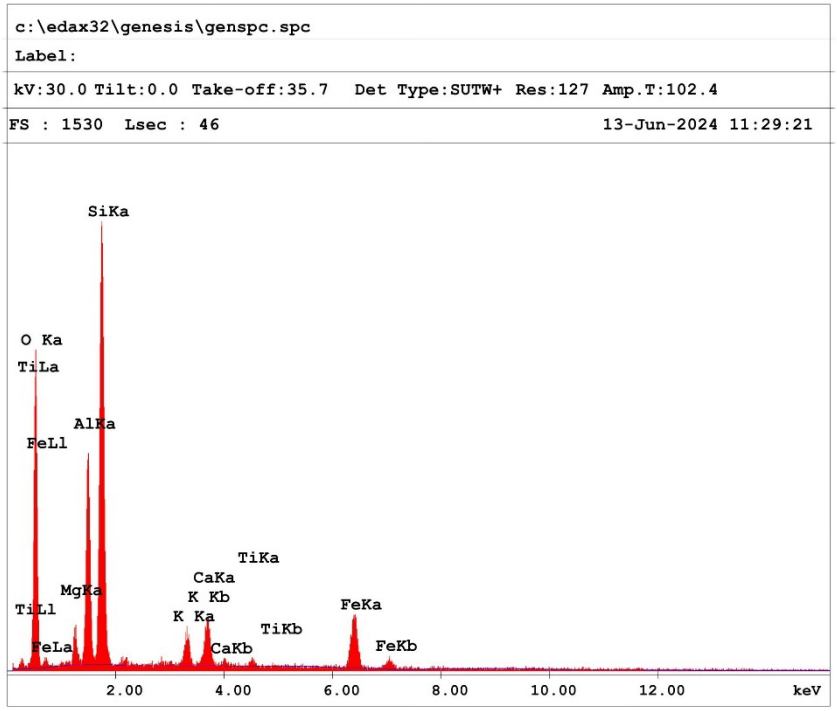

EDAX ZAF Quantification (Standardless)
Element Normalized
SEC Table : Default

Element	Wt %	At %	K-Ratio	Z	A	F
O K	47.52	63.02	0.1266	1.0285	0.2588	1.0006
MgK	2.44	2.13	0.0088	0.9915	0.3582	1.0092
AlK	11.75	9.24	0.0536	0.9633	0.4686	1.0110
SiK	27.56	20.82	0.1295	0.9924	0.4731	1.0009
K K	1.77	0.96	0.0131	0.9415	0.7791	1.0073
CaK	2.67	1.41	0.0215	0.9634	0.8313	1.0045
TiK	0.45	0.20	0.0037	0.8848	0.9076	1.0092
FeK	5.84	2.22	0.0515	0.8909	0.9914	1.0000
Total	100.00	100.00				

c:\edax32\genesis\genspc.spc

Element	Net Inte.	Bkgd Inte.	Inte. Error	P/B
O K	98.57	1.04	1.50	94.54
MgK	13.66	3.13	4.81	4.37
AlK	87.34	3.30	1.64	26.45
SiK	206.29	3.71	1.04	55.54
K K	17.27	3.26	4.16	5.30
CaK	26.61	3.58	3.22	7.42
TiK	3.89	3.65	12.68	1.07
FeK	36.73	2.56	2.60	14.33

Figure E.3. EDX Graphs

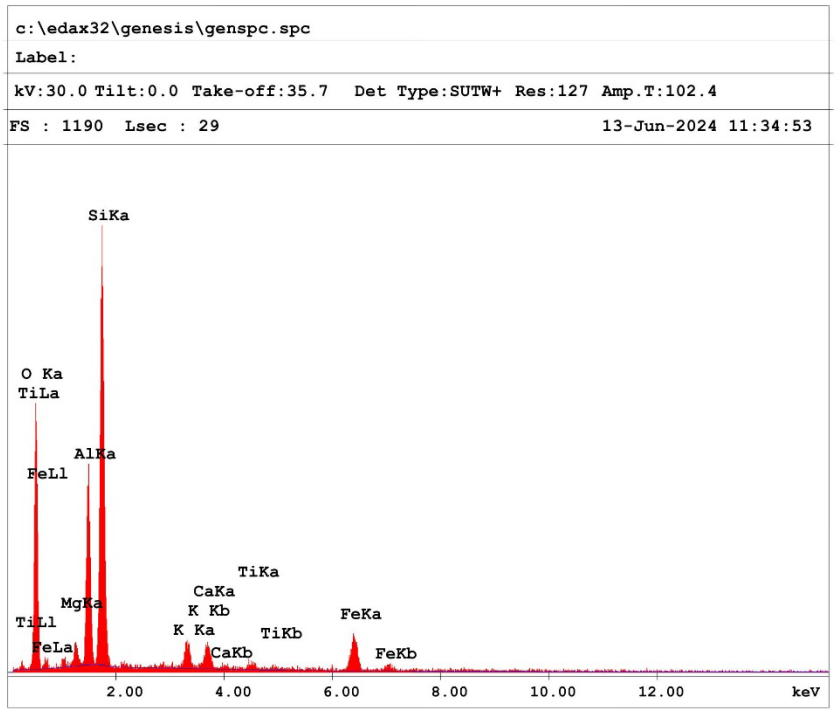

EDAX ZAF Quantification (Standardless)
Element Normalized
SEC Table : Default

Element	Wt %	At %	K-Ratio	Z	A	F
O K	47.69	62.85	0.1287	1.0276	0.2625	1.0006
MgK	1.88	1.63	0.0070	0.9906	0.3691	1.0100
AlK	12.22	9.55	0.0581	0.9625	0.4879	1.0119
SiK	29.37	22.05	0.1404	0.9916	0.4819	1.0007
K K	1.85	1.00	0.0135	0.9404	0.7731	1.0053
CaK	1.67	0.88	0.0134	0.9624	0.8257	1.0040
TiK	0.57	0.25	0.0047	0.8839	0.9103	1.0075
FeK	4.74	1.79	0.0418	0.8900	0.9923	1.0000
Total	100.00	100.00				

c:\edax32\genesis\genspc.spc

Element	Net Inte.	Bkgd Inte.	Inte. Error	P/B
O K	101.53	1.43	1.86	70.95
MgK	10.97	3.95	7.31	2.78
AlK	95.74	4.67	1.98	20.51
SiK	226.41	5.04	1.25	44.90
K K	18.09	3.07	5.02	5.90
CaK	16.76	3.00	5.25	5.59
TiK	5.01	2.45	11.60	2.04
FeK	30.15	1.43	3.52	21.07

Figure E.4. EDX Graphs

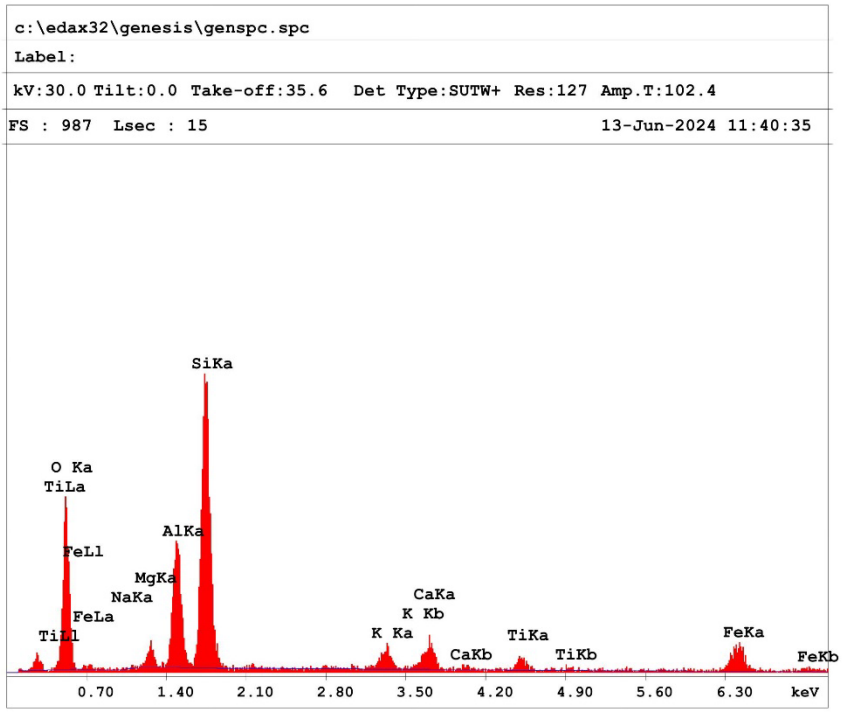

EDAX ZAF Quantification (Standardless)
Element Normalized
SEC Table : Default

Element	Wt %	At %	K-Ratio	Z	A	F
O K	45.05	60.56	0.1128	1.0298	0.2430	1.0006
NaK	0.13	0.12	0.0003	0.9673	0.2537	1.0054
MgK	2.51	2.22	0.0092	0.9927	0.3670	1.0099
AlK	11.95	9.52	0.0557	0.9645	0.4774	1.0119
SiK	29.56	22.64	0.1402	0.9936	0.4770	1.0009
K K	1.88	1.04	0.0138	0.9428	0.7696	1.0074
CaK	2.46	1.32	0.0196	0.9648	0.8226	1.0053
TiK	1.43	0.64	0.0115	0.8860	0.9031	1.0076
FeK	5.03	1.94	0.0442	0.8921	0.9866	1.0000
Total	100.00	100.00				

c:\edax32\genesis\genspc.spc

Element	Net Inte.	Bkgd Inte.	Inte. Error	P/B
O K	97.42	1.92	2.61	50.70
NaK	0.51	2.82	122.47	0.18
MgK	16.01	5.12	8.10	3.12
AlK	100.69	5.06	2.65	19.90
SiK	248.06	5.19	1.64	47.81
K K	20.24	3.84	6.61	5.27
CaK	27.03	3.97	5.54	6.81
TiK	13.64	3.07	8.25	4.44
FeK	35.03	1.79	4.49	19.54

Figure E.5. EDX Graphs

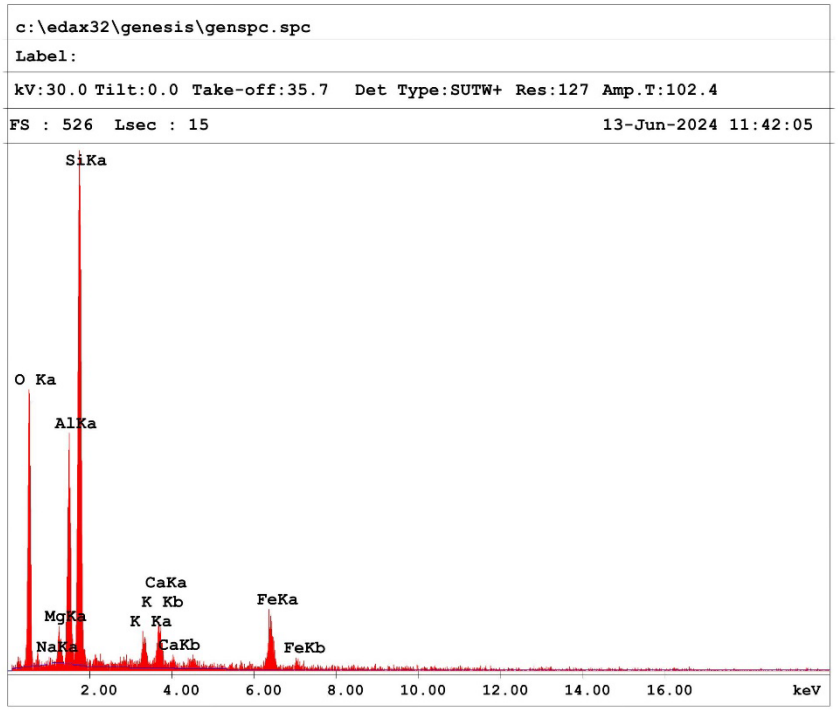

EDAX ZAF Quantification (Standardless)
Element Normalized
SEC Table : Default

Element	Wt %	At %	K-Ratio	Z	A	F
O K	45.16	60.53	0.1186	1.0286	0.2550	1.0007
NaK	0.21	0.20	0.0005	0.9662	0.2553	1.0055
MgK	2.21	1.95	0.0082	0.9916	0.3685	1.0101
AlK	11.37	9.03	0.0535	0.9635	0.4827	1.0127
SiK	31.30	23.89	0.1513	0.9925	0.4867	1.0008
K K	1.69	0.93	0.0122	0.9417	0.7649	1.0062
CaK	2.48	1.32	0.0196	0.9636	0.8203	1.0036
FeK	5.59	2.14	0.0493	0.8910	0.9905	1.0000
Total	100.00	100.00				

c:\edax32\genesis\genspc.spc

Element	Net Inte.	Bkgd Inte.	Inte. Error	P/B
O K	93.77	1.55	2.66	60.67
NaK	0.77	3.16	87.40	0.24
MgK	12.94	4.12	9.02	3.14
AlK	88.55	3.61	2.80	24.55
SiK	244.78	3.22	1.64	76.02
K K	16.42	1.93	6.96	8.50
CaK	24.73	2.13	5.52	11.64
FeK	35.68	0.90	4.35	39.57

Figure E.6. EDX Graphs

F. GRAPHICAL ABSTRACT OF THE RESEARCH

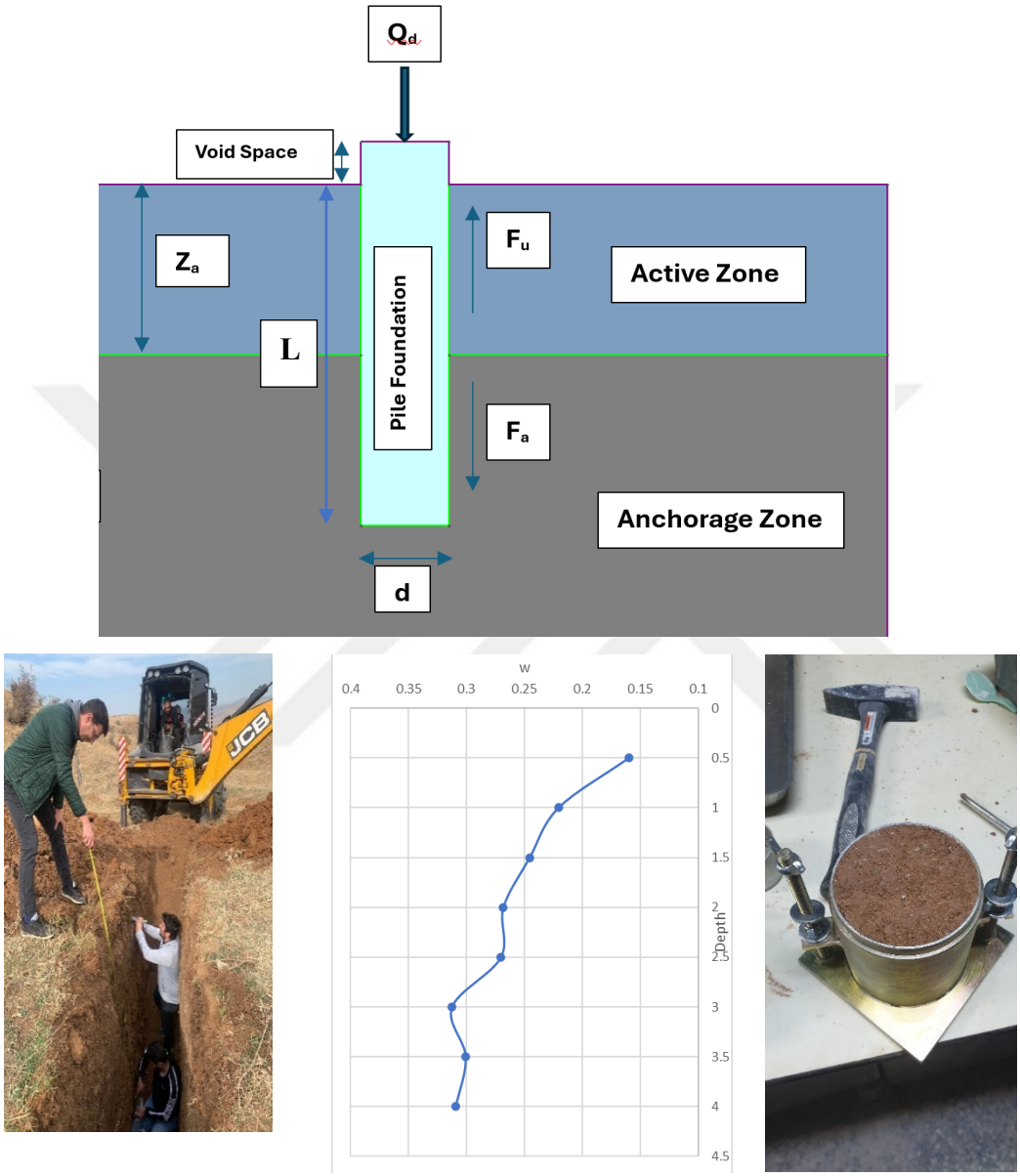

Figure F.1. Site Selection

Oedometer test

Triaxial test

Test for Axis translation method

MBT

Figure F.2. Laboratory Tests

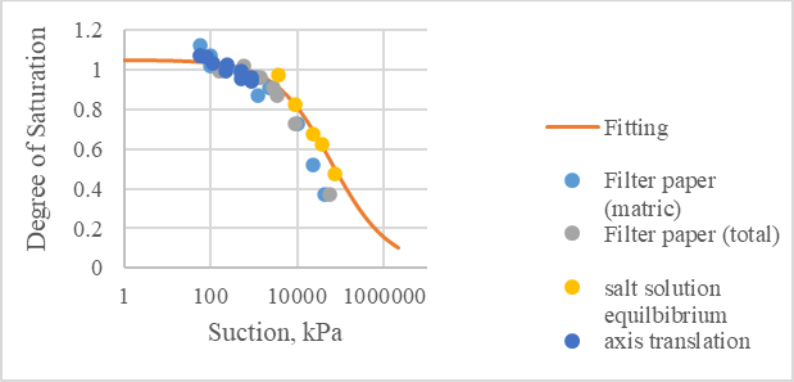

Figure F.3. SWRC

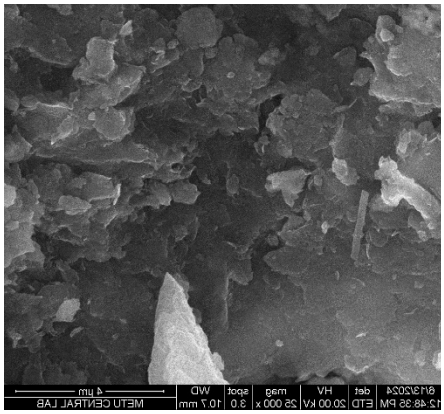

SEM

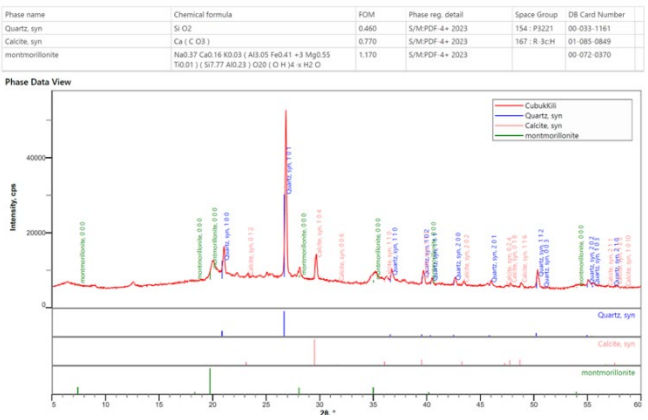

XRD

Figure F.4. Mineralogical Analyses

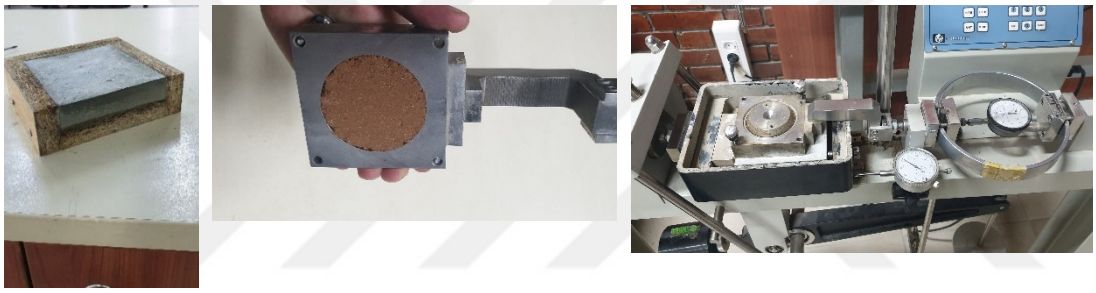

Figure F.5. Interface Direct Shear Test between concrete and clay

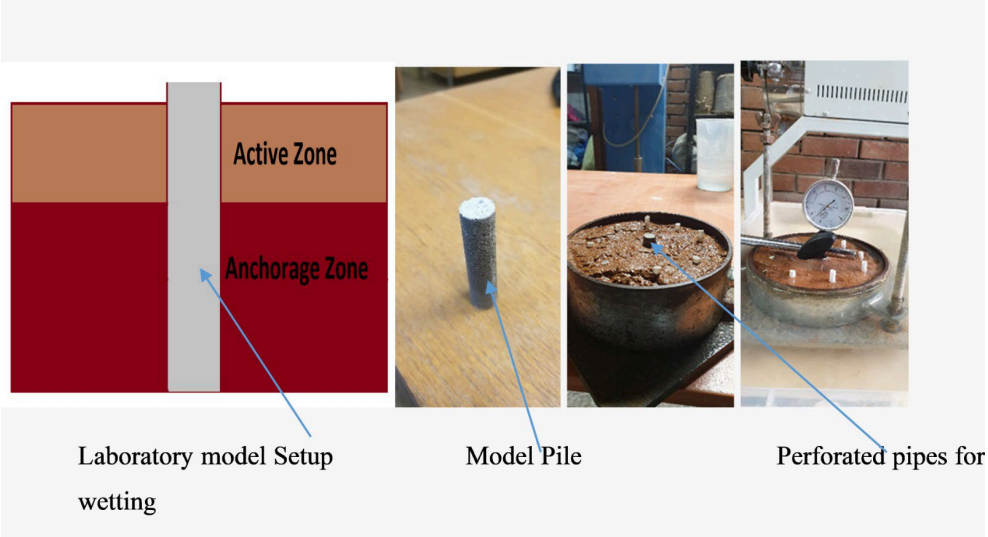

Figure F.6. Laboratory model setup

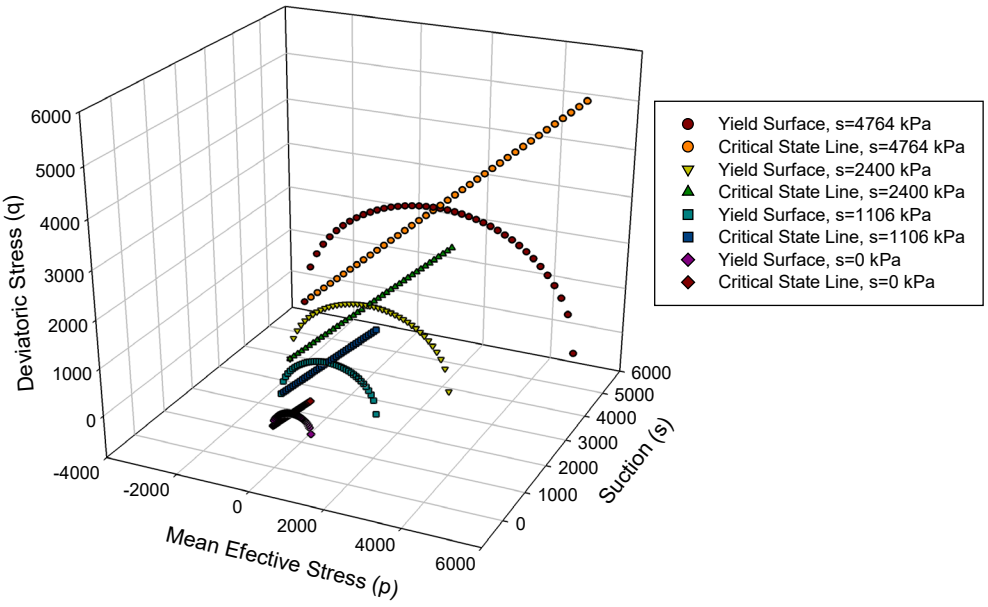

(a)

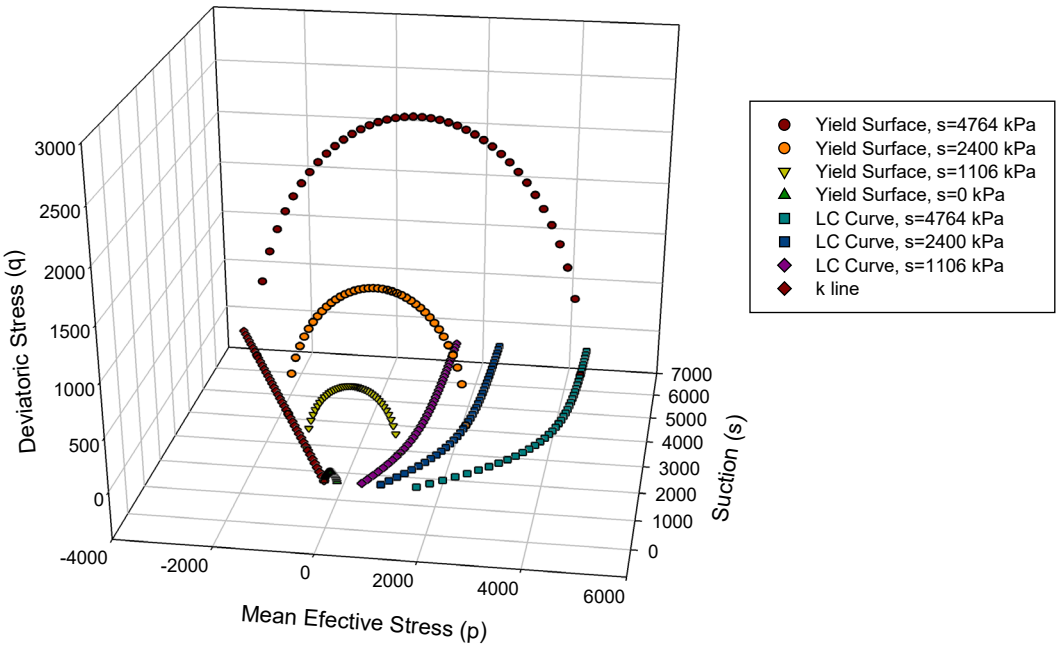

(b)

Figure F.7. BBM Model

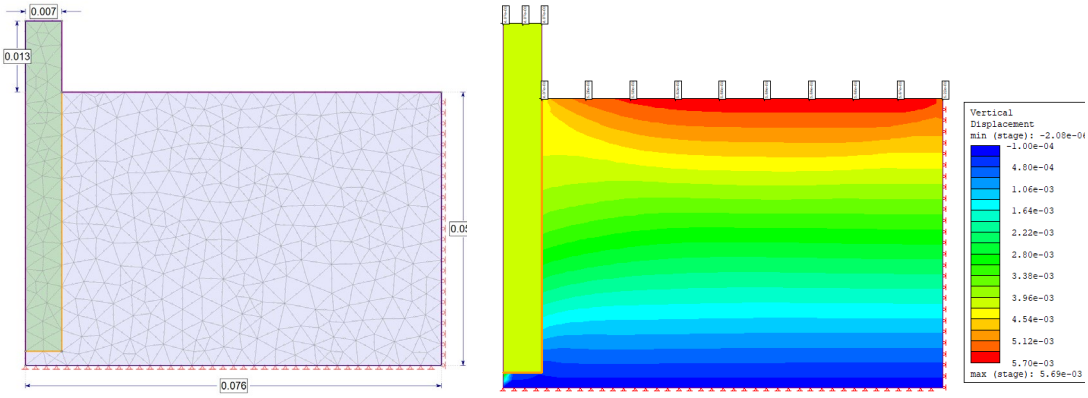

Figure F.8. Computer, Axisymmetric RS-2 model

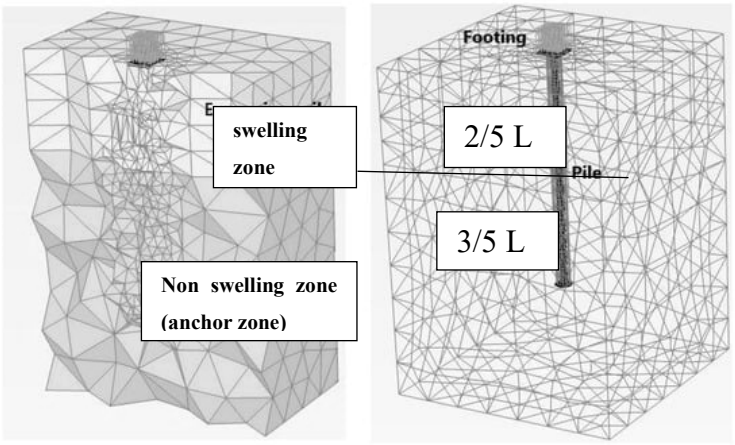

Figure F.9. Recommendation for pile design in Cubuk-Ankara clay

G. CURRICULUM VITAE

PERSONAL INFORMATION

Surname, Name : Yildirim, Sefa

EDUCATION

Degree	Institution	Year of Graduation
MS	University of Georgia Engineering	2017
BS	Ataturk University Civil Engineering	2012
High School	Rezan Has High School, Istanbul	2006

WORK EXPERIENCE

Year	Place	Enrollment
2018-Present	DSI Genel Mud.	Geotechnical Engineer

FOREIGN

LANGUAGES

Advanced English

PUBLICATIONS

1. Cetin, K. O., Ayhan, B. U., Cüceoğlu, F., & Yildirim, S. (2025). Performance of Reyhanlı Dam during February 6, 2023 Kahramanmaraş-Türkiye earthquake sequence. *Soil Dynamics and Earthquake Engineering, 194*, 109369.
2. Onder Cetin, K., Cuceoglu, F., Ayhan, B. U., Yildirim, S., Aydin, S., Demirdogen, S., ... & Moss, R. E. S. (2024). Performance of hydraulic structures during 6 February 2023 Kahramanmaraş, Türkiye, earthquake sequence. *Earthquake Spectra, 40*(4), 2231-2267.
3. Demirdogen, S., & Yildirim, S. (2024). Sarıçay Dam: a case study on in-depth seismic evaluation, deformation modulus and key geotechnical parameters. *Quarterly Journal of Engineering Geology and Hydrogeology, 57*(3), qjegh2024-002.

4. Demirdogen, S., & Yildirim, S. (2024). The disturbance factor of Hoek–Brown failure criterion in dam foundations. Geotechnical and *Geological Engineering, 42*(1), 817-825.

HOBBIES

Playing Bridge, Chess, Tennis